



Technische Universität München

Ingenieur fakultät Bau Geo Umwelt

Lehrstuhl für Ingenieurgeologie

Analysis of Performance and Wear of Electrical Rock Hammer Drills

Florian M. Menschik

Vollständiger Abdruck der von der Ingenieur fakultät Bau Geo Umwelt der Technischen Universität München zur Erlangung des akademischen Grades eines

Doktor Ingenieurs (Dr.-Ing.)

genehmigten Dissertation.

Vorsitzender: Univ.-Prof. Dr.-Ing. habil. Christian Grosse

Prüfer der Dissertation:

1. Univ.-Prof. Dr. rer. nat. Kurosch Thuro
2. Ass.-Prof. Dr. techn. Alexander Preh
Technische Universität Wien, Österreich

Die Dissertation wurde am 01.10.2015 bei der Technischen Universität München eingereicht und durch die Ingenieur fakultät Bau Geo Umwelt am 27.11.2015 angenommen.

Table of content

I	Acknowledgements.....	V
II	Abstract.....	VI
III	Zusammenfassung	VIII
IV	Table of figures.....	X
V	List of tables	XVI
VI	List of formulas.....	XVII
VII	List of MySQL queries.....	XVIII
1	Introduction	1
2	Mission objectives.....	2
3	State of the art	3
3.1	Drillability and performance and wear of drills.....	3
3.2	Database technology	3
3.3	Numerical Modelling of stress and disturbed zones	3
4	Geography and geology of the project sites	4
4.1	Gold mines.....	5
4.1.1	Location and short description	5
4.1.2	Geological overview	6
4.2	Platinum mines.....	10
4.2.1	Location and short description	10
4.2.2	Geological overview	10
4.3	Other mines.....	12
4.4	Quarries and other test rocks.....	14
5	Testing methodology	21
5.1	Sampling	21
5.2	Determination of rock mechanical properties in laboratory and field	21
5.2.1	Rock strength determination	21
5.2.2	Abrasivity	29
5.2.3	Determination of further properties	36
5.3	Determination of the drill data.....	38
5.3.1	Drill head design	38
5.3.2	Testing under defined conditions	39
5.3.3	Field testing and on-site testing.....	40
5.3.4	Analysis and evaluation of drill testing	42

6	Sample description, results and result interpretation	44
6.1	Description of all samples.....	46
6.1.1	Gold samples.....	46
6.1.2	Platinum samples.....	48
6.1.3	Samples of other mines	52
6.1.4	Quarries and test rock samples	57
6.2	Number of tested specimen of each rock samples	69
6.3	Uniaxial compression test	69
6.4	Point load test	71
6.5	Brazilian tensile test	72
6.6	Abrasivity tests	73
6.6.1	Cerchar abrasivity test	73
6.6.2	LCPC abrasivity test.....	75
6.6.3	Conclusion of all abrasivity tests.....	77
6.7	Ultrasonic test	78
6.8	Quartzite and Metaconglomerate of Tautona gold mine for the numerical modelling	79
6.9	Drill head data	79
6.9.1	Performance	79
6.9.2	Wear.....	81
7	Data management and data processing in engineering geology.....	83
7.1	General database structure.....	83
7.2	Dictionary of further general functions and code snippets used in our database system	84
7.3	The rock database of the TUM.....	85
7.3.1	Programming of the database	86
7.3.2	Database structure and web interface	86
7.3.3	Data processing (recommended work flow).....	92
8	Numerical modelling in 2D and 3D	101
8.1	Geotechnical Model setup	101
8.1.1	Geometry	101
8.1.2	Material properties	102
8.2	2D Models (MSc) and recent models	105
8.2.1	Stope without transportation gallery	107
8.2.2	One Stope with the consideration of a transportation gallery.....	108
8.2.3	Stope with transportation gallery taking the rounded edges into account	109
8.2.4	Two stacked stopes with transportation galleries.....	110

8.3	3D Models.....	111
8.3.1	FLAC 3D	112
8.3.2	RS ³	113
8.4	Summary of all considered numerical models	114
9	Discussion.....	115
9.1	Comparison of rock and drill data	115
9.1.1	Performance	116
9.1.2	Wear.....	121
9.1.3	Rock landscape.....	125
9.2	Discussion of the used DBMS and Migration of data and DBMS to another system.....	128
9.3	Stress data in 3D modelling and in the field.....	129
10	Conclusions	132
11	Recommendations for predicting drilling performance and wear based on rock properties	133
12	References.....	135
12.1	Literature, standards and maps	135
12.2	Online references	139
13	Appendices.....	i
A)	Database structure – entities (tables) and attributes (fields) with properties	i
A.1)	Explanation of database structure	i
A.2)	User management module.....	i
A.3)	General project data module	i
A.4)	Laboratory data module.....	iii
A.5)	Hilti add on module	vi

This thesis is dedicated to the loving memory of my Mum.

For all the love and help she gave to me
and her words of encouragement to lift my spirits she said to me during the time of my studies
although she had to live through the darkest hours of her life!

Sadly it was not granted to her to see the end of this work.



Erika Menschik

* 19.12.1953

† 24.07.2015

I Acknowledgements

First of all, I would like to thank Prof. Dr. Kurosch Thuro for the opportunity to do this research and all the support he gave to me during the whole creation process. I would also offer my special thanks to my co supervisor Assistant Prof. Dipl.-Ing. Dr. techn. Alexander Preh for ideas and the extensive discussions. I'm also thankful for all advice and help my mentor Dr. Heiko Käsling had for me.

Furthermore, I would like to extend my thanks to Dr. Michael Bayerl, Konrad Artmann und Arne Echterbruch of Hilti Entwicklungsgesellschaft mbH. They made this thesis possible and supported me with all needed data and information. Thanks for the financial support of Hilti AG over a period of 2.5 years.

Also on Hilti side I have special thanks to Stefan Götzfried. He helped me during many tests in lab and field not only with man power but with ideas and work arounds to solve problems we encountered during our site visits. I will keep especially our field trips to Sargans and Miltenberg very special in my mind!

For all the support in South Africa during my site visits I'm very thankful to Wayne Dowie and his colleagues, who help me with all the planning and logistics and to Tebogo Keogatile and Johan Fourie, who made almost everything possible during my mine visits. Especially the burning permission for my digital camera will always remain in my mind! Great thanks are going to all of the guys of the visited mines. They supported Johan, Tebogo and me wherever it was possible without hesitating.

At Technische Universität München I would like to thank Vladimir Ruttner, Prof. Dr. Albert Gilg and Mathias Köster for the technical and scientific support for the creation of the thin sections and the analysis and interpretation of the x-ray diffraction result. For all support in creation and improving my drawings for this thesis and for the best scans of geological maps ever I would like to offer my special thanks to Klaus Haas. I'm also very grateful for the help and the work of all our Hiwi's which did a great job at the laboratory.

My special thanks for the technical support at Technische Universität München goes to Friedrich Ettl, our true soul for almost everything. He helped during my field tests and with creativity and the right tools we solved minor or major problems in no time. I will always keep the Pan Am pocket knife in honor.

I'm very thankful to my students Christian Eitschberger, Matthias Quessel, Oliver Engelmann, Michael Zupfer, Phillip Klinger and Guangzhe Zhang, which contributed to this thesis with their studies for a better process understanding, programming and collecting data.

Very special thanks are going to Dr. Silvia Beer for all the discussions and all talks and coffee breaks we had during the great time while we were sitting in the same boat (office) and especially in the end while I was finalizing this thesis during a field trip in Teplá (Bohemia/Czech Republic).

My sincere thanks also go to Dr. Gerhard Lehrberger, who held my back clear as network administrator at our chair and for the amazing team work in our corporately teaching classes and field trips.

For supporting me with the possibility for my drill tests and test material I would like to thank all miners and employees and the companies of all visited quarries and mines.

Thanks to all of my friends for all nice distractions, adventures and events, which helped me to recreate and to come back to work with a fresh mind.

One before last but not least by far I'm unlimited grateful for all the support my family gave to me. There I have very special thanks to my sadly departed Mother and my ex-wife Svenja. Both supported me sacrificially during the whole time of my thesis.

Finally I'm very thankful that I had my best friend and now spouse Dr. Tina Sellmeier on my side, especially in the last months of my work, for advice, backup and all her help she gave to me. No words can express my gratefulness!

II Abstract

There are many models established and used for predicting wear and performance of pneumatic and hydraulic rock drills. But since the use of electrical rock drills started not long ago, only few testing programs were conducted on this kind of tool. The current thesis deals with one aspect of the drilling process, the drill head (drill bit) itself. It's an important issue for the analysis and the testing procedure to have an optimized workflow in terms of drilling. Thus a high number of different tests have to be conducted to create a fitting model to choose the most adequate drill head for the occurring geology. In a cooperation between Hilti AG and the Chair of Engineering Geology at TUM a research project has been carried out to create an optimized testing procedure for drill heads of electrical rock drills.

First of all, a fundamental data structure had to be established. For this issue an online based database was programmed providing a web interface which allows all project partners to access the data and to perform first analyses. We started with a general database system, which can be expanded with add-ons to fulfill all necessary requirements. This first system is able to manage data of customers, projects and all conducted laboratory tests like UCS, point load test or abrasiveness tests like CAI and LCPC. By means of this tool we grant quick access to our data. To meet all needs for drill head testing, we created the first add-on for the data management of drill head testing. This data contains not only information about the tested drill head but also about the geology of the project site, depth, underground and the occurring rock types which are directly related to our laboratory data. Applying this tool, a quick analysis of performance and wear is accessible.

For the drill head testing itself we carried out well established laboratory tests and compared them to drill head test data gained in field tests. The conducted laboratory tests included the uniaxial compressive strength test, the Brazilian tensile test, the point load test (laboratory and field test), the CERCHAR test, the LCPC test, the determination of the equivalent quartz content in thin section (qualitative) and the x-ray diffraction analysis (quantitative) as well as the determination of p-wave velocity with ultrasonic testing (laboratory and field test). To achieve comparable results, we conducted drill tests in the laboratory and in the field to measure the following parameters: the drill depth and netto drill time to obtain information about the performance; the weight and the caliber diameter of the drill head in order to determine the wear. This data was used for correlation analyses to develop a simple model for the selection of the right drill head according to the geology and the rock mechanical properties of the drilled rocks. We tested different rocks starting with weak sandstones with uniaxial compressive strength of 40 MPa to basalt with uniaxial compressive strength of more than 400 MPa. We were able to demonstrate a significant correlation between the destruction work, the indirect tensile strength and the point load index for the performance. For analyzing the parameter of wear we tested rocks with equivalent quartz content between 20 % (basalt) and more than 80 % (quartzite). The results provide no evidence of a singular correlation with a particular parameter. It could be shown, that the wear potential is determined by an interaction of several factors like rock strength, abrasive potential, mineral content and micro structure of the rocks.

Additionally, we analyzed the occurring stresses in a deep underground mine in South Africa by the help of Finite Element and Finite Differences simulations in 2D and 3D using the codes Phase² (RS²), RS³ from Rocscience and FLAC 3D from Itasca. All models provide certain evidence of high stress zones and yielding which can be interpreted as pre fractured zones. These zones can be found in the models with a distance of 1-2 m of the wall within the rock mass. Breaking of the rock mass, cracks and spalling are the effects of such high stress, and could also be observed in the field but only in areas which were mined longer time ago, especially at the transportation galleries and in the back side of the stopes. Due to the depth of the drill holes (length of a round) of max. 1.2 m and the occurrence of these pre fractured zones and out of our observations the time, which is needed to create this zone, a positive influence on the drilling process, especially a higher performance or lower wear, could not be shown.

The current thesis provides a recommendation for a procedure for drill head testing by means of field and laboratory test set-ups. The aim is to optimize the selection of the most appropriate drill head according to rock conditions and give benchmarks for drilling performance and tool wear as well as design parameters for further development of drill heads (drilling bits).

III Zusammenfassung

Pneumatische und hydraulische Schlagbohrhämmer sind heutzutage in Bergwerken, Steinbrüchen und auf Tunnel- und Kavernenbaustellen fast nicht mehr wegzudenken. Daher gibt es auch viele Arbeiten über die Prognose von Leistung und Verschleiß dieser Geräte. Seit ein paar Jahren existieren nun auch elektrische Schlagbohrhämmer auf dem Markt. Diese Arbeit beschäftigt sich daher mit der Analyse der Leistungs- und Verschleißcharakteristika dieser Geräte. Dabei wird speziell die Bohrkronen näher untersucht. Da sehr viele unterschiedliche Versuche durchgeführt wurden und diese auch für alle Projektpartner, die an weit verbreiteten Standorten zu finden sind, einsehbar und überprüfbar sein sollen, sind für diese Studie ein optimierter Testablauf und ein konsistentes Datenmanagement unverzichtbar. Diese Arbeit soll ein Modell für die Auswahl der passenden Werkzeuge gemäß der jeweils ermittelten Kennwerte erarbeiten und eine Empfehlung für einen optimierten Testablauf liefern. Sie ist Inhalt einer Forschungsk Kooperation zwischen der Hilti AG und dem Lehrstuhl für Ingenieurgeologie der TUM.

Zu Beginn muss eine passende Dateninfrastruktur geschaffen werden. Um den Anforderungen einer ausgezeichneten Datenhaltung nachzukommen, wurde eine Online-Datenbank programmiert, die der Zugänglichkeit aller Daten für die Projektpartner, der Dateneingabe und -pflege und einer einfachen Analyse aller Versuchsdaten dient. Um die Datenbank auch für künftige Anforderungen offen zu gestalten, wurde sie in mehrere Module unterteilt. Die Basismodule dienen der Verwaltung unserer Labordaten inklusive der Auftraggeber-, der Projekt- und Probandaten. Wir verwalten damit im Moment alle Einaxialen Druck-, Punktlast-, Spaltzug-, CAI-, LCPC- und Ultraschallversuche, die in unserem Labor durchgeführt werden.

Diese Basismodule können je nach Anforderung um zusätzliche Erweiterungsmodule (add-ons) ergänzt werden, um damit die Anforderungen aus neuen Projekten zu erfüllen. So wurde für diese Arbeit bereits eine erste Erweiterung zur Analyse von Bohrgeschwindigkeits- und Verschleißmessungen geschaffen, die auch eine Abfrage der am besten geeigneten Bohrkronen bietet. Hier werden die Daten aus Bohrversuchen mit felsmechanischen Eigenschaften und Informationen über die beprobten Bergwerke und Steinbrüche verknüpft und ermöglichen so eine schnelle Analyse von Leistung und Verschleiß einer Bohrkronen in Abhängigkeit von den geologischen Gegebenheiten des Standortes.

Zur Korrelation der Bohrkopftestdaten wurden Versuche ausgewählt, die zu den industriellen Standardversuchen gehören und die durch viele Labors weltweit standardisiert durchgeführt werden können. Wir führten Einaxiale Druck-, Punktlast- (Gelände- und Laborversuch), Spaltzug-, CAI- und LCPC-Versuche durch, ermittelten die p-Wellen-Geschwindigkeit (Gelände- und Laborversuch) und ermittelten den Mineralbestand und den äquivalenten Quarzgehalt mittels Dünnschliffmikroskopie (qualitativ) und Röntgendiffraktometrieanalyse (quantitativ). Zur Ermittlung der Kennwerte der elektrischen Schlagbohrhämmer wie auch der Bohrkronen wurden mit baugleichen Bohrmaschinen Bohrversuche im Gelände, im Versuchsstollen (Hagerbach) und im Labor durchgeführt. In jedem Versuch wurden die Nettobohrzeit und die Bohrlochtiefe gemessen. Zusätzlich wurden der Bohrkronendurchmesser und die Masse der Bohrkronen bestimmt, um Rückschlüsse auf den Verschleiß zu ziehen. Anschließend wurden die Felskennwerte mit den Bohrerkenwerten korreliert, um ein einfaches empirisches Modell zur Prognose von Leistung und Verschleiß zu erstellen und somit die Auswahl der Bohrkronen zu erleichtern. Um ausreichend Daten zu erhalten und um eine möglichst große Bandbreite an unterschiedlichen Gesteinen zu testen, wurden Proben ausgewählt, die eine Einaxiale Druckfestigkeit zwischen 40 (Sandsteine) und 400 MPa (Basalt) aufweisen. Die von uns durchgeführten Versuche zeigen eine starke Abhängigkeit von Bohrgeschwindigkeit und Zerstörungsarbeit, Spaltzugfestigkeit und Punktlastindex.

Der Verschleiß wurde an Proben mit einem äquivalenten Quarzgehalt zwischen 20 und 80 % gemessen und ergab keinen eindeutigen Zusammenhang. Der Verschleiß hängt eher von einem Zusammenspiel von Festigkeit, Abrasivität, Mineralbestand und Gefüge ab.

Da sich ein paar Versuchsstandorte in tiefliegenden Bergwerken, wie z.B. der Tautona Goldmine (Südafrika) mit einer maximalen Tiefe von bis zu 3,9 km, befinden, sind auch die auftretenden Spannungen interessant. Daher wurden in Ergänzung zu den durchgeführten Bohrversuchen auch mehrere 2D/3D-Finite-Elemente- und 3D-Finite-Differenzen-Modellierungen durchgeführt. Dabei kamen die Programme Phase² (RS²), RS³ von Rocscience und FLAC 3D aus dem Hause Itasca zum Einsatz. Alle Modelle zeigten Bereiche mit sehr hohen Spannungen und Deformationen in etwa 1-2 m Entfernung zum Ausbruchrand, die als Auflockerungszonen gedeutet werden können. Diese Bereiche konnten auch Untertage beobachtet werden, vor allem entlang von Strecken, die bereits über einen längeren Zeitraum offenstanden. An der Ortsbrust, an der etwa alle zwei Tage eine Sprengung stattfindet, konnten solche aufgelockerten Bereiche nicht beobachtet werden. Eine Abhängigkeit von Verschleiß und Bohrgeschwindigkeit zu den auftretenden Spannungen konnte nicht eindeutig geklärt werden. Aufgrund der großen Schwankungen der Bohrgeschwindigkeiten ist es aber sehr wahrscheinlich, dass sich die Spannungen auf den Bohrprozess auswirken.

Die diese Arbeit abschließende Empfehlung umfasst alle nötigen Feld- und Laborversuche, die nötig sind, um mit wenigen, gezielten Versuchen neue Bergwerke und Bohrkronen zu testen und damit die Auswahl der zu den geologischen Verhältnissen passenden Bohrkrone zu erleichtern.

IV Table of figures

Fig. 1: Illustration of the Hilti TE MD20 rotary hammer with TE MW90 water leg (www-1).	1
Fig. 2: Generalized map of South Africa illustrating the positions of all test sites. Blue stars: platinum; black stars: diamonds; green stars: copper; red stars: gold.	4
Fig. 3: General stratigraphy of the Witwatersrand basin around Johannesburg (GUILBERT & PARK JR. 1986: 757, edited).	6
Fig. 4: Geological map of the Witwatersrand Basin including information about the mining depths and the mine locations (THE GEOLOGICAL SOCIETY OF SOUTH AFRICA 1986).	7
Fig. 5: Cross section through Witwatersrand Basin showing the sedimentary series and some paleo placer fans (GUILBERT & PARK JR. 1986: 757).	7
Fig. 6: Gold bearing reef formations and their distribution within the sedimentary series of the Witwatersrand Basin (FRIMMEL 2005: 8, edited).	8
Fig. 7: Illustration of the location of all gold fields in the Witwatersrand Basin (GUILBERT & PARK JR. 1986).	9
Fig. 8: Geological map of the vicinity of all analyzed platinum mines. Excerpt of HAMMERBECK & ALLOCK (1985) (1 Brakfontein; 2 Twickenham; 3 Hackney; 4 Blue Ridge).	11
Fig. 9: Stratigraphic column of the layered intrusion part of the Bushveld igneous complex with all important reefs (SCHOUWSTRA et al. 2000: 34). Additionally, the typical rock types for each zone are plotted (PETTERS 1991: 145).	11
Fig. 10: Geological map of the vicinity of all analyzed mines. Excerpt of the geological map of Winburg (BESTER 1998).	12
Fig. 11: Geological map of Selebi Phikwe and its vicinity (MAIER et al. 2008).	13
Fig. 12: Generalized map of Germany, Switzerland, Liechtenstein and Austria with most of the European test sites plotted.	14
Fig. 13: Geological map of the southwestern area of the bohemian massive showing the most important granite quarries (LEHRBERGER 2013: 39).	15
Fig. 14: Simplified geological map of the Mecsek Mountains in southern Hungary (KLÖTZLI et al. 2004).	16
Fig. 15: Excerpt of the geological map of Hallein, showing the dominant stratigraphic units of the Haselgebirgs-Formations and the location of the quarry of Golling (PLÖCHINGER 1987).	17
Fig. 16: Excerpt of the geological map of Switzerland illustrating the main geological units and the location of the Hagerbach Test Gallery (SPICHER 1980).	17
Fig. 17: Geological map the city of Miltenberg, showing the location of the quarry (SCHWARZMEIER & WEINELT 1993).	18
Fig. 18: Excerpt of the geological map of the vicinity of the KTB in Upper Palatinate (DILL et al. 1991).	19
Fig. 19: Geological map of the surrounding of quarry Pechbrunn. The map was created based on the geodata provided by DIMROTH & SÖLLNER (1964) and RAUM (2013).	20
Fig. 20: Front view of Compression-Testing-Machine (according to manufacturer information).	22

- Fig. 21: Schematic sketch of the axial strain-stress curve of the uniaxial compression test. The destruction work is indicated as the grey area enclosed by the curve; $\delta\sigma$ and $\delta\varepsilon$ are used for calculating the modulus of deformation (first derivation of the linear curve segment). 23
- Fig. 22: Illustration of the classification scheme of the Uniaxial Compressive Strength (ISRM 1978a, edited). 25
- Fig. 23: Illustration of the point load field testing device: Left load frame including the test cones; right hydraulic manual pump (Picture: Johan Fourie). 26
- Fig. 24: Sketch of the point load test, the measured variables and the applied force. 27
- Fig. 25: Schematic sketch of the indirect tensile force in Brazilian tensile strength testing with the applied forces. 28
- Fig. 26: Illustration of the CERCHAR-device for the determination of the CERCHAR-Abrasivity-Index (according to WEST 1989, modified). 30
- Fig. 27: Schematic sketch of the steel pin before (a) and after (b) testing. 30
- Fig. 28: Left: Abrasimeter with a 700 W electric motor (1), sample container (2) and funnel tube (3) for the filling of the sample container (closed during operation). Right: Mounted metal impeller, which rotates with a speed of 4500 rpm for 5 minutes through the sample. 32
- Fig. 29: LCPC impeller before (left) and after (right) test run, indicating the abrasiveness of the material. 33
- Fig. 30: LCPC sample before (left) and after (right) test run. The grain size ranges between 4 and 6.3 mm before testing. 33
- Fig. 31: Grinding hardness according to ROSIWAL (mean values) plotted against the scratch hardness according to MOHS in a semi logarithmic diagram (THURO 1996) including the appropriate a semi logarithmic regression curve (appears as straight line) with its statistical parameters. 36
- Fig. 32: Testing setup for transmission testing determining p-wave velocity. 37
- Fig. 33: Testing frame for ultrasonic tests. Left: extensional Wave frame; Right: Transmission testing frame which was mainly used for this research. 37
- Fig. 34: Sketch of all important parameters which have been changed during the research project in order to optimize the drill head performance, the wear and to adapt the drill head perfectly to the occurring geology. 39
- Fig. 35: In line drill test set-up with a drill rig at the Hagerbach Test Gallery (Switzerland) (Picture: Stefan Götzfried). 39
- Fig. 36: Sketch of different drills illustrating varying contact force setups due to different working geometry. (A) Lower contact force; (B) Increased contact force; (C) Maximum contact force (In-line condition). 40
- Fig. 37: Field drill testing in progress. One person is drilling and the second one is registering the drilling time for each hole. 41
- Fig. 38: Exemplified drill pattern and bore holes for rock sampling in the quarry of Miltenberg. 41
- Fig. 39: Exemplified performance diagram including the drill distance plotted versus the average speed per drill hole. 43
- Fig. 40: Exemplified diagram for the wear as the first derivation of the fitted curve; the drill distance is plotted against the drill head diameter. 43

Fig. 41: Gold bearing meta conglomerate of the Witwatersrand Supergroup (the sample is part of the rock collection of the Chair for Engineering Geology of TUM).	46
Fig. 42: Thin section of a typical Witwatersrand conglomerate. Upper left corner: recrystallized quartz grains (polygonal structure). In the middle: fibrous, strongly toothed quartz minerals. At the right side: bigger primary quartz grains with undulous extinction and saturated grain boundaries. Image width: 2.6 mm. Sample HIL-KLO-02.	47
Fig. 43: Specimen of anorthosite for the point load testing of Blue Ridge mine.	48
Fig. 44: Thin section of the anorthosites with poach chromite of Blue Ridge mine in dark field. Sample HIL-BLU-01 (Image width: 2.6 mm).	49
Fig. 45: Specimen of pyroxenite as an example for all considered platinum samples. HIL-BRA-01.	50
Fig. 46: Thin section overview of a pyroxenite sample from mine of Brakfontein. HIL-BRA-01.	51
Fig. 47: Specimen of a kimberlite rock of the mine Peakstar. Sample HIL-PEA-01.	52
Fig. 48: Thin section overview of a Peakstar kimberlite. The mineral content is described in Tab. 14. Sample HIL-PEA-01.	53
Fig. 49: Specimen of a waste material of the mine of Selebi Phikwe. Sample HIL-SPH-09.	54
Fig. 50: Thin section of waste material of Selebi Phikwe with an inserted gypsum layer. Sample HIL-SPH-09.	55
Fig. 51: Picture of specimen of a copper ore of Selebi Phikwe. Sample HIL-SPH-10.	56
Fig. 52: Photo of a thin section of copper ore of Selebi Phikwe. Sample HIL-SPH-10.	56
Fig. 53: Picture of a UCS specimen of Bayerwald granite. Sample HIL-BWG-01.	57
Fig. 54: Thin section of the Bayerwald granite; the dominant minerals are named in the sketch. Sample HIL-BWG-01.	58
Fig. 55: Picture of point load samples of the Erdösmecke granite. Sample HIL-ERD-01.	59
Fig. 56: Thin section of the Erdösmecke granite. Sample HIL-ERD-01 showing altered amphibole minerals, quartz grains with saturated grain boundaries and weathered biotite grains.	60
Fig. 57: Picture of a Brazilian test sample of the Golling anhydrite. Sample HIL-GOL-01.	61
Fig. 58: Thin section of the Golling anhydrite; the dominant minerals are named and marked in the photo. Sample HIL-GOL-01.	61
Fig. 59: Picture of UCS samples of the siliceous limestone of Hagerbach Test Gallery.	62
Fig. 60: Picture of the red, fine grained Miltenberg sandstone in an outcrop situation.	63
Fig. 61: Thin section of the Miltenberg sandstone with clear quartz and feldspar minerals. In some areas brown to red hematite can be found. Sample HIL-MIL-01.	64
Fig. 62: Picture of the UCS sample of amphibolite of quarry Oberbaumühle. HIL-OBM-01.	65
Fig. 63: Thin section overview of an amphibolite of the quarry Oberbaumühle (HIL-OBM-1).	66
Fig. 64: Picture of a UCS specimen of the Pechbrunn basalt. HIL-PEB-01.	67
Fig. 65: Thin section analysis of the Pechbrunn basalt. HIL-PEB-01. Fine grained matrix consisting of pyroxene, olivine, plagioclase and magnetite with porphyric feldspar, biotite and olivine components.	68

Fig. 66: Mean uniaxial compressive strength values of all test results for the total amount of samples. N is the number of tested specimen of the particular sample (* All samples of Hagerbach Test Gallery HIL-HAG were tested by Hagerbach Test Gallery GmbH).	70
Fig. 67: Mean point load indices of all test results for the total amount of samples.	72
Fig. 68: Mean tensile strength values of all test results for the total amount of samples.	73
Fig. 69: Illustration of the CERCHAR abrasivity results including the total amount of samples.	74
Fig. 70: Illustration of the LCPC abrasivity coefficient results including the total amount of samples.	76
Fig. 71: Illustration of the LCPC breakability coefficient results including the total amount of samples.	78
Fig. 72: Illustration of the average performance of all drill heads applied at all considered test sites.	80
Fig. 73: Correlation between drill head size and drill performance of all conducted tests with the same drill in Hagerbach Test Gallery.	80
Fig. 74: Illustration of the average performance of drill head 1 for all tested locations.	81
Fig. 75: Illustration of the average wear of all tested drill heads including the data gap, where no wear measurement was performed.	82
Fig. 76: Illustration of the average wear of drill head 1 for all tested locations including the data gap for mines without wear measurement.	82
Fig. 77: General Entity-Relationship-Model of a relational database.	84
Fig. 78: Entity-Relationship-Model of the base modules according to CHEN (1976) of the rock database (without add ons and user management) established at the Chair for Engineering Geology at TUM.	85
Fig. 79: General, schematic sketch of the TUM rock database-layout with all modules.	86
Fig. 80: Illustration of the navigation bar (left side) and single value query of the base view of the rock database of TUM.	88
Fig. 81: UCS information window for testing results of one specific sample.	89
Fig. 82: Navigation bar and mean value query with export function of the project view of the rock database of TUM.	90
Fig. 83: Project status window for all projects of one project partner.	90
Fig. 84: Illustration of the connection between case modules and the drill head add-on.	91
Fig. 85: Navigation bar for the Hilti view of the database incl. add on for drill head testing.	91
Fig. 86: Illustration of the automatic calculated analysis of drill test data within the web interface (anonymized).	92
Fig. 87: Data entry interface for new clients showing the navigation bar and the form itself.	94
Fig. 88: Interface for sample entry with the buttons “insert sample” and “insert similar sample” which allows to enter a similar sample with identical properties as the previously entered sample.	94
Fig. 89: Illustration of the management console for all client entries. Within this window edits are possible and the view of the project partner can be reached by clicking on the corresponding button.	95
Fig. 90: Editing window for the data manipulation of client data.	95
Fig. 91: Main page for laboratory test data showing all conducted tests for sample HIL-TAU-07.	96
Fig. 92: Data entry page for UCS laboratory test data.	96

Fig. 93: Drill head query window with the pull down menu for rock type selection and the text fields used for UCS and CAI queries.	98
Fig. 94: Illustration of a successful drill head query for sandstones with UCS=50 MPa and CAI=3.	100
Fig. 95: Geotechnical model (cross section) of Tautona gold mine as basis for the subsequent numerical models.	102
Fig. 96: Geotechnical model (longitudinal section) of Tautona gold mine as basis for the subsequent numerical models.	102
Fig. 97: Stress distribution of sigma 1 in case of an increased horizontal stress (K=2).	103
Fig. 98: Comparison of synthetic Hoek-Brown properties out of TUM uniaxial laboratory testing and the Hoek-Brown properties of the triaxial test data from HOEK (1965: 200).	105
Fig. 99: Stress distribution of sigma 1 calculated with Phase ² after the third excavation stage (MENSCHIK 2009: 27).	106
Fig. 100: Major stress distribution of model stope without transportation gallery.	107
Fig. 101: Illustration of sigma 1 in a detailed view of the lower side wall after the third excavation stages.	107
Fig. 102: Total displacement of the rock around the excavation after the third excavation stages.	108
Fig. 103: Plot of yielded elements after the third excavation stage.	108
Fig. 104: Major Stress distribution of the model of one stope with a transportation gallery.	109
Fig. 105: Detail view of the geotechnical model of the transportation gallery with rounded edges.	109
Fig. 106: Major Stress distribution of the model of one stope with the transportation gallery and rounded edges.	110
Fig. 107: Comparison of maximum shear strain of the models with sharp corners and rounded edges.	110
Fig. 108: Major Stress distribution of the model with two stacked stopes including transportation galleries.	111
Fig. 109: Development of yielded zone (yielded elements) during the excavation stages.	111
Fig. 110: Stress distribution of vertical stress of the FLAC3D model.	112
Fig. 111: Displacement of generalized FLAC3D model.	112
Fig. 112: Major Stress distribution of the RS ³ model including one stope without transportation galleries.	113
Fig. 113: Map of total displacements of the RS ³ model including one stope without transportation galleries.	113
Fig. 114: Major stress distribution of the RS ³ model including one stope with transportation galleries.	114
Fig. 115: Maximum major stress at a notch after first round after a completed excavation step of the RS ³ model including one stope with transportation galleries.	114
Fig. 116: Sketch of the physical drilling process during the rock drilling (THURO 1996: 14). Indicated with numbers are the zones in which the material excavation occurs (1 Zone where material is crushed due to compression; 2 Zone of radial fractures due to tensile stress; 3 Released rock chips which where loosend).	115

-
- Fig. 117: Diagram of uniaxial compressive strength versus average drilling performance, providing certain evidence of a logarithmic correlation. 117
- Fig. 118: Classification of brittleness as ratio of UCS/BTS of all tested rocks according to THURO (1996) showing the brittle behaviour of almost all samples except of the amphibolite of Oberbaumühle. 118
- Fig. 119: Diagram of the destruction work versus average drilling performance. The fitted curve suggests a logarithmic correlation between both parameters. 119
- Fig. 120: Diagram, illustrating the logarithmic correlation between the results of the Brazilian tensile strength and the average drilling performance. 120
- Fig. 121: Diagram illustrating the correlation between the point load index and the average drilling performance. The trend line indicates a correlation between these two parameters. 121
- Fig. 122: Diagram of CAI versus the average wear of the drill head. Due to the scattering of the data no sufficient trend line could be plotted. 122
- Fig. 123: Diagram of LAC versus average wear of the drill bit. Due to the scattering of the data no sufficient trend line could be plotted. 123
- Fig. 124: Diagram of equivalent quartz content versus average wear with linear fit for all data except of Oberbaumühle. 124
- Fig. 125: Diagram of rock abrasivity index versus average performance with linear fit for all data except of Oberbaumühle. 125
- Fig. 126: Constitutional model of a “rock landscape” for drill head selection as an analysis tool for the current thesis. The colored frames represent the scope of application of each of 4 different drill heads. 126
- Fig. 127: The final rock landscape for point load index vs. equivalent quartz content. Areas of highest performance and lowest wear are printed in blue (performance) and red (wear). The landscape is divided in two parts. The upper one for performance and the lower part for wear. The best working conditions for drill head 1 are printed as intersecting area of the blue and red marked area in yellow. 127
- Fig. 128: Top view on the excavation stope. The highest stress concentrations are located with the red circle with definitions of the mining procedure. 129
- Fig. 129: Histogram illustrating the drill speeds of the total amount of single drillings of drill head 1 in Tautona gold mine. 130
- Fig. 130: Stress induced loosening of rock mass at the side walls of the transportation gallery. 131
- Fig. 131: Diagram illustrating the strain burst potential using a correlation between the UCS and m_i (Diederichs 2007: 1085, Fig 2). 131

V List of tables

Tab. 1: List of all goldfields of the Witwatersrand district with count of minable gold and uranium bearing reefs (GUILBERT & PARK JR. 1986: 761).	5
Tab. 2: Brief summary of the considered gold mines covering the operator, max. depth, the year of opening and the position.	5
Tab. 3: Illustration of the mentioned platinum mines covering the operator, the max. depth, the year of opening and the position.	10
Tab. 4: Brief description of all other testing mines in southern Africa considered in the current research.	12
Tab. 5: A brief description of all quarries and test rock areas covered by this research.	15
Tab. 6: Classification of brittleness (SCHIMAZEK & KNATZ 1976: 117 and BECKER & LEMMES 1984: 74 in THURO 1996: 74).	29
Tab. 7: Abrasiveness classification using the CAI-Test (according to CERCHAR 1986: 7).	31
Tab. 8: Classification of the LCPC Abrasivity Coefficient LAC in accordance to the Cerchar Abrasivity Index CAI and the associated terminology.	34
Tab. 9: Classification of the LCPC Breakability Coefficient LBC, according to BÜCHI et al. (1995).	34
Tab. 10: List of all tested rock samples during the project.	44
Tab. 11: Summary of all mean test results for rock strength of all included mining locations.	45
Tab. 12: Summary of the mean test results for abrasivity and other tests of all considered mining locations.	45
Tab. 13: Mineral content and equivalent quartz content of platinum samples.	51
Tab. 14: Mineral content and equivalent quartz content of kimberlite samples.	53
Tab. 15: Mineral content and equivalent quartz content of Selebi Phikwe-samples.	57
Tab. 16: Mineral content and equivalent quartz content of Bayerwald granite samples.	58
Tab. 17: Mineral content and equivalent quartz content of Erdösmecke granite samples.	60
Tab. 18: Mineral content and equivalent quartz content of the samples of Golling.	62
Tab. 19: Mineral content and equivalent quartz content of Miltenberg sandstone samples.	64
Tab. 20: Mineral content and equivalent quartz content of amphibolite samples of Oberbaumühle.	66
Tab. 21: Mineral content and equivalent quartz content of Pechbrunn samples.	68
Tab. 22: Planned count of specimen per sample for each laboratory test.	69
Tab. 23: Exact values of all conducted CERCHAR abrasivity tests.	75
Tab. 24: Exact values of all conducted LCPC abrasivity tests.	77
Tab. 25: Mean p wave velocities of all test results for all samples. N is the number of tested specimen of the particular mine or quarry.	79
Tab. 26: Rock mechanical properties of quartzites.	79
Tab. 27: Table of all tables of base module and short description of it first order relation within the database.	87

Tab. 28: Complete list of possible laboratory test codes for our name concept.	93
Tab. 29: Typical object names within the rock database with example.	93
Tab. 30: Required structure of the csv file for drill head testing data.	97
Tab. 31: Properties of quartzite used for numerical modelling in Phase ² and RS ³ .	103
Tab. 32: Properties of gold bearing quartzite used for numerical modelling in Phase ² and RS ³ .	104
Tab. 33: Mohr-Coulomb properties of gold bearing quartzites used for numerical modelling in FLAC 3D.	105

VI List of formulas

Eqn. 1: Calculation of failure stress as compressive strength σ_u .	23
Eqn. 2: Calculation of adjusted compressive strength $\sigma_{u(2)}$.	23
Eqn. 3: Calculation of the modulus of deformation:	24
Eqn. 4: Calculation of the destruction work:	24
Eqn. 5: Calculation of the point load index I_s .	27
Eqn. 6: Calculation of the Point-Load-Index correlating to standard sample dimension of 50 x 50 x 50 mm.	27
Eqn. 7: Calculation of uniaxial compressive strength derived from I_{50} .	28
Eqn. 8: Calculation of the Brazilian Tensile Strength.	29
Eqn. 9: Calculation of brittleness z .	29
Eqn. 10: Calculation of the Cerchar Abrasiveness Index (CAI).	31
Eqn. 11: Calculation of the LCPC Abrasivity Coefficient.	34
Eqn. 12: Calculation of the LCPC Breakability Coefficient.	34
Eqn. 13: Determination of the Equivalent Quartz Content using the grinding hardness according to Rosiwal (1916).	35
Eqn. 14: Calculation of velocity of longitudinal waves.	38
Eqn. 15: Calculation of average performance in [cm/min].	42
Eqn. 16: Calculation of average performance in [min/m].	42
Eqn. 17: Calculation of average wear in [$\mu\text{m}/\text{m}$].	42
Eqn. 18: Calculation of average wear in [$\mu\text{g}/\text{m}$].	42
Eqn. 19: Definition of the performance drop.	43
Eqn. 20: Equation for an estimation of vertical stress.	101
Eqn. 21: Calculation of the RAI with UCS and EQc as parameters PLINNINGER (2002: 95).	124

VII List of MySQL queries

- Query 1: General syntax of MySQL queries where the queried information is stored in the Fields 1, 2 and 5 of both entities shown in Fig. 77..... 84
- Query 2: Syntax for the “Single Value Query” for uniaxial compression test of one specific sample. %s is a php-variable going back to the http-form of the webpage and is generated automatically from the selection stated with the help of the tool header. This variable represents the value of the primary key for one specific sample within the sample table (tblproben). 88
- Query 3: Exemplary mean value query MySQL statement of all test results of all specimen of all sample of one project..... 89
- Query 4: Simplified SQL query for dataset entry for a new client. The \$-symbol is part of php code and defines variables which are filled with data with the help of an html-php-form. 93
- Query 5: Drill head query. Selection for the three best drill heads using the UCS as selection criteria value for an entry of UCS=100. All elements written with a \$ character are variables which are coming from the php code and were calculated from the entered values at the web interface. 98
- Query 6: Drill head query. Selection for the three best performing drill heads using the rock type as selection criteria values. \$rocktype is a variable within the php code and is directly entered through the user. 99

1 Introduction

Electrical rock hammer drills are quite new in the extensive field of underground excavation tools. They are commonly used in only a few mines spread around the world. They are in usage in some mines of the German stone coal, in different mines in South Africa and in several other mines scattered around the world. Some of the South African mines belong to the deepest mines in the world. For example, Tautona Gold Mine which reaches in a depth of 3.9 km.

These rock drills are easy to handle and due to their electric motor with a nominal voltage of 220-230 V they can be used with a general power supply unit. Electric current has the advantage that it can be transported long distances almost without any loss. Compared to pneumatic rock drills this is a huge pro considering the increasing length of cable or pipe with increasing depth of some mines. Due to the high depth long air pipes are needed to transport pressurized air, which is produced on the surface in consequence of the big dimension of the compressed air plant, down the mine to the stope. Because of the length of the lines and the wide spreading of stopes and tunnels many couplings, which are sometimes leaking, are needed. Also the lines between the couplings are sometimes punctured. These facts can lead to a decreasing pressure at the stope and thus lower impact energy of the rock drill. At this point the electrical rock drills show their true potential. As long as there is electricity they are working with almost constant power and efficiency. Although they have much less impact energy than pneumatic and hydraulic drills, at the challenging subsurface conditions mentioned above they can outperform their competitor.

Hilti AG is a big manufacturer of different tools for construction and mining like jack hammers, core drills and diamond circular saws. One of their products for mining is the first of those electrical rock hammer drills ever built (www-1). The Hilti TE MD20 (Fig. 1).



Fig. 1: Illustration of the Hilti TE MD20 rotary hammer with TE MW90 water leg (www-1).

During the development of this machine Hilti encountered several questions concerning the drilled material and the interaction between machine and rock. The drilled rocks for German Stone Coal are quite soft and have a low abrasivity, whereas the encountered rocks in South Africa show the opposite properties. The rocks can be characterized as quartzites and anorthosites with an increased rock strength and abrasiveness. The preconditions and the high vertical stress caused by the high overburden can influence the drilling process.

To achieve more efficiency Hilti started to optimize several aspects of the TE MD 20; e.g. a research project covering the drill head was launched in 2009. To analyze the performance of drill heads, Hilti set-up a statistical approach with different drill head types used in one geological setting. Further a scientific study

of the drill head testing including the numerical modeling (FEM) of the occurring stresses was performed by means of a master thesis project (MENSCHIK 2009). The current Ph.D.-Thesis represents the enhanced work based on the mentioned Master Thesis.

2 Mission objectives

The difference in performance and wear are conquering at different locations are depending on many factors. This Thesis will deal with the influence of rock mechanical parameters on the drilling process. It is important to know the impact on our tool to choose the right drill head for each purpose.

Within this thesis we aim a new and scientific perspective over electrical rock drills, expanding our first scientific results (MENSCHIK 2009) with further test sites and other rock types. By means of the current project we wanted to show the following aspects concerning wear and geological material:

- performance of this rock drills and especially of the drill heads
- correlation to rock mechanical parameters like rock strength, abrasivity and mineral composition.

We decided to take several standard tests into account which can be conducted in a fast and easy way, are worldwide standardized and well known to the community. As main factors we identified the rock strength and the abrasiveness of rocks. The first task was to correlate single properties of the rocks to drill test properties. This correlation was done in many theses before and is often applied in industry.

To choose the right laboratory test we started to look at the drill process in more detail. The drilling process can be divided in two phases. At first the impact and secondly the rotation of the drill head on the rock surface. A typical test to determine the resistance of the rock to impacts and to estimate the performance is the uniaxial compression test. The uniaxial compressive strength could be the main property to look at. Also the energy which is produced by each hit of the machine could be compared to the energy which is needed to fracture the rock. Thus a good point could be the destruction work w_z or the failure energy. To obtain a faster testing and especially avoid the sampling and the transportation the application of a point load field testing device is thinkable and is in interest of this thesis. Another point could be the rotating movement which could use tensile stress to scratch of smaller parts of the rock face. A suitable test for this effect is the Brazilian tensile test.

To analyze the wearing potential of a rock, several abrasiveness test are suitable. We decided to test the sensitivity of the CERCHAR test, the LCPC test and the determination of the equivalent quartz content to the occurring wear of the drill bit.

Due to various tests, different types of drill heads and a bunch of mines and rock types a high amount of data remains inevitable. Due to the demanding data storage as well as the global spreading of the project partners we also needed an enhanced approach to data management for testing machines and rocks. In previous times Excel-sheets were used to transfer all test data via email from partner to partner. This way of data management can be considered as obsolete, it's very easy to overwrite, lose or duplicate data by mistake. To improve the situation, we planned to set up a database system to conquer all requirements of data management and consistency.

This database system is basis of an analyzing-tool for drill data in almost real time in order to facilitate the choice of the right drill head taking the geology of a certain mine into account.

In most of the South African mines the overburden is about and over 2000 m so that we encounter much higher vertical stresses than in for the test mines typical conditions. One of the key aspects is the influence of increased stress rates on the drilling process. Another main issue in combination with high stress is the possibility of using this stress and its effects for a higher productivity. To answer this questions, we started to develop numerical models in 2D and 3D and compared them to occurring stress phenomena on site.

3 State of the art

3.1 Drillability and performance and wear of drills

Drillability and the prediction of performance and wear of rock drills is a well-known field for pneumatic and hydraulic drills. Many theses like THURO (1996) have worked in this field. In THURO (1996) an almost complete history of the most important publication in this field can be found. Many theses provide data which leads to only minor importance of the drill head. But this thesis is working on electrical rock drills which have a lower hit energy and therefore the drill head could play a bigger role. Also there are no other publications about the drilling performance of electrical rock drills because this tool is not as long established in mining and is still not often in use. But for deep mining these tools can provide drilling performance totally independent of the depth where the tool is used.

With this thesis we are using similar methods as they were suggested in e.g. THURO (1996), PLINNINGER (2002), GEHRING (1995) or SCHIMAZEK & KNATZ (1976).

3.2 Database technology

The idea of the use of database systems to handle big data and to work with many people around the world is omnipresent. Starting at simple address book software going over internet platforms for almost any purpose and ending at complex data management suites for big companies specially programmed for their purpose.

Database systems found their way into almost every niche of everyday life but also in many lines of business. And in today's age of bits and bytes and with actual progression of information technology, computers will be used for even more purposes in future. The possibilities and the calculation-accuracy are much better and higher than 10 years ago. Data analysis can be obtained on a much higher level than before. But not only the results are improving, also the data volume is rapidly increasing - in size as well as in number of files. To work at the state-of-the-art according to all standards for big projects, an increasing number of laboratory and field tests are needed and much more data are obtained than in former times - always with the aim of reaching a better and more precise understanding of the building-underground material-interaction during construction work.

At this point the use of relational database systems is total common and this table based saving of data is used in many programs. The fundamental idea to save data in tables and get them in relation to each other with the use of unique data keys is a very old idea and was founded by CODD (1970). This basic idea is still in use and the only change is in the database management systems which are using this idea to save data. CHEN (1976) developed the theoretical model behind almost any database. The Entity-Relationship-Model. These old theories are still in work in newer database systems. One very good example for the use of relational database systems for saving and analyzing project data gives us FELLINGER & BERGLER (2009) with their case study of the use of such a database system at the project Harter Platte in Linz. This program is 2Doc and is built from the company Pöyry Infra GmbH.

The idea of using an online database for saving of rock properties is also not a new one. Many companies and organizations are using such database systems for their purpose. Unfortunately, most databases are not accessible and cannot be found in literature.

3.3 Numerical Modelling of stress and disturbed zones

Looking at stress for deep underground excavations and discussing the use or the problems induced by high stress is a big issue at these days. Looking at the content of recent issues of rock mechanic magazines it is clear that this is an important question. All deep buildings were modeled thus this becomes more and more the state of the art for the analysis of stability. Most times the important question is the occurring stress the

displacements or the type of failure. Depending on the problem and the type of rocks respectively the type of mechanism which was in center of research the used code differs. So is the use of FEM/FDM (Finite Element Method/Finite Differences Method) typical for analysis of stress in almost undisturbed, homogenous material where no cracking is expected. For broken material respectively material which will break during the modeling process the use of DEM (Distinct Element Method) is best. As we want to use the higher stress rates of deep underground mines as positive effect on the performance we take different codes of the FEM/DEM side.

4 Geography and geology of the project sites

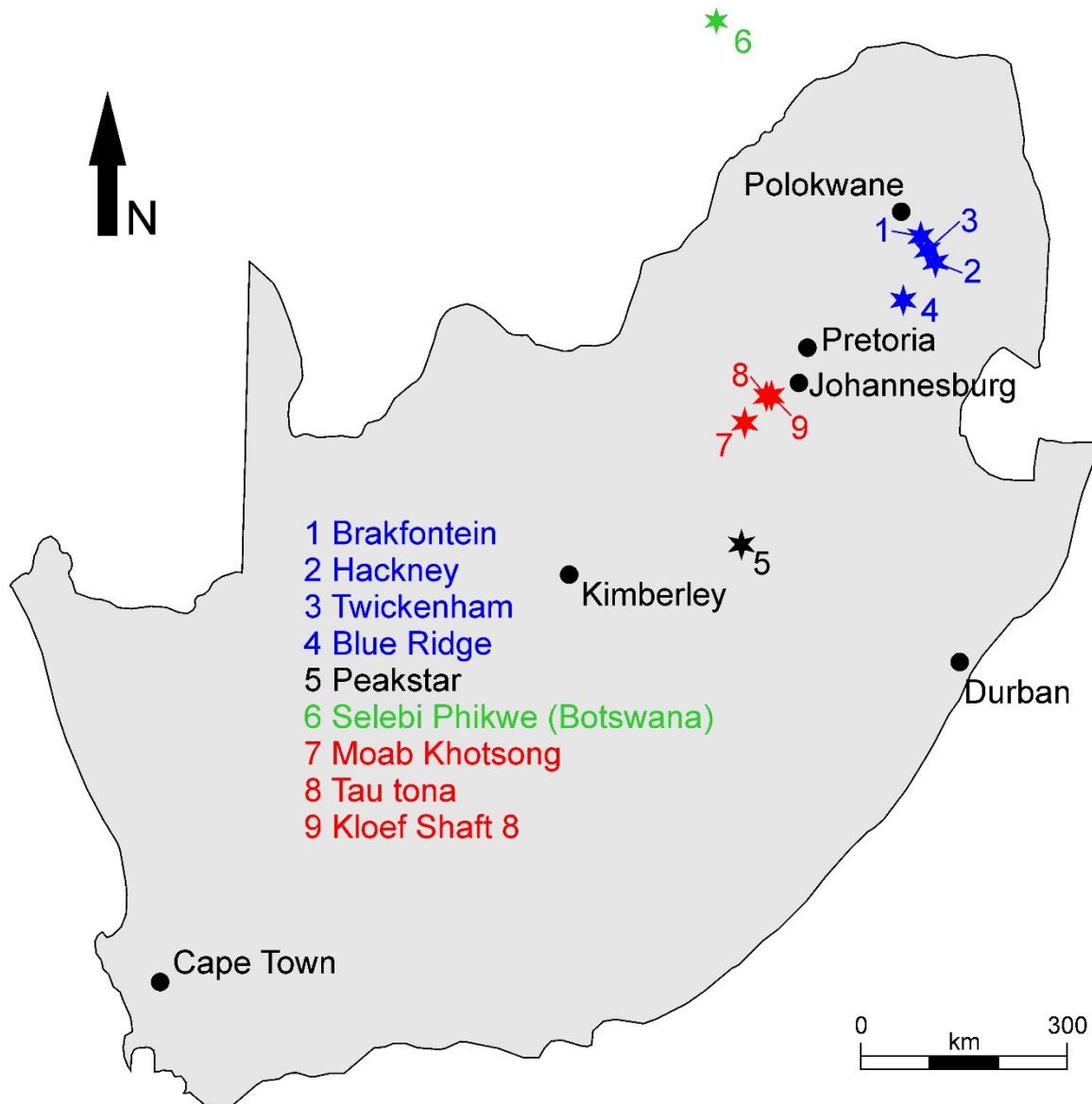


Fig. 2: Generalized map of South Africa illustrating the positions of all test sites. Blue stars: platinum; black stars: diamonds; green stars: copper; red stars: gold.

During the project rocks from very different places were analyzed to obtain data for different rock conditions taking the combination of abrasivity and rock strength into account. All this data is combined in a rock matrix for the decision-taking of the required drill head. The following chapter gives a short overview of all analyzed project sites - their position, geology and other details about the operation. The aim of the current thesis was not to achieve a highly detailed view of each project site but wherever possible additional

detailed literature is given in the corresponding section. Maps of all project sites are shown in Fig. 2 for all African sites and in Fig. 12 for European sites. Only the gold mine operations are explained in more detail, because the geological vicinity is the main input to all numerical models. This chapter deals only with general descriptions and data from literature. The description of total number of samples tested during the current thesis can be found in 6.1.

4.1 Gold mines

4.1.1 Location and short description

All analyzed gold mines are gathered in the vicinity of Johannesburg in the so called Witwatersrand Basin. The name is derived from a mountain ridge, partly surrounding the basin, the "ridge of white waters", which exceeds through the provinces Gauteng and Mpumalanga. This ridge consists mostly of pale quartzites. This Basin is well known for its high gold and uranium content bearing rocks which have been mined for centuries. The basin itself is divided in 6 fields (Tab. 1). Due to good conditions mining started at the end of the 19. Century in 1886 (EALES 2007: 288) and produced about 50,000 t of gold. The Highest gold contents can be found within paleo placers the so called reefs. A count of minable reefs for each goldfield is listed in Tab. 1. A brief description of the three mines can be found in Tab. 2.

Tab. 1: List of all goldfields of the Witwatersrand district with count of minable gold and uranium bearing reefs (GUILBERT & PARK JR. 1986: 761).

Name of goldfield	Count of usable reefs
Welkom goldfield	4
Klerksdorp goldfield	7
Carletonville goldfield	3
West Rand goldfield	10
East Rand goldfield	9
Evander goldfield	1

Tab. 2: Brief summary of the considered gold mines covering the operator, max. depth, the year of opening and the position.

	Kloof	Moab Khotsong	Tautona
Operator	Sibanye Gold	AngloGold Ashanti	AngloGold Ashanti
Max. Depth [m]	3500	2600	3900
Year of opening	2000	2003	1962
Coordinates (WGS84)	S26° 23.086' E27° 35.344'	S26° 59.219' E26° 47.920'	S26° 24.884' E27° 25.728'

Moab Khotsong is the shallowest of the analyzed gold mines with a depth of up to 2600 m (www-2). The mine is located in the province Free State, South Africa, near the city of Klerksdorp. At the mine Kloof the operating depth goes down to 3500 m below the surface (www-3). And with a depth of up to 3900 m Tautona gold mine is one of the deepest mines in the world. Both mining fields are located in the Province

of Gauteng near Carletonville (Johannesburg). All mines are active operations and are operated as stoping mines. Tautona and Moab Khotsong are operated by AngloGold Ashanti, Kloof is operated by Sibanye Gold.

4.1.2 Geological overview

The Witwatersrand basin is an old sedimentary basin filled with thick layers of alluvial material (paleo placers) of the surrounding bedrock mountains. Due to the age and the formerly high overburden these sedimentary rocks were slightly metamorphosed. The general cross section of the stratigraphy, which is described in this chapter section, can be found in Fig. 3; the corresponding excerpt detail of the geological and structural map of the Witwatersrand Basin (THE GEOLOGICAL SOCIETY OF SOUTH AFRICA 1986) with all mines plotted can be found in Fig. 4.

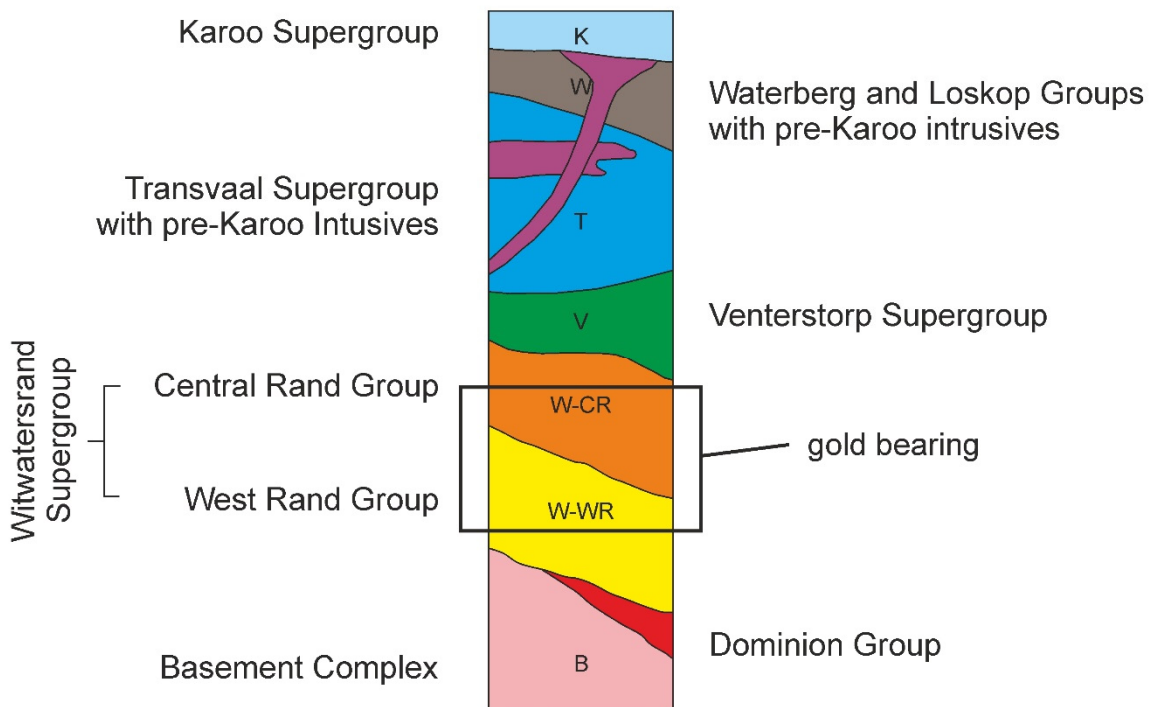


Fig. 3: General stratigraphy of the Witwatersrand basin around Johannesburg (GUILBERT & PARK JR. 1986: 757, edited).

The following paragraph refers to GUILBERT & PARK JR. (1986) unless otherwise noted.

The bedrock (Basement complex) with lower Archean age is part of the oldest rocks within the project area and has an age of about 3000 Ma. The rocks are part of the Kapvaal craton and form the basement of the whole basin. The bedrock can also be observed apart from the Witwatersrand basin where these rocks build dome shaped mountains and represent the source material for all sedimentary and metasedimentary rocks filling the Witwatersrand basin. The bedrock consists of granites, granitic gneisses and other for greenstone belts typical rocks (SCHLÜTER 2008), for example the Limpopo belt, which is described in more detail in chapter 4.2.2. In some areas these oldest crystalline rocks are discordantly overlaid by thin conglomerate and metaconglomerate layers and eventually thicker lava layers (Dominion Group), but in the main areas the latter strata is missing. These meta conglomerates are also the first gold and uranium bearing layers.

The basement is buried underneath about 8 km (HENNING et al. 1938: 30) of clastic sediments and their metamorphic products. This sedimentary package is called Witwatersrand Supergroup and can be characterized as the host rock for most of gold bearing reefs being mined in this area. The thickness of the Supergroup varies and reaches its maximum in the center of the basin. A cross section through the

Witwatersrand conglomerates can be found in Fig. 5. The Witwatersrand Supergroup is divided in West Rand (older) and Central Rand (younger) Group. The names of these groups originate from the outcrops at the surface. West Rand Group quartzites are located at the west rand mountain range, Central Rand Group material exists only in the inner part of the basin. The West Rand Group consists of alternating, fluvial sedimentary layers of shales, quartzites, coarse sandstone (gritstones) and conglomerates. Within this subgroup only few reefs with low gold content can be found. The detailed stratigraphic profile in Fig. 6 gives insight into the sequence of the rock strata of Witwatersrand Supergroup and the important reefs.

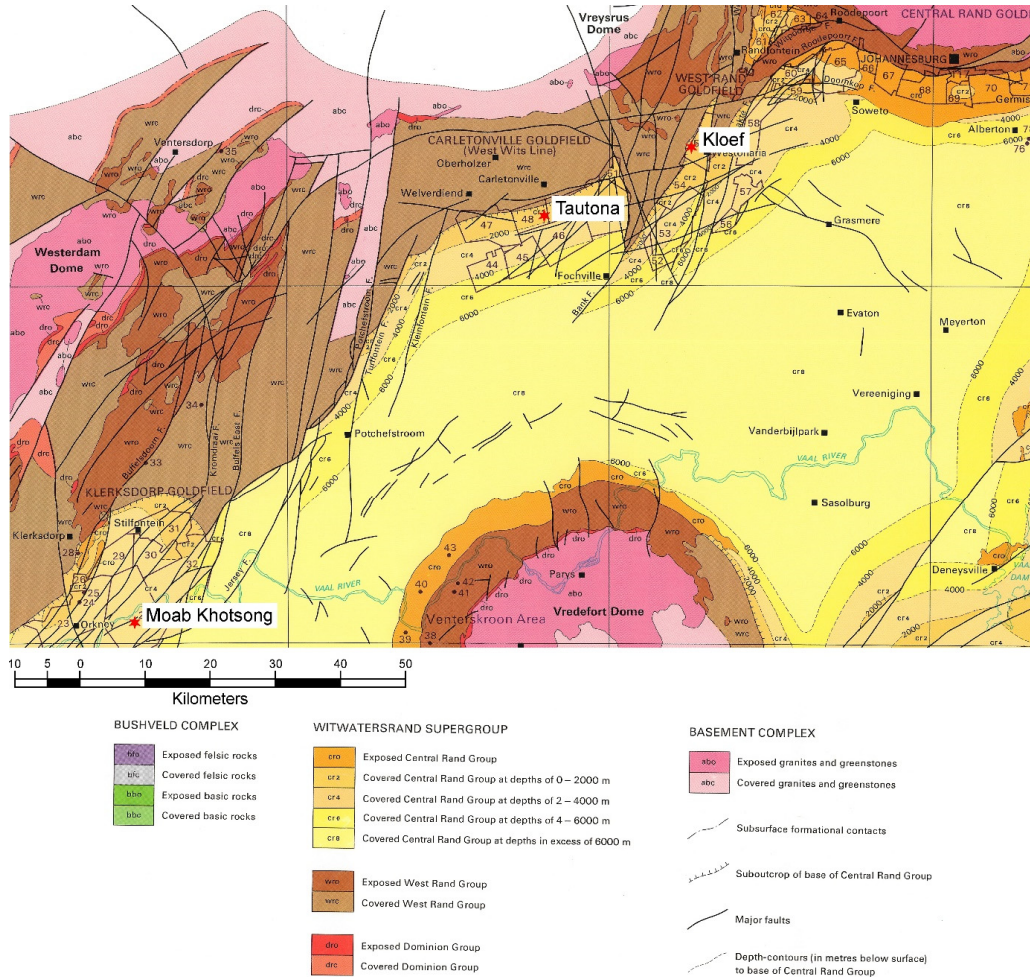


Fig. 4: Geological map of the Witwatersrand Basin including information about the mining depths and the mine locations (THE GEOLOGICAL SOCIETY OF SOUTH AFRICA 1986).

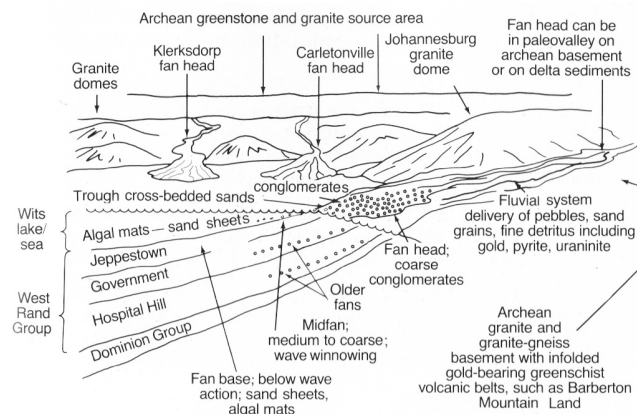


Fig. 5: Cross section through Witwatersrand Basin showing the sedimentary series and some paleo placer fans (GUILBERT & PARK JR. 1986: 757).

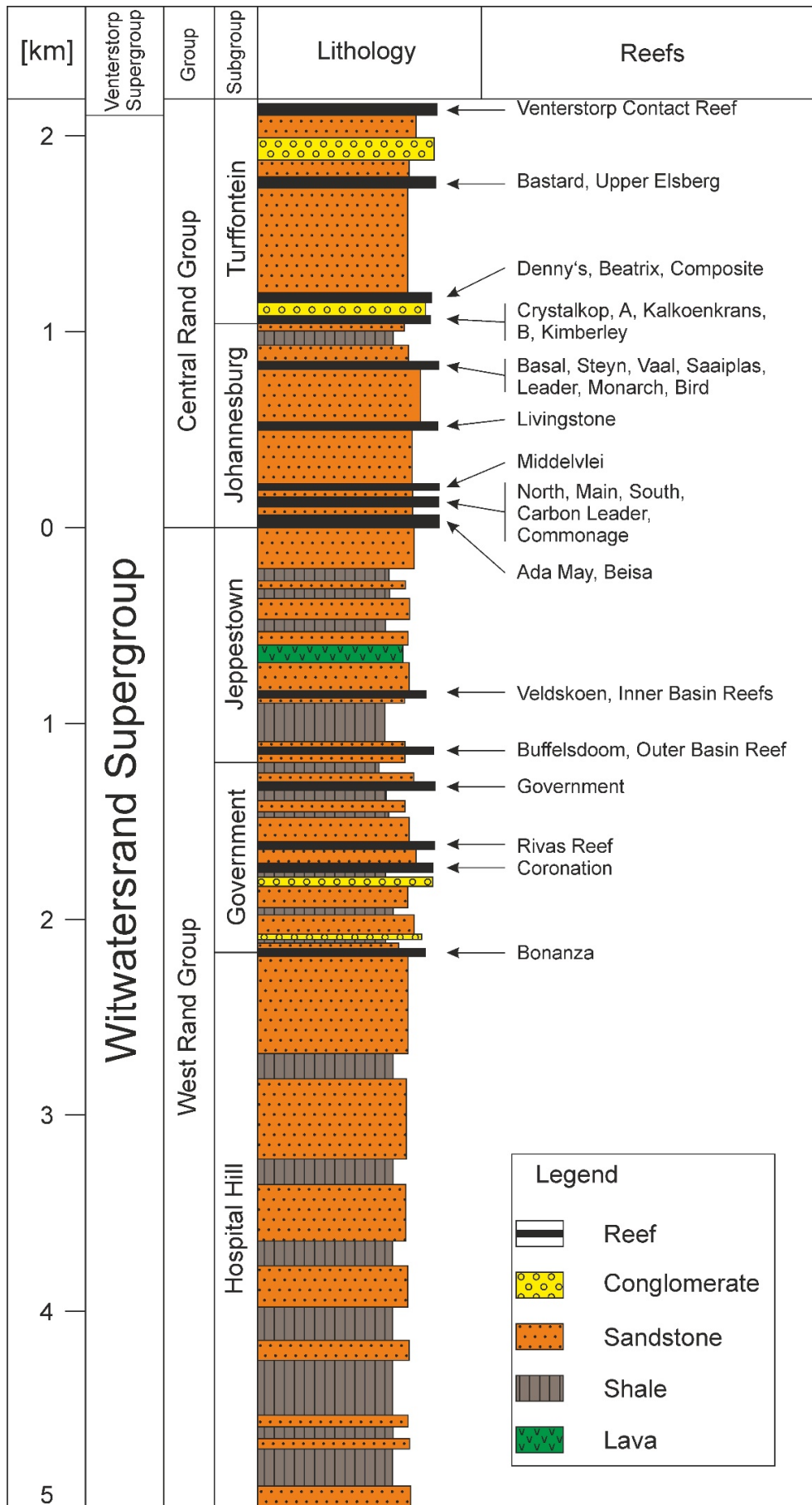


Fig. 6: Gold bearing reef formations and their distribution within the sedimentary series of the Witwatersrand Basin (FRIMMEL 2005: 8, edited).

The sedimentary milieu and the conditions have been changing with ongoing sedimentation from fluvial to limnic (FRIMMEL 2005: 9). As the sea level rose over time more and more different types of sediments were accumulated and deltaic deposits were created (Fig. 5).

With increasing water volume of this paleo sea the flow velocity decreased and the sedimentation of paleo placers started. Coarse quartzitic conglomerates, sandstones, metaconglomerates and –sandstones with intermediary gold bearing reefs are the main occurring rock types within the Central Rand Group. Referring to POHL (2005) the main deposit stage for the Witwatersrand sediments has an age of 3074 and 2714 Ma. Each goldfield refers to one deltaic fan head containing gold bearing reefs (Fig. 5 and Fig. 7). In comparison to the total volume of sediments of the Witwatersrand Supergroup the gold bearing rocks account for 6 to 12 %.

The development of the mentioned deposits goes back to the collision of terranes and the building of the Kapvaal craton. Parallel to this process the area of the present basin was tectonically lowered and many depressions and domes were formed. Between these domes the alluvial fans (Fig. 7), enriched with paleo placers containing heavy minerals, could be formed. Besides other typical heavy minerals these placers consist of well-rounded pyrite, a notable amount of uraninite (UO₂) and rounded gold grains. The alluvial fans are developed as limnic deltaic sediments. Due to the alluvial to limnic facies layers containing coal or algae were deposited. The strata are used nowadays as stratigraphic marker horizons for the development and the exploration of the mines. Especially for the deepening of the mines it is very important to follow these layers, because the dipping of the reefs varies due to the complex building of the deltaic sediment and the inclination angle of the edges of the basin. The dipping of the reefs can also be disturbed according to faults, step fault systems, folds and other sedimentary structures. The general dip angle of the reefs can be averaged with 20° in western direction.

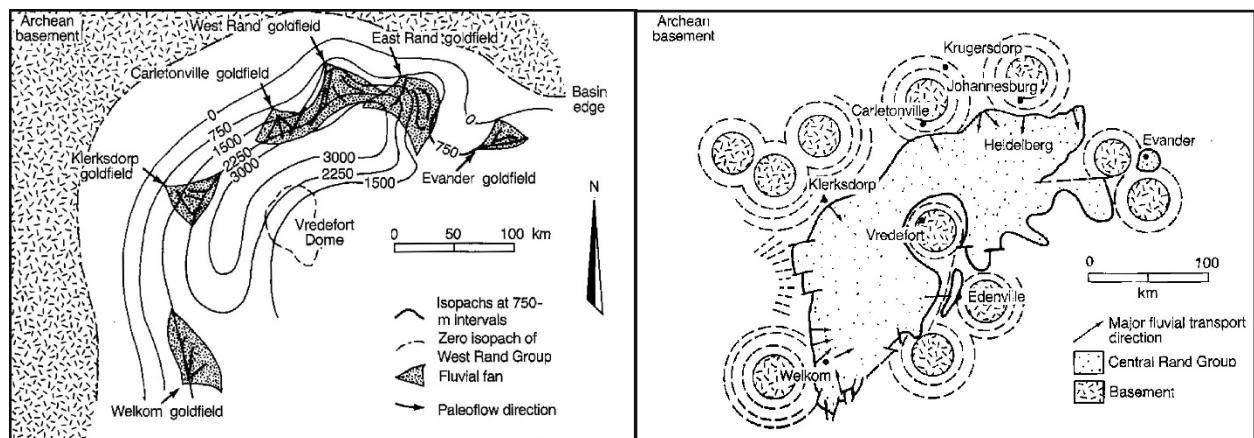


Fig. 7: Illustration of the location of all gold fields in the Witwatersrand Basin (GUILBERT & PARK JR. 1986).

During the decay of the last movements of the terrane collision mainly basic lava ascended, cutting through the thick sedimentary layers and producing huge and thick volcanic strata on top of the sediments of the Witwatersrand Supergroup. The effusive rocks built most of to the Venterstorp Supergroup. Inferior single clastic strata were deposited between the thick volcanic layers. Within this group layers with considerable gold content can occur (SCHLÜTER 2008: 232). But the deposits are not wide spread, slender and are therefore mostly not important for mining. The complete Venterstorp Supergroup has a thickness of about 1,500 to 3,000 m (HENNING et al. 1938: 20).

The massive rock layers of Venterstorp Supergroup are not encountered in the production levels of the considered gold mines. Only for building the transportation and production shafts these rocks have to be excavated, whereas magmatic veins and dykes belonging to the Venterstorp and younger magmatic formations can be observed on the mines' production levels.

At inferior parts of this area the Venterstorp Supergroup is superposed by the Transvaal Supergroup. These Rocks are only observed on surface and therefore have no relevance for the mining industry although they are reaching a thickness of over 3,000 m in some areas (HENNING et al. 1938: 20). The mentioned rocks as well as their educts are, same as the Witwatersrand rocks, clastic sediments and quartzites. (HENNING et al. 1938: 29). In addition to the clastic rocks dolomite and limestone-formations can be found. These rocks were deposited as eroded material of the surrounding mountain ranges during the generation of a new basin.

4.2 Platinum mines

4.2.1 Location and short description

The first in 2009 analyzed platinum mine was the Blue Ridge mine. It is situated between Pretoria and Polokwane (Pietersburg) near the city of Middleburg in the Province of Mpumalanga. The mine is in maintenance (www-4) at the current stage but was active at the start of this research project. Due to this fact samples were prepared and analyzed but no further drill testing was possible to accomplish. This mine reaches a depth of around 300 m for the production.

The other three platinum mines, Brakfontein, Twickenham and Hackney (named from North to South) are located near Polokwane (Pietersburg) in the direct vicinity of the City of Lebowakgomo in the Province Limpopo, South Africa, exceeding along the road R37. All three mines are still active, classical stoping mines and provide mining depths of up to 2,000 m. The most production levels are built in a shallower depth, between surface and 700 m due to cost efficiency reasons.

A brief description with all key factors of the four mines can be found in Tab. 3.

Tab. 3: Illustration of the mentioned platinum mines covering the operator, the max. depth, the year of opening and the position.

	Blue Ridge	Brakfontein	Hackney	Twickenham
Operator	Aquarius Platinum Limited (pdf report 2013)	Anooraq Resources Corporation	Anglo Platinum	Anglo Platinum
Max. depth [m]	300	800	250	300
Year of opening	2001	1969	2005	2005
Coordinates (WGS84)	S25 14.783 E29 34.067E	S24 18.768 E29 55.461	S24 27.676 E30 03.542	S24 24.842 E30 01.296

4.2.2 Geological overview

An excerpt of the geological map 1:4,000,000 of Southern Africa of HAMMERBECK & ALLOCK (1985) (Fig. 8) shows the distribution of all analyzed platinum mines and the regional geology of the project sites.

The main targets for platinum mining in this area are the two well-known reefs: the Merensky reef and the UG2 reef. Both belong to the Bushveld Complex which is the almost exclusive formation for platinum recovery in South Africa (SCHLÜTER 2008: 235).

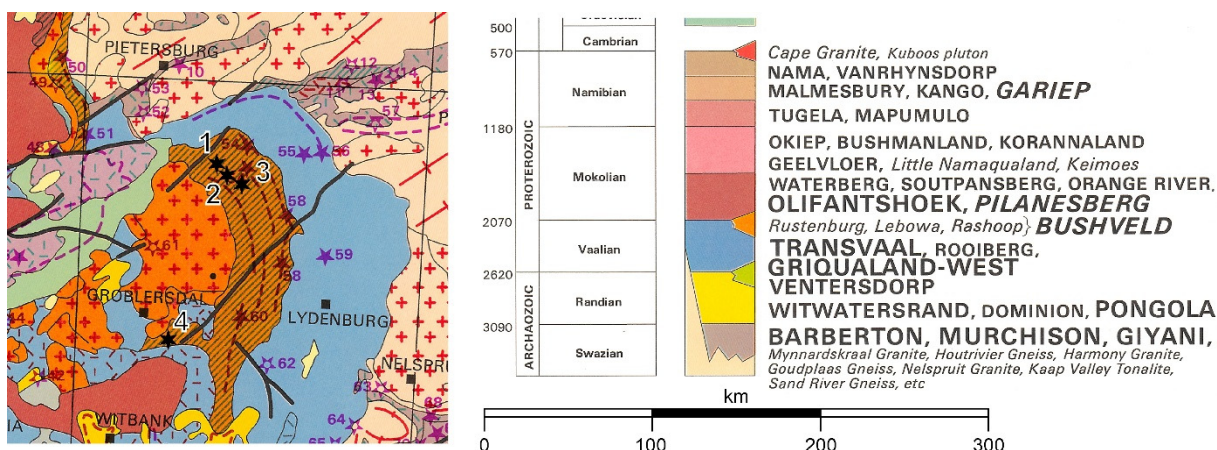


Fig. 8: Geological map of the vicinity of all analyzed platinum mines. Excerpt of HAMMERBECK & ALLOCK (1985) (1 Brakfontein; 2 Twickenham; 3 Hackney; 4 Blue Ridge).

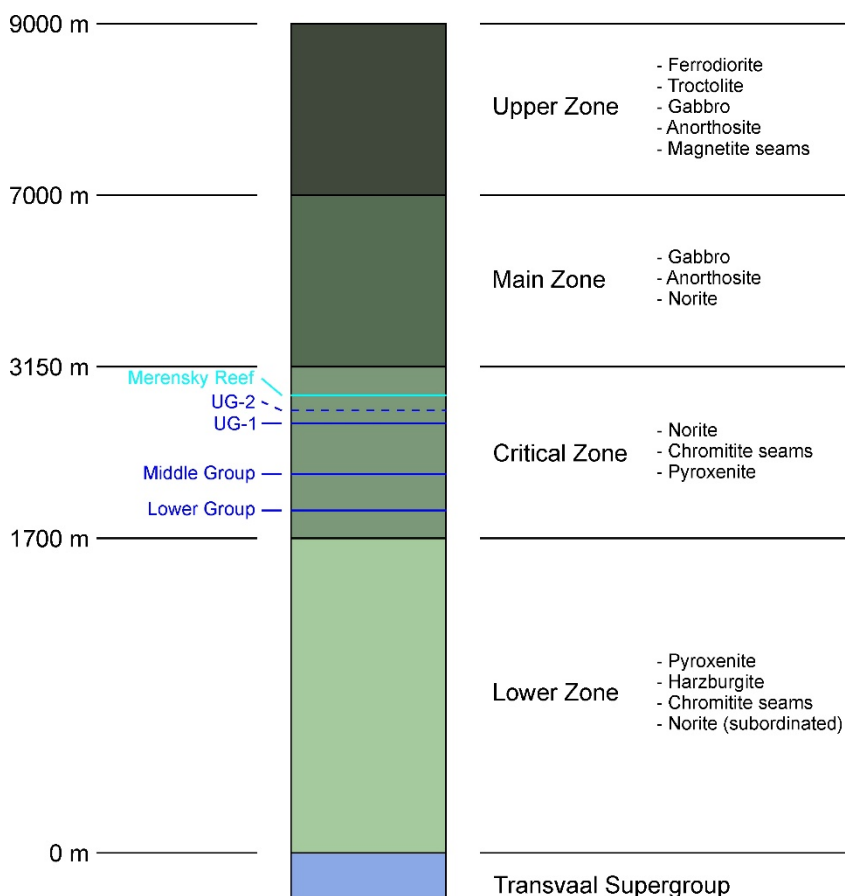


Fig. 9: Stratigraphic column of the layered intrusion part of the Bushveld igneous complex with all important reefs (SCHOUWSTRA et al. 2000: 34). Additionally, the typical rock types for each zone are plotted (PETTERS 1991: 145).

The Bushveld Complex is the largest layered intrusion on the entire earth and is covering an area of 65,000 km² (PETTERS 1991: 144). The formation is situated in the center of the Transvaal craton basin in the area between Pilanesberg Volcano (West), Lydenberg (East), Pretoria (South) and Potgietersrus (North). The Bushveld igneous complex was formed around 2055 to 2060 Ma (VILJOEN & REIMOLD 1999: 6) before present and consists of granites and granitoids in the center-part (PETTERS 1991: 144). The border area is mainly dominated by layered mafic rocks, like gabbros, anorthosites and norites. These layers are dipping with 10-25° towards the center (PETTERS 1991: 144 ff). The layered part of the intrusion can

be divided in 4 zones which are shown in Fig. 9. The Upper Zone, Main Zone and Lower Zone are not relevant for platinum mining. Only the “Critical Zone” containing the Merensky Reef and the UG-2 beside of other reefs is target of all mining operations in South Africa and therefore the only rock for research purposes of the current thesis.

The Merensky Reef is a pyroxenite with varying thickness of 40-120 cm (CAWTHORN & BOERST 2006: 1509) and has a near constant grade of PGE of 5 to 8 g/t.

The UG-2 surrounding rock is a pyroxenite with a thickness of about 25 m (MONDAL & MATHEZ 2007: 496), but the reef itself is a chromitite and is poor in gold, copper and nickel but very rich in platinum group elements (PGE). The PGE grade is stated to be exceeding the grade of the Merensky reef by a factor of 1.5 (EALES 2007: 321). The reef has a thickness of about 70 cm (MONDAL & MATHEZ 2007: 496).

4.3 Other mines

A brief description with all key factors of the four mines can be found in Tab. 4.

Tab. 4: Brief description of all other testing mines in southern Africa considered in the current research.

	Peakstar	Selebi Phikwe
Operator	Sibanye Gold	AngloGold Ashanti
Max. Depth [m]	3500	2600
Year of opening	2000	2003
Coordinates (WGS84)	S26° 23.086' E27° 35.344'	S26° 59.219' E26° 47.920'

4.3.1.1 Peakstar

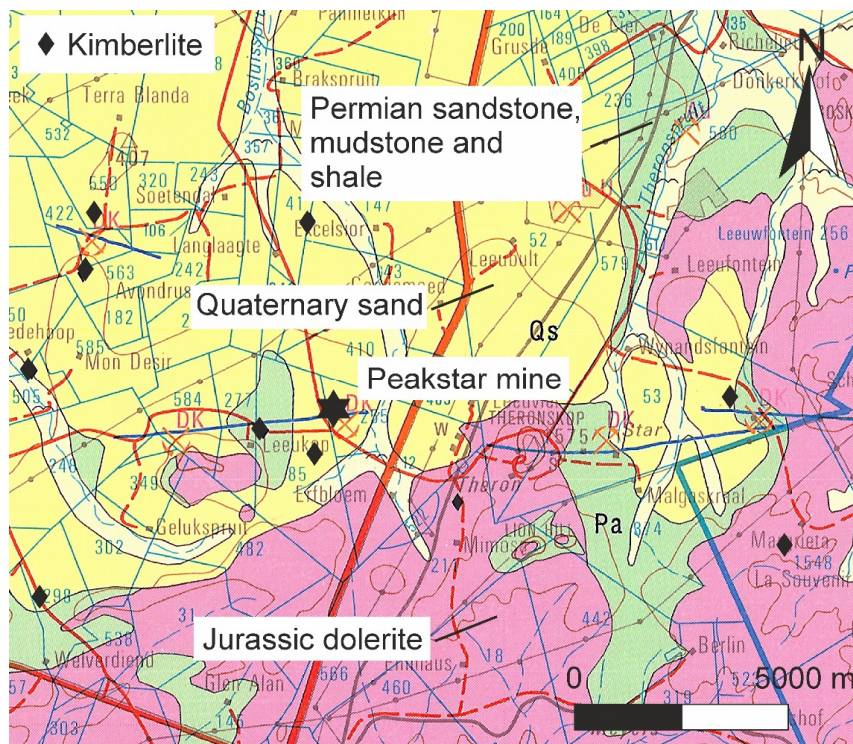


Fig. 10: Geological map of the vicinity of all analyzed mines. Excerpt of the geological map of Winburg (BESTER 1998).

Peakstar mine is a diamond mining operation around 35 km south of the city of Welkom in the province of Free State, South Africa. Fig. 10 shows the location and the surrounding geology of this project site. This mine operates down to a depth of around 100 m and is mined from bottom to top level following the steep standing, very narrow pipes of kimberlites in very soft clayey and sandy material.

Kimberlites are magmatic ultramafic rocks belonging to the group of peridotites. These rocks represent mostly the root of very old volcanic activity. In South Africa the main part of kimberlites has a mid to late cretaceous age. Kimberlites contain a huge amount of olivine and phlogopite and accessory diamonds. The latter is the reason for the importance of the rocks to the mining industry.

4.3.1.2 Selebi Phikwe

The Selebi Phikwe copper and nickel mine is located near the equivalent named town Selebi Phikwe in the eastern part of Botswana. The mine is operated by BCL Limited and was started as two small surface mining operations in the 1960s. The mining complex at a bigger scale started its operation in 1973. At the current stage this mine is classified as a deep mining project and thus shows a maximum depth of 1400 m (www-5).

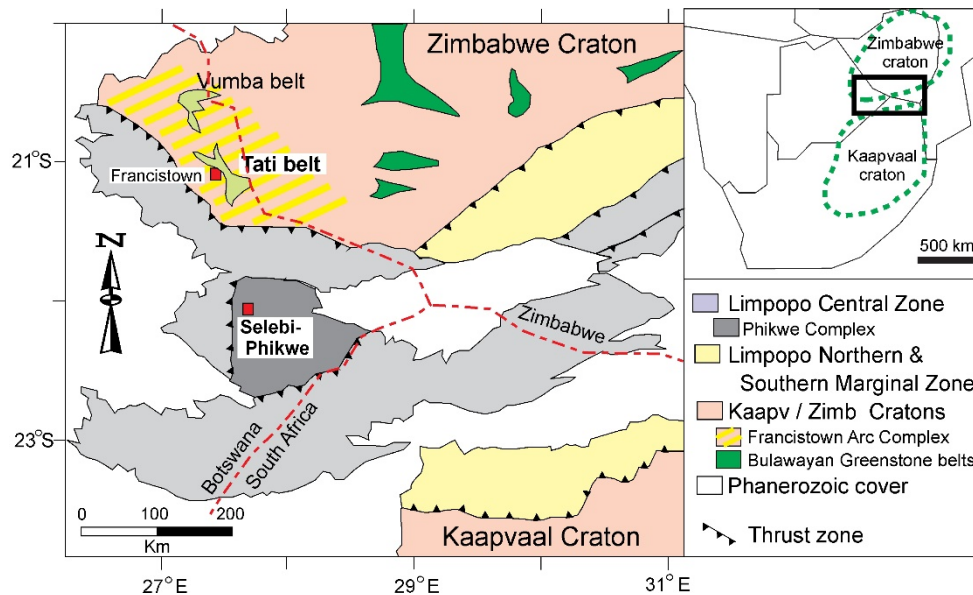


Fig. 11: Geological map of Selebi Phikwe and its vicinity (MAIER et al. 2008).

The host rocks, containing a high grade of copper and nickel, are a high grade metamorphosed gabbro-norites, pyroxenite and peridotites which have intruded into the rocks of the central zone of the Limpopo belt.

The schematic geological map of the mining area of Selebi Phikwe can be found in Fig. 11. The underlying and mined rock mass of Selebi Phikwe is of Archean age and is consists of gneissic granitoids associated with metasedimentary and metavolcanic rocks. These rocks are part of the Limpopo Belt between Zimbabwe and Kapvaal Craton, which was mentioned before (4.2.2). In some areas this bedrock is covered by Phanerozoic rocks of the Karroo Group. This overburden could only be found in the upper parts of the mine construction and is not considered in the current thesis.

4.4 Quarries and other test rocks



Fig. 12: Generalized map of Germany, Switzerland, Liechtenstein and Austria with most of the European test sites plotted.

A brief description with the most important facts of all analyzed quarries and test rocks can be found in Tab. 5.

Tab. 5: A brief description of all quarries and test rock areas covered by this research.

	Bayerwald Granite	Erdösmecke	Golling	Hagerbach	Miltenberg	Oberbaumühle	Pechbrunn
Operator	Different operators	closed	Moldan GmbH	Versuchsstollen Hagerbach AG	Peter Wassum GmbH	Basalt AG	Basalt AG
Max. Depth [m]	surface	surface	surface	100	surface	surface	surface
Coordinates (WGS84)	Different quarries	46.148193, 18.518074	N47 36.943 E13 12.997	N 47 4.590 E 9 23.346	N49 42.735 E09 15.315	N49 48.714 E12 09.212	N49 57.572 E12 09.858

4.4.1.1 Bayerwald Granite

These granites are coming from different quarries of the Bavarian Forest. A Map of important quarries mining the Bayerwald Granites can be found in Fig. 13.

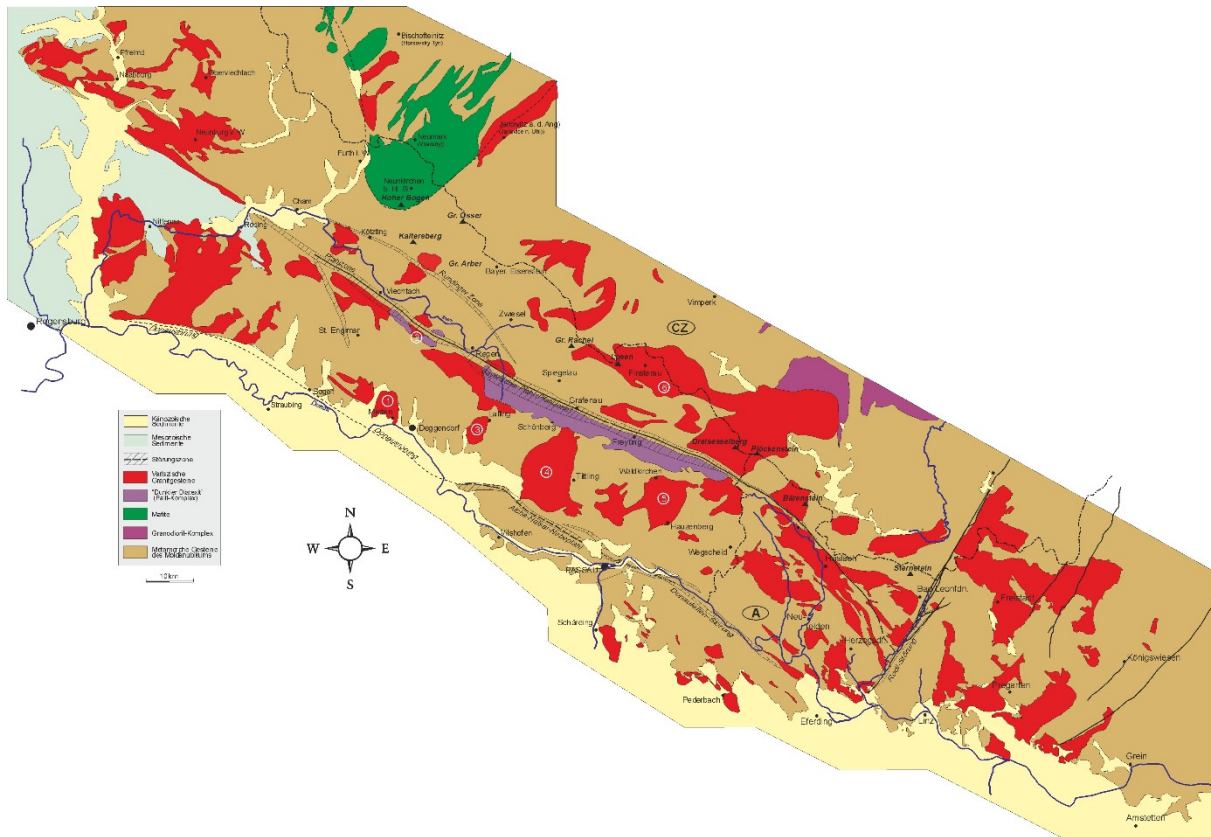


Fig. 13: Geological map of the southwestern area of the Bohemian Massif showing the most important granite quarries (LEHRBERGER 2013: 39).

In spite of various occurrences at the surface the material is a very homogenous and isotropic rock. Thus it is the number one test rock for drill testing for Hilti.

During the maximum of the Variscan orogenesis these rocks intruded as magma in gneisses of the Bohemian Massif of the Bavarian Forest around 320 Ma ago (LEHRBERGER 2013: 33), where they had enough time and depth to crystallize as the plutonic granite. Due to the crystallization process feldspar, quartz, glimmer and other minerals could grow to bigger size and influencing with their mineral structure the interaction of the rock with the used tool.

4.4.1.2 Erdösmecke

This granite quarry is located 3 km south of the town of Erdösmecke in Hungary in the Mountain Range of the Mecsek Mountains (Fig. 14).

The occurring granites are part of the Mórág unit which is part of the Tisia Terrane. The Tisia Terrane is an alpine Nappe consisting of different sub terranes. The Mórág Unit is one of these sub units and contains different intrusive plutons of variscan age which were transformed to high-grade gneisses and migmatites.

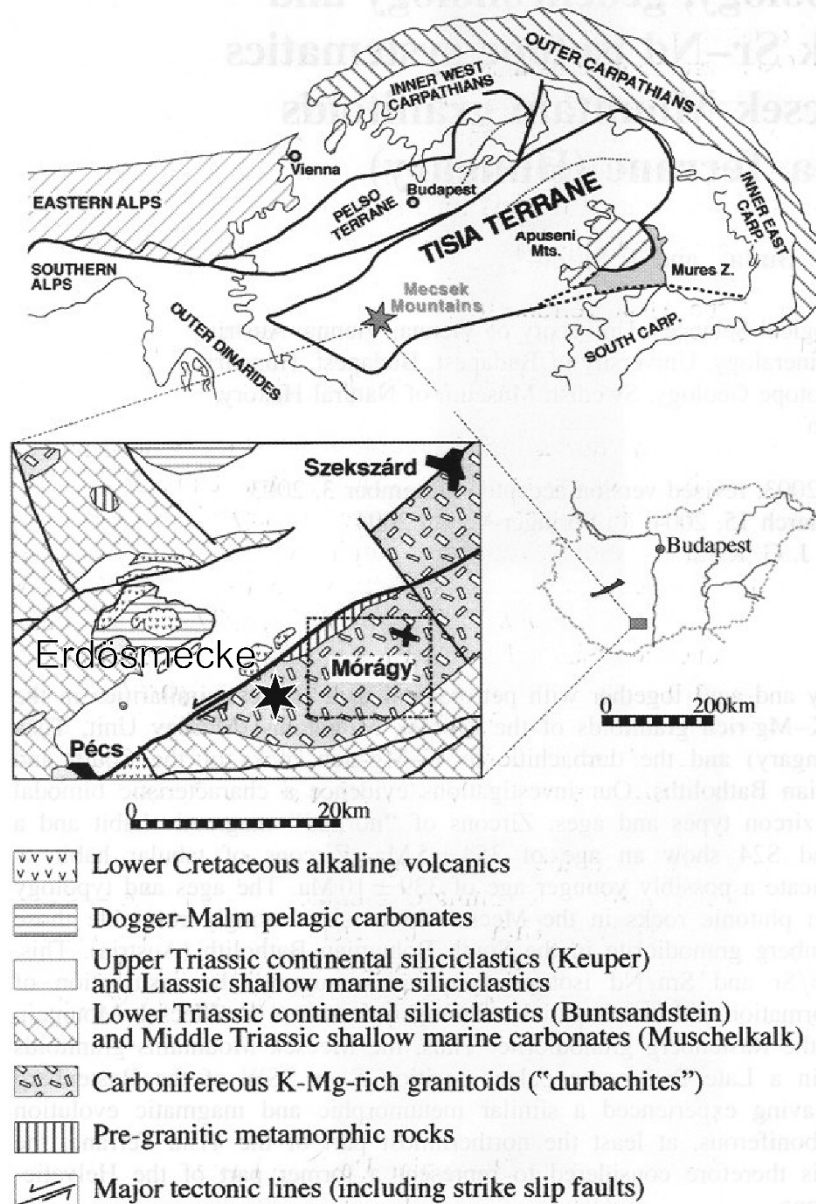


Fig. 14: Simplified geological map of the Mecsek Mountains in southern Hungary (KLÖTZLI et al. 2004).

4.4.1.3 Golling

The quarry of Golling is operated by the Moldan Baustoffe GmbH which is part of the Salzburger Sand- & Kieswerke GmbH and is situated at Moosegg (Grubach) around 5 km northeast of Golling at the river Salzach. This quarry was at mentioned for the first time in 1613; in 1853 the first industrial mining of gypsum and anhydrite under the direction of Christian Moldan KG as the first company started (PLÖCHINGER 1990: 55). The quarry is still active, producing gypsum for the construction industry.

The quarried rock belongs to the stratigraphic units of the Haselgebirge (Fig. 15). The Haselgebirge is a sedimentary, tectonically influenced breccia consisting of anhydrite, gypsum and clay components surrounded by a salt and fine grained clay matrix. The material was deposited in Upper Permian in a smooth and shallow lagoon filled with hypersaline ocean water from the Tethys.

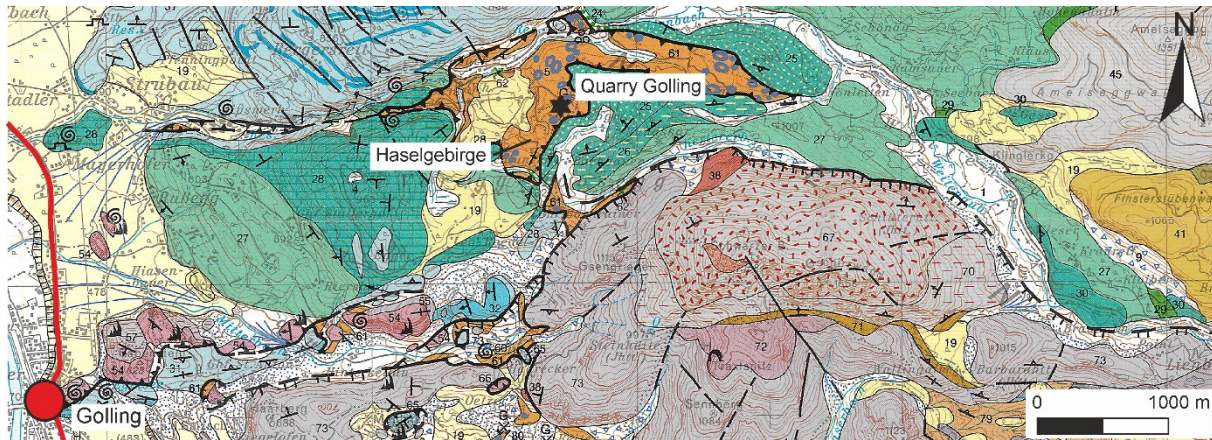


Fig. 15: Excerpt of the geological map of Hallein, showing the dominant stratigraphic units of the Haselgebirgs-Formations and the location of the quarry of Golling (PLÖCHINGER 1987).

4.4.1.4 Hagerbach Test Gallery

The Hagerbach Test Gallery is located 5 km northwest of town of Sargans, in Switzerland at the Highway 3. The Test Gallery portal is situated at the basis of mount Gonzen. It was opened in 1970 and is used for different kinds test set-ups. Starting with burning tests of trains to the generation climatic tunnel models, many companies are using this site for 1:1 scale testing. The operating company “Versuchsstollen Hagerbach AG”, is managing the site and is performing own on site research as well as running a subsurface testing laboratory. Several test results used in the current thesis, which are specially marked in chapter 6, were generated in this underground laboratory.

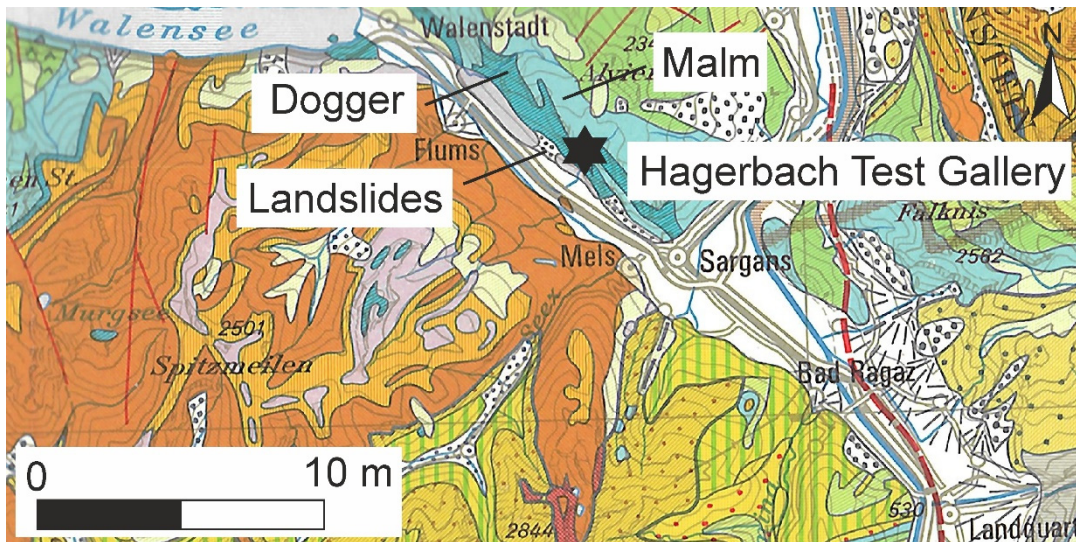


Fig. 16: Excerpt of the geological map of Switzerland illustrating the main geological units and the location of the Hagerbach Test Gallery (SPICHER 1980).

As shown in Fig. 16 the Testing Gallery is located inside the mountain ridge of the Gonzen, which consists of Jurassic rocks from Dogger and Malm. These rocks were pushed northwards as unit of different kind of rock strata on top of the rocks of the Zentralmassiv (WEISSERT & STÖSSEL 2010: 45). Today we can exemplify this on the occurrence of nappes like the Wildhorndecke and Morclesdecke.

The typical rocks observed in Hagerbach Testing Gallery at the Hilti test site are black colored shales of minor strength and siliceous limestone. Both materials are strongly disturbed in their bedding and no clear strata can be observed. The testing during this thesis was exceptionally accomplished in the strata of the siliceous limestone.

4.4.1.5 Miltenberg

The active quarry of Miltenberg is situated at the state road ST2309 near the town of Miltenberg at the river Main in the county of Lower Franconia, Germany. The quarry is operated by concern “Peter Wassum GmbH” which is specialized in all kinds of natural dimension stones. This Quarry is only one of some quarries in this area which are mining all similar sandstones of the Buntsandstein unit.

The red and white striped sandstones are called Miltenberg Sandstone and are a variety of the Red Main Sandstone with Lower Triassic age. The rocks belong to the lower Buntsandstein, especially to the Gelnhausen- and Salmünster-Series (GRIMM et al. 1990: 386 [Nr. 066]). An excerpt of the geological map can be found Fig. 17.

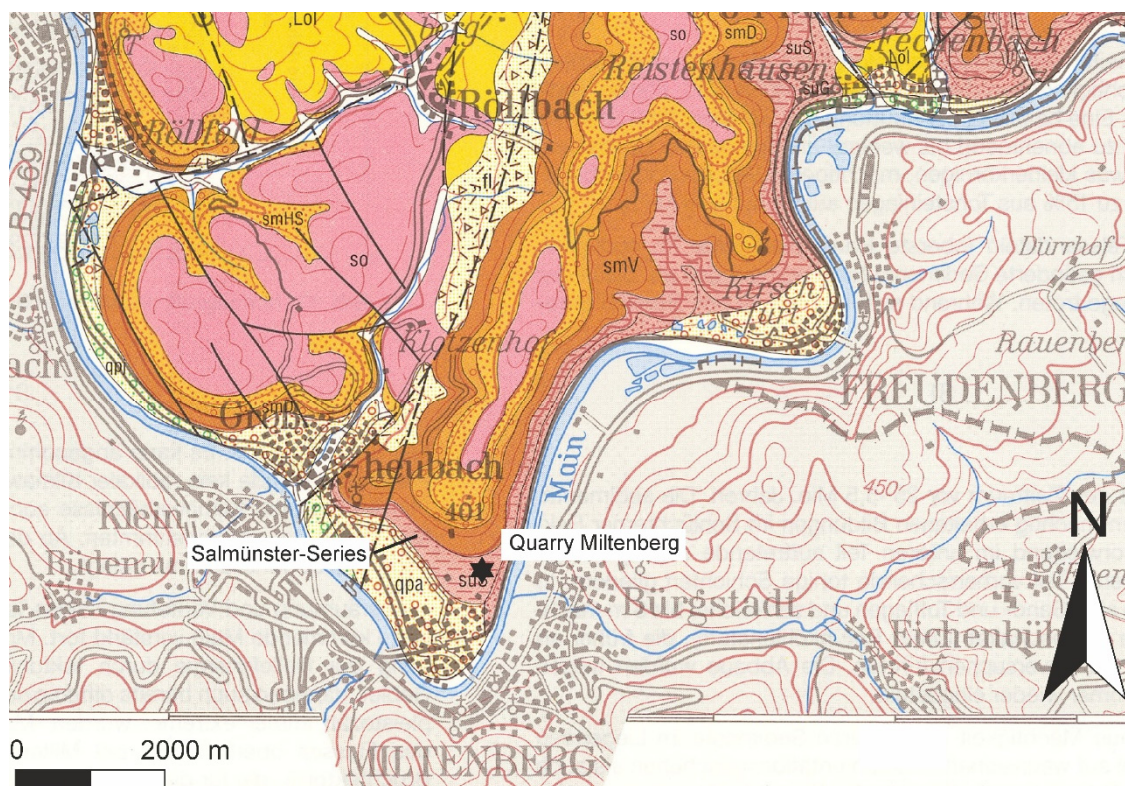


Fig. 17: Geological map the city of Miltenberg, showing the location of the quarry (SCHWARZMEIER & WEINELT 1993).

The start of the regression of the Tethys during the upper Permian was continued during the Lower Triassic. The beginning of the Lower Triassic can be correlated with the start of the sedimentation of the so called Buntsandstein-Formation. During this period of earth history, the coastal stripe of the Tethys was moving northwards in Germany and the connection to the world sea was lost. At the same time the subsidence of the Germanic basin which started in the upper Permian continued. Due to the conditions in central Germany fluviatile, limnic and terrestrial sediments were deposited, where the Miltenberg Sandstones belongs to.

4.4.1.6 Oberbaumühle

The Quarry Oberbaumühle is operated by the concern “Basalt AG” and is located north of the town of Windischeschenbach in Upper Palatinate, in Germany. The quarry extends mostly along the Fichtelnaab on its western bank (left bank).

The opened material consists of amphibolite of the Neustädter Scholle which is part of the Zone of Erbendorf – Vohenstrauß of the Bohemikum SCHÜSSLER (1990). The educts of the amphibolite were gabbros which have been subducted and transformed due to a mid to high pressure metamorphosis STETTNER (1992). During the period of subduction, the overburden reached up to 40 km (STETTNER 1992) and the rocks were highly restrained. Due to the conditions as well as the high horizontal stresses, the rock mass today is highly fractured and shows a very narrow discontinuity spacing. Fig. 18 shows the geology and the location of this quarry.

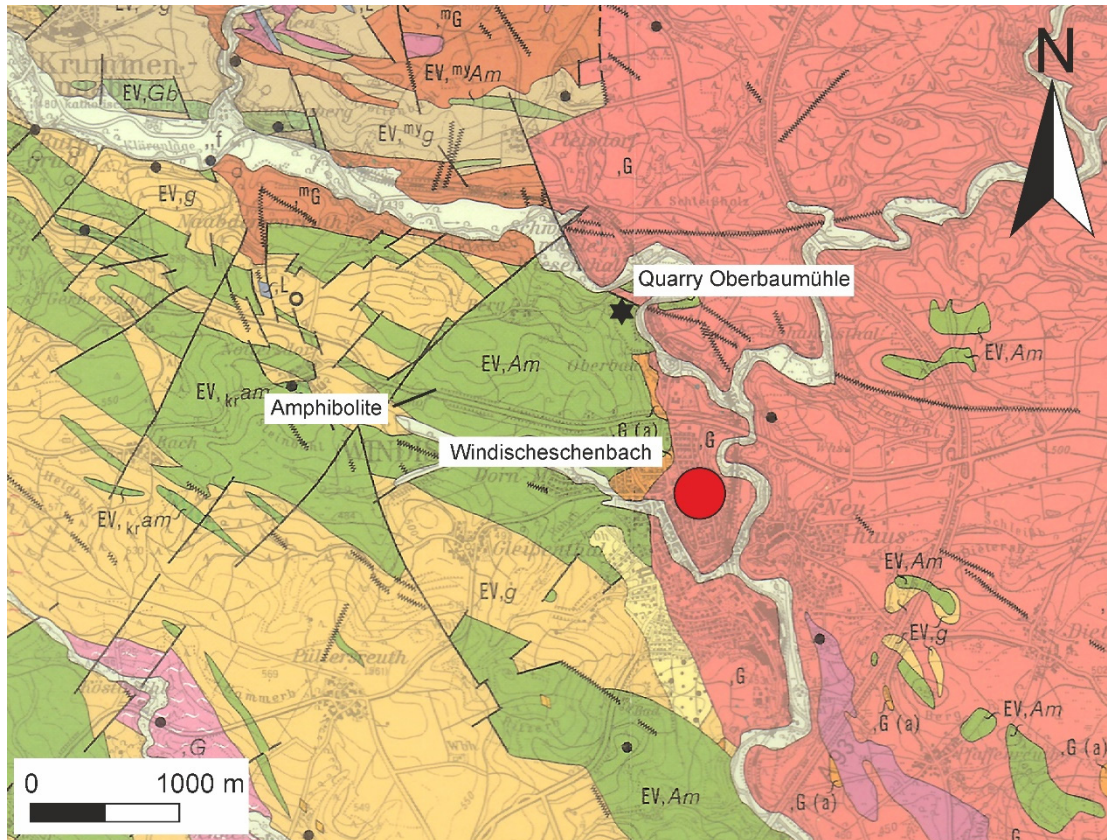


Fig. 18: Excerpt of the geological map of the vicinity of the KTB in Upper Palatinate (DILL et al. 1991).

4.4.1.7 Pechbrunn

The rock quarry Pechbrunn is situated 8 km southeast of the town of Marktredwitz in Upper Palatinate in Germany. The quarry was built on the northwestern slope of the mount “Großer Teichelberg”. In the quarry basalt and basalt tuffite are mined which are used as split and gravel especially as crushed stones for railway traces due to the high rock strength. The quarry operated by the concern “Basalt AG”.

The volcanic rocks consist of mainly basic volcanic rocks of the so called tertiary volcanism. It's the main eruptive zone was located around the Vogelsberg but also occurred in the spacious area of the Upper Palatinate in accordance with the Egger Rift Valley and started 65 Ma MESCHÉDE (2015) before today. Fig. 19 shows the geology and the location of this quarry.

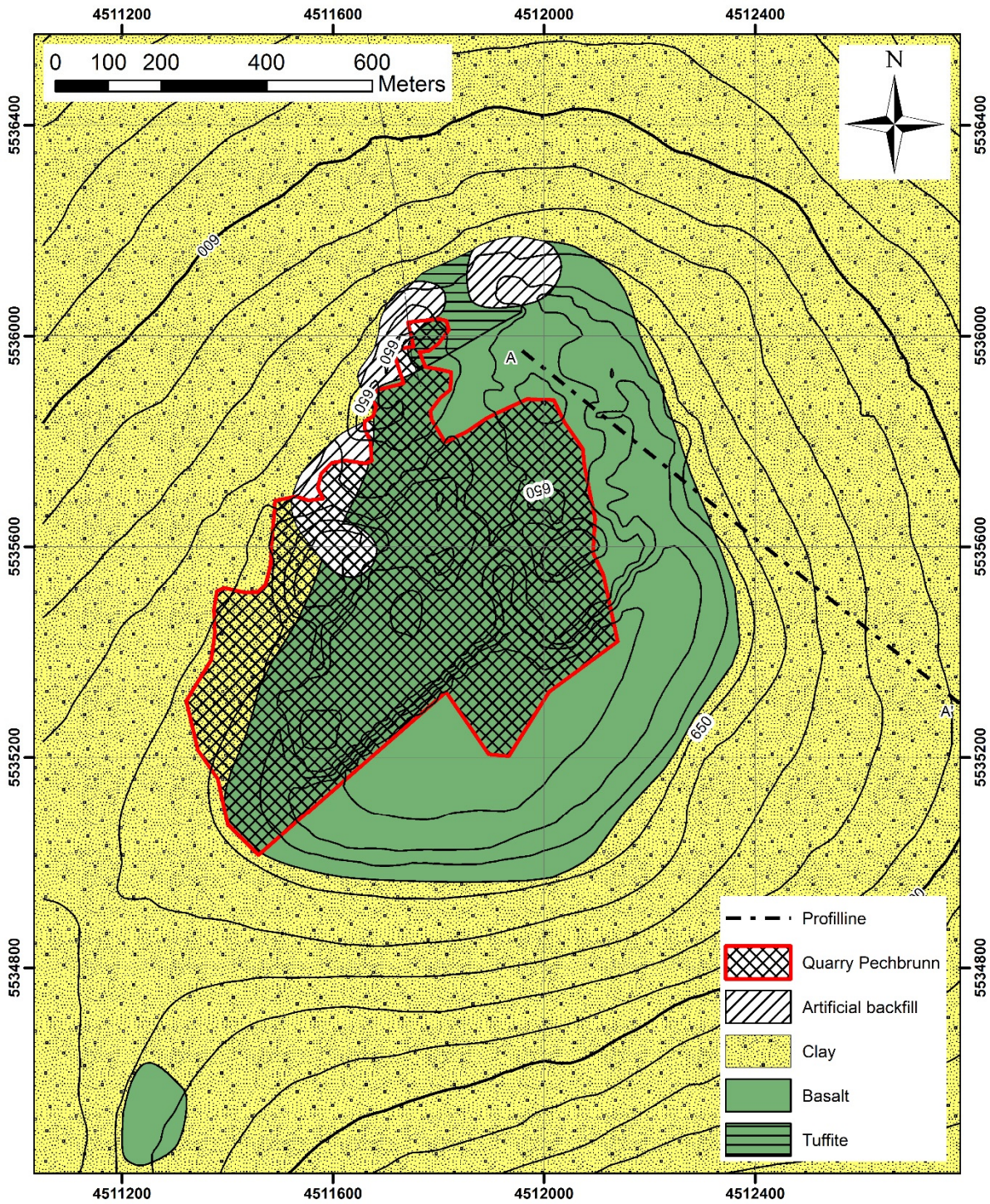


Fig. 19: Geological map of the surrounding of quarry Pechbrunn. The map was created based on the geodata provided by DIMROTH & SÖLLNER (1964) and RAUM (2013).

5 Testing methodology

To improve the drill performance and the wear of drill heads in relation to the occurring geology and stope geometry several field and laboratory tests were conducted. We tested various drill head designs and we started to consider a new way of data management. The current chapter deals with the basics of all of these points.

5.1 Sampling

The first samples were collected from employees of Hilti AG. This applies to all samples of Blue Ridge, Kloof, Selebi Phikwe and Tautona from the mines and to Bayerwald Granite, Erdösmecke and Hagerbach from the quarries and test rock sites.

Wherever it was possible at the remaining sites (Miltenberg, Pechbrunn, Oberbaumühle, and Golling) to draw drill cores in direct connection to the drill tested rock we collected several core samples in-situ. If this was not possible we collected bigger blocks (Moab Khotsong, Hackney, Brakfontein, Twickenham, and Peakstar) to drill cores in our laboratory.

Wherever possible samples were taken directly from the rock face which is drilled for the drill test data. These samples were drilled with a diamond core drill. The common sample diameter during the project was chosen as 50 or 80 mm. If the in-situ sample generation was not successful, larger blocks of equivalent material were taken into, sawn and cored in the laboratory.

5.2 Determination of rock mechanical properties in laboratory and field

5.2.1 Rock strength determination

5.2.1.1 Uniaxial compression test

We tested 63 specimens of 19 different samples from 12 different project sites. All testing was performed in the rock laboratory of the chair for Engineering Geology according to the recommendations of ISRM (1978a), DGEG (1979) and DGGT (2004). Specimen preparation and dimension meet also the requirements of ASTM D2938 (2002) and ASTM D7012 (2013).

Sample preparation

The cylindrical specimens were drilled out of bigger rock samples with a diamond core drill with an inner diameter of about 50 or 80 mm. As often mentioned in literature and also encountered during our own investigations, foliated and hence anisotropic rocks show a clear correlation of the uniaxial compressive strength with the angle between foliation and loading direction (THURO 1996: 57). To receive correct values for the uniaxial compressive strength, it is necessary to keep the angle between foliation and loading direction at 90 degrees. With an angle of less than 90 degrees, an early failure of the rock sample will occur and some kind of shear strength instead of the uniaxial compressive strength will be measured. The current research follows this rule whenever it was possible. Due to difficult sampling conditions the angle between drill axis and discontinuity of some specimens differs from 90°. Whenever this issue occurs it is mentioned in the test documentation and it was considered for further calculations.

After drilling, the specimens are cut to a length which corresponds to the length/diameter ratio (L/D) of 2:1 whenever it was possible. Due to poor sampling conditions or sample quality, some samples had a lower height so smaller specimens had to be sawn.

The specimens end faces were grinded by a lapping machine to the required flatness, parallelism of both end faces (coplanar) and perpendicularity of end faces to core axis. The smoothness was controlled with a straightedge.

Testing apparatus and conducting the test

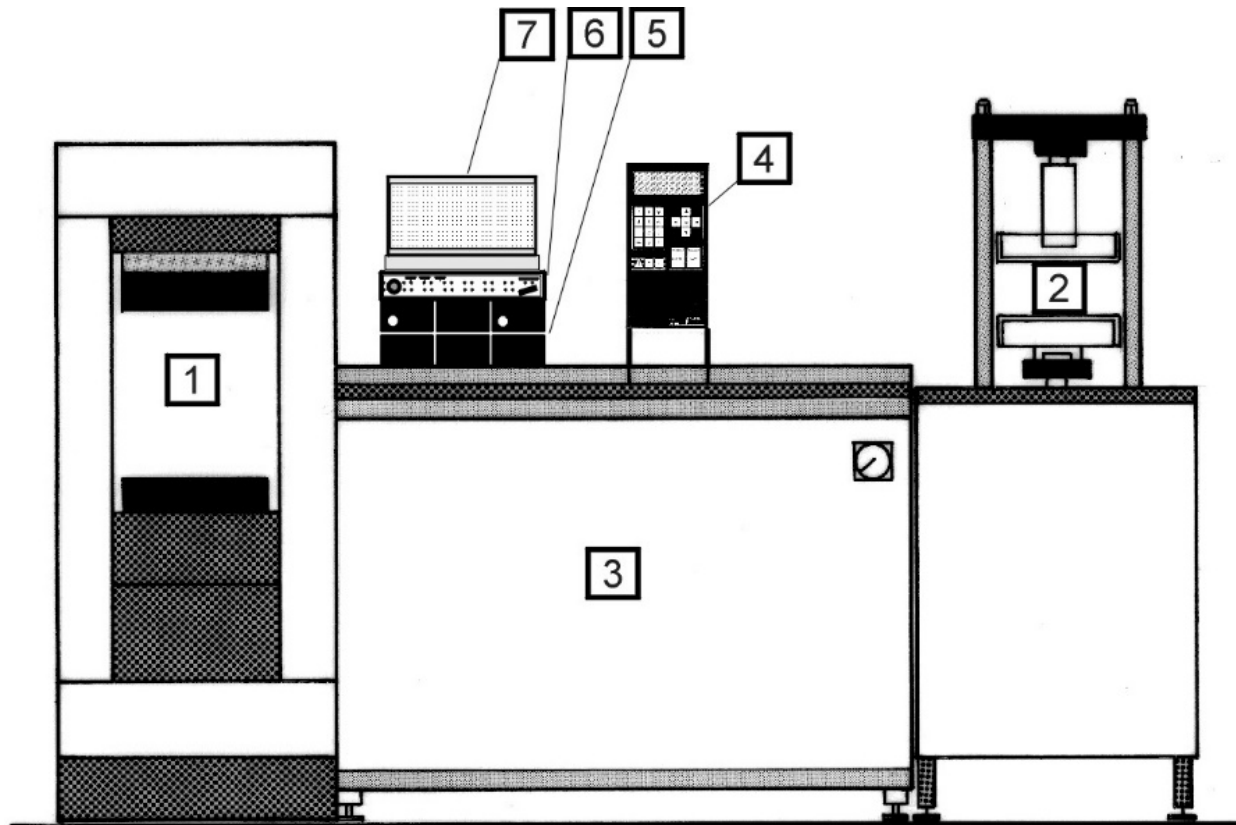


Fig. 20: Front view of Compression-Testing-Machine (according to manufacturer information).

- | | |
|---|--|
| 1) Loading frame 1 (2000 kN nominal load) | 2) Loading frame 2 (200 kN nominal load) |
| 3) „Powerbox“ (hydraulic unit) | 4) „ToniTrol“ control unit |
| 5) Measurement amplifiers for deformation recording | 6) HBM Spider 8 – buffer amplifier |
| 7) Desktop PC with reporting software named „TestXpert“ | |

For all compression tests in the laboratory we are using a servo-controlled hydraulic press (Fig. 20). This press loads the sample and measures the actual load continuously till failure of the specimen. Uniaxial compression tests are solely conducted with the big loading frame (1 in Fig. 20) with a nominal Load of 2000 kN. The machine fits the accuracy requirements of class 1 in the German standard DIN 51220 (2003). All dimensions of each sample are measured with an electronic caliper; for weighing the sample a sensitive, electronic scale was used.

The samples were loaded with a constant deformation rate of 0.06 to 0.08 mm/min (depending on the length of the tested sample) until total failure of the rock occurred. The axial deformation of the sample was measured using three digital inductive displacement transducers parallel connected to record the stress-strain curve.

Analysis and evaluation

All data is collected with a computer with the software “TestXpert” from Zwick. This software records time, deformation and current applied force, conduct all further calculation and creates the final documentation of the test.

For this study the software determines uniaxial compressive strength σ_u , modulus of deformation V and destruction work w_z .

The compressive strength (σ_u) is calculated as follows (Eqn. 1).

Eqn. 1: Calculation of failure stress as compressive strength σ_u .

$$\sigma_u = \frac{F_{max}}{A}$$

<i>with:</i>	σ_u	<i>Uniaxial compressive strength</i>	<i>[MPa]</i>
	F_{max}	<i>Failure load of sample</i>	<i>[kN]</i>
	A	<i>Cross-section area of the sample</i>	<i>[mm²]</i>

In order to the given standards and recommendations, the compressive strength (σ_u) has to be adjusted, if the sample length/diameter ratio is less than 2. The revised compressive strength $\sigma_{u(2)}$ has been calculated using Eqn. 2 from (OBERT & DUVAL 1967) cross-section area of the sample).

Eqn. 2: Calculation of adjusted compressive strength $\sigma_{u(2)}$.

$$\sigma_{u(2)} = \frac{8 \cdot \sigma_u}{7 + 2 \cdot \frac{D}{L}}$$

<i>with:</i>	$\sigma_{u(2)}$	<i>Revised compressive strength</i>	<i>[MPa]</i>
	σ_u	<i>Uniaxial compressive strength</i>	<i>[MPa]</i>
	D	<i>Diameter of sample</i>	<i>[mm]</i>
	L	<i>Length of sample</i>	<i>[mm]</i>

The modulus of deformation is determined as grade of the linear part of the graph of the recorded axial strain-stress-diagram shown in Fig. 21 and calculated with Eqn. 3.

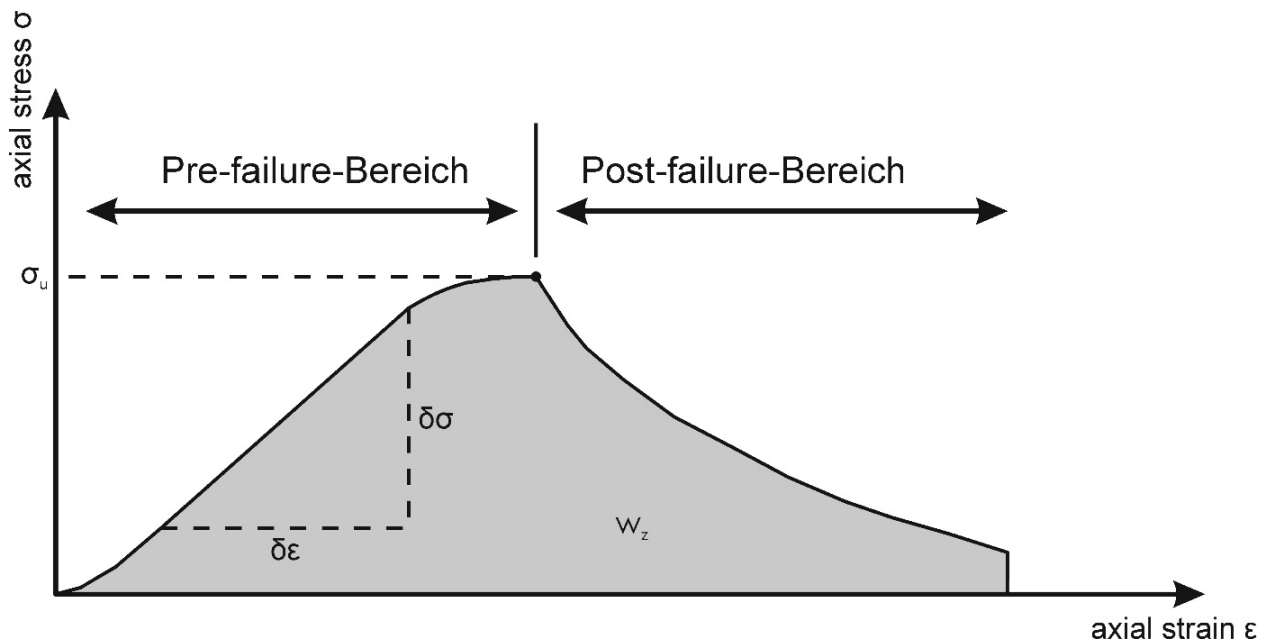


Fig. 21: Schematic sketch of the axial strain-stress curve of the uniaxial compression test. The destruction work is indicated as the grey area enclosed by the curve; $\delta\sigma$ and $\delta\varepsilon$ are used for calculating the modulus of deformation (first derivation of the linear curve segment).

Eqn. 3: Calculation of the modulus of deformation:

$$V = \frac{\delta\sigma}{\delta\varepsilon}$$

<i>with</i>	V	<i>Modulus of deformation</i>	$[MPa]$
	$\delta\sigma$	<i>Differential axial stress</i>	$[MPa]$
	$\delta\varepsilon$	<i>Differential axial strain</i>	$[-]$

and

$$\varepsilon = \frac{\delta L}{L}$$

<i>with</i>	ε	<i>Axial strain</i>	$[-]$
	δL	<i>Change in Length during test</i>	$[mm]$
	L	<i>Original length of sample</i>	$[mm]$

The area below the axial strain-stress-curve is defined as the destruction work w_z (Fig. 21, Eqn. 4).

Eqn. 4: Calculation of the destruction work:

$$w_z = \int \sigma d\varepsilon$$

<i>with</i>	w_z	<i>Destruction work</i>	$[kJ/m^3]$
	σ	<i>Axial stress</i>	$[MPa]$
	ε	<i>Axial strain</i>	$[-]$

The classification of uniaxial compressive strength is on the basis of a recommendation of the ISRM (1978a) and is shown in Fig. 22.

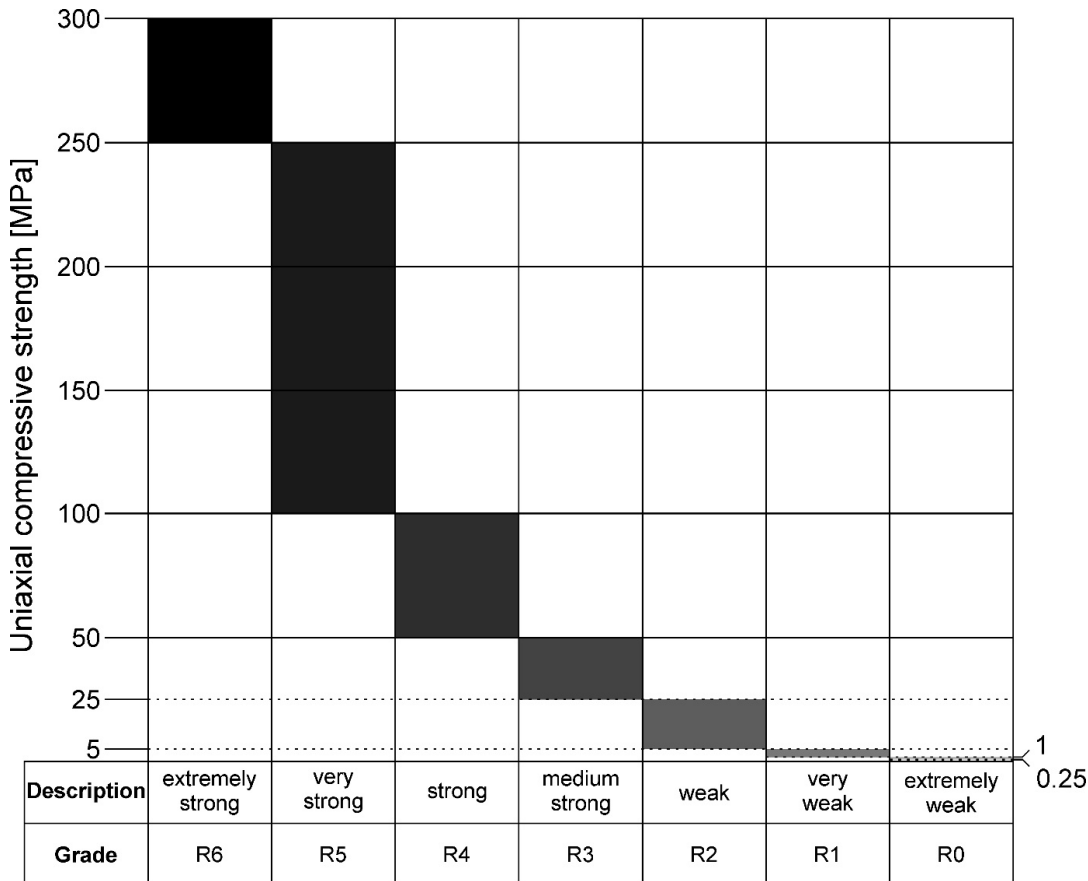


Fig. 22: Illustration of the classification scheme of the Uniaxial Compressive Strength (ISRM 1978a, edited).

5.2.1.2 Point load test (field and lab)

The point load test was conducted on 39 samples. It is used as an indirect method to determine the uniaxial compressive strength of rock samples. The test was performed according to ISRM (1985) and DGGT (2010). The point load test was performed as laboratory test and as field test.

Sample preparation

The test during field investigation can be performed with irregular but compact samples. No further sample preparation is required.

For the laboratory testing several cubic specimens (“block test”) were cut out of the rock sample. The standardized sample size of 50 x 50 x 50 mm was tried to achieve whenever it was possible. In exceptional cases at least a length-width ratio of 1:1 was used. When preparing the specimens, special attention was paid to gain samples with as few discontinuities as possible.

Testing device and conduction of the tests

For the field test a hydraulic hand pump equipped with a loading frame including point load testing pins and electronic manometer with a drag indicator is used (Fig. 23). The irregular sample is loaded with a non-constant loading rate till failure occurs. The maximum pressure is recorded and converted in stress.



Fig. 23: Illustration of the point load field testing device: Left load frame including the test cones; right hydraulic manual pump (Picture: Johan Fourie).

For this test in laboratory the same servo-controlled hydraulic press mentioned in chapter 5.2.1.1 (Fig. 20) was used. For the point load test the small loading frame (200 kN nominal load) is sufficient for loading the sample and measuring the occurring failure load. The machine fits the accuracy requirements of class 1 in the German standard DIN 51220 (2003). The loading frame can be equipped with point load testing pins as shown in the schematic view in Fig. 24.

The samples were loaded with a constant stress rate of 0.5 MPa/s until total failure of the specimen occurred. The failure load and time is measured with the Software “TestXpert” from Zwick. This software is also used for final analysis and creation of the documentation of the test. After the test the exact failure surface is determined with a sliding caliper performing 2 perpendicular measurements.

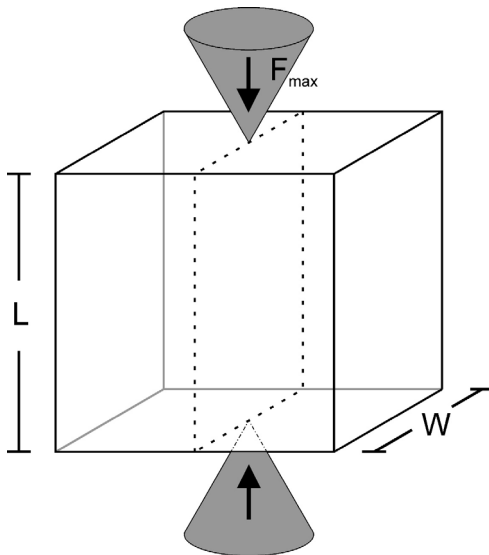


Fig. 24: Sketch of the point load test, the measured variables and the applied force.

Analysis and Evaluation

From the failure load and the failure surface the point load index I_s is derived using the following equation (Eqn. 5)

Eqn. 5: Calculation of the point load index I_s .

$$I_s = \frac{F_{max}}{D_e^2}$$

with I_s Point load index [MPa]
 F_{max} Failure load of sample [kN]

and

$$D_e^2 = W \cdot L$$

with D_e^2 Area of failure surface [mm²]
 W Width of failure surface [mm]
 L Length of failure surface [mm]

Due to scaling effects occurring with different sample size all results were correlated with Brook's equation (BROOK 1993) (Eqn. 6) to a standard sample size of 50 x 50 x 50 mm.

Eqn. 6: Calculation of the Point-Load-Index correlating to standard sample dimension of 50 x 50 x 50 mm.

$$I_{50} = f \cdot \frac{F_{max}}{D_e^2}$$

with I_{50} Point load index correlating to standard sample size [MPa]
 F_{max} Failure load of sample [kN]
 D_e^2 Area of failure surface [mm²]
 f Correction factor [-]

and

$$f = \left(\frac{D_e^2}{2500} \right)^{0.225}$$

From the I_{50} the uniaxial compressive strength σ_m is derived using the correlation factor c (Eqn. 7). c is an empirically determined constant. Generally $c = 20$ but in some cases when point load tests and uniaxial compressive strength test were conducted c can be determined and used for further calculations. Within this work c will be specified for each test.

Eqn. 7: Calculation of uniaxial compressive strength derived from I_{50} .

$$\sigma_m = c \cdot I_{50}$$

with	σ_m	Derived uniaxial compressive strength	[MPa]
	c	Correlation factor	[-]
	I_{50}	Point load index correlating to standard sample size	[MPa]

5.2.1.3 Brazilian tensile test

The Brazilian Tensile Strength Test according to the German recommendation no. 10 of the DGGT (2008) is used as an indirect method to determine the tensile strength of rock samples. During the current PhD thesis this test was conducted on a total of 60 samples. Fig. 25 shows a schematic test setup with all occurring forces.

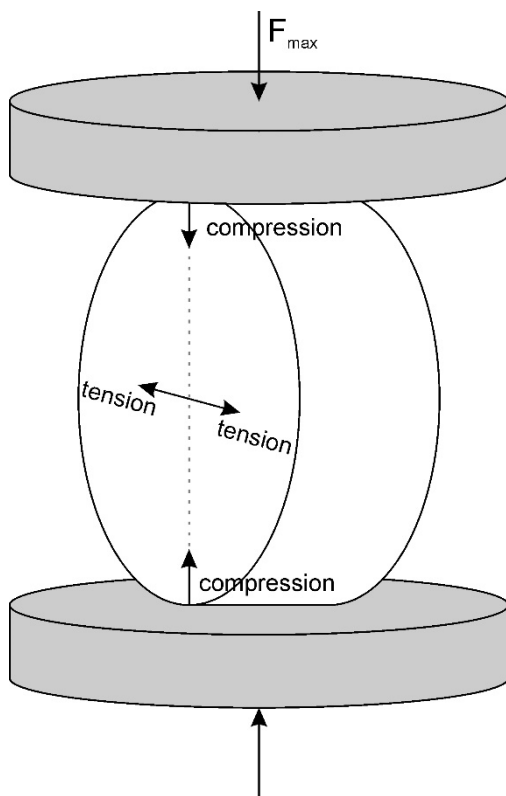


Fig. 25: Schematic sketch of the indirect tensile force in Brazilian tensile strength testing with the applied forces.

Sample preparation

Cylindrical specimens with a length-diameter ratio of 0.5 (+/- 0.2) were drilled out of bigger rock samples, where great effort was put into the sample preparation in order to gain samples with as few discontinuities as possible.

Testing device

For this test also the small loading frame (200 kN nominal load) of the servo-controlled hydraulic press (Fig. 20) was applied and recording of the failure load of the cylindrical specimen was accomplished. The loading frame is equipped with Brazilian tensile strength loading brace. Before the test the exact dimensions

of the sample are determined using a sliding caliper (2 perpendicular measurements). Afterwards the samples are loaded until failure and the maximum load is recorded using the software *TestXpert*.

Analysis and evaluation

From the failure load and the area of the failure surface, the Brazilian Tensile Strength $\sigma_{t,bts}$ is determined using the Eqn. 8.

Eqn. 8: Calculation of the Brazilian Tensile Strength.

$$\sigma_{t,BTS} = \frac{2 \cdot F_{max}}{\pi \cdot D \cdot L}$$

<i>with</i>	$\sigma_{t,BTS}$	<i>Brazilian tensile strength</i>	<i>[MPa]</i>
	F_{max}	<i>Failure load of sample</i>	<i>[kN]</i>
	D	<i>Diameter of sample</i>	<i>[mm]</i>
	L	<i>Length of sample</i>	<i>[mm]</i>

The ratio of $\sigma_{t,BTS}$ and σ_u is used as indicator for brittleness, respectively the ductility of a rock (Eqn. 9, Tab. 6). This classification is used in many theses but is in discussion at the moment by the PhD thesis of Wilfing (in preparation).

Eqn. 9: Calculation of brittleness z .

$$z = \frac{\sigma_u}{\sigma_{t,BTS}}$$

<i>with</i>	z	<i>Brittleness of sample</i>	<i>[-]</i>
	σ_u	<i>Uniaxial compressive strength</i>	<i>[MPa]</i>
	$\sigma_{t,BTS}$	<i>Brazilian tensile strength</i>	<i>[MPa]</i>

Tab. 6: Classification of brittleness (SCHIMAZEK & KNATZ 1976: 117 and BECKER & LEMMES 1984: 74 in THURO 1996: 74).

z [-]	Classification
> 20	very brittle
20 - 10	brittle
10 - 5	ductile
< 5	very ductile

5.2.2 Abrasivity

5.2.2.1 Cerchar abrasivity test

The Cerchar Abrasivity Test was conducted on 24 specimens according to the testing recommendation of Centre d'Études et Recherches de Charbonnages de France CERCHAR (1986) and ALBER et al. (2014).

Sample preparation

For this test rock samples with a rough surface were used. The surface roughness was produced by fracturing the rock with the point load or the Brazilian tensile test. Due to the testing condition for point load test and Brazilian tensile test, this failure surface was perpendicular to all potential occurring discontinuities.

Testing device

The testing device (Fig. 26) is in accordance with the modified CERCHAR-device presented in WEST (1989).

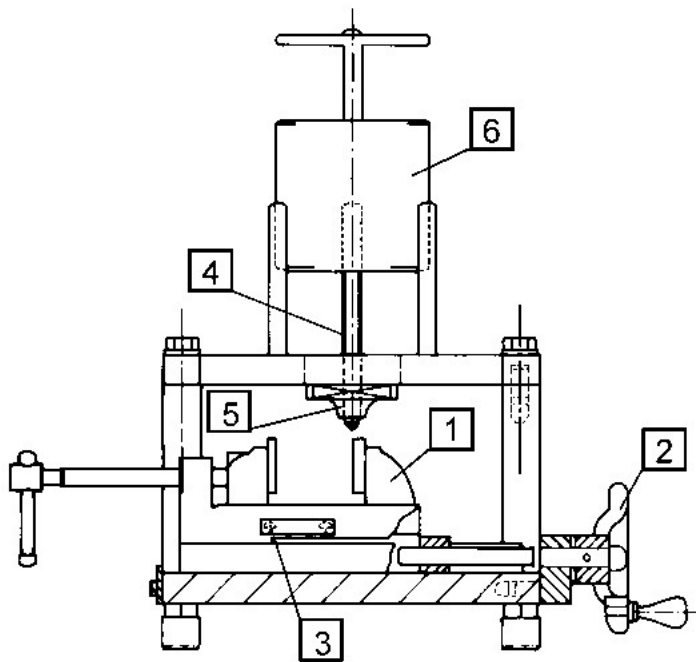


Fig. 26: Illustration of the CERCHAR-device for the determination of the CERCHAR-Abrasivity-Index (according to WEST 1989, modified).

- | | | |
|----------------|-----------------|--------------------|
| 1) Device | 2) crank handle | 3) precision slide |
| 4) testing pin | 5) pin guide | 6) weight |

A steel testing pin with defined geometry and quality (HRC 54-56) is scratched over 10 mm of the rough surface of the specimen. The steel pin is loaded with a static weight of 7 kg. Each sample is scratched 5 times.

Analysis and evaluation

For test analysis the worn steel pin (Fig. 27) is examined with a reflected-light binocular with a measuring scale and the diameter of the flattened area is determined with the accuracy of 0.02 mm. As recommended by Käsling et al. (KÄSLING et al. 2006) each steel needle is measured in 4 perpendicular directions and the results are averaged.

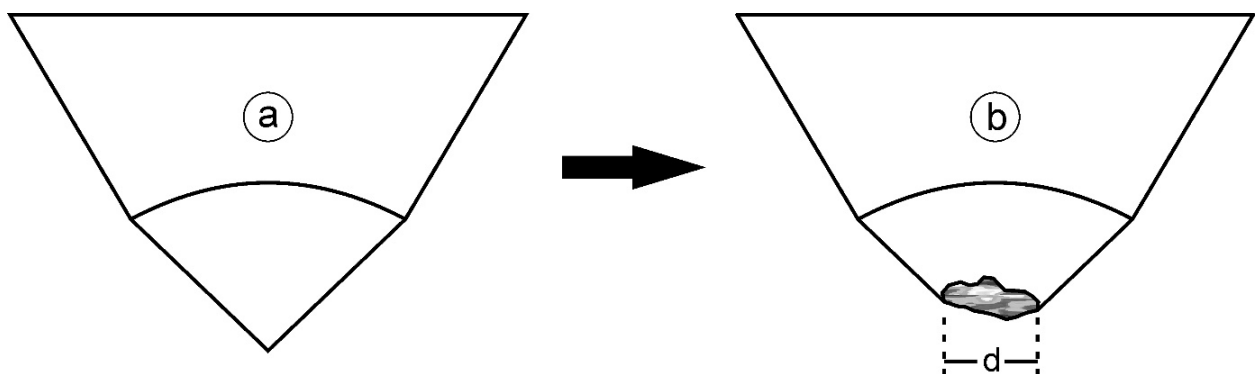


Fig. 27: Schematic sketch of the steel pin before (a) and after (b) testing.

The CERCHAR Abrasiveness Index (**CAI**) is calculated using Eqn. 10 and the wear of the steel needle (d). An evaluation of the abrasiveness is performed according to the classification table below (Tab. 7).

Eqn. 10: Calculation of the Cerchar Abrasiveness Index (CAI).

$$CAI = d \cdot 10$$

with CAI Cerchar Abrasiveness Index [-]
 d Wear of the steel pin [mm]

Tab. 7: Abrasiveness classification using the CAI-Test (according to CERCHAR 1986: 7).

CAI	Classification
0.3-0.5	not very abrasive
0.5-1.0	slightly abrasive
1.0-2.0	medium abrasiveness
2.0-4.0	very abrasive
4.0-6.0	extremely abrasive

5.2.2.2 LCPC abrasivity test

LCPC Abrasivity test was performed on 26 specimens according to the French standard (normalisation française AFNOR) P 18-579 (1990), THURO & KÄSLING (2009) and KÄSLING & THURO (2010). The LCPC Abrasivity Test was developed for the determination of the abrasiveness and breakability of hard rock by the *Laboratoire Central des Ponts et des Chaussées* (LCPC). For this thesis the LCPC Abrasivity Coefficient LAC [g/t] and the LCPC Breakability Coefficient LBC [%] are determined.

Sample preparation

For this test 500 g \pm 0.02 g of sample material are needed. Therefore, the sample is broken with a jaw breaker to a grain size of 4 to 6.3 mm. Smaller particles are removed with dry sieving.

Testing device

The LCPC Abrasivity Tests were performed at the Chair for Engineering Geology of the Technische Universität München using an abrasivity testing device („abrasimeter“) shown in Fig. 28 according to the French standard P 18-579 (1990).



Fig. 28: Left: Abrasimeter with a 700 W electric motor (1), sample container (2) and funnel tube (3) for the filling of the sample container (closed during operation). Right: Mounted metal impeller, which rotates with a speed of 4500 rpm for 5 minutes through the sample.

The rectangular metal impeller with standardized Rockwell hardness (B 60-75) and dimensions (5 x 25 x 50 mm) shown in Fig. 29 is weighed with an accuracy of 0.01 g. After weighing the impeller and closing of the sample container, 500 g of the dried, broken sample were filled into the machine through the sample funnel on top of the machine. After sealing the funnel, the machine is started and rotates the impeller within the sample with 4500 rpm for exactly 5 min inside the sample container.

The sample container with the tested sample is carefully dismantled to preserve all of the test material. The fraction smaller than 1.6 mm of the broken sample is determined with sieving and weighing with an accuracy of 0.01 g for the LCPC Breakability Coefficient LBC. For the determination of the LCPC Abrasivity Coefficient LAC the impeller is again weighed with an accuracy of 0.01 g.

Analysis and evaluation

During the abrasion test, with the rotation of the impeller the steel gets worn and eroded at the edges and on the surfaces thus the material gets less and the impeller is lighter (Fig. 29). Also the rock material gets worn and the grains are crushed (Fig. 30). This effect is influenced by the breakability of the rock.



Fig. 29: LCPC impeller before (left) and after (right) test run, indicating the abrasiveness of the material.



Fig. 30: LCPC sample before (left) and after (right) test run. The grain size ranges between 4 and 6.3 mm before testing.

As measure for abrasivity the LCPC Abrasivity Coefficient is determined by the mass loss of the metal impeller during this test as shown in Eqn. 11.

Eqn. 11: Calculation of the LCPC Abrasivity Coefficient.

$$LAC = \frac{m_{F0} - m_F}{m_s}$$

<i>with</i>	m_{F0}	<i>Mass of metal impeller prior test</i>	<i>[g]</i>
	m_F	<i>Mass of metal impeller after test</i>	<i>[g]</i>
	m_s	<i>Total sample mass</i>	<i>[t]</i>

For rocks the LAC typically ranges between 0 and 2000 g/t. This range is characterized by 6 classes which are shown in Tab. 8. This classification is adapted to CAI classification. The usual classes introduced by BÜCHI et al. (1995) do not support this correlation and therefore are not used.

Tab. 8: Classification of the LCPC Abrasivity Coefficient LAC in accordance to the Cerchar Abrasivity Index CAI and the associated terminology.

LAC [g/t]	CAI	Abrasivity terminology	Examples as hard rock and as components of granular soil
0 – 50	0 – 0.3	not abrasive	wood, turf
50 – 100	0.3 – 0.5	not very abrasive	clay-silt stone, marl
100 – 250	0.5 – 1.0	slightly abrasive	schist, sandstone (fine grained, argillaceous cement), limestone (pure), marble (pure)
250 – 500	1.0 – 2.0	medium abrasiveness	limestone (sandy), marble (containing quartz) sandstone (calcareous cement)
500 – 1250	2.0 – 4.0	very abrasive	sandstone (quartzitic cement), porphyry, andesite, basalt, phyllite, mica schist, some amphibolite
1250 – 2000	4.0 – 6.0	extremely abrasive	(vein-) quartz, granite, quartzite, eclogite, gneiss, some amphibolite

The LCPC Breakability Coefficient (LBC) is calculated incorporating the total sample mass and the mass fraction smaller than 1.6 mm after the test run using Eqn. 12. The LBC is classified according to Tab. 9.

Eqn. 12: Calculation of the LCPC Breakability Coefficient.

$$LBC = \frac{100 \cdot m_{1,6}}{m_s}$$

<i>with</i>	$m_{1,6}$	<i>Mass fraction with grain size <1.6 mm</i>	<i>[g]</i>
	m_s	<i>Total sample mass</i>	<i>[g]</i>

Tab. 9: Classification of the LCPC Breakability Coefficient LBC, according to BÜCHI et al. (1995).

LBC [%]	Breakability-Classification
0 – 25	very poor
25 – 50	medium poor
50 – 75	medium
75 – 100	medium high
> 100	very high

5.2.2.3 Thin section and X-Ray Diffraction analysis

The mineral content was determined for every sample.

Sample preparation

From every sample a petrographic thin section of 25 µm thickness of for qualitative analysis and an estimation of mineral content was prepared.

For a full quantitative X-Ray diffraction analysis, a fine powder from every sample was created. To achieve a grain size smaller than 0.5 mm the samples were disaggregated by using an agate mortar. Two grams of the sample were ground for 8 minutes with 10 ml of isopropyl alcohol in a McCrone Micronising Mill using agate cylinder elements. The suspension was filtered, dried, and homogenized in an agate mortar by hand.

Testing facilities

The used microscope equipment is a ZEISS-microscope with 32- to 500-times magnified. The pictures of the thin sections were recorder with a digital camera.

The XRD analyses (2-70° 2θ) were performed on top-loaded powder mounts using a Philips-Panalytical PW 1800 X-ray diffractometer (CuKα, graphite monochromator, 10 mm automatic divergence slit, step-scan 0.02° 2θ increments per second, counting time 1s per increment, 40 mA, 40 kV).

Determination of mineral content

The minerals were identified under the microscope during the qualitative analysis by their optical characters. The structural fabric, potential weathering, preexisting cracks and other peculiarities were assessed.

The identification of crystalline mineral phases was carried out using the characteristic diffraction lines and their d-values with the program IDENTIFY (Philips-Panalytical). Clay minerals were identified using the basal diffraction lines on oriented mounts and their changes on glycolization and heating to 550 °C (MOORE & REYNOLDS 1997). The crystalline phases in the whole rock powder were quantified using the Rietveld-program BGMN (BERGMANN et al. 1998).

Determination of the Equivalent Quartz Content

Another important parameter in the context of rock-abrasivity classification is the equivalent quartz content EQc. It is a value which describes the content of abrasive minerals within the sample and reflects their abrasiveness in relation to quartz, since quartz, with a Mohs hardness of 7, is considered to be the most important mineral for abrasiveness of rock. The equivalent quartz content is influenced by minerals with a hardness higher than steel (about 7 on the Mohs scale) but also by minerals with much lower hardness.

The EQc is determined by the sum of all mineral content multiplied by their corresponding abrasion resistance related to quartz (Eqn. 13). Thereby minerals with a higher hardness than 5.5 on Mohs scale contribute significantly to the EQc.

Eqn. 13: Determination of the Equivalent Quartz Content using the grinding hardness according to Rosiwal (1916).

$$EQc = \sum_{i=1}^n A_i \cdot S_i$$

<i>with</i>	A_i	<i>Percentage of the particular mineral</i>	<i>[%]</i>
	S_i	<i>Rosiwal-grinding hardness (related to quartz)</i>	<i>[%]</i>
	n	<i>Number of all considered minerals</i>	<i>[-]</i>

The determination of the grinding hardness (considered equivalent to the abrasion resistance in this context) is related to the recommendation of ROSIWAL (1896) and ROSIWAL (1916). The dependency between the scratch hardness according to MOHS and the grinding hardness according to ROSIWAL (1896 and 1916) is given in Fig. 31. By use of this diagram, the grinding hardness of minerals can be estimated, even if it was not determined in a laboratory test.

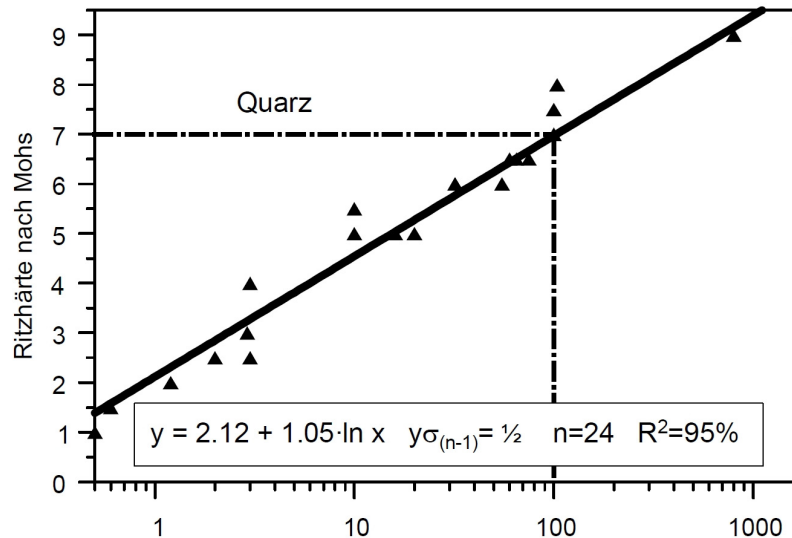


Fig. 31: Grinding hardness according to ROSIWAL (mean values) plotted against the scratch hardness according to MOHS in a semi logarithmic diagram (THURO 1996) including the appropriate a semi logarithmic regression curve (appears as straight line) with its statistical parameters.

5.2.3 Determination of further properties

5.2.3.1 Ultrasonic tests

We determine the p-wave velocity of our rock samples with a simple ultrasonic transmission test (longitudinal wave) according to DIN EN 14579 (2005). The transmission test can also be performed in the field. The tests are conducted on standardized samples in the rock laboratory. For samples with irregular geometry e.g. in the field the p-wave velocity can also be determined.

Sample preparation

Irregular formed samples out in the field don't need further preparation as long as they have a nearly square-built layout respectively sample length is minor to sample width for best results. But generally speaking almost any sample can be tested.

For conducting the test in laboratory standardized samples are used. In most cases cylindrical samples with smoothed end faces and a diameter to length proportion of at least 1:2 which are prepared for uniaxial compressive strength tests will be used.

Testing apparatus and conducting the Test

We are testing with a complete system from Geotron Elektronik consisting of an ultrasonic generator (USG-40), a preamplifier (VV40) an oscilloscope (Scopemeter, PicoScope 4000) and one transmitter and one receiver probe. The type of transmitter and receiver are depending on testing conditions (p-wave/elastic properties) and measured length of the sample. The oscilloscope is connected to a computer on which the testing Software (Lighthouse UMPC) is installed. Before sample testing starts the whole system has to be calibrated using a runtime standard with known elastic and mechanical properties. The calibration and the sample testing are done in a similar way. Changes in terms of conducting for the different tests will be mentioned in the text. The testing setup for transmission testing is shown in Fig. 32.

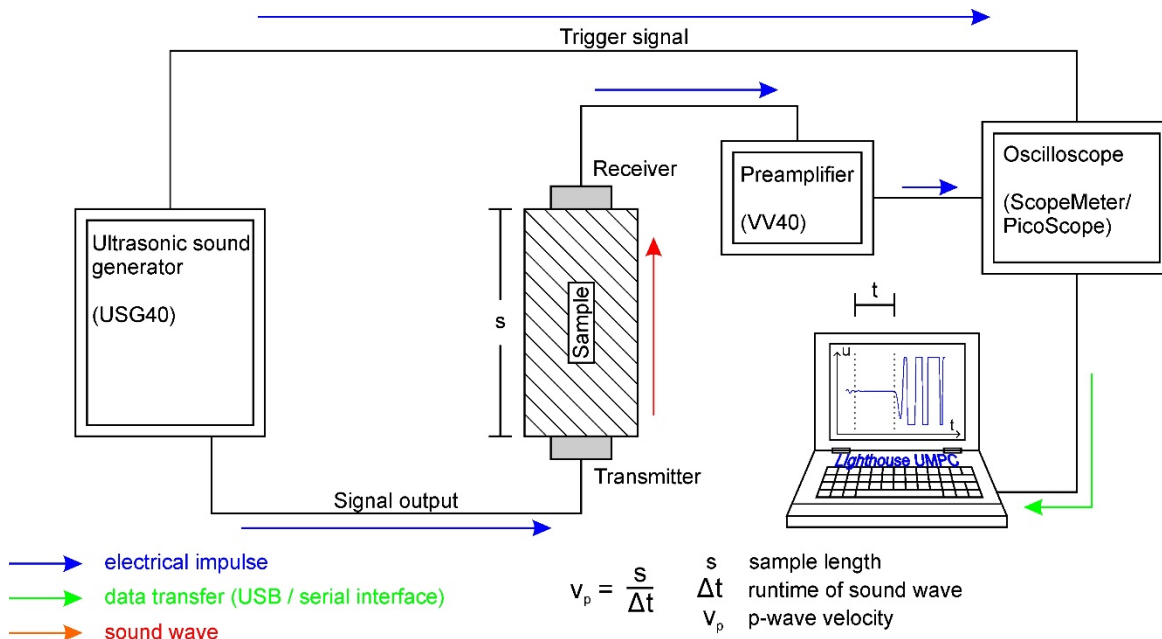


Fig. 32: Testing setup for transmission testing determining p-wave velocity.

The sample or the standard is installed in a testing frame as shown in Fig. 33. We use two equivalent constructed test frames with built in detector heads for a faster testing procedure for longitudinal and quasilongitudinal measurements on one sample. The sample/standard is fixed and loaded with air pressure of 2-4 Bar within the test frame for better contact between specimen and detector heads. Sometimes a contact fluid is needed to improve the contact surface. This contact fluid has not to be renewed between calibration and sample testing. After loading the sample, the ultrasonic wave is generated by the help of the ultrasonic sound generator (USG 40) which stimulates the piezoelectric probe. The wave runs through the sample and is detected by a second detector head which leads the signal to an oscilloscope detecting the wave. For the transmission test a preamplifier is required between the detector head and the oscilloscope. The oscilloscope translates the wave signal in a computer signal and sends the data to the connected computer.

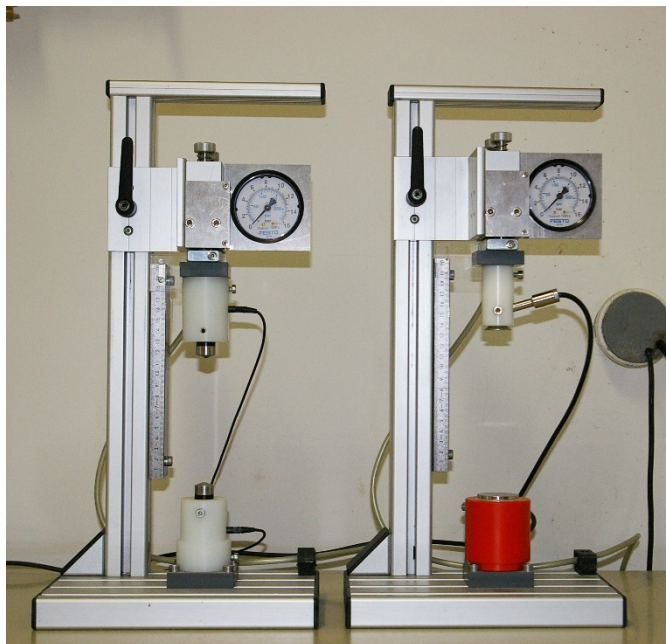


Fig. 33: Testing frame for ultrasonic tests. Left: extensional Wave frame; Right: Transmission testing frame which was mainly used for this research.

Analysis and evaluation

For the determination of p-wave velocity v_p the sample length is measured with an accuracy of 0.01 mm. Due to larger test dimensions and irregular samples the sample dimensions are only determined with a folding ruler and a caliper with an accuracy of 1 mm during field testing. With the sample length and the runtime of the wave inside the sample, v_p can be calculated (Eqn. 14) using the Software Lighthouse UMPC.

Eqn. 14: Calculation of velocity of longitudinal waves.

$$v_p = \frac{L}{\Delta t}$$

<i>with</i>	v_p	<i>p-wave velocity of the sample</i>	<i>[m/s]</i>
	L	<i>Sample length</i>	<i>[m]</i>
	Δt	<i>Runtime of ultrasonic wave in the sample</i>	<i>[s]</i>

5.3 Determination of the drill data

For the determination of the drill data, drill tests were conducted in the field and in the Hilti test laboratory. All tests were conducted using similar rock drills of the type TE MD 20 and different drill heads. To gather comparable data in addition to several different drill heads, as described in the previous chapter, one standard bit was used in all tests.

5.3.1 Drill head design

To create a decision map for the right drill head according to geology respectively rock mechanical properties, several drill head layouts were tested. These layouts differ in drill head diameter and button configuration and count. Additionally, another series of similar drill heads with differing design were tested to get the best performance and wear properties for one layout.

To optimize the drill head design 7 parameters were changed and different drill head specimen were tested to obtain data to create a tool to choose the most appropriate drill head for each geology.

The following 7 parameters are illustrated which were changed during the test period are visualized in Fig. 34:

- Angle between hard metal buttons (A-1)
- Angle between hard metal buttons and flush hole axis (A-2)
- Approach angle of hard metal buttons (B)
- Diameter of hard metal buttons
- Arrangement and number of flush holes (top/side/sloped)
- Shape of the hard metal buttons
- Shape of the flush channel on the side of the drill head

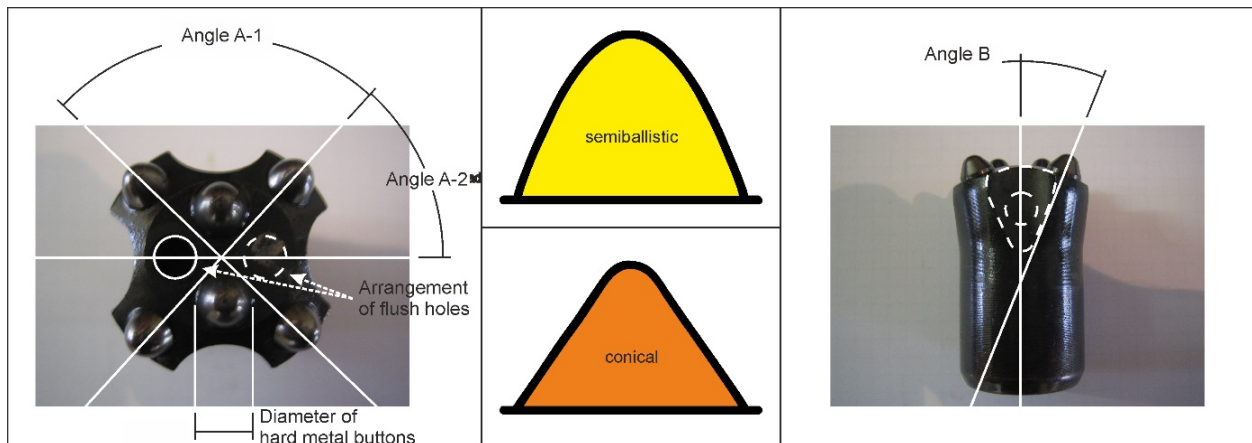


Fig. 34: Sketch of all important parameters which have been changed during the research project in order to optimize the drill head performance, the wear and to adapt the drill head perfectly to the occurring geology.

Due to confidentiality all drill heads which are published in this thesis are anonymized. All aliases are unique and clearly connected to only one drill head to achieve a comprehensibly comparison among all drill heads.

5.3.2 Testing under defined conditions

The testing under defined conditions was conducted at the Hagerbach Test Gallery (Switzerland), at various quarries and in the Hilti Testing Laboratory in Kaufering (Germany). For the current testing the rock drill is installed on a drill rig (Fig. 35) or on a similar but nonmoving drill mount for four parallel rock drills in the test laboratory. To minimize the effects of different contact forces due to the test setting, the water leg and the drill are setup in one line (in line) with the drill rod (Setup C in Fig. 36). The water leg is operated with similar pressure to maintain an equal force on the drill head for every conducted test. The energy and the water comes from the general power supply of the mine/quarry and is almost infinite available.



Fig. 35: In line drill test set-up with a drill rig at the Hagerbach Test Gallery (Switzerland) (Picture: Stefan Götzfried).

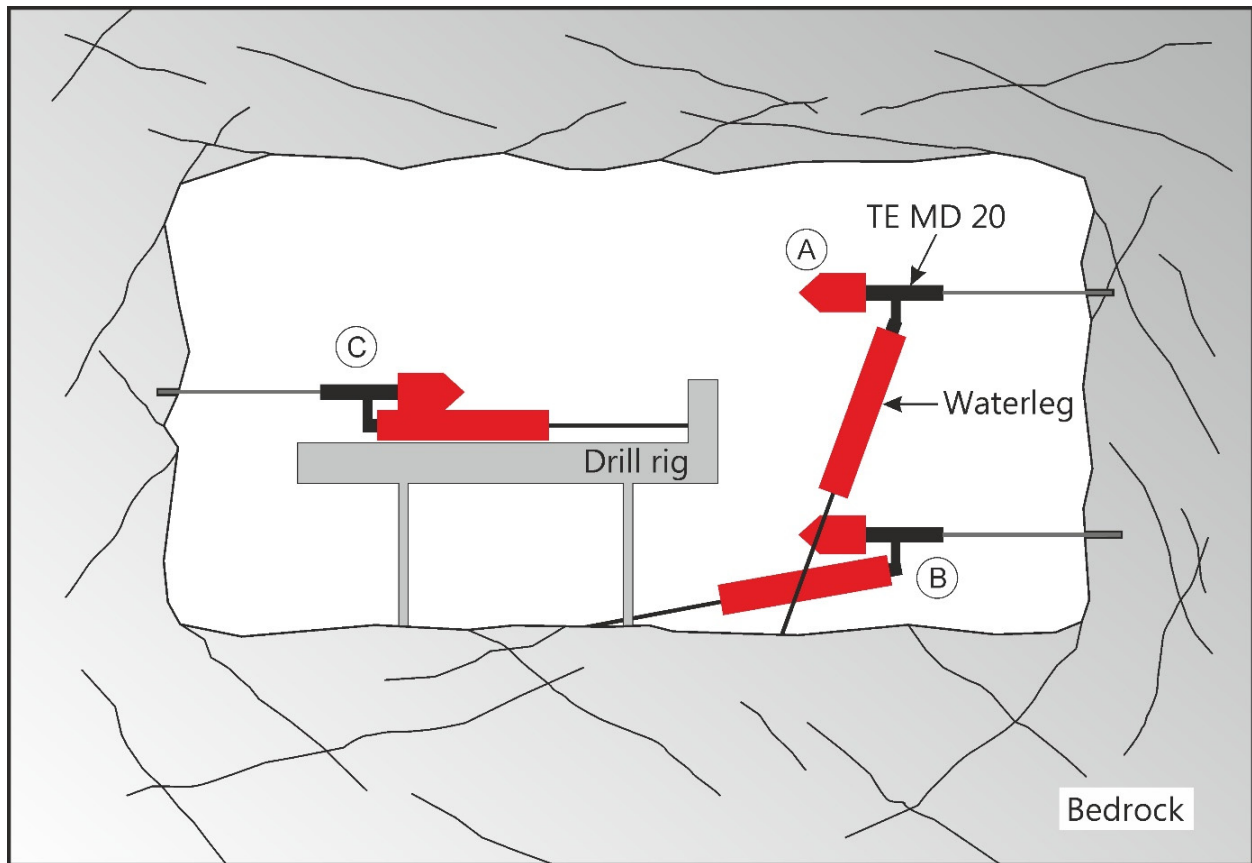


Fig. 36: Sketch of different drills illustrating varying contact force setups due to different working geometry. (A) Lower contact force; (B) Increased contact force; (C) Maximum contact force (In-line condition).

The netto time which is needed to drill one hole is timed in seconds with a stopwatch and is noted. The depth of all drill holes was determined in cm with the use of a folding ruler. The diameter of the drill head is measured with a sliding caliper to determine the weight loss and the loss in diameter of the head. The occurrence of any problem like jamming of the drill head, loss of flush fluid or electrical power outage was noted.

5.3.3 Field testing and on-site testing

Unfortunately, the drill rig is very bulky and hard to transport and setup. Depending on the site conditions it is in several cases impossible to use. Due to this circumstance hand controlled drill tests are sometimes required. For the manual testing the rock drill is connected to a power generator and is flushed by the help of a water pump. The drill itself is hand driven as shown in Fig. 37. Due to the weight and the unhandiness of the drill, the drill rod and the waterleg, it is impractical to drill in a regular drill pattern (Fig. 38). The spacing between the holes and the sampling holes should be chosen large enough to avoid any interference of the drill holes.

The netto time which is needed to drill one hole is timed in seconds with a stopwatch and is noted. All drill hole-depths were determined in cm with the use of a folding ruler. The diameter of the drill head is measured with a sliding caliper to determine the weight loss and the loss in diameter of the head. Any occurrence of problems like jamming of the drill head, loss of flush fluid or electrical power outage was also noted. For all handheld drill tests the inline condition (C in Fig. 36) could not be achieved. Only case A and B in Fig. 36 could be realized. Due to this fact for all tests the height from the ground was measured with a folding ruler to analyze the influence of geometry for the drilling process.



Fig. 37: Field drill testing in progress. One person is drilling and the second one is registering the drilling time for each hole.



Fig. 38: Exemplified drill pattern and bore holes for rock sampling in the quarry of Miltenberg.

5.3.4 Analysis and evaluation of drill testing

For the drill testing all data is collected in tables. Interesting facts for each drill head are the average performance, average wear, drill life time and of minor importance the performance drop. The definition of all properties follows in this chapter.

The average performance is the arithmetic mean of the performance p of all drillings. It's measured as cm/min or min/m following Eqn. 15 and Eqn. 16.

Eqn. 15: Calculation of average performance in [cm/min].

$$\bar{p} = \frac{1}{n} \sum_{i=1}^n \frac{x_i}{t_i}$$

<i>with</i>	p	<i>Performance of the drill</i>	[cm/min]
	n	<i>Number of drill holes</i>	[-]
	x	<i>Depth of each drill hole</i>	[cm]
	t	<i>Netto drill time for each hole</i>	[min]

Eqn. 16: Calculation of average performance in [min/m].

$$\bar{p} = \frac{1}{n} \sum_{i=1}^n \frac{t_i}{x_i}$$

The average wear is the arithmetic mean of the drill head diameter (Eqn. 17) or material loss (Eqn. 18) over the drilling length. Due to the size of the blasting cartridge the final diameter of the drilling hole is an important factor. Due to this fact we concentrated the thesis on the gauge wear only.

Eqn. 17: Calculation of average wear in [μ m/m].

$$w_d = \frac{\Delta d}{x_{total}}$$

<i>with</i>	w_d	<i>Wear of a drill head</i>	[μ m/m]
	Δd	<i>Change in caliber diameter of drill head</i>	[μ m]
	x_{total}	<i>Sum of all depths of each drill hole</i>	[m]

Eqn. 18: Calculation of average wear in [μ g/m].

$$w_m = \frac{\Delta m}{x_{total}}$$

<i>with</i>	w_m	<i>Wear of a drill head</i>	[μ g/m]
	Δm	<i>Mass loss of drill head</i>	[μ g]
	x_{total}	<i>Sum of all depths of each drill hole</i>	[m]

The drill lifetime is defined as maximum distance drilled with one drill head till it is sorted out due to wreckage or passing the threshold of wear which is set up by the drilling operator. This parameter is outdated with the introduction of p_{10} .

For all tests wherever it is possible, respectively for all drill tests where at least 20 drillings were possible, the performance drop p_d is calculated as ratio of the average performance of the first 10 drillings and the average performance of the last 10 drillings (Eqn. 19).

Eqn. 19: Definition of the performance drop.

$$p_d = \frac{\frac{1}{10} \sum_{i=n-10}^n \frac{x_i}{t_i}}{\frac{1}{10} \sum_{i=1}^{10} \frac{x_i}{t_i}}$$

All test are plotted inside our database as performance plot (Fig. 39) and as wear plot (Fig. 40).

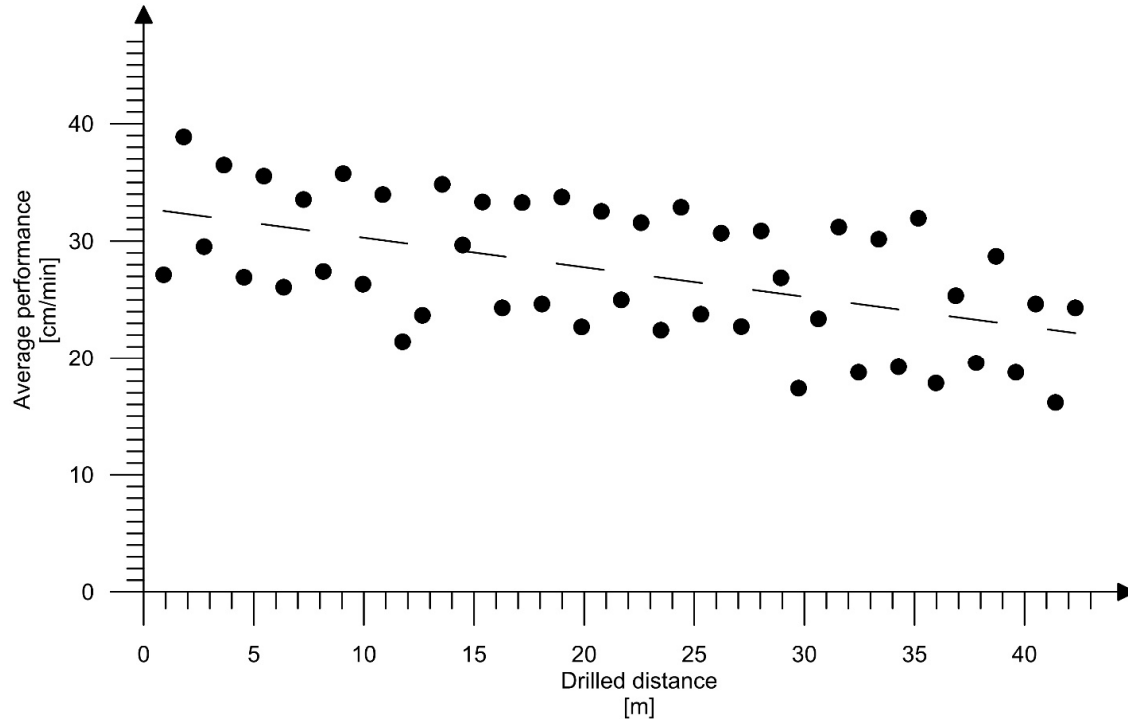


Fig. 39: Exemplified performance diagram including the drill distance plotted versus the average speed per drill hole.

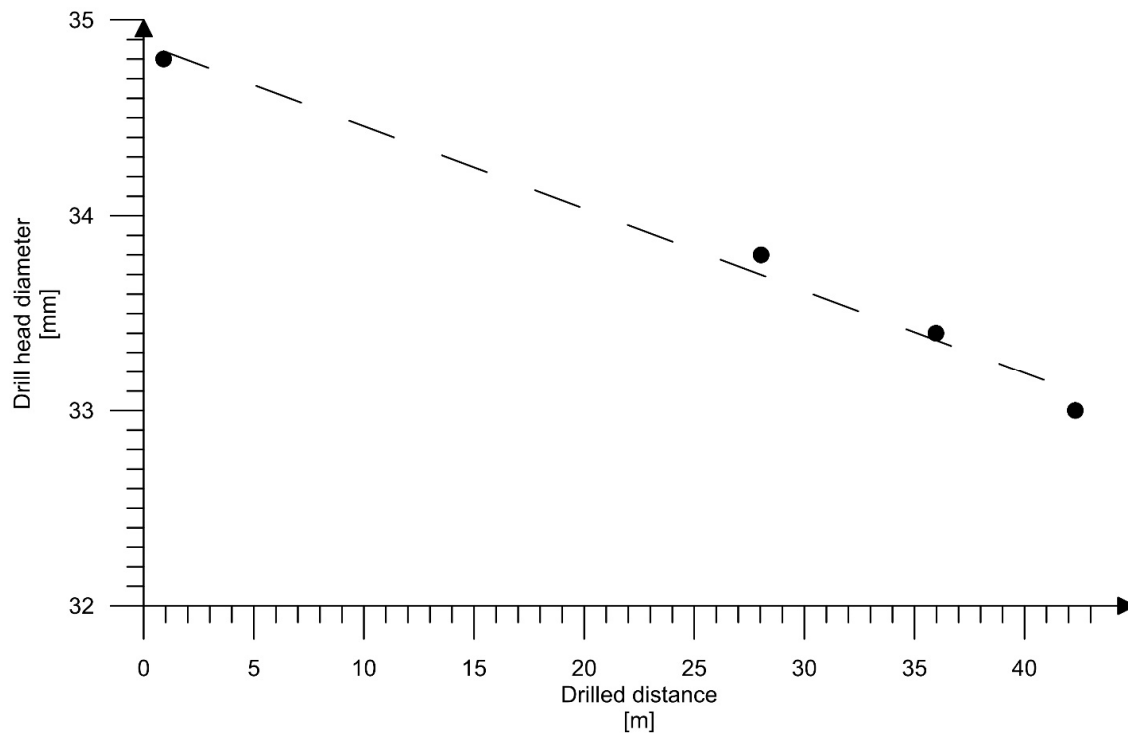


Fig. 40: Exemplified diagram for the wear as the first derivation of the fitted curve; the drill distance is plotted against the drill head diameter.

6 Sample description, results and result interpretation

The macroscopic and microscopic description of all samples and the test results of all laboratory and field tests are summarized and explained in the following chapter. A description of all tested rock samples can be found in Tab. 10.

Tab. 10: List of all tested rock samples during the project.

Sample name	Project name	Rock type	Further descriptions
HIL-KLF-02	Kloof #8	Quartzite	
HIL-KLF-03	Kloof #8	Quartzite	
HIL-KLF-04	Kloof #8	Quartzite	
HIL-KLF-05	Kloof #8	Quartzite	
HIL-KLF-06	Kloof #8	Quartzite	
HIL-TAU-07	Tautona	Quartzite	
HIL-TAU-08	Tautona	Quartzite	
HIL-TAU-F1	Tautona	Quartzite	Hanging Wall
HIL-TAU-F2	Tautona	Quartzite	Foot wall
HIL-TAU-F3	Tautona	Quartzite	Reef
HIL-MOA-F1	Moab Kothsong	Quartzite	Hanging Wall
HIL-MOA-F2	Moab Kothsong	Quartzite	Foot wall
HIL-MOA-F3	Moab Kothsong	Quartzite	Reef
HIL-BLU-01	Blue Ridge	Anorthosite Chromite	
HIL-BF-1	Brakfontein	Anorthosite	Ore
HIL-BF-2	Brakfontein	Anorthosite	Waste
HIL-BF-F1	Brakfontein	Anorthosite	Waste
HIL-BF-F2	Brakfontein	Anorthosite	Ore
HIL-HAC-1	Hackney	Anorthosite	Ore
HIL-HAC-2	Hackney	Anorthosite	Waste
HIL-HAC-F1	Hackney	Anorthosite	Waste
HIL-HAC-F2	Hackney	Anorthosite	Ore
HIL-TWI-F1	Twickenham	Anorthosite	Waste
HIL-TWI-F2	Twickenham	Anorthosite	Ore
HIL-PEA-1	Peakstar	Kimberlite	
HIL-PEA-F1	Peakstar	Kimberlite	
HIL-SPH-09	Selebi Phikwe	Gabbro	
HIL-SPH-10	Selebi Phikwe	Gabbro	
HIL-BWG-1	Bayerwald Granite	Granite	
HIL-ERD-01	Erdösmecke	Granite	
HIL-GOL-01	Golling	Anhydrite	
HIL-MIL-1	Miltenberg	Sandstone	
HIL-MIL-2	Miltenberg	Sandstone	
HIL-MIL-3	Miltenberg	Sandstone	
HIL-OBM-1	Oberbaumühle	Amphibolite	
HIL-PEB-1	Pechbrunn	Basalt	

The following tables (Tab. 11 and Tab. 12) summarizes all mean values of all tested samples during this thesis.

Tab. 11: Summary of all mean test results for rock strength of all included mining locations.

Mine/Quarry	UCS	wz	V	BTS	PLT	UCS (plt)
	[MPa]	[kJ/m ³]	[GPa]	[MPa]	[MPa]	[MPa]
Kloof #8	140,67	249	64,71	9,3	8,81	132,15
Tautona	179,47	477,97	49,88	13,35	11,5	172,5
Moab	161,25				10,75	161,25
Blue Ridge	193,75				7,75	193,75
Brakfontein	103,42	123,77	58,82	7,3	3,75	93,75
Hackney	146,05	217,25	91,87	9,45	5,75	143,75
Twickenham	167,5				6,7	167,5
Peakstar	77,63			7,83	6	120
Selebi Phikwe	139,73			11,65	10,2	204
Bayerwald	184,18	545,43	41,82	11,8	8,95	179
Erdösmecke	137,57	324,5	46,85	11,85	7,44	148,8
Golling	85,33	210,13	71,38	4,85	5,3	106
Hagerbach	118,3					
Miltenberg	36,09	181,32	7,75	3,7	2,24	44,8
Oberbaumühle	59,36	639,27	59,36	17,7	14,41	288,2
Pechbrunn	412,53	1246,57	76,24	22,95	16,12	322,4

Tab. 12: Summary of the mean test results for abrasivity and other tests of all considered mining locations.

Mine/Quarry	CAI	LAC	LBC	EQc	vp
	[-]	[g/t]	[%]	[%]	[m/s]
Kloof #8	4,95	1240	38,5	80,48	
Tautona	4,8	1319,5	37	82,55	5640,58
Moab					5014,42
Blue Ridge	4,7	1100	53	33,6	
Brakfontein	3,5	1140	79	38,1	5136,08
Hackney	3,65	1560	59	37,72	6598,54
Twickenham					
Peakstar	0,9	180	33	6,4	3510,53
Selebi Phikwe	4	1090	43	38,65	
Bayerwald	4,4	1039	43	59,9	
Erdösmecke	4,1	1140	35	64,26	
Golling	1,6	60	55	3,5	5747,2
Hagerbach	5,4				
Miltenberg	1,4	460	96,5	59,46	2498,27
Oberbaumühle	3,3	500	19	41,04	6285,08
Pechbrunn	2,6	499	15	23,71	6424,06

6.1 Description of all samples

6.1.1 Gold samples

Most important rocks for the mining process for all three gold mines are quartzites and meta-conglomerates and are part of the Central Rand Group of Witwatersrand Supergroup.



Fig. 41: Gold bearing meta conglomerate of the Witwatersrand Supergroup (the sample is part of the rock collection of the Chair for Engineering Geology of TUM).

The Witwatersrand conglomerates are -petrographic speaking- no real conglomerates any more. They are slightly metamorphosed quartzitic sandstones and quartz rich conglomerates and are classified as quartzites and meta quartz conglomerates. They show greenschist facial metamorphosis grade due to their maximum temperature of about 350 °C, although the overburden reached up to 20 km (POHL 2005: 180).

There are two main varieties existing. One coarser one with bigger grains as shown in Fig. 41 and one finer grained type which can be addressed as real quartzite. Both have a light green to light to dark greyish color and are very dense and are built mostly of clastic quartz grains with a grain size of a view mm up to about 5 cm surrounded with a fine grained matrix. All grains are edge rounded and are bond with a siliceous matrix. Only quart and light mica as muscovite and sometimes pyrite can be identified by a macroscopic observation.

Both varieties show under the microscope strongly toothed quartz grains (partially with undulous extinction) with saturated grain boundaries beside of recrystallized quartz grains (Fig. 42). Isolated and subordinated light mica minerals (muscovite and chlorite) can be found within the matrix but also covering some grains like a thin skin. They show only very small grain sizes of max. 0.5 mm. Very spread but mostly very small pyrite minerals can be found. Pyrite can sometimes also build nests and bigger grain sizes and can then be observed macroscopic. Pyrite is like all other grains mostly well to edge rounded and shows grain sizes up to 1 mm.

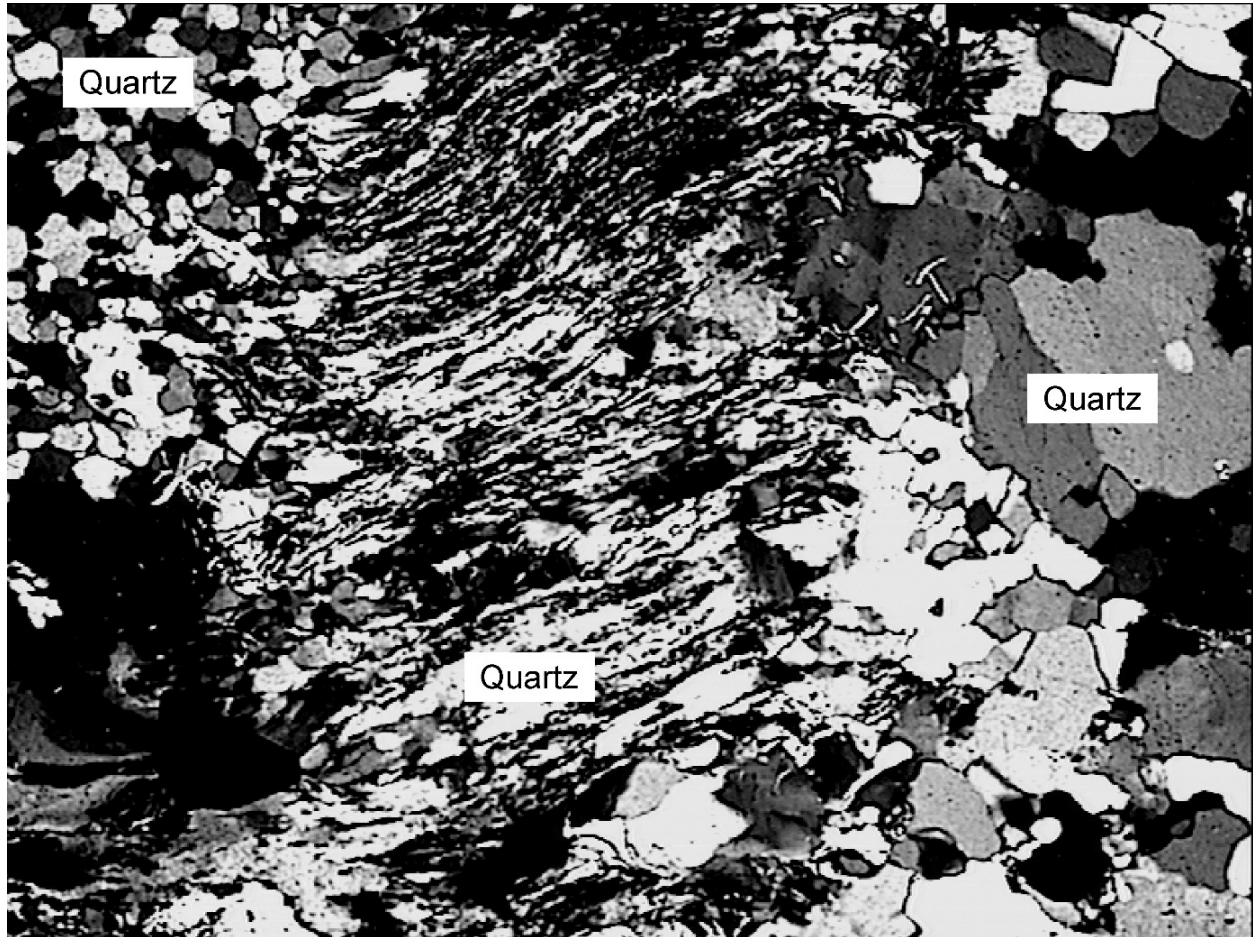


Fig. 42: Thin section of a typical Witwatersrand conglomerate. Upper left corner: recrystallized quartz grains (polygonal structure). In the middle: fibrous, strongly toothed quartz minerals. At the right side: bigger primary quartz grains with undulous extinction and saturated grain boundaries. Image width: 2.6 mm. Sample HIL-KLO-02.

Additionally, uranium minerals, especially uraninite (UO_2) exists. Uranium minerals can reach higher, economically recoverable concentrations, therewith an extraction like it is done in uranium rand mine is suitable. From economic point of view, the most valuable component of this formation is still the solid gold. The reefs, in which the gold occurs in economically recoverable concentration, are often bound to coarser varieties of the metaconglomerate. Highest thickness of the reefs is about 1 m. Most of the time the reef is not thicker than 20-30 cm. The maximum gold content is reported with about 45 g/t but nowadays in recent parts of the gold mine typically content between 5 to 10 g/t are found.

The XRD analysis results are showing a typical mineral content of quartz with contents between 77 and 85 %, mica (muscovite, chlorite and pyrophyllite) between 5 and 25 % and pyrite between 0 and 5 %. Only Sample HIL-KLF-05 shows a higher mica content of 45 % and a quartz content of only 53 %.

All samples, except HIL-KLF-05, having an equivalent quartz content of around 80 %.

6.1.2 Platinum samples

6.1.2.1 Blue Ridge

The dark, nearly blackish rock is dense and only the major minerals like anorthosite (feldspar), chromite and some phlogopite can be recognized by a macroscopic observation (Fig. 43).



Fig. 43: Specimen of anorthosite for the point load testing of Blue Ridge mine.

Regarding the thin section analysis there are opaque minerals of the tight chromite (42 % of the mineral content) with grains up to 0.2 mm in diameter which float in a matrix of mainly anorthosite (a feldspar variation) with excellent fissility along the crystal structure. Some tight pyroxene, a well fissionable phlogopite (a mica) and the abrasive quartz are irregularly distributed in the matrix. Quartz is only represented by 7 % of the mineral content as given by the x-ray diffractometer-analysis. Pyroxene and phlogopite are represented by 10 respectively 8 % of the mineral content.

The XRD analysis result shows a mineral content of chromitite of 42 %, feldspar of 33, pyroxene of 10 %, and phlogopite of 8 % and quartz of 7 %. The equivalent quartz content is 33.6 %.

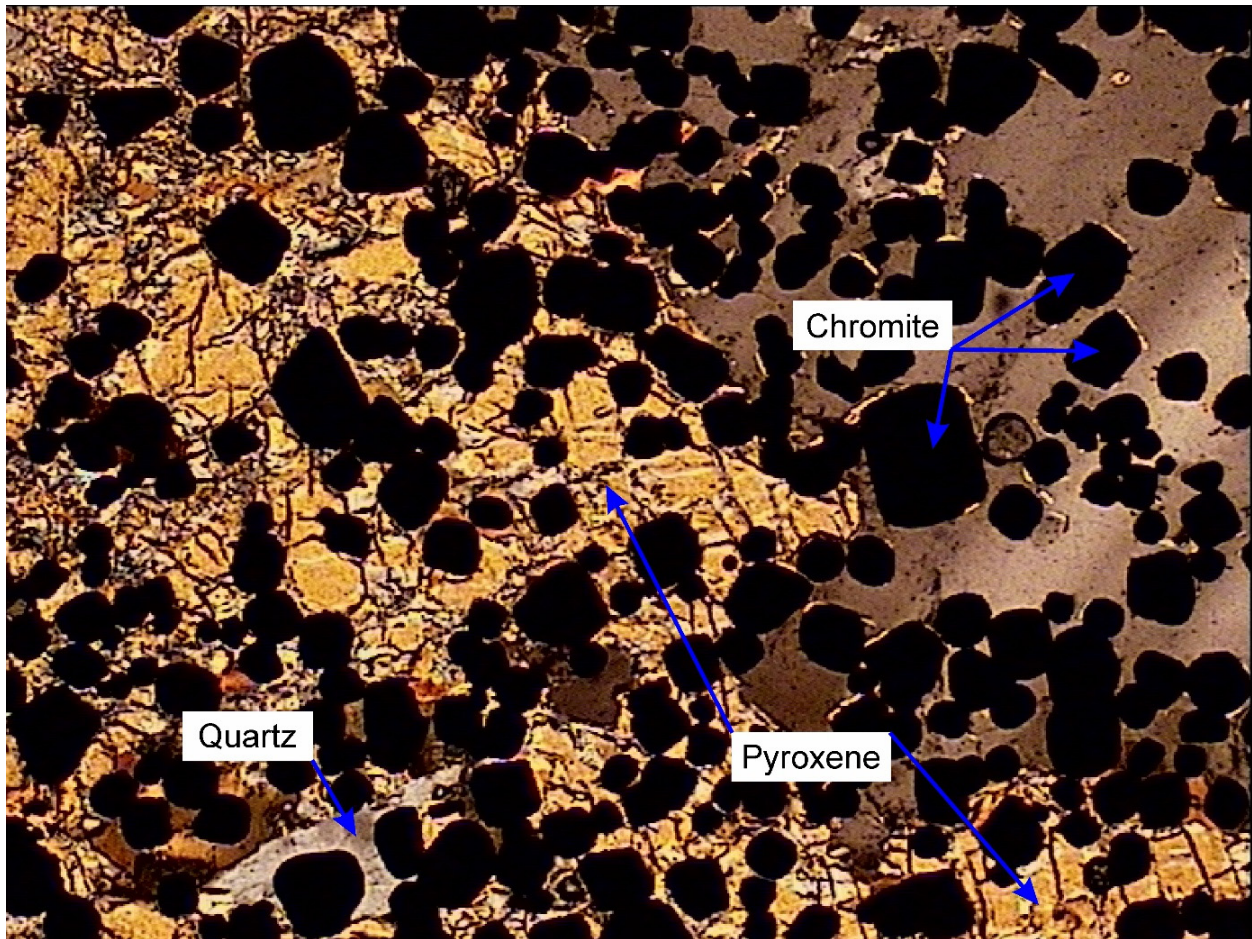


Fig. 44: Thin section of the anorthosites with poach chromite of Blue Ridge mine in dark field. Sample HIL-BLU-01 (Image width: 2.6 mm).

6.1.2.2 Brakfontein, Twickenham and Hackney.

The mid to light greyish rock (Fig. 45) has macroscopic observable pores, up to 1 mm, and contains feldspar and pyroxene minerals with a grain size up to 5 mm in a fine grained matrix with no minerals identifiable. It's homogenous, isotropic and slightly porphyritic. No further structure or texture like fluidal texture is observable. The rock weathers with brownish to greenish colors, where the feldspar minerals are visible slightly weathered. With additional weathering the pore space is getting bigger.

This rock can be classified as Pyroxenite.



Fig. 45: Specimen of pyroxenite as an example for all considered platinum samples. HIL-BRA-01.

In thin section (Fig. 46) pyroxene and feldspar were clearly as main content identifiable. Quartz with undulous extinction, amphiboles with clear cleaving faces and biotite were accessory contained.

All these results were confirmed with XRD analysis. The results of XRD and the equivalent quartz content is shown in Tab. 13. All platinum samples are lying between 33 and 39 % for EQc.

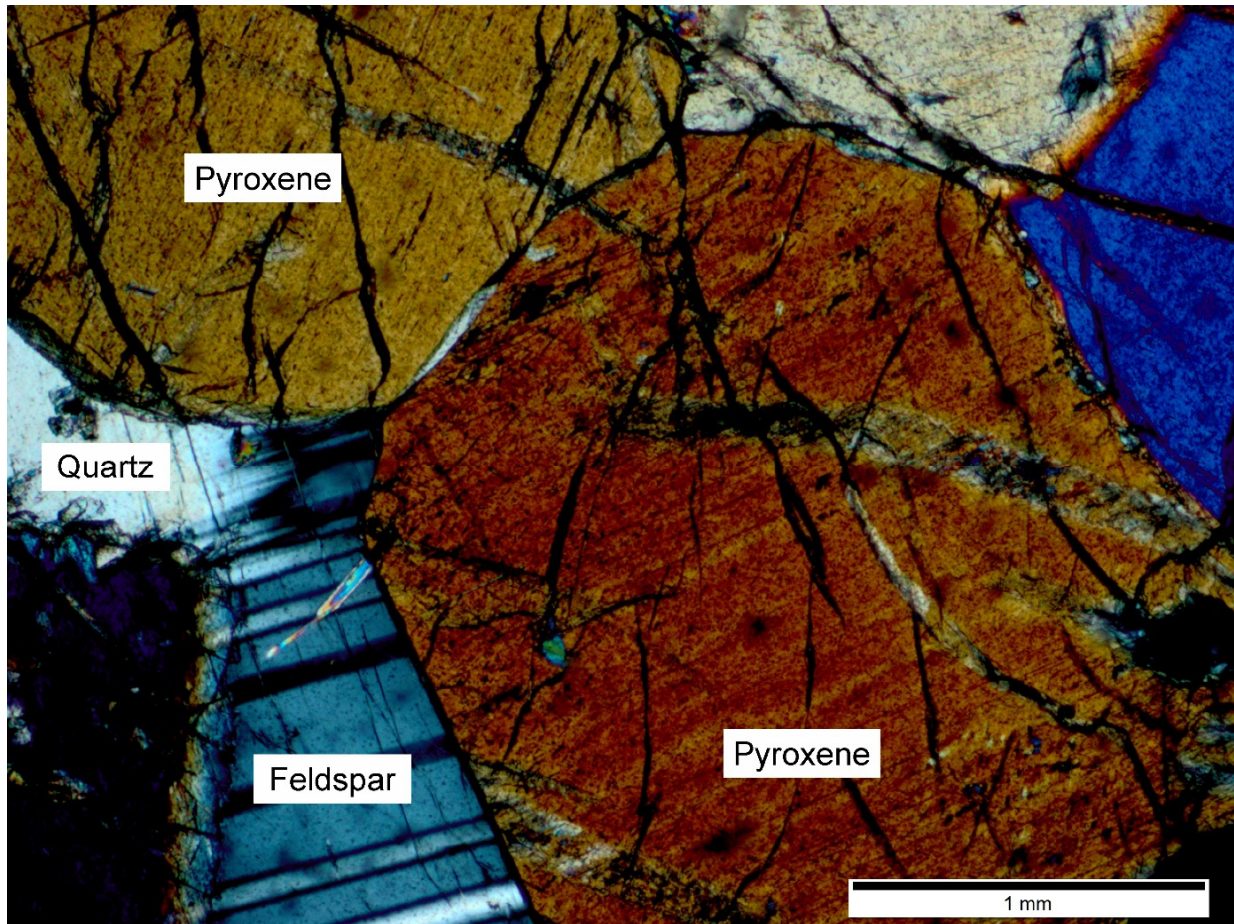


Fig. 46: Thin section overview of a pyroxenite sample from mine of Brakfontein. HIL-BRA-01.

Tab. 13: Mineral content and equivalent quartz content of platinum samples.

Mineral	Grinding hardness after Rosiwal	Brakfontein		Hackney	
		Mineral Content	EQc	Mineral Content	EQc
Pyroxene	22-65	70	30,45	64	27,84
Feldspar	3-40	23	4,95	27	5,81
Amphibole	18-30	2	0,48		
Quartz	100	1	1	2	2
Olivine	80	1	0,8		
Serpentine	4	1	0,04		
Magnetite	34	1	0,34		
Mica (Biotite/Phlogopite)	1,8-5,6	1	0,04	2	0,07
Talc	0,03			3	0,0009
Opaque minerals	100			2	2
Sum		100	38,10	100	37,72

Due to the similarity of all samples of Twickenham mine and the other platinum mines and the close location to each other and to safety reasons of the mine itself no other samples could be taken for further analyzes.

6.1.3 Samples of other mines

6.1.3.1 Peakstar

This dark greyish to anthracite colored (Fig. 47) rock sample has smaller pyroxene and phlogopite minerals with a grain size of up to 8 mm in a fine grained matrix. It has a slightly porphyritic structure and is very dense. The mineral content as found in thin section analysis was dolomite, serpentine, feldspar, biotite and phlogopite as main content and talc, calcite, apatite and opaque minerals as secondary content.



Fig. 47: Specimen of a kimberlite rock of the mine Peakstar. Sample HIL-PEA-01.

The results of XRD and the equivalent quartz content is shown in Tab. 14.

In thin section (Fig. 48) a dark green to black matrix is visible. The olivine minerals are partly altered to serpentine. Biotite and phlogopite are accessory contained. All bigger minerals show reaction seams around the grain boundaries. Some opaque minerals can be found throughout the thin section. Also feldspar minerals can be identified which can be possibly classified as plagioclase. Also apatite is contained.

Tab. 14: Mineral content and equivalent quartz content of kimberlite samples.

Mineral	Grinding hardness after Rosiwal [%]	Peakstar	
		Mineral Content [%]	EQc [%]
Talc	0,03	7,0	0,0
Biotite/Phlogopite	1,8-5,6	23,0	0,8
Apatite	5	1,0	0,1
Dolomite	4	25,0	1,0
Serpentine	4	22,0	0,9
Plagioclase	3-27	17,0	2,6
Calcite	1,9-3,9	4,0	0,1
Opaque minerals	100	1,0	1,0
Sum		100	6,4

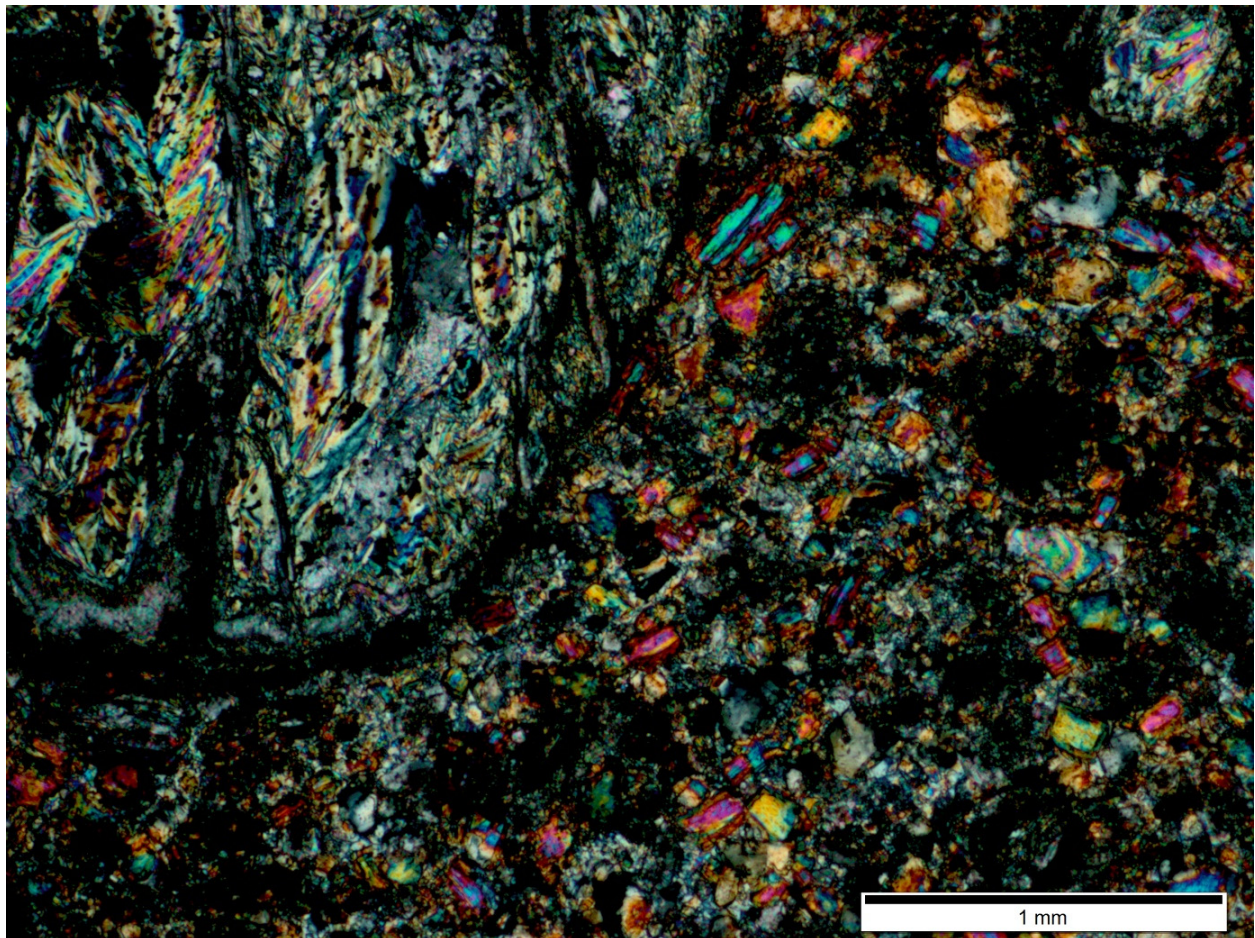


Fig. 48: Thin section overview of a Peakstar kimberlite. The mineral content is described in Tab. 14. Sample HIL-PEA-01.

6.1.3.2 Selebi Phikwe

From Selebi Phikwe we analyzed two different samples. One of the waste material (HIL-SPH-09) in which most of the drilling occurs and one sample of copper ore (HIL-SPH-10).

The waste material (Fig. 49) is a middle to fine grained dark grey green to dark brown spotted Amphibolite with a dense structure. A faintly distinguishable foliation can macroscopic be recognized. In thin section the main components plagioclase, biotite and amphiboles were identifiable. But also quartz is incorporated with a content of around 5 %.

Main content (>5 %):

Plagioclase 55 %, Biotite 20 %, and Amphibole 20 %

Secondary content (<5 %, > 1%):

Quartz 5 %

Minor Content (<1%):

Apatite, Zircon, Opaque Minerals (Pyrite, Ilmenite? /Magnetite?)

In thin section (Fig. 50) a polygonal, slight to clear toothed grain structure is identifiable. Plagioclase-, amphibole- and quartzgrains are oval and parallel directed to foliation. Mica discs show an even clearer tight foliation. Plagioclase grains are polygonal slightly toothed and the grain size vary between 0.5 to 1 mm. Twin-fins are clear bend and show symptoms of deformation. Grains are partly blurred due to marginal alteration (growth of mikrolithes). They show light zonal structure with undulous extinction. The amphiboles show dark green to light brown pleochroism and occur as polygonal aggregates with grain sizes between 0.5 to 1 mm. Biotite has a grain size between 0.1 to 1 mm. Quartz grains show undulous extinction and grain sizes between 0.1 to 0.8 mm. The feldspar minerals and quartz grains shows a subparallel, cementated micro fissure structure, which is slightly tilted to foliation. This rock sample can be classified as Gabbro.

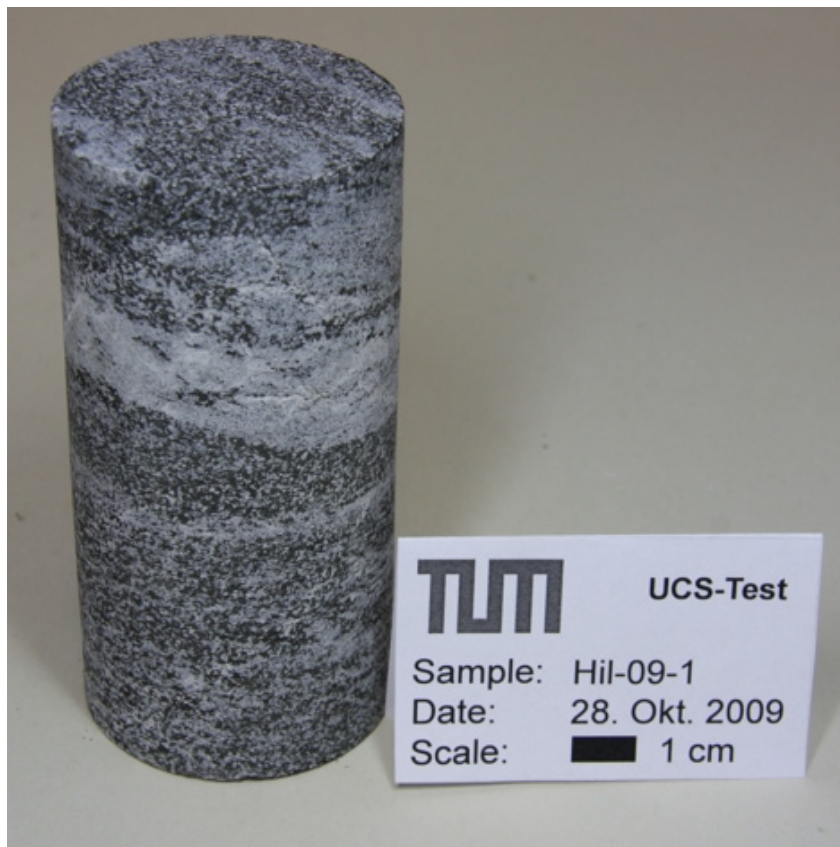


Fig. 49: Specimen of a waste material of the mine of Selebi Phikwe. Sample HIL-SPH-09.

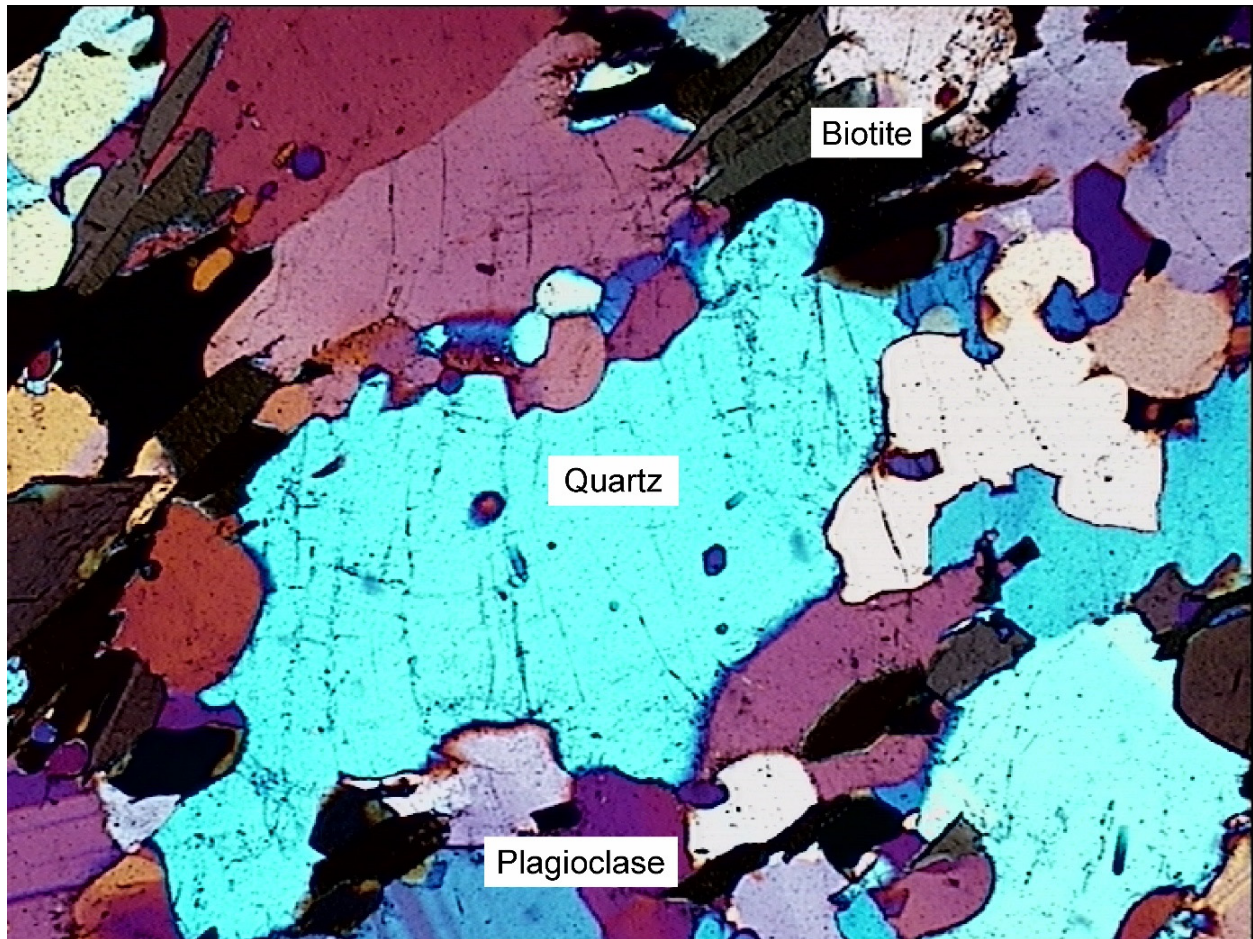


Fig. 50: Thin section of waste material of Selebi Phikwe with an inserted gypsum layer. Sample HIL-SPH-09.

The ore itself (Fig. 51) is a pyrrhotite-chalkopyrite-sulfide ore in a black to dark grey green, middle to coarse grained matrix. It has a dense structure. On the contrary to the waste material no foliation is distinguishable. In thin section (Fig. 52) the main components are amphiboles, pyroxene and opaque minerals as pyrrhotite and chalcopyrite. Minor contained minerals are talc and phlogopite. The grains have an irregular, polygonal slightly toothed structure. Amphibole grains are hypidiomorphic to xenomorphic, round and 0.2 - 2 mm in grain size. Pyroxene grain size is up to 1 cm. Pyroxenes are partly serpentinized. Serpentine occurs fine laminated to fibrous subparallel between pyroxenes. Opaque minerals occur mostly as fissure-, crotch- and pore filling. Mica is max. 1 mm in diameter. Talc appears in small clusters and inclusions. Aggregates reach a size between 0.1 to 0.5 mm. A with sulfide minerals filled network of fissures is clearly identifiable which is punching through the structure. Independent of grain material and position. Fissures are often tear fissures. This rock is a copper ore can be classified as pyroxenhornblendit.

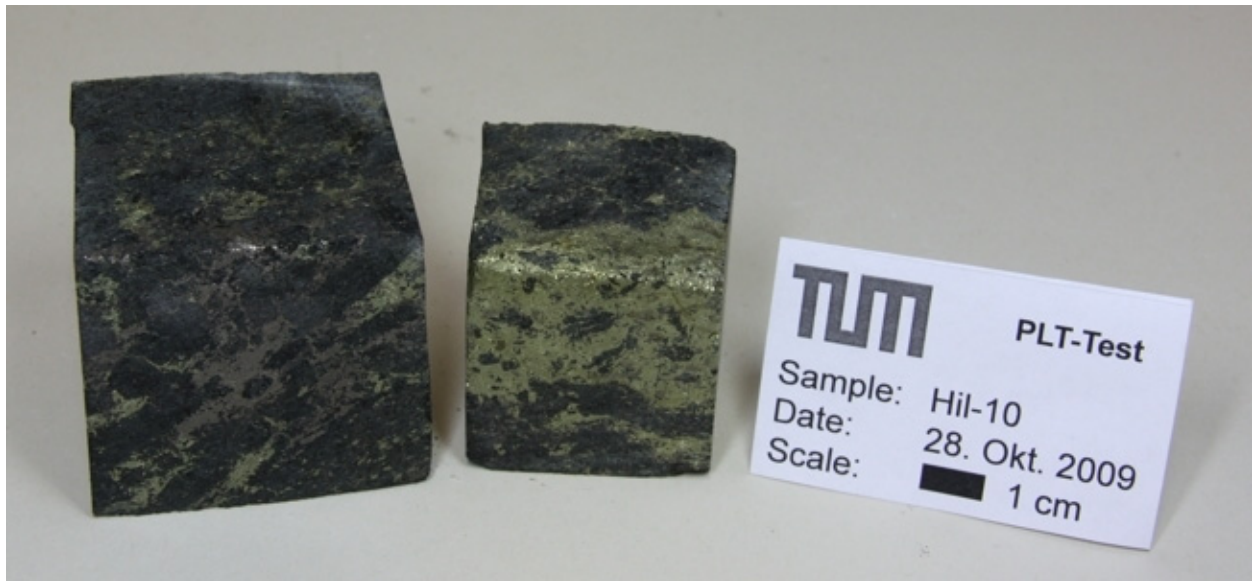


Fig. 51: Picture of specimen of a copper ore of Selebi Phikwe. Sample HIL-SPH-10.

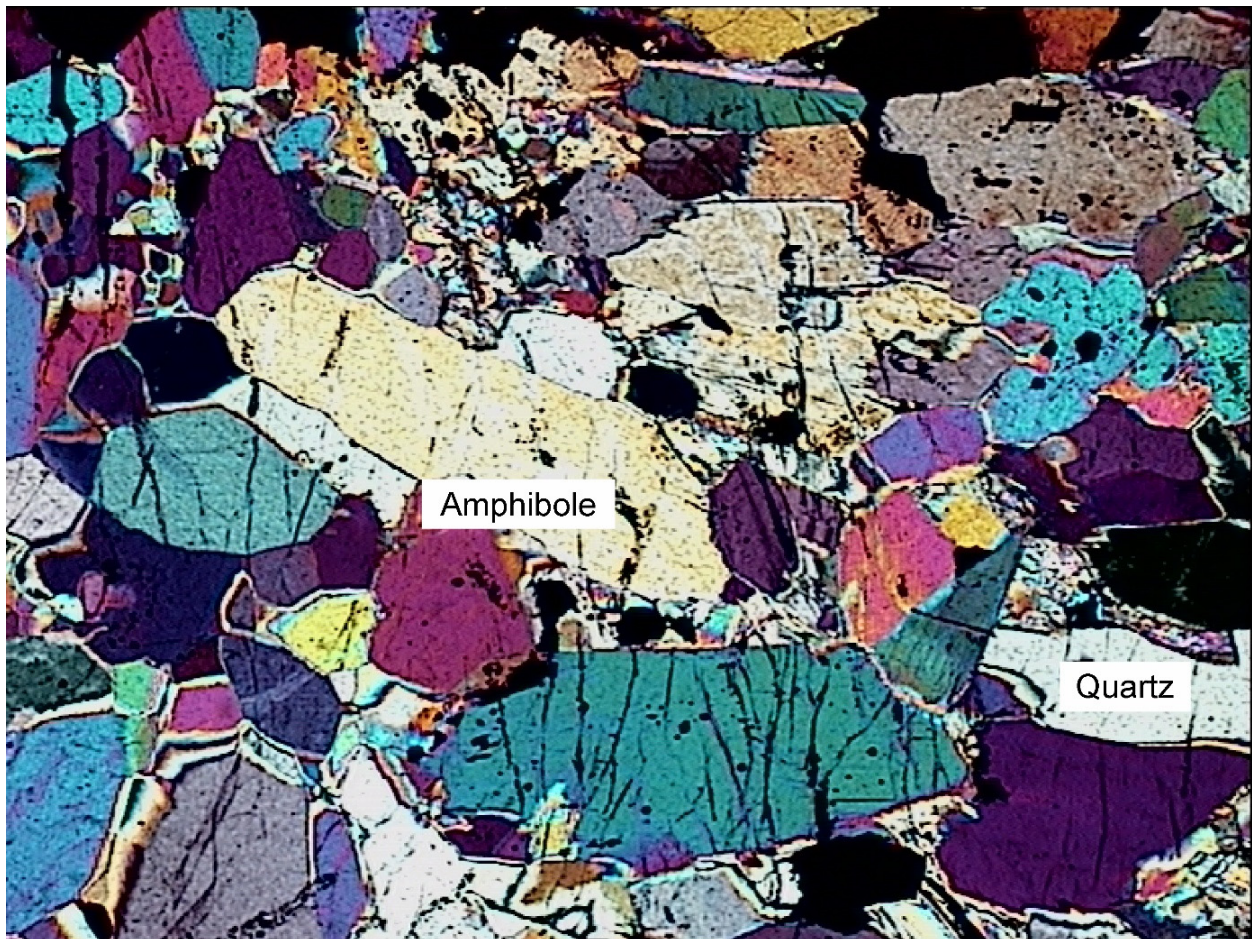


Fig. 52: Photo of a thin section of copper ore of Selebi Phikwe. Sample HIL-SPH-10.

The results of XRD and the equivalent quartz content of both samples is shown in Tab. 15.

Tab. 15: Mineral content and equivalent quartz content of Selebi Phikwe-samples.

Mineral	Grinding hardness after Rosiwal [%]	HIL-SPH-09		HIL-SPH-10	
		Mineral Content [%]	EQc [%]	Mineral Content [%]	EQc [%]
Quartz	100	22,0	22,0	18,0	18,0
Phlogopite/Biotite	3	13,0	0,4	5,0	0,2
Amphibole	25	19,0	4,8	39,0	9,8
Plagioclase	30	45,0	13,5	28,0	8,4
Apatite	4,5	1,0	0,0	10,0	0,3
Sum		100	40,7	100	36,6

6.1.4 Quarries and test rock samples

6.1.4.1 Bayerwald Granite

The Bayerwald granite (Fig. 53) is a light greyish rock and is a medium-grained plutonic rock with a maximum grain size of 1-2 mm. Feldspar, quartz and mica (muscovite and biotite) can be clearly identified macroscopic. The exact mineral content and the equivalent quartz content is shown in Tab. 16. The rock is very homogeneous and isotropic. No fluidal textures are recognizable.

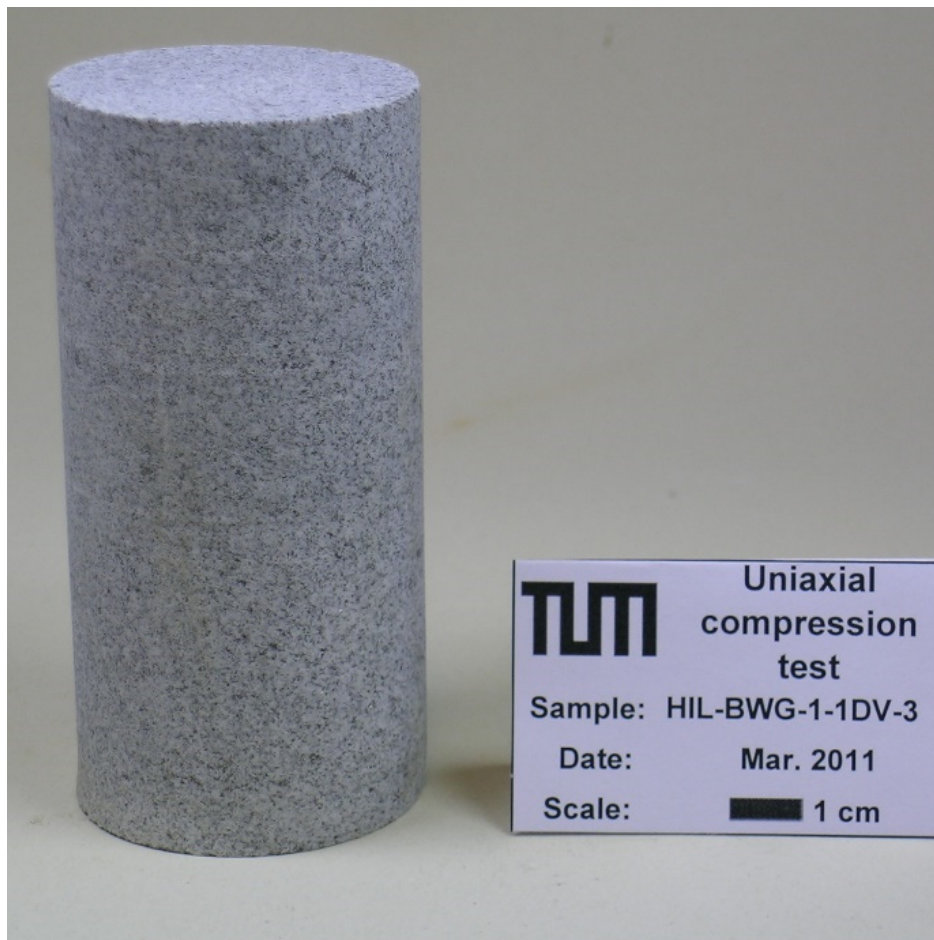


Fig. 53: Picture of a UCS specimen of Bayerwald granite. Sample HIL-BWG-01.

Tab. 16: Mineral content and equivalent quartz content of Bayerwald granite samples.

Mineral	Grinding hardness after Rosiwal [%]	Bayerwald granite	
		Mineral Content [%]	EQc [%]
Feldspar	40	48,0	19,20
Quartz	100	37,4	37,40
Biotite	5,6	9,2	0,52
Muscovite	6	3,2	0,20
Amphibole	25	1,4	0,35
Zircon	367	0,6	2,20
Chlorite	1	0,2	0,00
Sum		100	59,9

In thin section (Fig. 54) the strongly tooting of the quartz minerals is clearly identifiable. Biotite is clustered in small nests and is slightly foliated. The feldspar minerals are altered to sericite.

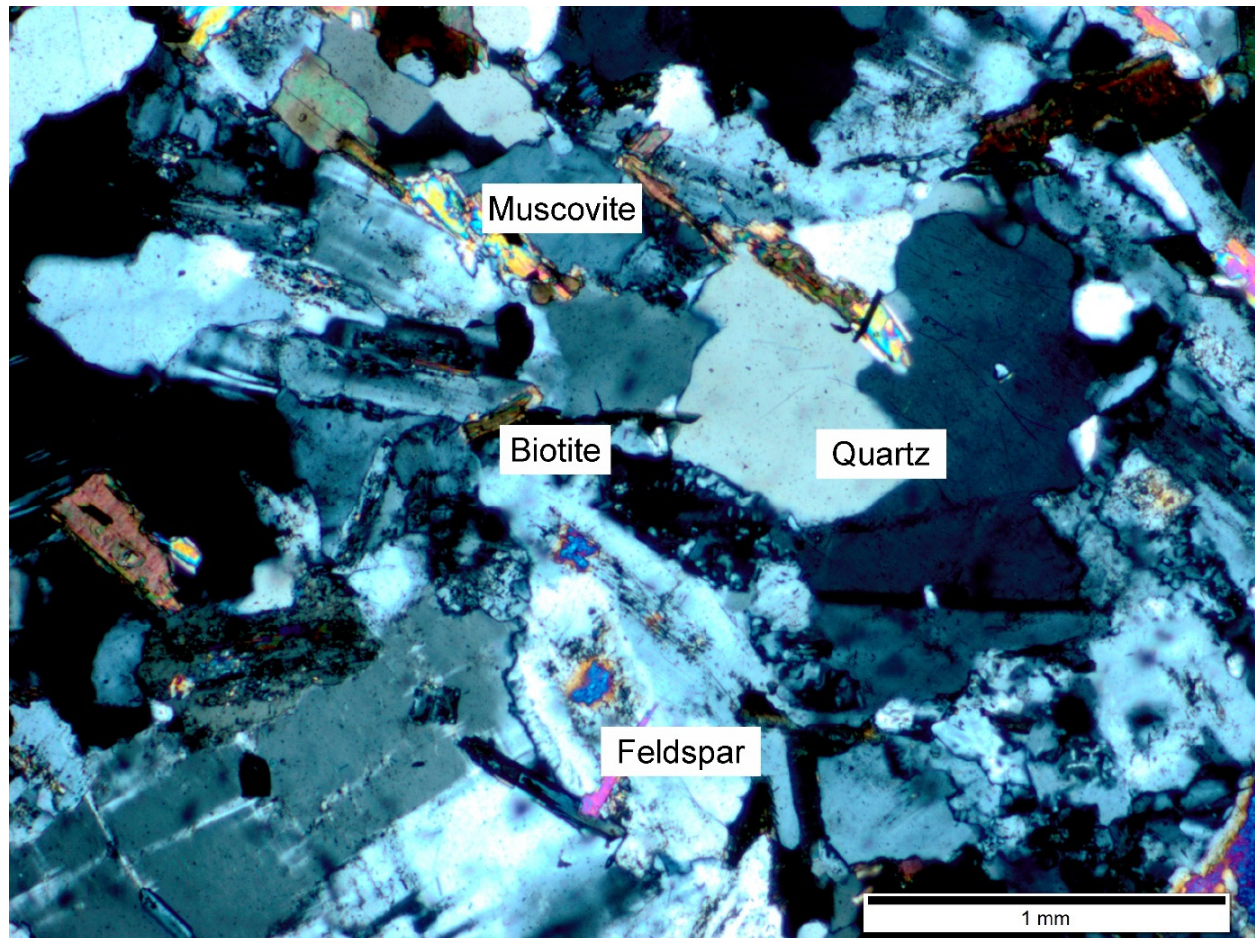


Fig. 54: Thin section of the Bayerwald granite; the dominant minerals are named in the sketch. Sample HIL-BWG-01.

6.1.4.2 Erdösmecke

The granite of Erdösmecke (Fig. 55) bright, greyish, coarse-grained plutonic rock with a maximum grain size of 10 mm. No fluidal textures are recognizable. Feldspar, quartz and biotite can be clearly identified macroscopic. The feldspar minerals have a grain size of up to 10 mm. The exact mineral content and the equivalent quartz content is shown in Tab. 17. The rock is very homogeneous and isotropic. The quartz grains are partly toothed (Fig. 56) and the feldspar minerals show symptoms of weathering and are slightly altered.



Fig. 55: Picture of point load samples of the Erdösmecke granite. Sample HIL-ERD-01.

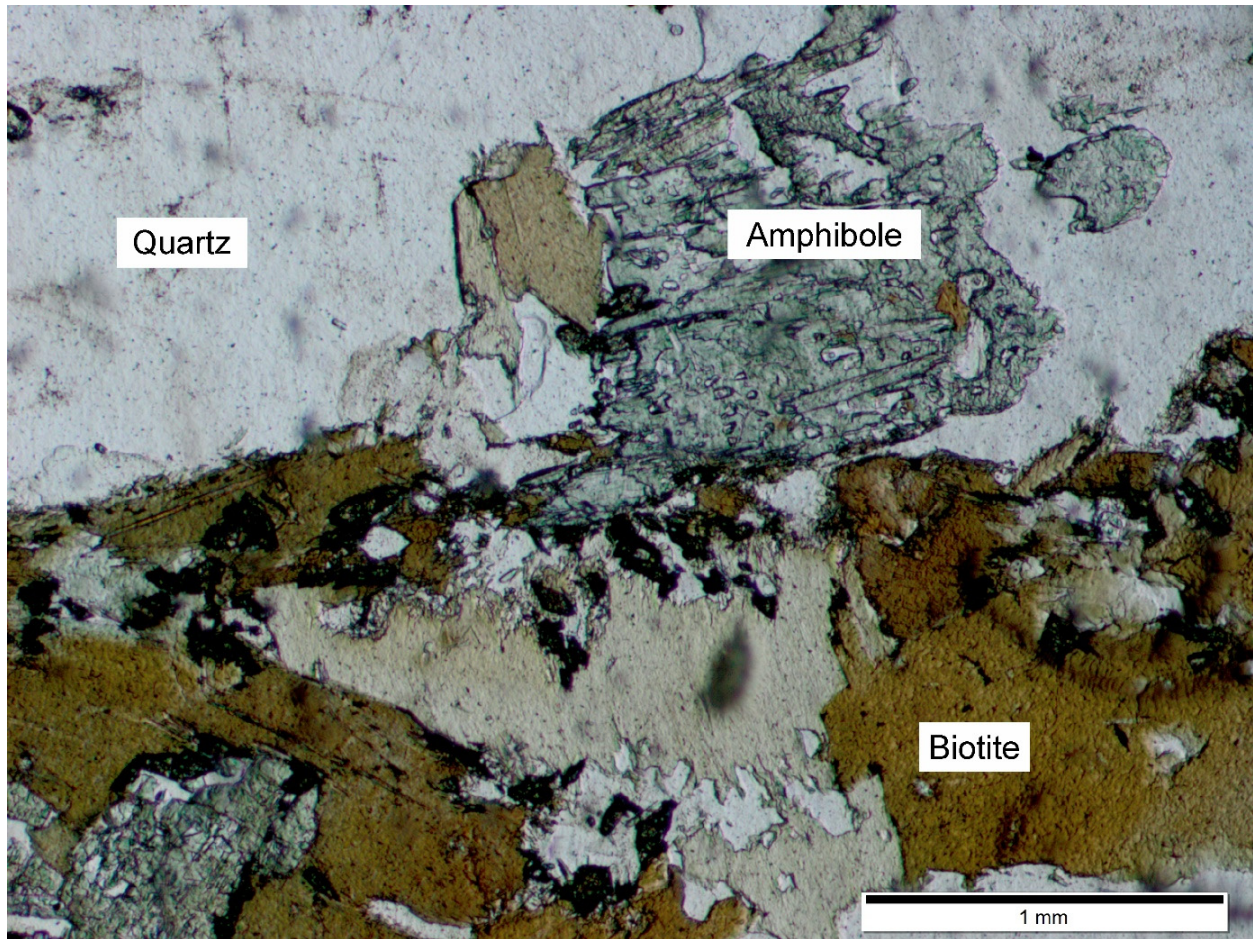


Fig. 56: Thin section of the Erdösmecke granite. Sample HIL-ERD-01 showing altered amphibole minerals, quartz grains with saturated grain boundaries and weathered biotite grains.

In thin section (Fig. 56) the saturated quartz grain boundaries are visible and bigger grains of biotite. The biotite minerals are slightly weathered. Amphibole minerals are slightly fissured and weathered. Some quartz grains are slightly fractured.

Tab. 17: Mineral content and equivalent quartz content of Erdösmecke granite samples.

Mineral	Grinding hardness after Rosiwal [%]	Erdösmecke	
		Mineral Content [%]	EQc [%]
Feldspar	40	47,5	19
Quartz	100	42,0	42
Biotite	5,6	7,3	0,41
Amphibole	25	2,6	0,65
Zircon	367	0,6	2,20
Sum		100	64,26

6.1.4.3 Golling

The rocks of Golling (Fig. 57) are light greyish fine crystalized very dense and bulky anhydrites with a maximum grain size of 1-2 mm. No fluidal textures are recognizable. Mostly anhydrite minerals can be clearly identified macroscopic. The exact mineral content and the equivalent quartz content is shown in Tab. 18. The rock is very homogeneous and isotropic.



Fig. 57: Picture of a Brazilian test sample of the Golling anhydrite. Sample HIL-GOL-01.

In thin section (Fig. 58) the high content of anhydrite is clearly visible. The mineral grains have saturated boundaries. Feldspar is partly altered to sericite. Quartz is only few contained as small grains with a size of max. 0.2 mm.

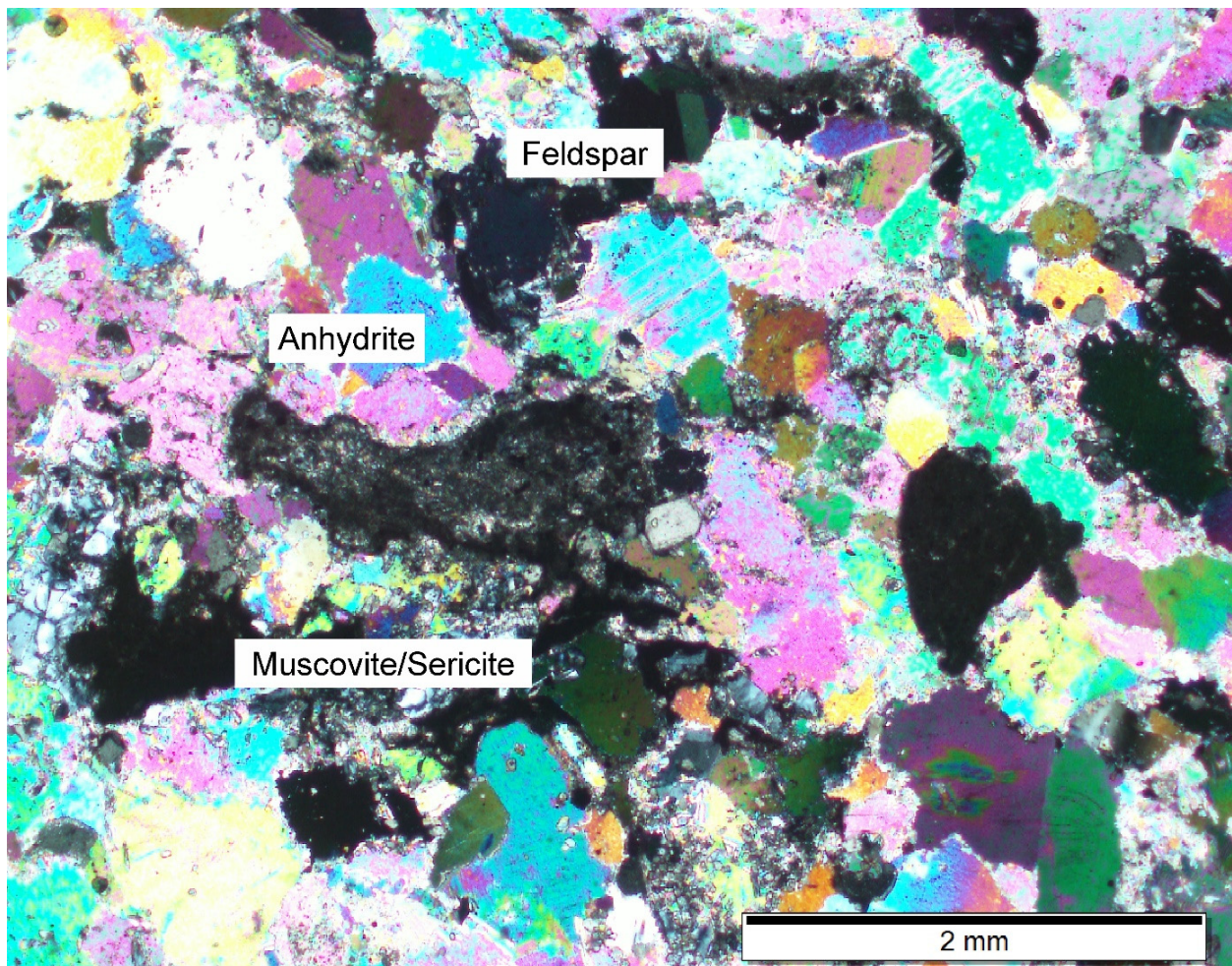


Fig. 58: Thin section of the Golling anhydrite; the dominant minerals are named and marked in the photo. Sample HIL-GOL-01.

Tab. 18: Mineral content and equivalent quartz content of the samples of Golling.

Mineral	Grinding hardness after Rosiwal [%]	Golling	
		Mineral Content [%]	EQc [%]
Anhydrite	0	90,4	0
Magnesite	34	5,4	1,84
Quartz	100	0,4	0,4
Muscovite	1,5-6,1	0,5	0,02
Pyrite	56	0,8	0,45
Feldspar	3-40	2,5	0,79
Sum		100	3,50

6.1.4.4 Hagerbach Test Gallery

The so called siliceous limestone of the Hagerbach Test Gallery (Fig. 59) is a fine to medium grained sedimentary, clastic rock. It has a high quartz content of up to 40 %. The quartz minerals are mostly coarse sand particles and partly very fine grained dissolved and in the pore space recrystallized. Some calcite minerals can be identified macroscopic. Bigger clasts of radiolarite with a grain size of up to 4 mm can be found.



Fig. 59: Picture of UCS samples of the siliceous limestone of Hagerbach Test Gallery.

6.1.4.5 Miltenberg



Fig. 60: Picture of the red, fine grained Miltenberg sandstone in an outcrop situation.

The brownish to red colored Miltenberg Sandstone (Fig. 60) can be classified as quartz sandstone with quartzitic cement. The mineral sand grains are fine to medium grained with a grain size of 0.1-0.3 mm. They are bad sorted and unequal shaped to edge rounded.

An overview of the mineral content is shown in Fig. 61 the exact content and the average equivalent quartz content can be found in Tab. 19. The quartz grains show healed fissures and undulous extinction. The quartz grains are edge rounded. Around the quartz grained as well as inside the matrix is very fine grained hematite. Microscopic (Fig. 61) are feldspar, muscovite, biotite, rutile and zircon identifiable. The feldspar reaches contents between 20-25 %, all other minerals are only accessory.

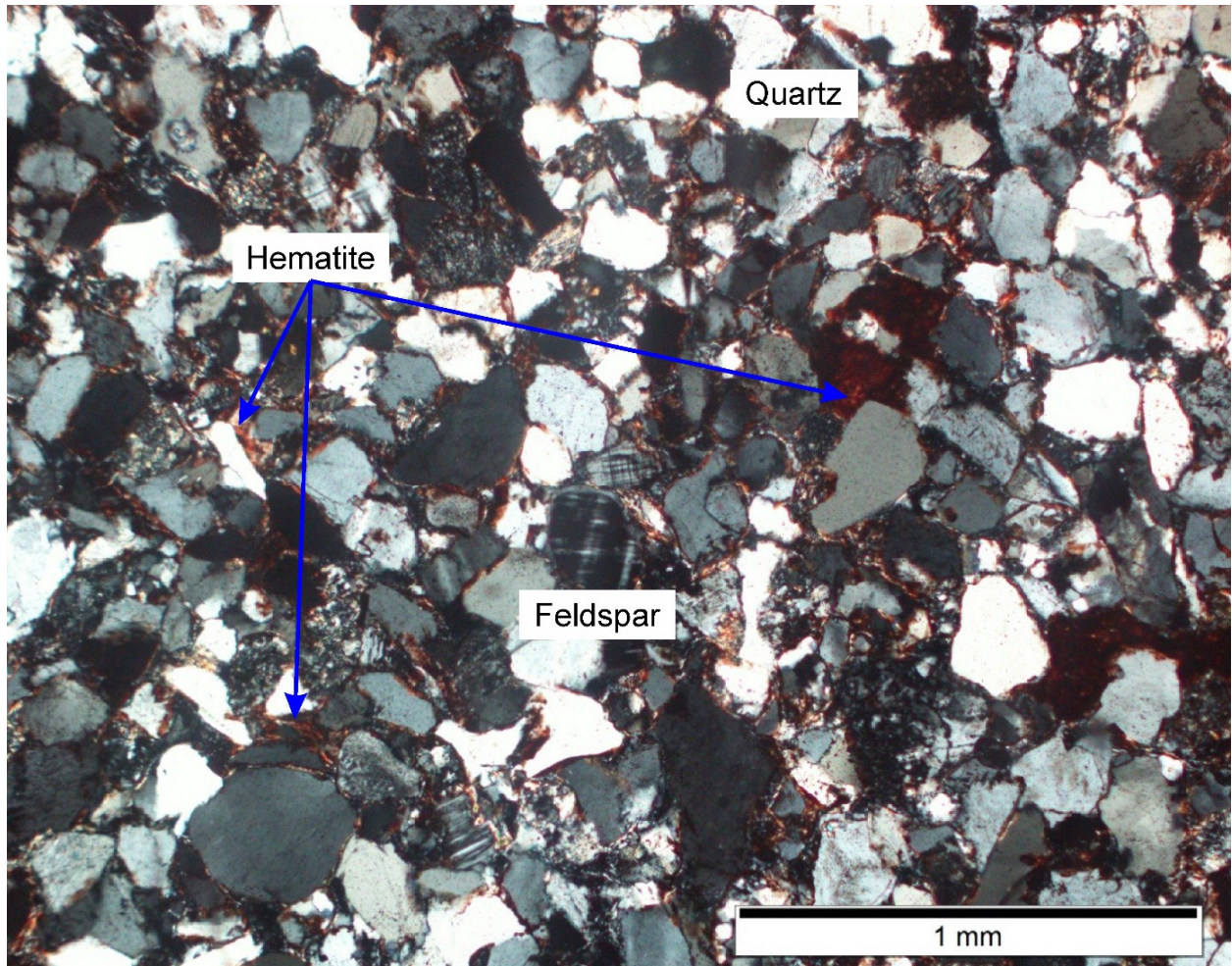


Fig. 61: Thin section of the Miltenberg sandstone with clear quartz and feldspar minerals. In some areas brown to red hematite can be found. Sample HIL-MIL-01.

Tab. 19: Mineral content and equivalent quartz content of Miltenberg sandstone samples.

Mineral	Grinding hardness after Rosiwal [%]	Miltenberg Sandstone	
		Mineral Content [%]	EQc [%]
Quartz	100	72,0	72
Feldspar	3-40	21,0	4,83
Hematite	25	0,21	0,053
Mica	1,5-6,1	6	0,228
Accessory (Clay minerals)	1	0,79	079
Sum		100	77,9

6.1.4.6 Oberbaumühle

The amphibolite of quarry Oberbaumühle (Fig. 62) is a dark green to grey to black dense rock. The rock has many fissures filled with light plagioclase and quartz. Sometimes bigger feldspar lenses can be found. The rock is strongly foliated and layered. Two layers are alternating.

An overview of the mineral content is shown as thin section in Fig. 63, the detailed analysis can be found in Tab. 20. One amphibole rich layer with garnet and a second plagioclase layer containing sometimes quartz grains. As accessory mica, apatite, zircon as well as ore minerals can be found. The rock is strongly disturbed, the garnet minerals are showing dissolving at their surface and are strongly fissured. The plagioclase minerals are often altered to sericite.



Fig. 62: Picture of the UCS sample of amphibolite of quarry Oberbaumühle. HIL-OBM-01.

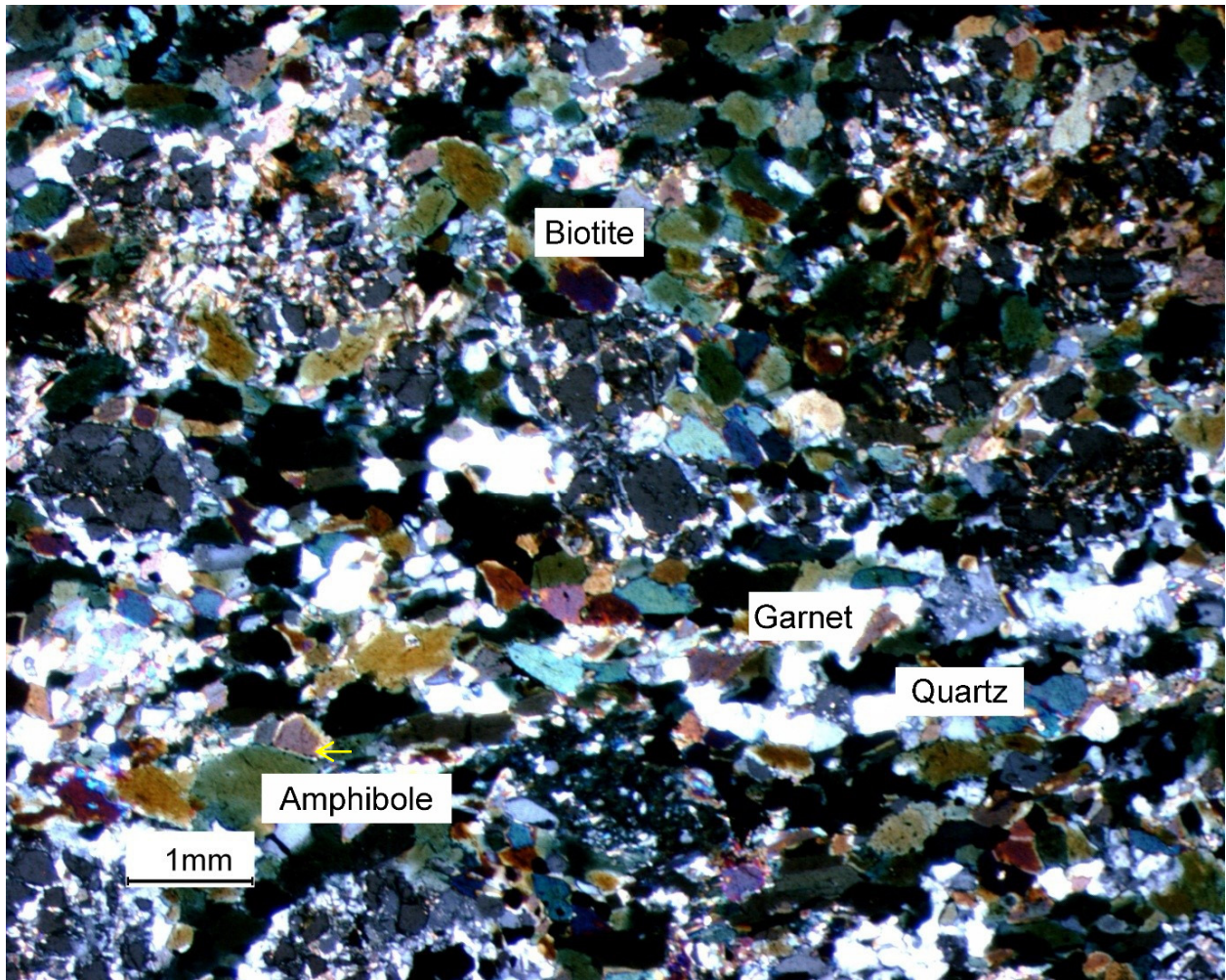


Fig. 63: Thin section overview of an amphibolite of the quarry Oberbaumühle (HIL-OBM-1).

Tab. 20: Mineral content and equivalent quartz content of amphibolite samples of Oberbaumühle.

Mineral	Grinding hardness after Rosiwal [%]	Oberbaumühle amphibolite	
		Mineral Content [%]	EQc [%]
Amphibole	18-30	41	9,84
Plagioclase	3-27	35	5,25
Garnet	203-210	10	20,65
Biotite	1,8-5,6	8	0,3
Quartz	100	5	5
Sum		100	41,04

6.1.4.7 Pechbrunn

The basalt of Pechbrunn (Fig. 64) is a dark grey rock and is a very fine grained volcanic rock. No fluidal textures are recognizable. Feldspar minerals are porphyritic distributed in a very fine matrix. Pyroxene minerals are sometimes altered to amphibole. Xenomorphic olivine minerals are clustered in nests and often show rounded edges. The exact mineral content and the equivalent quartz content is shown in Tab. 21. The rock is very dense, homogeneous and isotropic. Main content of the sample is pyroxene, plagioclase and magnetite as shown in the thin section in Fig. 65. Accessory are biotite and apatite contained.



Fig. 64: Picture of a UCS specimen of the Pechbrunn basalt. HIL-PEB-01.

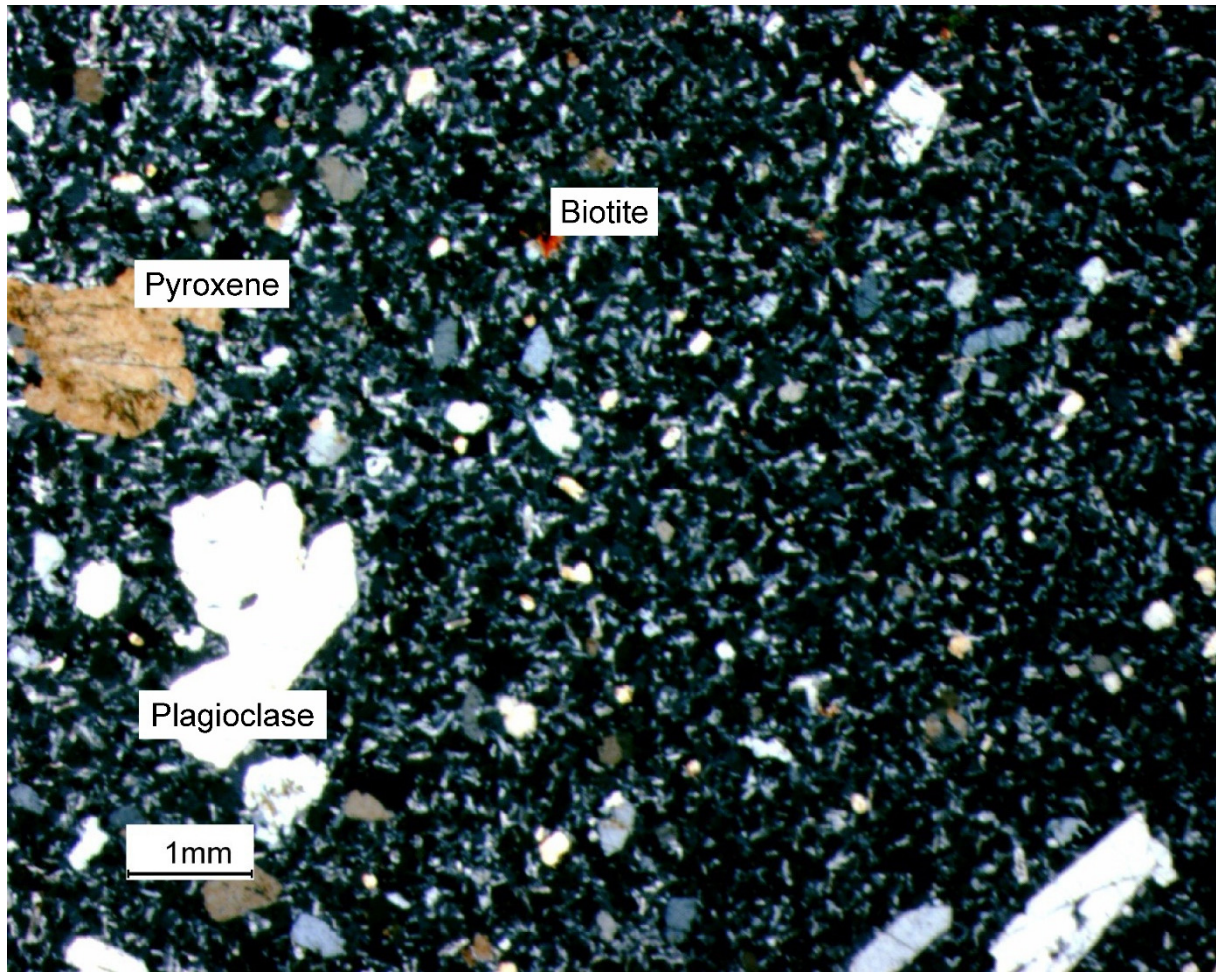


Fig. 65: Thin section analysis of the Pechbrunn basalt. HIL-PEB-01. Fine grained matrix consisting of pyroxene, olivine, plagioclase and magnetite with porphyritic feldspar, biotite and olivine components.

Tab. 21: Mineral content and equivalent quartz content of Pechbrunn samples.

Mineral	Grinding hardness after Rosiwal [%]	Pechbrunn basalt	
		Mineral Content [%]	EQc [%]
Pyroxene	18-30	56	13,44
Plagioclase	3-27	33	4,95
Magnetite	34	8	2,72
Olivine	80	2	1,6
Accessory	100	1	1
Sum		100	23,71

6.2 Number of tested specimen of each rock samples

Wherever it was possible we performed all tests on at least following number (Tab. 22) of rock specimen per sample. Due to problems with sample collection and preparation a discrepancy between real count and planned count of specimen for the different tests is possible. The final number of specimen per sample of a specific test can be looked up in the particular chapter of the test result.

Tab. 22: Planned count of specimen per sample for each laboratory test.

Laboratory test	Planned count of specimen
Uniaxial compression test	3
Point load test	1 (10 cubes)
Brazilian tensile test	3
Cerchar abrasivity test	1
LCPC abrasivity test	1
Thin section analysis	1
Ultrasonic test (v_p)	1 for each UCT specimen
Ultrasonic test (DW)	1

6.3 Uniaxial compression test

The mean uniaxial compressive strength (σ_u) and the final count of specimen per sample are shown in Fig. 66. The values for σ_u of all samples lie between 25 and 415 MPa. According to ISRM (1978a) the tested rocks can be classified as medium strong (R3) to extremely strong (R6) rock material. As planned for this thesis we were able to test different samples of most common and problematic strength value ranges and could combine this data with drill data.

Gold mines

The South African quartzites of Kloof and Tautona gold mines show σ_u values of between 120 and 240 MPa. The typical value is about 150 MPa but can be local extremely higher as sample HIL-TAU-07 shows. For the numerical models the highest values are used to create the worst case scenario for the drill head. The values of HIL-TAU-08 are more scattered due to pre-existing cracks and fissures of the sample itself.

The V modulus is varying between 26 and 68 GPa with a mean of 57 MPa. The destruction work w_z varies between 178 and 645 kJ/m³ with a mean of 363 kJ/m³. The variability in both properties is also depending on the pre-existing damage.

Platinum mines

For platinum the uniaxial compressive strength of all tested rocks varies between 37 and 205 MPa. The mean value for Brakfontein mine is 103 MPa, for Hackney the mean is around 110 MPa. Both mines can reach in dependence of pre fracturing of the rock very low values which occurred for the sample HIL-HAC-02. Also higher values of up to 200 MPa were thinkable due to missing fractures and missing discontinuities.

The V modulus is varying between 8 and 155 GPa. The mean is 72 GPa. The destruction work w_z varies between 77 and 480 kJ/m³. The mean is 161 kJ/m³.

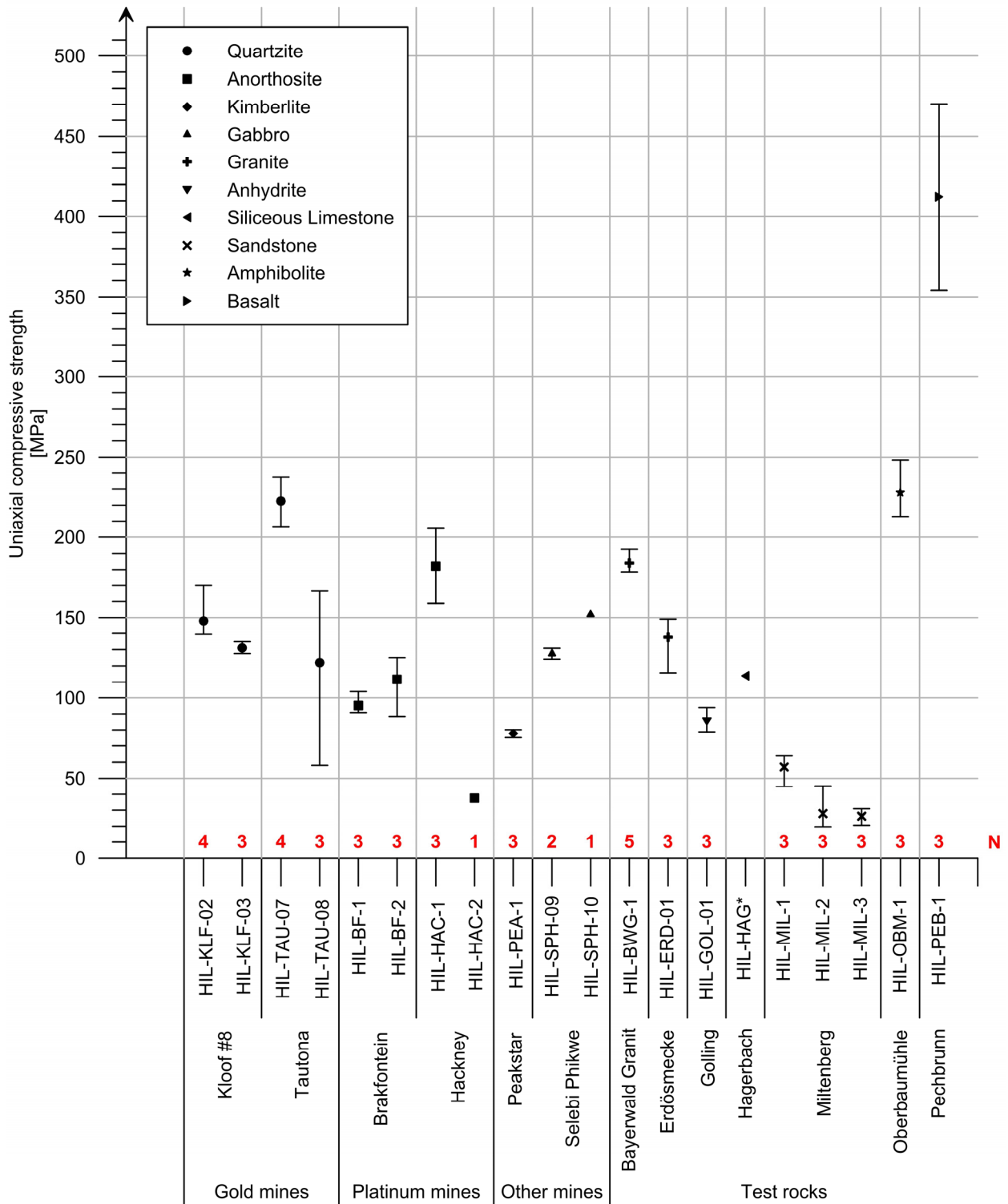


Fig. 66: Mean uniaxial compressive strength values of all test results for the total amount of samples. N is the number of tested specimen of the particular sample (* All samples of Hagerbach Test Gallery HIL-HAG were tested by Hagerbach Test Gallery GmbH).

Other mines

The tested kimberlite reach values between 75 and 80 MPa which can be higher in another kimberlite in field. All sample specimen failed at discontinuities. The upper limit for UCS is taken from point load tests. The V modulus is varying 17 to 19 GPa. The destruction work w_z lies between 161 and 369 kJ/m³

The Uniaxial Compressive Strength for the copper ore of Selebi Phikwe is determined with 152 MPa, the waste material of Selebi Phikwe reaches values between 124 und 131 MPa. The V modulus is for all samples of Selebi Phikwe between 62 and 65 GPa. The destruction work w_z varies between 14.5 and 500 kJ/m³.

Test rocks

The Bayerwald granite reaches Uniaxial Compressive Strength values between 178 and 193 MPa with an average of 184 MPa and is classified as very strong (R5). The V modulus lies between 36 and 57 GPa. The destruction work w_z varies between 426 and 628 kJ/m³.

The basalt of Bennau reaches UCS values between 260 and 348 MPa with an average of 309 MPa and is classified as extremely strong (R6). The V modulus lies between 65 and 99 GPa. The destruction work w_z varies between 621 and 956 kJ/m³.

The granite of Erdösmecke reaches UCS values between 115 and 149 MPa with an average of 138 MPa and is classified as very strong (R5). The V modulus lies between 43 and 48 GPa. The destruction work w_z varies between 305 and 343 kJ/m³.

The anhydrite of Golling reaches UCS values between 78 and 94 MPa with an average of 85 MPa and is classified as strong (R4). The V modulus lies between 69 and 74 GPa. The destruction work w_z varies between 134 and 278 kJ/m³.

The siliceous limestone of Hagerbach Test Gallery which was tested by Hagerbach Versuchsstollen GmbH with an average of 113 MPa and is classified as very strong (R5).

The rocks with the lowest σ_u were the sandstones from Miltenberg quarry. They show values between 25 and 63 MPa. HIL-MIL-2 and -3 are samples from rock layers of poorer quality but HIL-MIL-1 is a dimension stone layer with best quality. This can also be found in the rock properties. This was the sandstone sample with the highest strength and the best properties. The Miltenberg sandstone can be classified as weak for the lower qualities and as medium strong for HIL-MIL-1. The V modulus lies between 3 and 11 GPa. The destruction work w_z varies between 96 and 295 kJ/m³.

The amphibolite of Oberbaumühle reaches UCS values between 212 and 248 MPa with an average of 228 MPa and is classified as very strong (R5). The V modulus lies between 58 and 61 GPa. The destruction work w_z varies between 606 and 700 kJ/m³.

The basalt of Pechbrunn reaches UCS values between 354 and 470 MPa with an average of 413 MPa and is classified as extremely strong (R6). The V modulus lies between 74 and 78 GPa. The destruction work w_z varies between 955 and 1586 kJ/m³.

6.4 Point load test

To complete data about rock strength we performed point load tests. This is done for Moab Khotsong, Blue Ridge and Twickenham. For calculating the uniaxial compressive strength, the correlation factor of similar rocks is used. For all Gold samples of Moab, a correlation factor c of 15 was used which was determined for Kloof and Tautona samples for all platinum rocks the c was determined as 25 for Samples of Brakfontein and Hackney. All other samples were calculated with 20. The mean values and minimum and maximum can be found in Fig. 67. The point load results are lying between 2 and 17 MPa which is coping the wanted range of strength values for this testing series. Strongly correlated to σ_u the highest values can be found in

Pechbrunn for basalt with an I_{50} of 16.12 MPa. The lowest values are as expected in Miltenberg sandstone with 1.02 MPa as minimum. The quartzite of Tautona gold mine has an unexpected low mean I_{50} of 11.10 MPa and is lying in the upper midfield of all results but the maximum was the highest point load index of all tests with 17.9 MPa. This can be explained with the sampling method and the testing method. Some samples were collected with core drilling in the rock face. These samples were quite intact and provided the highest values. Samples with lower values were collected in the excavated material after blasting with much pre-damage.

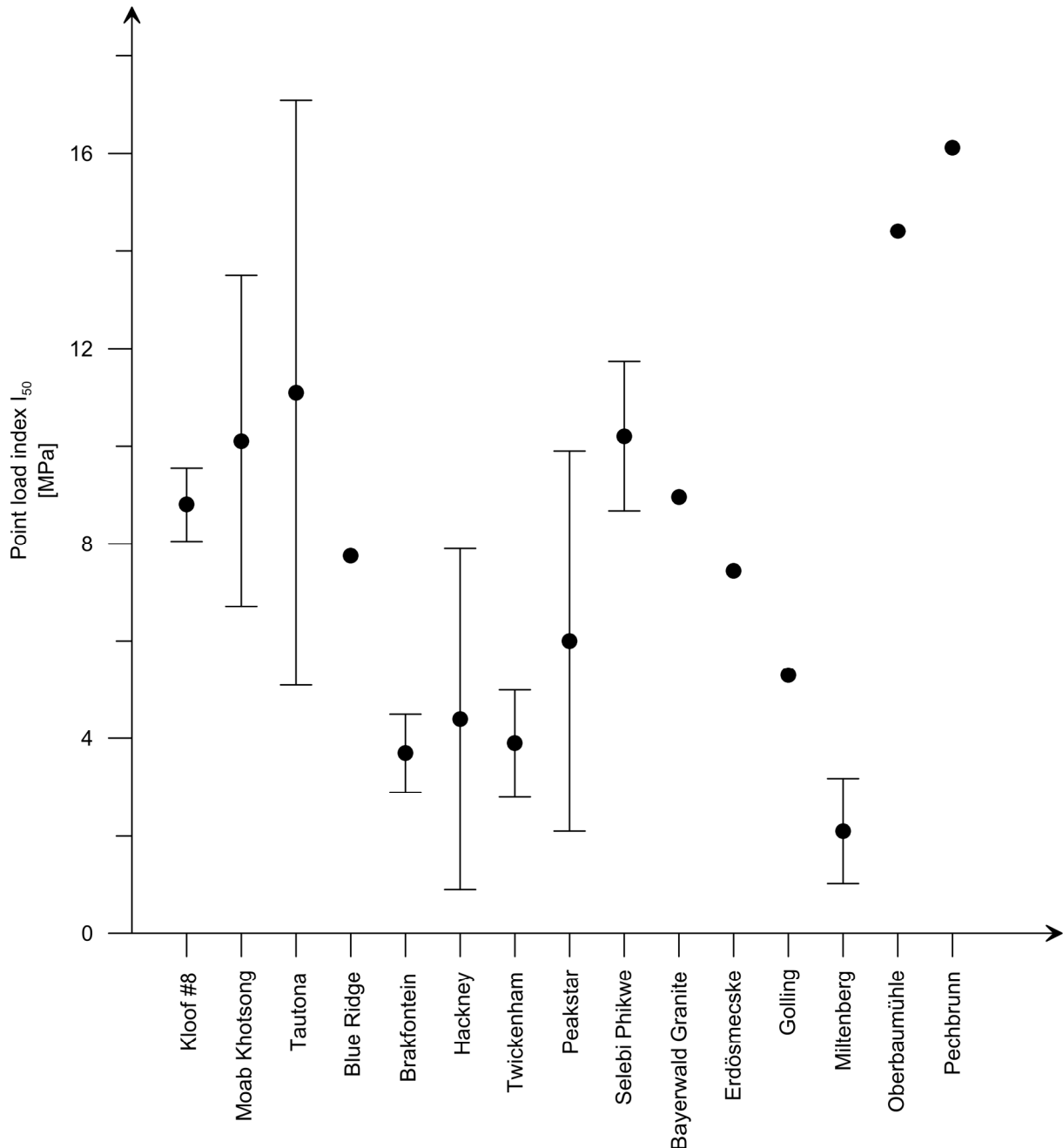


Fig. 67: Mean point load indices of all test results for the total amount of samples.

6.5 Brazilian tensile test

The mean values and minimum and maximum of Brazilian tensile strength of all tested samples can be found in Fig. 68. The Brazilian tensile strength results of all samples are lying between 3 and 23 MPa. The

highest values in, in correlation with σ_u can be found in Pechbrunn. This basalt reach values for $\sigma_{t,BTS}$ of 22.9 MPa. The lowest values are in Miltenberg for the Buntsandstein with 3.98 MPa.

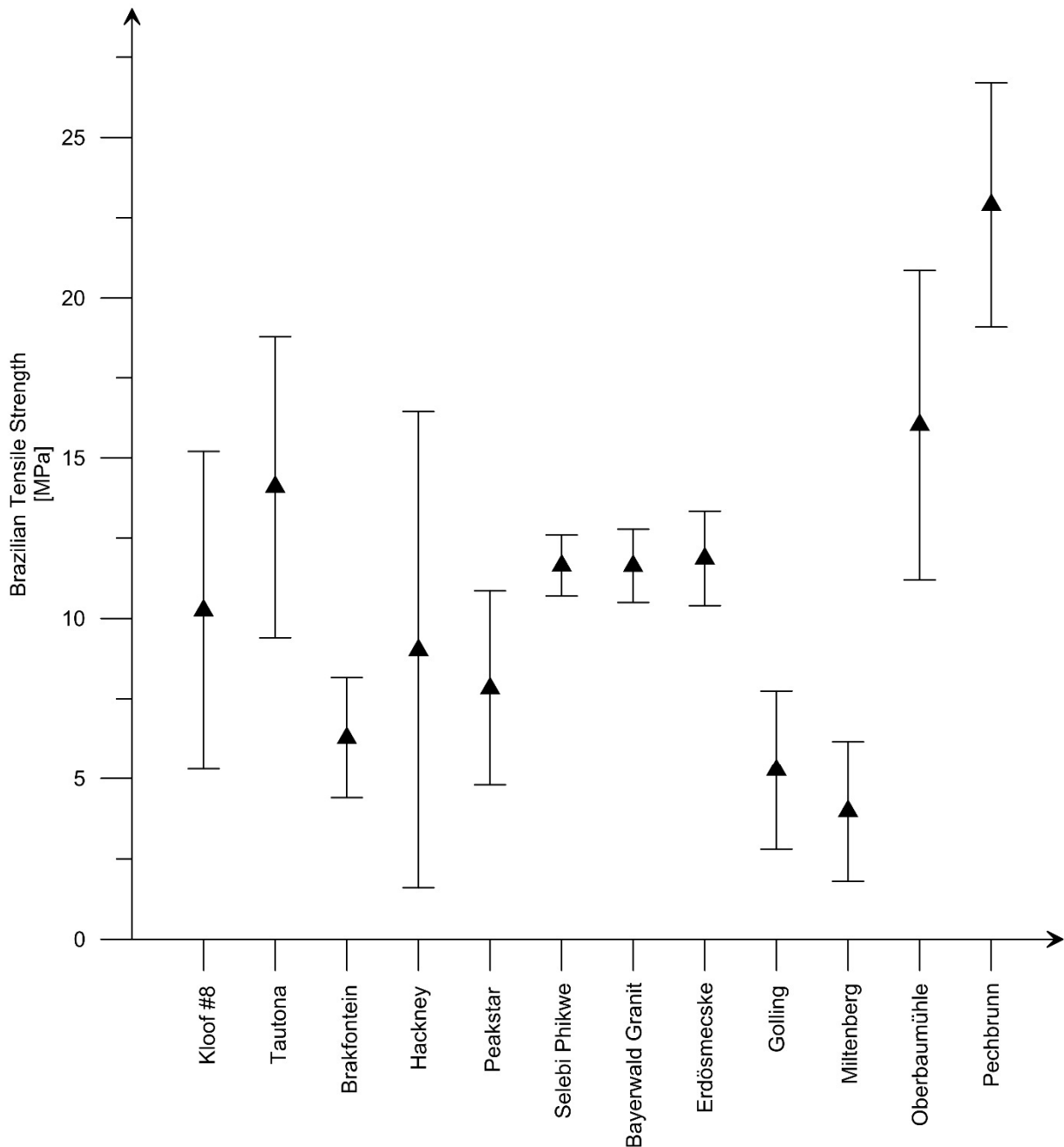


Fig. 68: Mean tensile strength values of all test results for the total amount of samples.

6.6 Abrasivity tests

6.6.1 Cerchar abrasivity test

A comparison of all testing results are shown in Fig. 69. All testing results in detail can be looked up in Tab. 23. Most samples reached for the rock type expected values. Except the samples of Peakstar and of Miltenberg. The abrasivity of the Peakstar kimberlite is unexpected low, because the kimberlite is host rock for diamond mining. But in all laboratory test no diamond minerals could be verified. Though the abrasivity is very low to the breakability of all other occurring minerals. Another unexpected value is found for the Miltenberg quartz sandstones. Due to the high quartz content the abrasivity should be higher. But due to

the low rock strength the testing pin is scratching deeper in the rock and the steel pin isn't as much worn as it would be expected. The Rock strength, especially low rock strength is an important and misleading factor for this test. The extremely high test results for the Hagerbach samples were produced by the Hagerbach Versuchsstollen GmbH and are maybe caused by too weak steel for the testing pin. This could neither be confirmed nor neglected but due to no further problems for all analyzes this value was used.

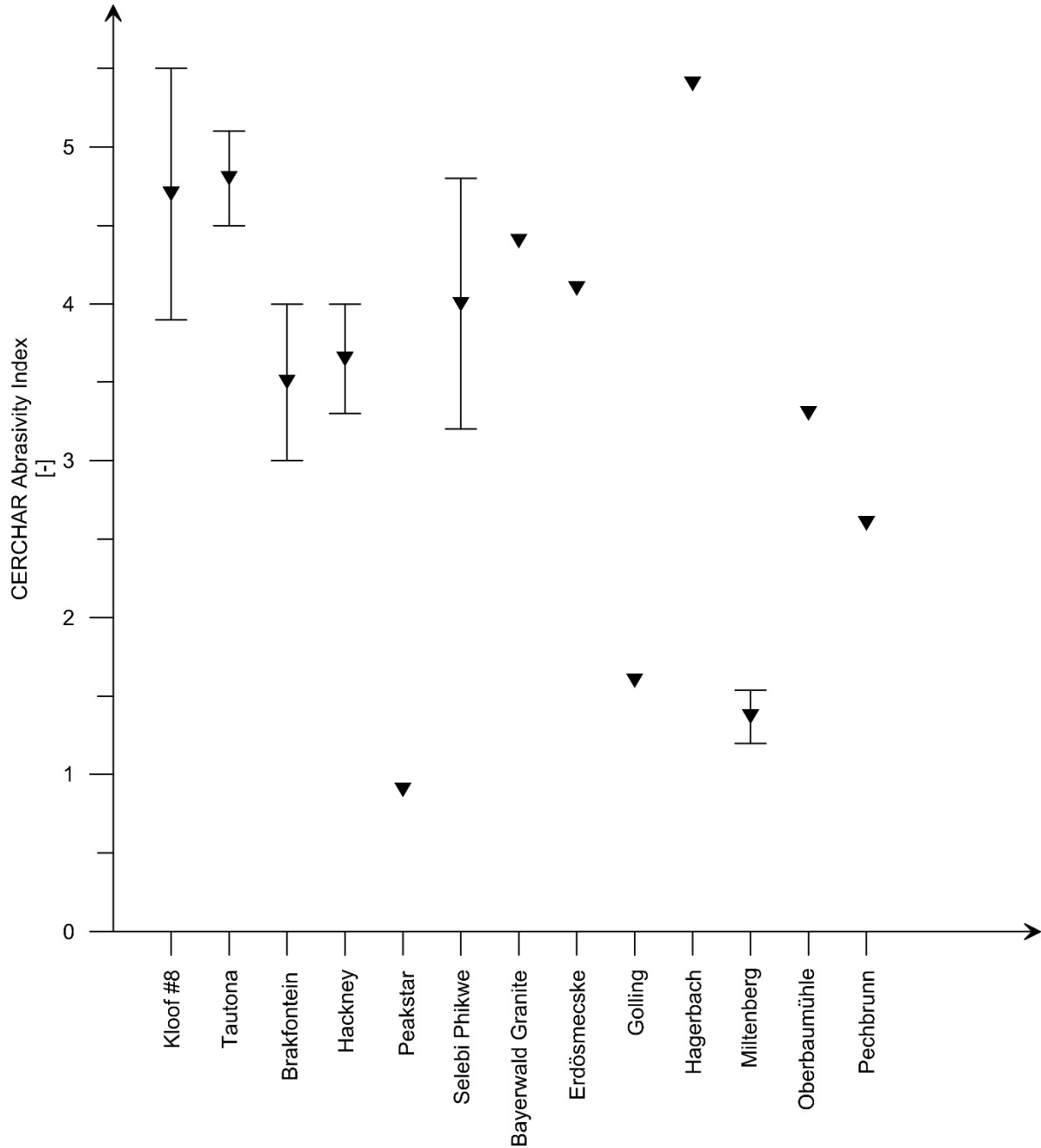


Fig. 69: Illustration of the CERCHAR abrasivity results including the total amount of samples.

Tab. 23: Exact values of all conducted CERCHAR abrasivity tests.

Mine/Quarry	Sample name	CAI [-]	Standard-deviation	Classification
Brakfontein	HIL-BF-1-CAI-1	3	0,55	very abrasive
Brakfontein	HIL-BF-2-CAI-1	4	0,33	very abrasive
Blue Ridge	HIL-BLU-01-CAI-01	4,7	0,3	extremely abrasive
Bayerwald Granit	HIL-BWG-1-CAI-1	4,4	0,38	extremely abrasive
Erdösmecke	HIL-ERD-01-CAI-1	4,1	0,65	extremely abrasive
Golling	HIL-GOL-01-CAI-1	1,6	0,4	medium abrasiveness
Hackney	HIL-HAC-1-CAI-1	4	0,47	very abrasive
Hackney	HIL-HAC-2-CAI-1	3,3	0,31	very abrasive
Kloof #8	HIL-KLF-02-CAI-1	6	0,7	extremely abrasive
Kloof #8	HIL-KLF-03-CAI-1	3,9	0,6	very abrasive
Kloof #8	HIL-KLF-05-CAI-1	4,2	0,3	extremely abrasive
Miltenberg	HIL-MIL-1-CAI-1	1,3	0,05	medium abrasiveness
Miltenberg	HIL-MIL-2-CAI-1	1,2	0,1	medium abrasiveness
Miltenberg	HIL-MIL-3-CAI-1	1,6	0,23	medium abrasiveness
Oberbaumühle	HIL-OBM-1-CAI-1	3,3	0,62	very abrasive
Peakstar	HIL-PEA-1-CAI-1	0,9	1,02	slightly abrasive
Pechbrunn	HIL-PEB-1-CAI-1	2,6	0,42	very abrasive
Selebi Phikwe	HIL-SPH-09-CAI-1	4,8	1	extremely abrasive
Selebi Phikwe	HIL-SPH-10-CAI-1	3,2	0,5	very abrasive
Tautona	HIL-TAU-07-CAI-1	5,1	0,6	extremely abrasive
Tautona	HIL-TAU-08-CAI-1	4,5	0,6	extremely abrasive

6.6.2 LCPC abrasivity test

A comparison of all testing results are shown in Fig. 70. All testing results in detail can be looked up in Tab. 24. Most samples reached for the rock type expected value. Except the samples of Peakstar and of Miltenberg. The abrasivity of the Peakstar kimberlite is unexpected low, because the kimberlite is host rock for diamond mining. But in all laboratory test no diamond minerals could be verified. Though the abrasivity is very low to the breakability of all other occurring minerals. Another unexpected value is found for the Miltenberg quartz sandstones. Due to the high quartz content the abrasivity is expected to be higher. But due to the low rock strength and the high breakability which is shown in the LBC of 94 to 99 % the quartz

grains were crushed and disintegrated and are not able to produce the expected wear of the metal impeller. Low rock strength and high breakability is an important factor for this test.

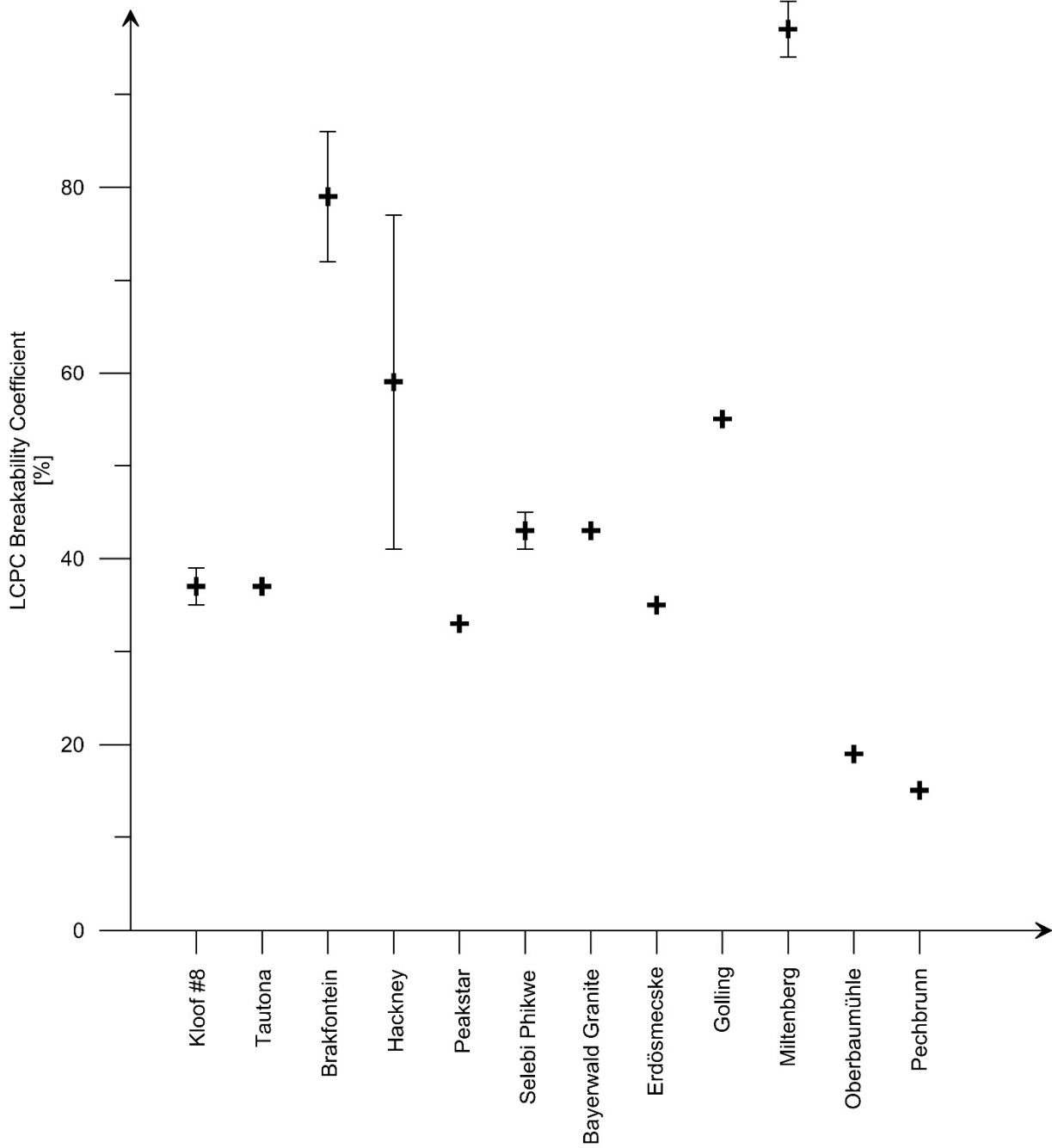


Fig. 70: Illustration of the LCPC abrasivity coefficient results including the total amount of samples.

Tab. 24: Exact values of all conducted LCPC abrasivity tests.

Mine/Quarry	Sample name	LAC [g/t]	Class	LBC [%]	Class
Brakfontein	HIL-BF-1-LCPC-1	1100	very abrasive	86	medium high
Brakfontein	HIL-BF-2-LCPC-1	1180	very abrasive	72	medium
Blue Ridge	HIL-BLU-01-LCPC-1	1100	very abrasive	53	medium
Bayerwald Granit	HIL-BWG-1-LCPC-1	1039	very abrasive	43	medium poor
Erdösmecke	HIL-ERD-01-LCPC-1	1140	very abrasive	35	medium poor
Golling	HIL-GOL-01-LCPC-1	60	not very abrasive	55	medium
Hackney	HIL-HAC-1-LCPC-1	1860	extremely abrasive	41	medium poor
Hackney	HIL-HAC-2-LCPC-1	1260	extremely abrasive	77	medium high
Kloof #8	HIL-KLF-02-LCPC-1	1300	extremely abrasive	42	medium poor
Kloof #8	HIL-KLF-03-LCPC-1	1240	very abrasive	35	medium poor
Kloof #8	HIL-KLF-04-LCPC-1	1180	very abrasive	36	medium poor
Kloof #8	HIL-KLF-05-LCPC-1	1180	very abrasive	36	medium poor
Kloof #8	HIL-KLF-06-LCPC-1	1180	very abrasive	36	medium poor
Miltenberg	HIL-MIL-1-LCPC-1	200	slightly abrasive	98	medium high
Miltenberg	HIL-MIL-2-LCPC-1	200	slightly abrasive	99	medium high
Miltenberg	HIL-MIL-3-LCPC-1	720	very abrasive	94	medium high
Oberbaumühle	HIL-OBM-1-LCPC-1	500	very abrasive	19	very poor
Peakstar	HIL-PEA-1-LCPC-1	180	slightly abrasive	33	medium poor
Pechbrunn	HIL-PEB-1-LCPC-1	499	medium abrasiveness	15	very poor
Selebi Phikwe	HIL-SPH-09-LCPC-1	1100	very abrasive	45	medium poor
Selebi Phikwe	HIL-SPH-10-LCPC-1	1080	very abrasive	41	medium poor
Tautona	HIL-TAU-07-LCPC-1	1439	extremely abrasive	37	medium poor
Tautona	HIL-TAU-08-LCPC-1	1200	very abrasive	37	medium poor

6.6.3 Conclusion of all abrasivity tests

The test results of CAI and LCPC testing are good correlating to each other. Also in comparison to the equivalent quartz content the test results are confirming the abrasivity of the rocks.

In all test results the dependence of the performed index tests to the rock strength is clearly visible and a problem to have in mind for all further testing of the drill head wear. This effect is observable with the samples of Golling and Miltenberg but also for the higher end of the abrasivity of the tested basalts of Pechbrunn. These samples have lower EQc but higher abrasivity index values due to the very high rock strength. This effect is supported by the test results for the breakability coefficient Fig. 71. When looking at the results of Miltenberg the LAC of 200 as minimum and the CAI of 1.6 are unexpected low as the EQc

is almost 60 %. But looking at the breakability of almost 100 % and the rock strength of 36 MPa it is clear that these index tests are not capable of representing the wear of these sandstones.

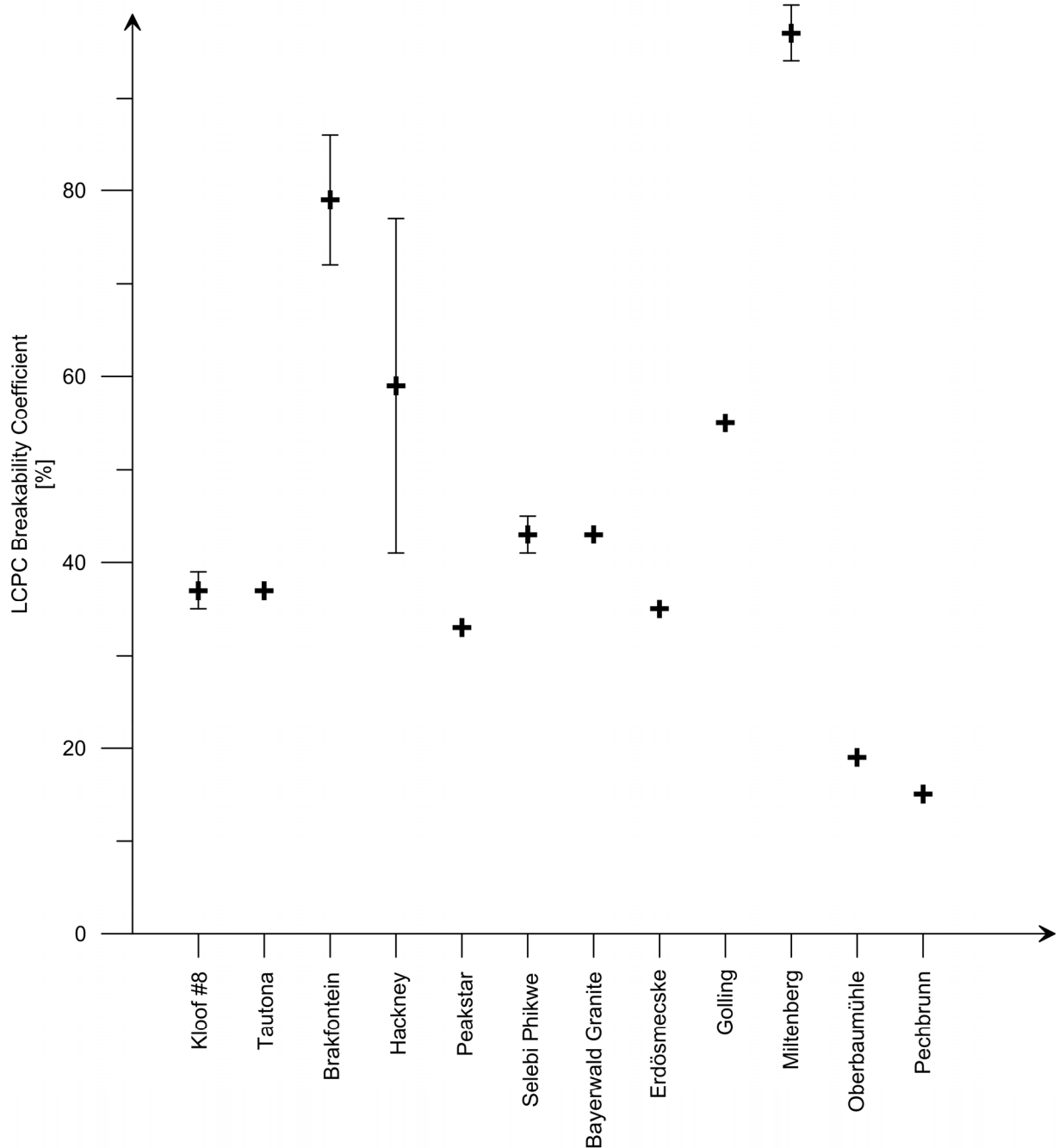


Fig. 71: Illustration of the LCPC breakability coefficient results including the total amount of samples.

6.7 Ultrasonic test

The conducted ultrasonic tests were performed to test the pre-damage of rock samples and as measure for porosity and pore filling grade. All test results are shown in Tab. 25. The denser the rock the higher the v_p and vice versa. The p-wave velocity is also strongly depending to rock strength. A very dense rock with a high rock strength like the Pechbrunn basalt has one of the highest velocities with 6424 m/s. The lowest velocity can be found at Miltenberg for the porous sandstone with low rock strength. It reaches only values of around 2500 m/s.

Tab. 25: Mean p wave velocities of all test results for all samples. N is the number of tested specimen of the particular mine or quarry.

Mine/Quarry	N	v_p
	[-]	[m/s]
Tautona	9	5640.58
Moab Khotsong	5	5014.42
Brakfontein	5	5136.08
Hackney	11	6598.54
Peakstar	3	3510.53
Golling	11	5747.2
Miltenberg	30	2498.27
Oberbaumühle	9	6285.08
Pechbrunn	9	6424.06

6.8 Quartzite and Metaconglomerate of Tautona gold mine for the numerical modelling

As the rocks of Tautona gold mine were the interesting rocks for our numerical simulations are in this chapter in Tab. 26 all results of Tautona gold mine summarized.

Tab. 26: Rock mechanical properties of quartzites.

	UCS			PLT	BTS		CAI	LCPC		v_p
	σ_u	V	w_z	I_{50}	$\sigma_{t,BTS}$	z	CAI	LAC	LBC	v_p
	[MPa]	[GPa]	[kJ/m ³]	[MPa]	[MPa]	[-]	[-]	[g/t]	[%]	[m/s]
Min	58	26	246	5.1	9	6.4	4.5	1200	37	5168
Mean	172	48	445.5	11.1	13.5	12.7	4,8	1319.5	37	5641
Max	237	68	645	17.9	17	13.9	5.1	1439	37	5909

The quartzites of Tautona gold mine can be classified as very strong (R5), brittle and very to extremely abrasive rocks.

6.9 Drill head data

The following chapter summarizes data of over 4700 drill holes of 76 single drill head tests. Most of the drill tests were conducted under the lead of Hilti AG.

6.9.1 Performance

Fig. 72 shows all performance data of all drill heads tested in laboratory and field. This data contains drill heads of different design and size. Due to these differences, especially to size, the performance and the wear could not be clearly correlated and it could be misleading in interpretation. The effect of different drill head size comes clear visible by looking at all conducted drill tests with different drill heads, differing in size, of one location. This is done in Fig. 73 for all tests in Hagerbach Test Gallery.

Thus all following chapters will concentrated only on data of drill head 1 (Fig. 74), which was also the most tested drill head, for all mines. This is also the only drill head which was tested at all locations.

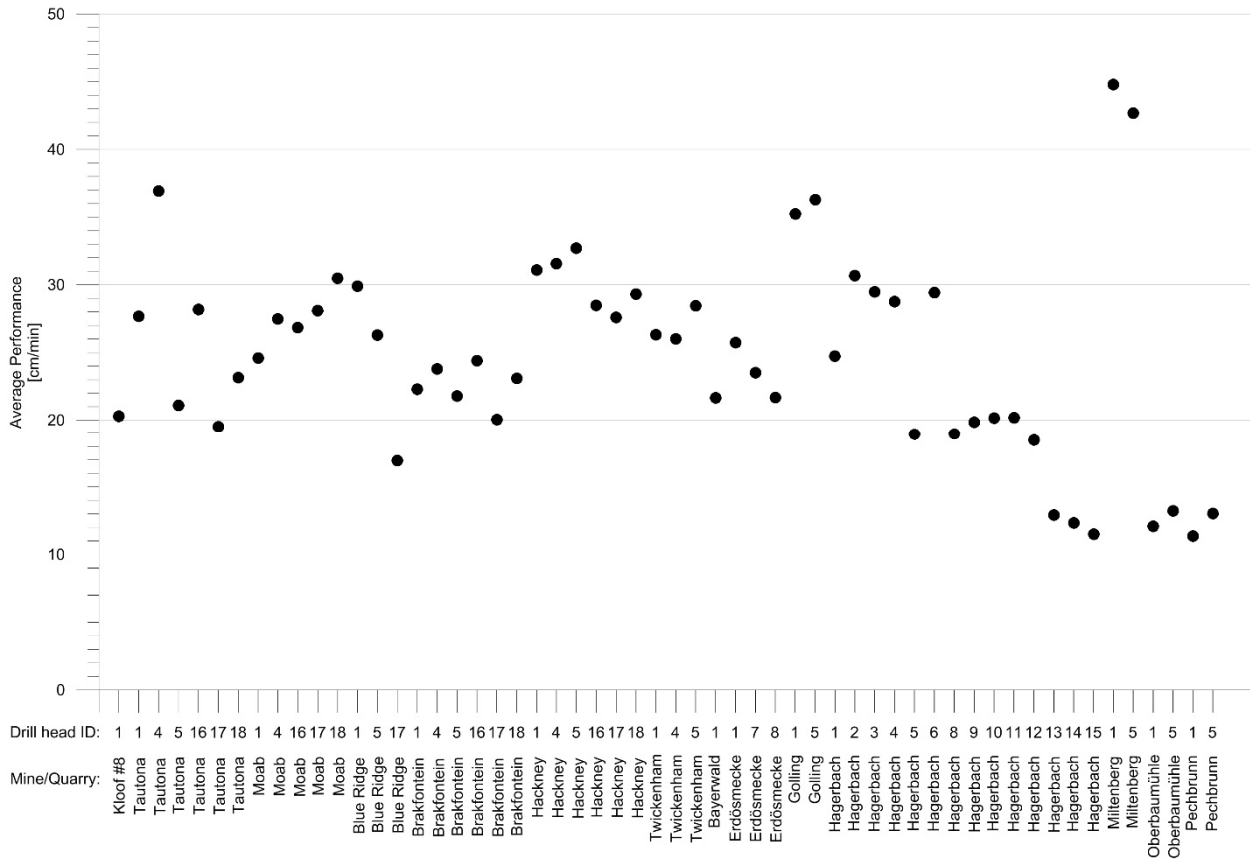


Fig. 72: Illustration of the average performance of all drill heads applied at all considered test sites.

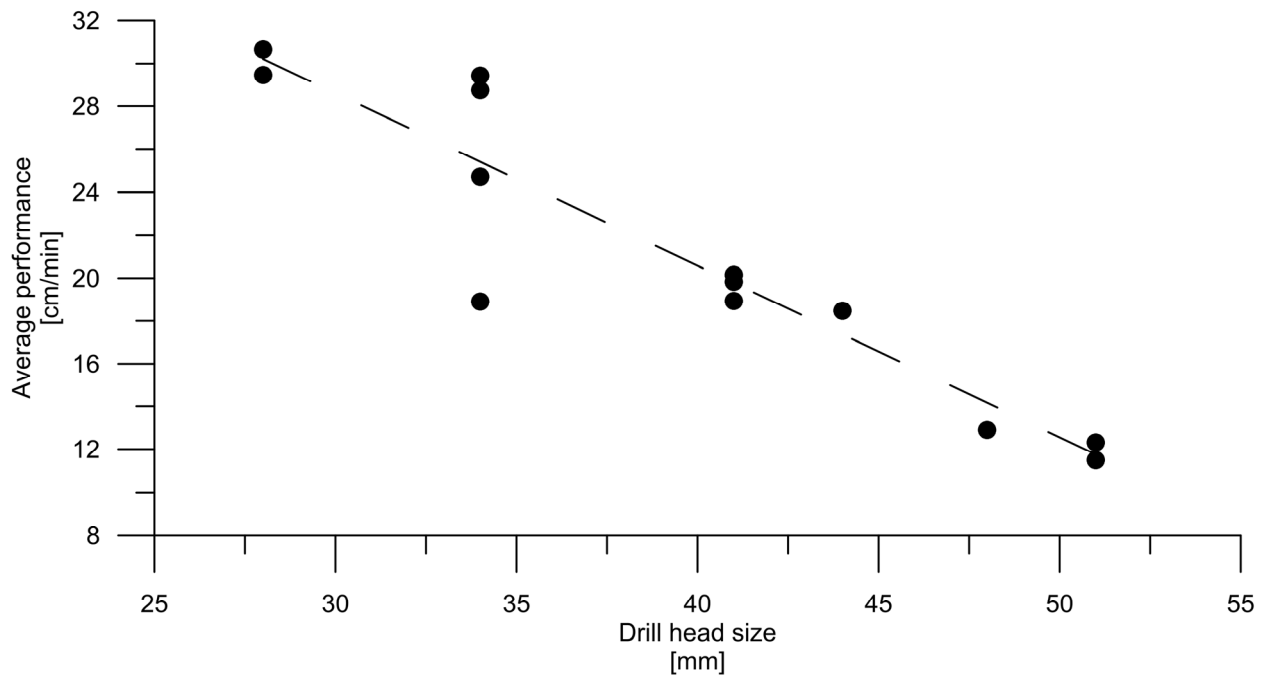


Fig. 73: Correlation between drill head size and drill performance of all conducted tests with the same drill in Hagerbach Test Gallery.

Looking at the overall performance the drill head 1 is drilling with a quite constant drill rate of 20 to 30 cm/min. Especially all quartzite (Kloof, Moab, Tautona), platinum rocks (Blue Ridge, Brakfontein, Hackney, Twickenham) and the main test rocks of Bayerwald granite and Hagerbach are in this midrange span. It's also clearly visible that rocks with lower rock strength like Golling anhydrite and Miltenberg

sandstone result in higher performance and areas with rock of higher strength leads to lower drill speed. This effect can be found at Pechbrunn and Oberbaumühle.

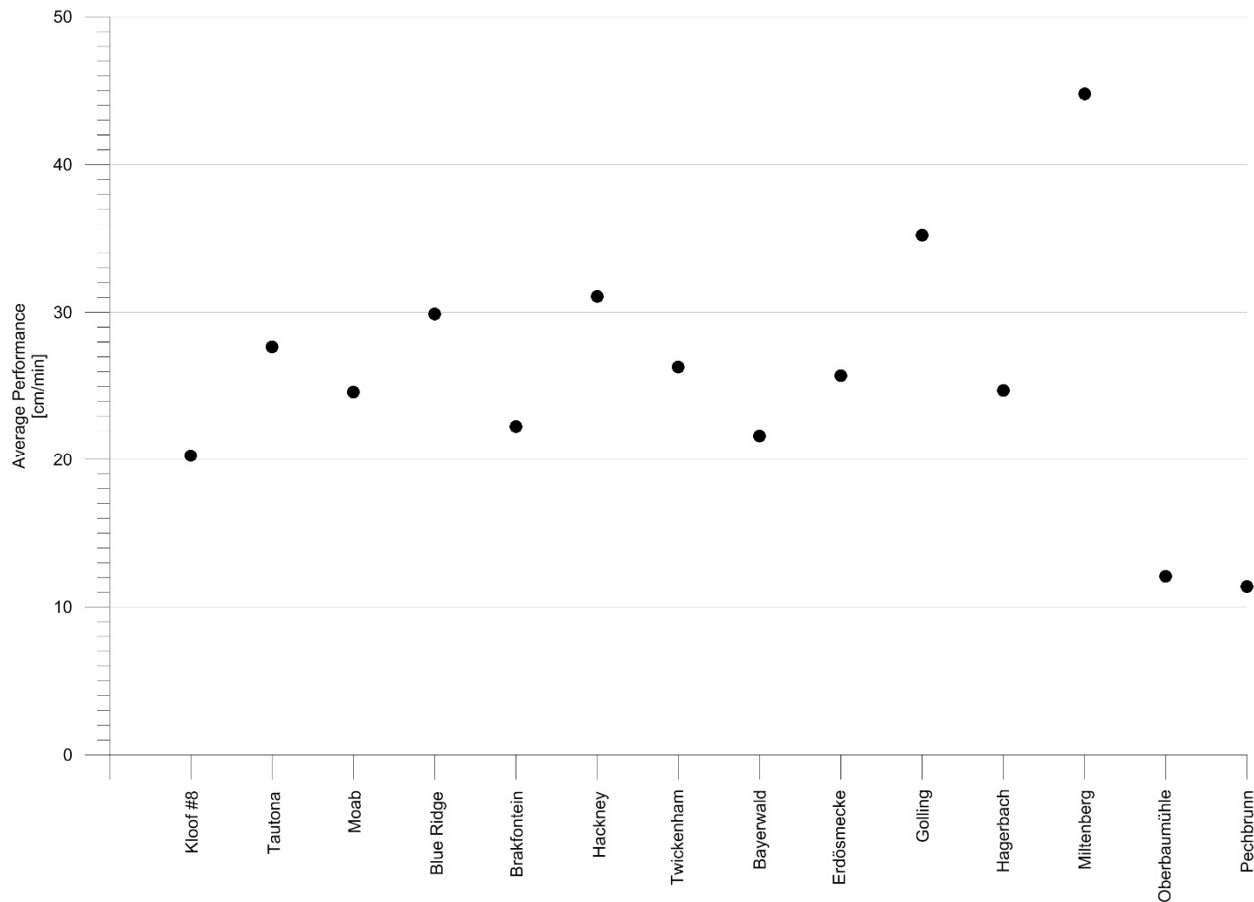


Fig. 74: Illustration of the average performance of drill head 1 for all tested locations.

6.9.2 Wear

In Fig. 75 all wear data of all conducted drill test is shown. For several drill heads no data about weight or diameter of the drill head was noted. But as written in the chapter before we are only looking at drill head 1. This is shown in Fig. 76. Here are also several drill tests without observations about the drill head wear. This point was the main issue for us to conduct additional drill tests in field in Germany. This was done in Golling, Miltenberg, Oberbaumühle and Pechbrunn. It's quite obvious looking at the data that samples with higher abrasive potential as the quartz rich sandstone and quartzite are leading to the highest wear of around 50 $\mu\text{m}/\text{m}$ loss in diameter. Rock samples with lower abrasive potential like the anorthosites of platinum mines or the anhydrite of Golling are leading to very low wear of only 5 $\mu\text{m}/\text{m}$. Looking at the data of Hagerbach it's quite astonishing that these siliceous limestones have also a very low wear potential in comparison to the high CAI value. Also the granite of Erdösmecke has a very low wear rate. This can be explained with the thin section analysis. All index tests like CAI and LCPC are testing fresh surfaces. But looking at the thin section in Fig. 56 the weathering can be found. This could be the reason for local higher breakability and lower wear.

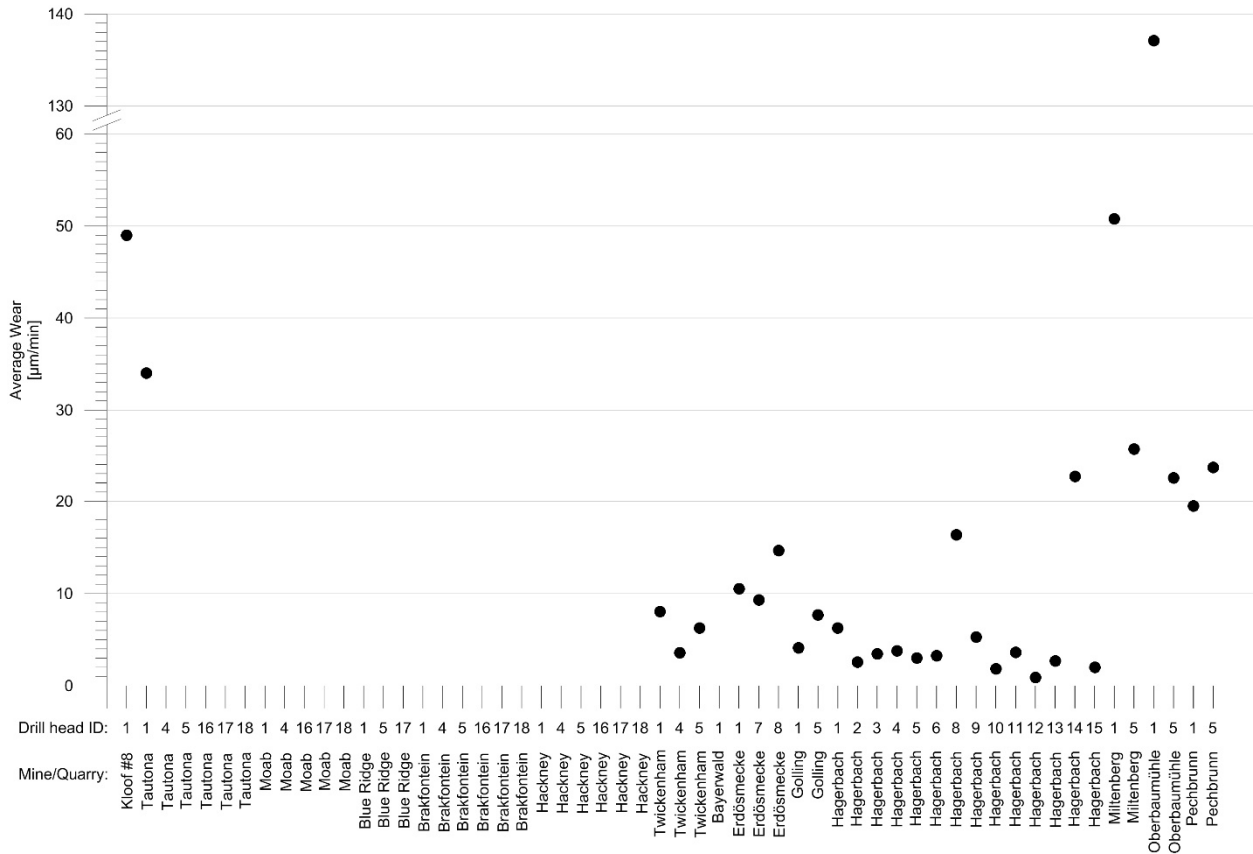


Fig. 75: Illustration of the average wear of all tested drill heads including the data gap, where no wear measurement was performed.

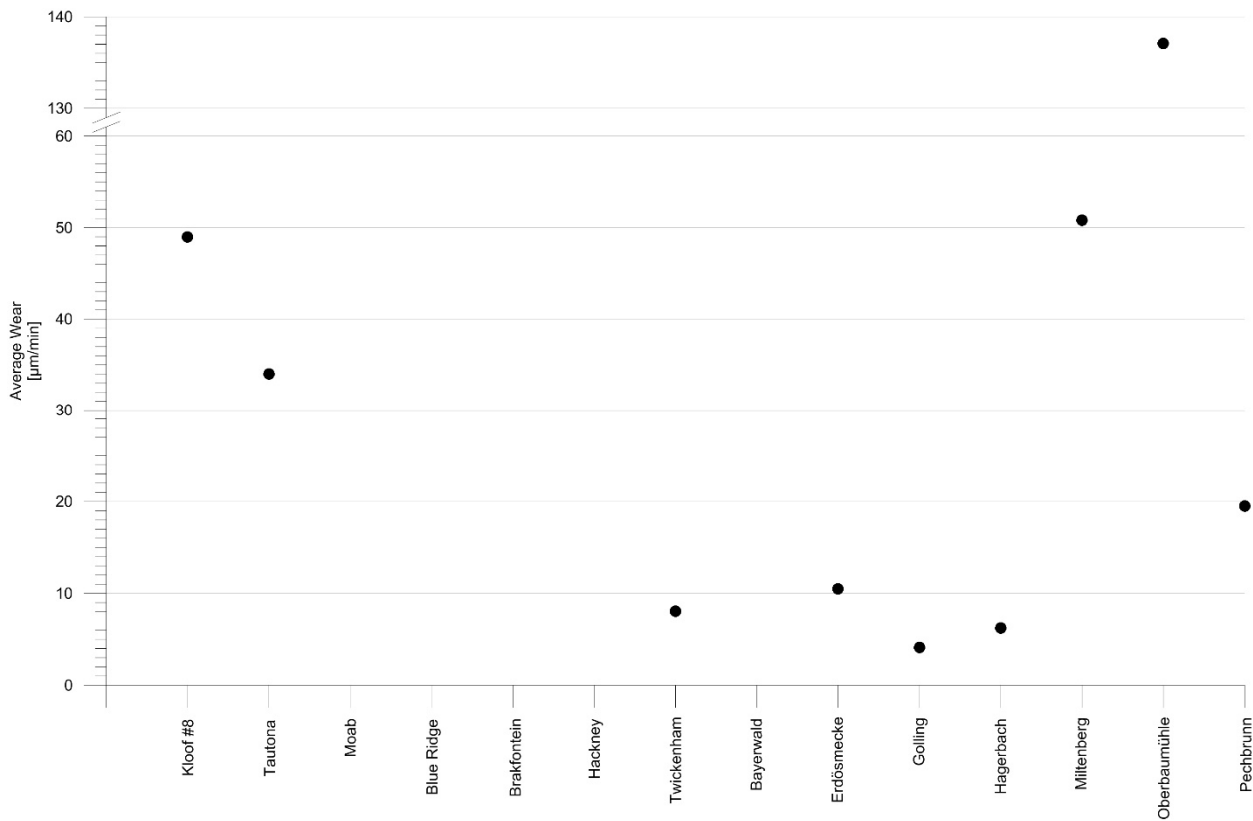


Fig. 76: Illustration of the average wear of drill head 1 for all tested locations including the data gap for mines without wear measurement.

7 Data management and data processing in engineering geology

Nowadays, in the age of bits and bytes and with actual progress in information technology, computers will be used various purposes. This trend is not only observable in private life but also in many lines of business.

The possibilities and the calculation-accuracy are much better and higher than 10 years ago. Data analysis can be obtained on a much higher level than before. But not only the results are improving; the data volume is rapidly increasing - not only in size, but also the amount of files. To work at the state-of-the-art according to all standards for big projects, an increasing number of laboratory and field tests are required. Due to the aim of reaching an enhanced and more precise understanding of the building-underground-interaction during construction work, the amount of data is increasing.

With the increasing data volume, we need to evolve new ways for providing easy-accessible data, in short and long term, and to ensure a comprehensible data structure.

In the current project various international partners are working together. The data are provided from South Africa and Botswana, Switzerland, Hungary, Austria and Germany. The data volume is extraordinary high due to numbers of different conducted test series. An excel spreadsheet for example can easily reach more than 10 MB (maximum capacity of most e-mail providers) and contains several hundred sheets.

Besides the issue of data volume, a universal and simple way of combining the complete set of field and laboratory data was needed to provide a comfortable access for all project partners.

The chair for Engineering Geology at Technische Universität München has developed a web-based database solution to handle all project relevant data in a more appropriate way. We optimized our data management and achieved a fast and easy way of collecting, documenting and analyzing the gained data. The second objective was to provide an easy access to the data for international project partners.

7.1 General database structure

A database system (DBS) is divided in two main parts (SAAKE et al. 2010). On the one hand data storage is needed, in which the data can be saved and accessed again. This first part is called the database itself. The second part manages all access to the database which is needed to maintain data safety, integrity and security. In an ideal case, a parallel multi-user environment is provided. This part is named as the database management system (DBMS).

The applied database type depends on the purpose for which the database is designed. There are several simple database models available, for example the network or hierarchic model. These models are typically used for cross-linked or treelike data structures like file management systems of common computer operating systems. In the file management systems, the data are saved data in single files from different spreadsheet and word processing programs (e.g. Microsoft Excel and Word), which are organized in different folders. A further type of database is the object oriented database. The models of this type can be effectively applied for a smaller amount of datasets, where each dataset contains a high amount of information. In the field of engineering or engineering geology many tests with much information occur. In this case we need to choose the most appropriate database model - the Entity Relationship (ER) Model. This is one of the most common models used in database systems (KEMPER & EICKLER 2011).

In this type of database the data are stored as table-datasets (entities) which are related to each other via identification numbers (ID) being saved in one column (Fields or attributes) per entity (Fig. 77). Due to the relations between the datasets and the building of so called master tables, redundant data and mistakes (e.g. spelling mistakes) can be avoided. This model type supports and combines huge data volumes in a fast way and is therefore very efficient for a rock testing database.

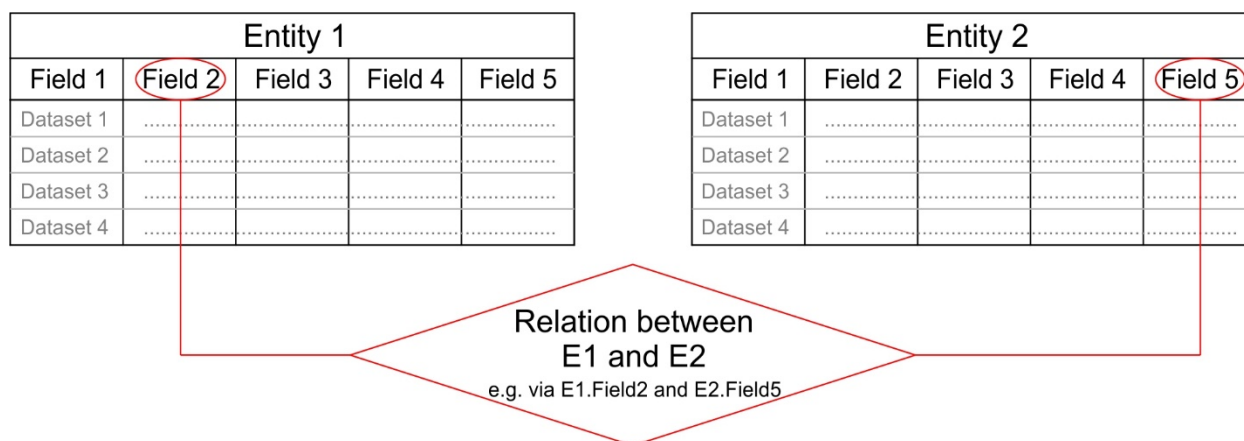


Fig. 77: General Entity-Relationship-Model of a relational database.

The connection (relation) of data can be obtained by the use of certain fields called primary and foreign keys. Primary keys are unique data which identify each dataset within the entity. In the example of Fig. 77 Field 1 can be seen as the primary key. The “Field 2” for entity 1 (E1.Field2) and the “field 5” for entity 2 (E2.Field5) are called the foreign keys, which are combining all datasets of both tables in a unique way. These relations are required to combine different types of entities (e.g. drill data and rock properties for the specific mine).

To access data which is stored in the mentioned way, you have to use a query language, like SQL (structured query language) to join the data from different tables and to present them in the most appropriate way. The general expression of the “relation”, mentioned in Fig. 77 above is shown in following Query 1 as code example.

Query 1: General syntax of MySQL queries where the queried information is stored in the Fields 1, 2 and 5 of both entities shown in Fig. 77.

```
SELECT E1.Field2, E1.Field 5, E2.Field2, E2.Field 5
FROM Entity 1 (E1), Entity 2 (E2)
WHERE E1.Field2 = E2.Field 5
ORDER BY E1.Field2 ASCENDING
```

In such MySQL queries **SELECT** declares which fields are presented, **FROM** defines each table in which the fields are stored and **WHERE** specifies the preconditions (foreign keys) in which the data is connected within the fields. With the **ORDER BY** tag all results can be sorted (**ASCENDING** or **DESCENDING**) for one or more fields.

7.2 Dictionary of further general functions and code snippets used in our database system

In this chapter all MySQL functions and code snippets used to program all queries for this database are explained in this chapter in alphabetical order.

AND/OR operators are used create query results with two or more conditions in the WHERE part of the MySQL statement.

AS is used to declare a new name for a queried field. It is mostly used in this database to rename calculated fields (AVG, MIN, MAX...).

AVG calculates the mean value of all values of a field or all values of a group (GROUP BY).

GROUP BY is used to combine different datasets with the same value for one field for further functions like AVG, MIN and MAX.

LEFT JOIN joins data of two entities where all data of the first entity (E1) is preserved and data of the second table (E2) is added. Each dataset of E1 with no corresponding data within E2 will be supplemented with <NULL> values for the added fields of E2. The foreign key which connects the data for this join is specified with the **ON** command.

ON is used to define foreign key fields to match for **LEFT/RIGHT JOIN**.

REPLACE is used to replace occurrences of defined strings with alternative values. This command is used within this thesis to replace decimal commas with decimal points and vice versa.

TRUNCATE cuts off the decimal part of a numerical value at the given decimal place.

7.3 The rock database of the TUM

There are several script languages and software suites available to realize an ER database. DB2, SQL, MySQL or Microsoft Access can be listed as some of the most common systems. To get an open and cost-efficient database system (DBS), the chair for Engineering Geology decided to develop a MySQL-database (at no charge) with an HTML-PHP web interface, which can be accessed throughout the world with any web-enabled device (computer, tablet or smartphone).

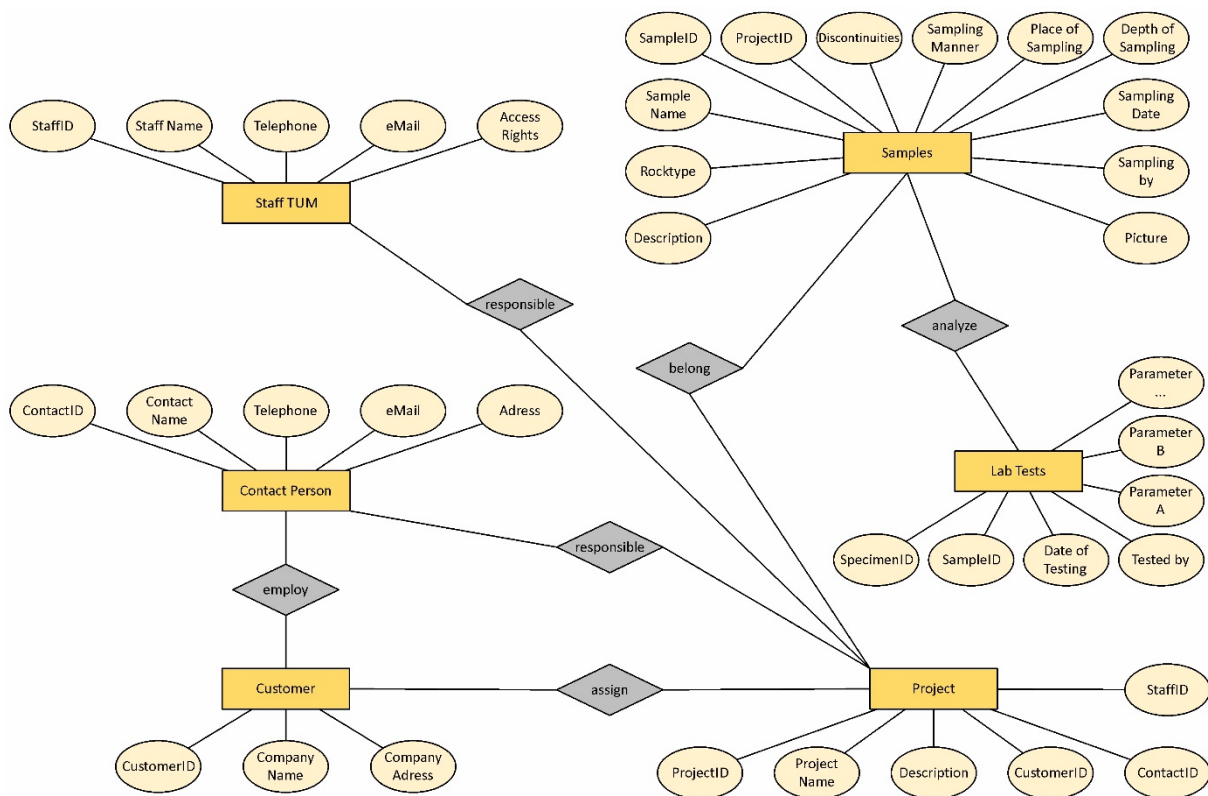


Fig. 78: Entity-Relationship-Model of the base modules according to CHEN (1976) of the rock database (without add ons and user management) established at the Chair for Engineering Geology at TUM.

Fig. 78 shows the ER model of the main part of the rock database. This schematic model provides the basis for the further programming of the database. It illustrates the connection between all entities and reveals which data combinations (queries) are possible when following the connection lines between the attributes (fields) of all entities.

The URL to the rock database is:

<http://www.geo.tum.de/rockdb>

7.3.1 Programming of the database

The programming of the database system (DBS) was started as part of the master's thesis of EITSCHBERGER (2010) and was further developed by Menschik during this PhD studies and afterwards.

The data are stored in tables in a MySQL database and can be accessed by the user due to a web interface (general usage) and a phpMyAdmin interface (administrative access), which grants easy access to the raw data. PhpMyAdmin is also a great possibility for introducing and testing new data queries and expansions for the database in advance of setting up a new part of the web interface. The web interface itself is built with the software Adobe Dreamweaver as a common HTML web page with php code inside.

A complete list of all entities (tables) and attributes (fields) is attached in appendix A.

7.3.2 Database structure and web interface

The database consists of the following four modules (Fig. 79): user management, general project data, laboratory data and add ons. The first three modules form the base component of our database and can be expanded with additional functionality using add ons.

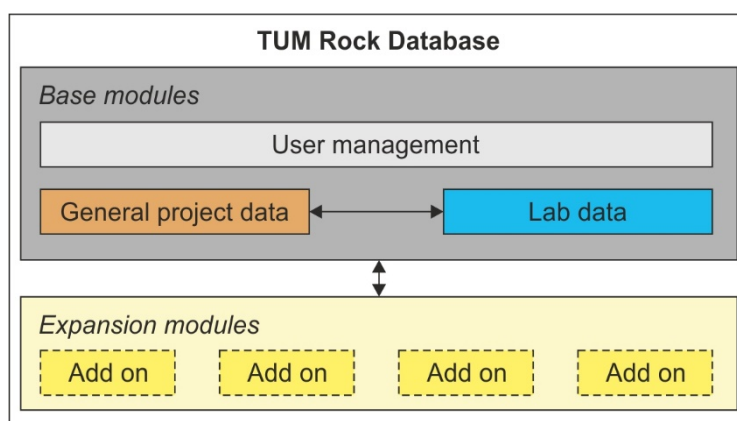


Fig. 79: General, schematic sketch of the TUM rock database-layout with all modules.

7.3.2.1 Base modules

The Base modules are the core of our database system and are managing all data coming from all laboratory tests conducted by the chair for Engineering Geology. These parts are stand-alone modules.

By means of the User management module all access to single data and the whole database is supervised. This module provides the base of granting access to data and later to special add ons only to respective customers and special users. It allows automatic data sharing restricted to project partners and no third party members. The display language is managed depending on the customer settings.

Currently there are 4 different kinds of user types. The administrators have access to all modules and thus are able to access all data. Users of the “full access”-type can write and read all data but are not allowed to create new users and change user properties. Users with “access to some content” are only able to read and write laboratory data. It's not possible to create new project, samples or persons using this account type. The “external” user is only able to read data from his or her own company. This user-type is not able to write any data and has no access to the data of other customers.

The user data is stored in a table (tblbenutzer) which is queried each time a user types in his credentials to log in the web interface. During the log-in procedure the user data is stored in session variables (superglobals) which are saved and valid throughout the whole webpage until the user logs out. These variables, especially the user type, is verified by the help of a php script and the access to the requested web page is granted or not.

All accesses to the web interface are recorded and stored for safety reasons. With this security part of the database it is possible to retrace all logins using the login date.

The project data module contains all project relevant data including the project name, the description and the customer data. In addition, the information about incoming samples, which are processed to test specimen, is collected and related to a certain project. This module is set to be the main connection between all additional data from other modules like laboratory and field test results and data coming with the add-ons. This connection is essential for all further analyses, plotting of test results and exporting data of the database.

This module is divided in 6 tables which are shown by following Tab. 27.

Tab. 27: Table of all tables of base module and short description of it first order relation within the database.

Name of table	Content	Directly related to
tblprojekte	project name project code project description	tblauftraggeber tblmitarbeiter tblproben
tblauftraggeber	Company name and address	tblprojekte tblauftraggeber
tblansprechpartner	Contact details of contact person (e.g. Name, Telephone, e-mail...)	tblauftraggeber
tblmitarbeiter	Contact Details of person in charge from TUM for the project	tblprojekte
tblproben	Data of all samples of one project (e.g. Rock type, name and description)	tblprojekte tblgesteinsart <u>connection to laboratory and field data</u>
tblgesteinsart	Reference table for rock types	tblproben

The entity “tblproben” is the direct connection to all test data and represents the link between all of project data module, the laboratory data module and all current and future add on modules.

All data derived from laboratory tests can be stored in the laboratory data module. Currently we are storing data from uniaxial compression, point load, Brazilian tensile, CERCHAR, LCPC and ultrasonic tests. This data can be entered and displayed using the web interface, which is accessible throughout the world via the internet by any normal web browser (e.g. Mozilla Firefox, Internet Explorer etc.) from almost any web-enabled device (Computer, tablet or smartphone). Each laboratory test has its own corresponding MySQL table in which all data is collected.

The database management system uses the login credentials to decide which modules and which part of the data can be accessed by a certain user. This automatic choice of tools and selection of data is defined as “view”. There are three “views” currently in application.

One administrative (“base view”); one for project partners (“project/external view”); and one as a special view for the first add on. The “base view”, accessed by administrators and users with “full access” and “access to only some extent”, is used for laboratory data entries and creation of new customer, project and sample datasets. This view is further applied for the creation and the editing of the user dataset for the user

management module. These administrators have access to all data. With this view all other parts and tools of the database system like single and mean value requests can be accessed.

The “project view”, which is only for “external” users, has only access to the query tools (single and mean values) to show the data corresponding belonging to their company and to the display the processing state of their inquired laboratory tests.

“Special views” are individually programmed for specific tasks of the corresponding add on and can only be accessed by the research partners. The first programmed “special view” is explained in more detail in the sub-section after next (Add ons on page 90).

7.3.2.2 Query tools

To access data in a more appropriate way we created several tools, already mentioned above, which allow simple analyses of the laboratory data. With the first tool it is possible to show all single laboratory tests in detail with the “all (single) value” query for one project.

With this “single value” query (Fig. 80) all laboratory tests of one single sample, of all project samples or certain client samples can displayed. One of these selection categories can be chosen with three drop down menus in the tool header. It is possible depending on the user view to query all laboratory test settings and properties or only all for the client available data which are stored in the database. It is further possible to display and download the laboratory form with additional information as pdf file. As an example of the used single value query (MySQL syntax) shown in this figure can be found in Query 2.

Query 2: Syntax for the “Single Value Query” for uniaxial compression test of one specific sample. %s is a php-variable going back to the http-form of the webpage and is generated automatically from the selection stated with the help of the tool header. This variable represents the value of the primary key for one specific sample within the sample table (tblproben).

```
SELECT 1DVProbenID, 1DVPruefkoerperID, 1DVPruefkoerper,
       1DVEinaxiale_Druckfestigkeit, 1DVE_Modul, 1DVV_Modul,
       1DVZerstoerungsarbeit, 1DVFormblatt, 1DVTyp, 1DVwb,
       tblauftraggeber.AufCode, tblprojekte.ProCode, tblproben.PrbName
FROM tbl1dv, tblauftraggeber, tblprojekte, tblproben
WHERE 1DVProbenID = %s AND tblauftraggeber.AufAuftraggeberID =
      tblprojekte.ProAuftraggeberID AND tblprojekte.ProProjektID =
      tblproben.PrbProjektID AND tblproben.PrbProbenID = tbl1dv.1DVProbenID
ORDER BY 1DVPruefkoerper ASC
```

Sample	Project	Rocktype	Rockname	UCS [MPa]	Young's Modulus [GPa]	V-Modulus [GPa]	Destructionwork [kJ/m ²]
Hilti -Samp-1-1DV-1	T	Quartzite	Quartzite	213.7	60.14	54.53	571.8
Hilti -Samp-1-1DV-2	T	Quartzite	Quartzite	206.2		52.75	469.1
Hilti -Samp-1-1DV-3	T	Quartzite	Quartzite	237.4		51.35	645.8
Hilti -Samp-1-1DV-4	T	Quartzite	Quartzite	232.9		68.49	513.5
Hilti -Samp-2-1DV-1	T	Quartzite	Quartzite	58.1		26.62	246.6
Hilti -Samp-2-1DV-2	T	Quartzite	Quartzite	166.5	55.83	44.52	538.2
Hilti -Samp-2-1DV-3	T	Quartzite	Quartzite	141.5		50.92	360.8

Fig. 80: Illustration of the navigation bar (left side) and single value query of the base view of the rock database of TUM.

With a click on the sample name a more detailed window opens (Fig. 81), more data for this sample test is shown and the laboratory form can be downloaded.

Sample:	HIL-Samp-1-1DV-1		
Date:	28.10.2009		
Person in charge:	Menschik/Käsling		
Length:	104,8 mm	Diameter:	50,0 mm
Density:	2,667 g/cm ³	Angle between Discontinuities:	80°
Uniaxial compressive strength:	213,7 MPa	V modulus:	54,53 GPa
Destruction Work:	571,8 kJ/m ³	Young's modulus:	60,14 GPa
Energy till failure:	571,8 kJ/m ³		
Form:	HIL-Samp-1-1DV-1.pdf		

Fig. 81: UCS information window for testing results of one specific sample.

The second tool is the “mean value” query. In addition to the display possibilities of single values of laboratory results, we introduced this query to get an overview of all values concerning one sample (Fig. 82). This tool enables the user to calculate the arithmetic mean values as well as display minimum and maximum either for all analysis results for the complete set of specimen concerning one specific sample of a certain project; or for the complete set of specimen of the total number of samples amongst all projects of one client as shown below. This query is defined as shown in Query 3.

Query 3: Exemplary mean value query MySQL statement of all test results of all specimen of all sample of one project.

```
SELECT proname AS Projekt, prbname AS Probe,
TRUNCATE(MIN(1DVEinaxiale_Druckfestigkeit),0) AS 1DV_min,
TRUNCATE(AVG(1DVEinaxiale_Druckfestigkeit),0) AS 1DV_avg,
TRUNCATE(MAX(1DVEinaxiale_Druckfestigkeit),0) AS 1DV_max,
TRUNCATE(MIN(1DVZerstoerungsarbeit),0) AS Wz_min,
TRUNCATE(AVG(1DVZerstoerungsarbeit),0) AS Wz_avg,
TRUNCATE(MAX(1DVZerstoerungsarbeit),0) AS Wz_max,
TRUNCATE(MIN(1DVE_Modul),0) AS E_Modul_min,
TRUNCATE(AVG(1DVE_Modul),0) AS E_Modul_avg,
TRUNCATE(MAX(1DVE_Modul),0) AS E_Modul_max,
TRUNCATE(MIN(1DVV_Modul),0) AS V_Modul_min,
TRUNCATE(AVG(1DVV_Modul),0) AS V_Modul_avg,
TRUNCATE(MAX(1DVV_Modul),0) AS V_Modul_max, TRUNCATE(MIN(PLTUCS),0) AS
PLT_min, TRUNCATE(AVG(PLTUCS),0) AS PLT_avg, TRUNCATE(MAX(PLTUCS),0)
AS PLT_max, TRUNCATE(MIN(SPZSpaltzugfestigkeit),0) AS SPZ_min,
TRUNCATE(AVG(SPZSpaltzugfestigkeit),0) AS SPZ_avg,
TRUNCATE(MAX(SPZSpaltzugfestigkeit),0) AS SPZ_max,
TRUNCATE(AVG(lcpclak),0) AS LAK_avg, TRUNCATE(AVG(lcpclbk),0) AS
LBK_avg, REPLACE(TRUNCATE(AVG(caiwert),1), '.', ',') AS CAI_avg,
TRUNCATE(MIN(USPvp_p),0) AS vp_min, TRUNCATE(AVG(USPvp_p),0) AS
vp_avg, TRUNCATE(MAX(USPvp_p),0) AS vp_max, 1DVProbenID, PLTProbenID,
SPZProbenID, LCPCProbenID, CAIProbenID, USPPProbenID
FROM tblauftraggeber, tblprojekte, tblproben LEFT JOIN tbl1dv ON 1dvprobenid
= prbprobenid LEFT JOIN tblplt ON pltprobenid = prbprobenid LEFT JOIN
tblspz ON spzprobenid = prbprobenid LEFT JOIN tbl1lcp ON lcpcprobenid
```

```

= prbprobenid LEFT JOIN tblcai ON caiprobenid = prbprobenid LEFT JOIN
tblus_p ON USPProbenID = prbprobenid
WHERE aufauftraggeberid = proauftraggeberid and prbprojektid = proprojektid
and proauftraggeberid = %s
GROUP BY prbprobenid
ORDER BY Projekt, aufcode, procode, prbname
    
```

These mean values can be exported as a csv file which is supported by most statistical software packages for further and more detailed analyses.

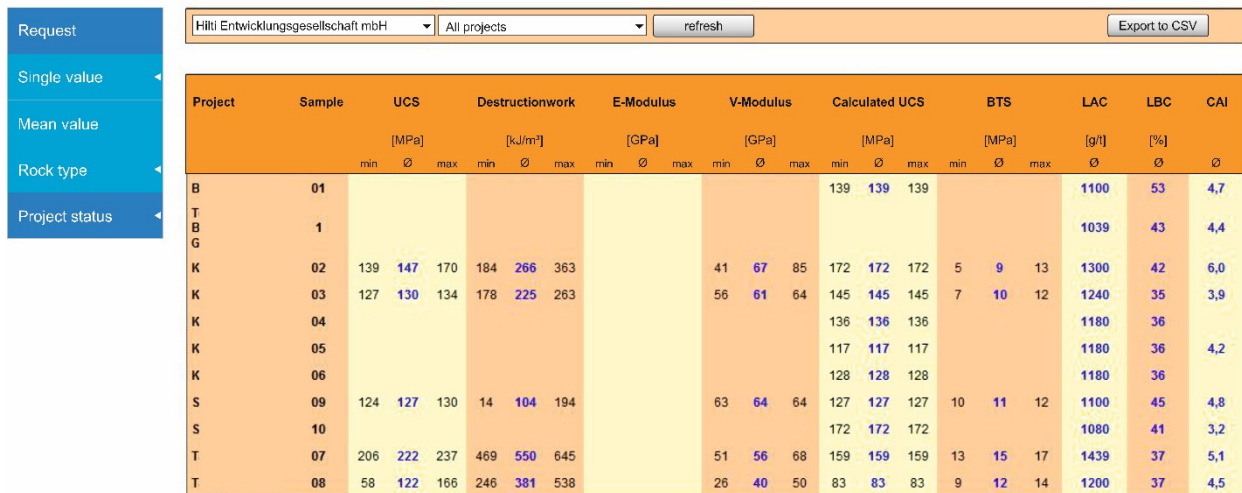


Fig. 82: Navigation bar and mean value query with export function of the project view of the rock database of TUM.

In the mean value calculation tool all single values can be accessed individually for each test on a certain sample by one single mouse click on the mean value. In the “single value” window it is possible to get further information about each sample in the same way as it is possible in the “single value query”.

It is intended to develop a plotting tool to display all data of one sample or one project in various diagrams (e.g. UCS vs. CAI of all samples of a project or all UCS of one sample in a boxplot). At current stage only Whisker-Box-Plots are supported for analysis for all single results of one sample.

By use of the third tool it is possible to request all mean values of all ever conducted laboratory tests for one specific or multiple specified rock types. This tool works similar to the mean value request.

The fourth and last tool is the project status query (Fig. 83). With this query tool all project partners are able to check the progress of inquired tests. This tool provides data on the testing progress, the status of the report, and the information about invoicing.

Processing status

Projects from Sample Company	Subproject	Status of lab testing		Status of lab report		Status of invoice	
Sample project 2	2	queued	19.03.2015	n/a		n/a	
Sample project 2	1	in progress	16.03.2015	in progress	16.03.2015	in progress	16.03.2015
Sample project 1		closed	01.03.2015	shipped	05.03.2015	payed	09.03.2015

Fig. 83: Project status window for all projects of one project partner.

7.3.2.3 Add ons

This type of modules is built for special requests and allows more specific analyses of existing and new types of collected data (e.g. field test data and their relation to preexisting laboratory data). This type of data is typically connected to one single project or sample (Fig. 84). The structure of an ER type database especially the relations between different data enables the customer by use of the database to perform combined analysis of laboratory and field test results.

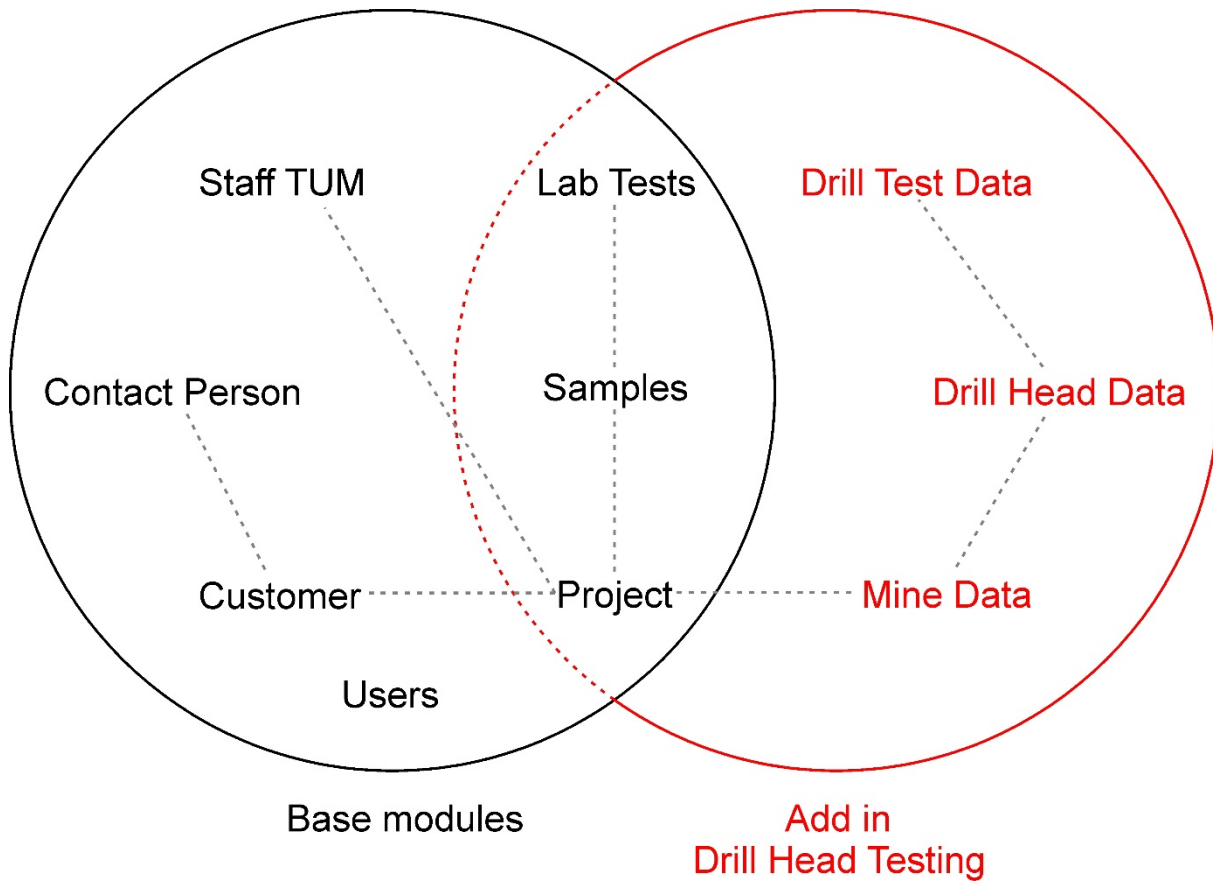


Fig. 84: Illustration of the connection between case modules and the drill head add-on.

The first add on (Fig. 85) is generated for the integration of drill head field testing data (performance and wear) and details of the test sites (quarries and mines distributed over the world) during the PhD studies of Menschik (ongoing). This module allows an easy correlation of rock mechanical properties with performance and wear data of the drill equipment in combination with rock type, depth, and other details of the test sites.



Fig. 85: Navigation bar for the Hilti view of the database incl. add on for drill head testing.

Within this add on containing a special view and several new queries were added to the project view. So the data of all tested mines and all tested drill heads is easily accessible within the web interface. By the help of one of the queries all drill head test data are visible. Beside the calculated mean values for wear and performance all data is plotted in scatter diagrams (Fig. 86) and all single values are listed beneath all plots. In addition to the new introduced queries descriptions of all conducted and in the database stored laboratory tests are available in the navigation panel.

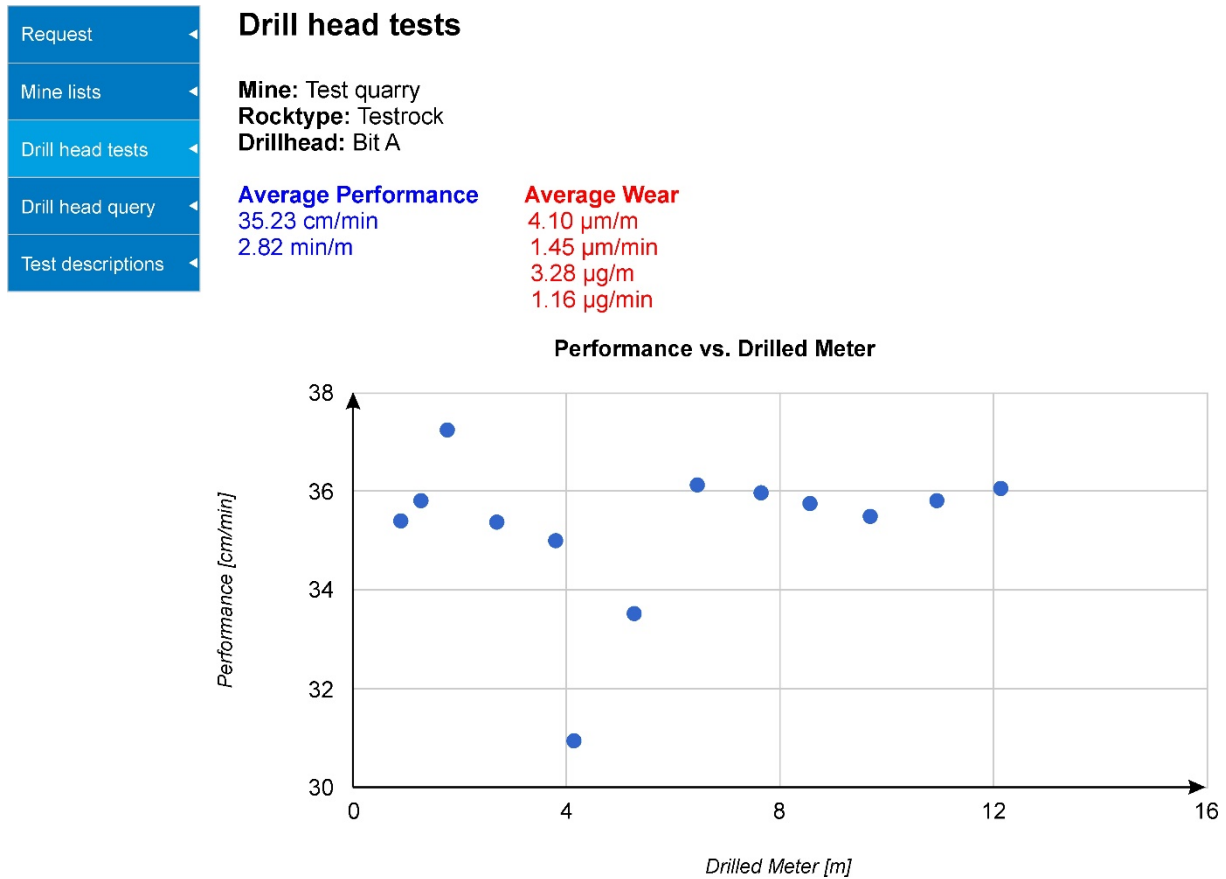


Fig. 86: Illustration of the automatic calculated analysis of drill test data within the web interface (anonymized).

The main aspect of this view is the drill head query which is explained in more detail in the section Data input for drill head add-on of the following chapter 7.3.3.

Though not all clients are familiar with the testing methodology a tool which allows to read all important facts and to gain all information about the used standards is introduced and can be accessed through the web interface.

7.3.3 Data processing (recommended work flow)

7.3.3.1 Name concept

To manage a bigger amount of data with a database system makes it indispensable to work with a name concept which generates unique, distinct and precise project, sample and test specimen names for every object within the database. Our name concept is according to our database structure. With the creation of a new entry for project partners, projects, samples or laboratory test results a unique three letter code has to be entered for each dataset. The name of each object, like of samples and specimen, then is derived from the combination of these stored codes. A complete list of possible laboratory test codes is shown in Tab. 28.

Our Name concept follows the following scheme:

CLI - PRJ - 001 - SPZ - 008

with: CLI Client code
PRJ Project code
001 Sample number
SPZ Name of the laboratory test
008 Specimen number for this specific test

Tab. 28: Complete list of possible laboratory test codes for our name concept.

3 letter code	Name of the laboratory test
1DV	Uniaxial compression test
SPZ	Brazilian tensile test
PLT	Point load test
LCPC	LCPC abrasivity test
CAI	CERCHAR abrasivity test
USP	p-wave velocity determination with ultrasonic test

Using this scheme to identify a specific object within our database typical names unfold which are presented in Tab. 29.

Tab. 29: Typical object names within the rock database with example.

	General object name	Example
Project	CLI - PRJ	HIL - TAU (Hilti Tautona-mine)
Sample ID	CLI - PRJ - 001	HIL - TAU - 01
Specimen ID for specific laboratory test	CLI - PRJ - 001 - 1DV - 001	HIL - TAU - 01 - 1DV - 04

7.3.3.2 General Data input and data manipulation

Data entry is done by using the web interface. The data entry sequence is conform to the name concept and it is not possible to enter projects or samples without setting client details in previous. First provided data must be details about the client and the person of contact. Second data must be further information about the project. For the third step the sample details must be entered. Only after this last step it is possible to enter laboratory results and forms and work with the newly entered data.

All data entries are made with the help of the web interface. A form within the web interface is programmed in html and php and sends all data, entered in the browser, to the MySQL database (Query 4).

Query 4: Simplified SQL query for dataset entry for a new client. The \$-symbol is part of php code and defines variables which are filled with data with the help of an html-php-form.

```
INSERT INTO tblauftraggeber (AufFirmenname, AufCode, AufStrasse,
    AufPostleitzahl, AufOrt)
VALUES ($AufFirmenname, $AufCode, $AufStrasse, $AufPostleitzahl, $AufOrt)
```

For each object type (Client, project, sample, test) are two data manipulation interfaces programmed. One for the new entry and one for editing of data. The interface for a new client entry according to Query 4 is shown in Fig. 87.

Fig. 87: Data entry interface for new clients showing the navigation bar and the form itself.

For samples and tests an additional tool within the new entry interface is provided to add similar samples and tests for one sample in a fast and easy way. With this tools, after entering all details for a specific sample, it is optional to enter a similar sample with only one click (Fig. 88). All details are transferred from the just added sample to the next one. This helps to add easily many similar samples or tests for a specific sample. The only necessity is the change of the sample id or specimen id.

New sample

Fig. 88: Interface for sample entry with the buttons “insert sample” and “insert similar sample” which allows to enter a similar sample with identical properties as the previously entered sample.

The second interface for data manipulation, the so called management area of each object type, creates, on calling the tool, a complete list of all elements of the chosen object type e.g. all Clients (Fig. 89). This list is loaded in several pages, which can be browsed with help of the small arrows underneath the data box, to keep track of all data. From this list all detailed data can be shown and edited with clicking on the edit button (Fig. 90).

Clients

Company name	City		
Client 1	Augsburg	Contact person	Edit
Client 2	Rosenheim	Contact person	Edit
Client 3	Düsseldorf	Contact person	Edit
Client 4	Bernried	Contact person	Edit
Client 5	Karlsruhe	Contact person	Edit
Client 6	Munich	Contact person	Edit
Client 7	Schrobenhausen	Contact person	Edit
Client 8	Schrobenhausen	Contact person	Edit
Hilti Entwicklungsgesellschaft mbH	Kaufering	Contact person	Edit
Client 10	Munich	Contact person	Edit



Client: 1 to 10 of 60

Fig. 89: Illustration of the management console for all client entries. Within this window edits are possible and the view of the project partner can be reached by clicking on the corresponding button.

Edit Client

Compan Name:	Hilti Entwicklungsgesellschaft mbH
3 letter code:	HIL
Adress:	Hiltistr. 6
Zip code:	86916
City:	Kaufering
<input type="button" value="edit client"/>	

Fig. 90: Editing window for the data manipulation of client data.

The creation of a new and the editing of existing contact persons of one client can be obtained in the same way with the use of the data management tools for clients (Fig. 89). From there it is possible to reach the editing (Fig. 90) and entry window for contact persons.

To generate and to manage data for project or samples the approach is also similar to all other data entries. There are two interfaces for each. One for data entry and one for data manipulation.

The laboratory test interface is slightly different. Before new laboratory test can be entered the user has to choose the Client, the project and the specific sample on which the test was conducted in exactly this sequence with the use of the drop down menu on top of the page (Fig. 91). After refreshing the page all previous conducted laboratory tests are listed and can be edited. It is easily possible to access the laboratory form for each test from this site by clicking on the pdf-symbol.

Hilti Entwicklungsgesellschaft mbH

Tautona

07

refresh

Enter new lab test:

UCS

BTS

PLT

LCPC

CAI

USP

Sample: HIL-TAU-07

Rock type: Quartzite

Rock: Quartzite

Lab test	Specimen ID	Date	Form	
Uniaxial comprssion test	HIL-TAU-07-1DV-1	28.10.2009		<input type="button" value="edit"/>
Uniaxial comprssion test	HIL-TAU-07-1DV-2	28.10.2009		<input type="button" value="edit"/>
Uniaxial comprssion test	HIL-TAU-07-1DV-3	28.10.2009		<input type="button" value="edit"/>
Uniaxial comprssion test	HIL-TAU-07-1DV-4	28.10.2009		<input type="button" value="edit"/>
Brazilian tensile test	HIL-TAU-07-SPZ-1	28.10.2009		<input type="button" value="edit"/>
Brazilian tensile test	HIL-TAU-07-SPZ-2	28.10.2009		<input type="button" value="edit"/>
Brazilian tensile test	HIL-TAU-07-SPZ-3	28.10.2009		<input type="button" value="edit"/>
Brazilian tensile test	HIL-TAU-07-SPZ-4	28.10.2009		<input type="button" value="edit"/>
Point load test	HIL-TAU-07-PLT-1	28.10.2009		<input type="button" value="edit"/>
LCPC test	HIL-TAU-07-LCPC-1	28.10.2009		<input type="button" value="edit"/>
CAI test	HIL-TAU-07-CAI-1	03.11.2009		<input type="button" value="edit"/>
CAI test	HIL-TAU-07-CAI-2	16.08.2012		<input type="button" value="edit"/>
p-wave velocity test	HIL-TAU-07-USP-1	16.08.2012		<input type="button" value="edit"/>

Fig. 91: Main page for laboratory test data showing all conducted tests for sample HIL-TAU-07.

With clicking on the blue buttons for the laboratory test the data entry window can be accessed and new laboratory test can be inserted in the database. This mask, shown in Fig. 92 for the uniaxial compression strength test, works quite similar to the entry mask for samples. After entering the data, it is possible to enter a similar laboratory test for the same sample by clicking on “enter similar laboratory test” or closing the entry mask and go back to the laboratory test main page by clicking on “insert laboratory test”. Both buttons will enter the data in the database.

Uniaxial compression test

Sample name: HIL-SAM-01

Specimen: last entered specimen: 04

Date of collection:

Test conductor:

Length: mm **Diameter:** mm

Density: g/cm³ **Angle of disc.:** °

UCS: Mpa **V modulus:** GPa

Destruction work: kJ/m³ **E modulus:** Gpa

Energy of failure: kJ/m³

Formular: no file selected.

Fig. 92: Data entry page for UCS laboratory test data.

Finally, it is also possible to enter data about the processing status of all laboratory test. This is very important for all co-workers to gain information about the status of all laboratory tests, the writing of the report and issuing the invoice. All this information is also important for the client. So this tool can also be accessed from the project view.

7.3.3.3 Data input for drill head add on

The main aspect for the drill head add on, beside of the access to drill head data, mine information and laboratory test data is a tool which allows the user to easily choose the right drill head for a new mining location with help of only some rock properties. To create a dynamic and learning tool we decided to choose an empirical selection of drill heads without creating a mathematical model. This tool is fed with all drill head testing data ever conducted and should be continuously added with further testing results.

First of all, the database has to be fed with all laboratory test data and all drill head testing results to work with. All laboratory test data is entered as mentioned above with the use of the base view. This is not possible from inside the Hilti add on and must be done as administrator or as user with full access or access to some content. External users are not allowed to enter data. Due to the complexity of drill head testing data it can only be entered with help of phpMyAdmin as csv file. This csv file has to be generated in previous and must contain all columns in the right order as mentioned in Tab. 30. The csv file can contain one drill test but it is also possible to enter several drill tests at once.

Tab. 30: Required structure of the csv file for drill head testing data.

Column name	Data type	description	Unit
DrilltestID	int(11)	Incremental number of all drill tests. Is automatically generated.	-
DrillID	int(11)	ID of the used drill head. Can be looked up with the drill parameter tool.	-
DrillHeadCount	int(11)	This is used as incremental numbering for different drill heads of the same type which are tested at the same location. Generally this is 1.	-
MineID	int(11)	ID of the Mine in which the test was conducted. Can be looked up with the Mine list tool.	-
HoleNr	tinyint(4)	Incremental numbering of drill holes.	-
HoleDepth	decimal(5,3)	Depth of the specific hole.	m
DepthinSum	decimal(6,3)	Sum of all depth of all holes for the specific drill head.	m
DrilltimeMin	tinyint(4)	Drill time minutes for this hole.	min
DrilltimeSec	tinyint(4)	Drill time seconds for this hole.	sec
Problems	tinyint(1)	Were there any problems during the drilling yes/no (1/0)	-
Problemdescription	text	Description of the problem. Only needed if Problems=1.	-
Diameter	decimal(6,3)	Outer diameter of drill head.	mm
Mass	decimal(6,2)	Mass of the drill head.	g
Operator	text	Name of the drill operator.	-

After entering all necessary data, the drill head query tool can be used. The algorithms behind the tool are SQL selections of the fastest 3 and the long-lasting 3 which were used under similar rock property conditions. As explained in chapters 6.9 and 9.1 for this tool the UCS and the CAI was chosen due to the high correlation between these values and the performance and the wear of the drill head. The average UCS

values of one sample, which are considered for the selection, have a range of +/- 50 MPa (Query 5) and the average CAI can vary with +/- 1.5.

It is also necessary to enter the rock type, because if there is now UCS-CAI combination inside the database it is possible to get a result from the rock type selection. This creates a second list of the fastest 3, the long-lasting 3 and the best drill head over all for one rock type without considering rock strength and abrasivity. Therefore Query 6 is used. All data is entered through a web interface (Fig. 93).

Fig. 93: Drill head query window with the pull down menu for rock type selection and the text fields used for UCS and CAI queries.

Query 5: Drill head query. Selection for the three best drill heads using the UCS as selection criteria value for an entry of UCS=100. All elements written with a \$ character are variables which are coming from the php code and were calculated from the entered values at the web interface.

```

SELECT Kennung, Minename, Rocktype, UCS, CAI, AVGPerformance, `Wear_mym-m`
FROM
(SELECT `hil-drill`.`DrillID`, `hil-drill`.`Kennung`, `hil-
drilldata`.`DrilltestID`, `hil-drilldata`.`DrillID` AS DrillID2, `hil-
drilldata`.`MineID`, TRUNCATE(100 * AVG(`hil-
drilldata`.`Bohrlochtiefe` / (`hil-drilldata`.`BohrzeitMin` + (`hil-
drilldata`.`BohrzeitSek` / 60))),2) AS `AVGPerformance`,
TRUNCATE((1000 * (MAX(`hil-drilldata`.`Durchmesser`) - MIN(`hil-
drilldata`.`Durchmesser`)) / (MAX(`hil-drilldata`.`TiefenSumme`))),2)
AS `Wear_mym-m`, `hil-mines`.`MineID` AS MineID2, `hil-mines`.`Name`
AS `Minename`, `hil-mines`.`ProjektID`, `tblproben`.`PrbProjektID`,
`tblproben`.`PrbProbenID`, `tblldv`.`1DVProbenID`,
TRUNCATE(AVG(`tblldv`.`1DVEinaxiale_Druckfestigkeit`),2) AS `UCS`,
`tblcai`.`CAIProbenID`, TRUNCATE(AVG(`tblcai`.`CAIWert`),2) AS `CAI`,
`hil-rocks`.`Rocktype`, `hil-rocks`.`RockID`, `hil-rocks`.`MineID` AS
MineID3
FROM `hil-drill`, `hil-drilldata`, `hil-mines`, `tblproben`, `tblldv`,
`tblcai`, `hil-rocks`
WHERE `hil-drill`.`DrillID`=`hil-drilldata`.`DrillID` AND `hil-
mines`.`MineID`=`hil-drilldata`.`MineID` AND `hil-
mines`.`ProjektID`=`tblproben`.`PrbProjektID` AND
`tblldv`.`1DVProbenID`=`tblproben`.`PrbProbenID` AND
`tblcai`.`CAIProbenID`=`tblproben`.`PrbProbenID` AND `hil-
rocks`.`MineID`=`hil-mines`.`MineID`
GROUP BY `hil-drilldata`.`DrilltestID`
ORDER BY `AVGPerformance` DESC
) AS Tab1
WHERE `UCS` > '$UCSslow' AND `UCS` < '$UCShigh' AND `CAI` > '$CAIlow' AND
`CAI` < '$CAIhigh'
LIMIT 3

```

Query 6: Drill head query. Selection for the three best performing drill heads using the rock type as selection criteria values. \$rocktype is a variable within the php code and is directly entered through the user.

```
SELECT `hil-drill`.`DrillID`, `hil-drill`.`Kennung`, `hil-
drilldata`.`DrilltestID`, `hil-drilldata`.`DrillID`, `hil-
drilldata`.`MineID`, TRUNCATE
(100 * AVG(`hil-drilldata`.`Bohrlochtiefe`/(`hil-
drilldata`.`BohrzeitMin`+(`hil-drilldata`.`BohrzeitSek`/60))),2) AS
`AVGPerformance`, TRUNCATE ( ( 1000 * ( MAX(`hil-
drilldata`.`Durchmesser`) - MIN(`hil-drilldata`.`Durchmesser`) ) / (
MAX(`hil-drilldata`.`TiefenSumme`) ) ),2 ) AS `Wear_mym-m`, `hil-
mines`.`MineID`, `hil-mines`.`Name` AS `Minename`, `hil-
mines`.`ProjektID`, `tblproben`.`PrbProjektID`,
`tblproben`.`PrbProbenID`, `tblldv`.`lDVPProbenID`,
TRUNCATE(AVG(`tblldv`.`lDVEinaxiale_Druckfestigkeit`),2) AS `UCS`,
`tblcai`.`CAIProbenID`, TRUNCATE(AVG(`tblcai`.`CAIWert`),2) AS `CAI`,
`hil-rocks`.`Rocktype`, `hil-rocks`.`RockID`, `hil-rocks`.`MineID`
FROM `hil-drill`, `hil-drilldata`, `hil-mines`, `tblproben`, `tblldv`,
`tblcai`, `hil-rocks`
WHERE `hil-drill`.`DrillID`=`hil-drilldata`.`DrillID` AND `hil-
mines`.`MineID`=`hil-drilldata`.`MineID` AND `hil-
mines`.`ProjektID`=`tblproben`.`PrbProjektID` AND
`tblldv`.`lDVPProbenID`=`tblproben`.`PrbProbenID` AND
`tblcai`.`CAIProbenID`=`tblproben`.`PrbProbenID` AND `hil-
rocks`.`MineID`=`hil-mines`.`MineID` AND `hil-
rocks`.`Rocktype`='$rocktype'
GROUP BY `hil-drilldata`.`DrilltestID`
ORDER BY `AVGPerformance` DESC
LIMIT 3
```

After performing the drill head query all data is calculated and presented in a web page containing up to 4 tables (Fig. 94). The upper rock type-query will always be successful so in any case a selection of drill heads is represented. Due to the high variability in rock properties the second query in dependence of rock strength and abrasivity will not always be successful. For this case a button was introduced which leads the user back to the data entry mask to change the rock parameters and perform another query. A recommendation for a suitable analysis workflow can be found in chapter 10.

Drill head query

Requested values:

Rock type: Sandstone
 UCS: 50 MPa (Limits: 0/100)
 CAI: 3 (Limits: 1.5/4.5)

Best performers in sandstone

Drill head	Mine	DrilltestID	Average UCS	Average CAI	Average Performance	Average wear
			[Mpa]	[-]	[cm/min]	[µm/m]
Drill head 1	Quarry Miltenberg	1	36.09	1.35	44.79	53.84
Drill head 2	Quarry Miltenberg	2	36.09	1.35	42.66	25.64

Long-living in sandstone

Drill head	Mine	DrilltestID	Average UCS	Average CAI	Average Performance	Average wear
			[Mpa]	[-]	[cm/min]	[µm/m]
Drill head 2	Quarry Miltenberg	2	36.09	1.35	42.66	25.64
Drill head 1	Quarry Miltenberg	1	36.09	1.35	44.79	53.84

Best performers for UCS between 0 and 100 Mpa and CAI between 1.5 and 4.5.

Drill head	Mine	DrilltestID	Average UCS	Average CAI	Average Performance	Average wear
			[Mpa]	[-]	[cm/min]	[µm/m]
Drill head 2	Quarry Golling	8	85.33	1.60	36.28	7.68
Drill head 1	Quarry Golling	7	85.33	1.60	35.23	4.10

Long-living for UCS between 0 and 100 Mpa and CAI between 1.5 and 4.5.

Drill head	Mine	DrilltestID	Average UCS	Average CAI	Average Performance	Average wear
			[Mpa]	[-]	[cm/min]	[µm/m]
Drill head 1	Quarry Golling	7	85.33	1.60	35.23	4.10
Drill head 2	Quarry Golling	8	85.33	1.60	36.28	7.68

[return to drill head query](#)

Fig. 94: Illustration of a successful drill head query for sandstones with UCS=50 MPa and CAI=3.

From the query results it is possible to reach more information about the drill head, the mine itself and all corresponding laboratory tests and the specific drill test by clicking on the requested item.

8 Numerical modelling in 2D and 3D

During the current thesis various numerical models in 2D and 3D were set up in order to contribute to an enhanced understanding of the occurring stress constellation in deep underground mines. One of the central questions was if high stress levels can be beneficial for the drilling process. We started with simulating the rock mass in cross and longitudinal sections with the 2D-FEM-code Phase² (Rocscience) (MENSCHIK 2009). For the doctoral thesis we investigated further 2D-Modells containing additional aspects as more complex geometry and additional stopes and extended the 2D-modells to 3D. To yield a better reconnaissance of the rock mass behavior, the generation of the disturbance zone and the high stress induced fracturing processes around the area of excavation, we applied the finite difference code FLAC 3D (Itasca) as well as the finite element code RS³ (Rocscience).

We decided to model Tautona gold mine (see chapter 4.1) due to the following facts:

- the high maximum mining depth of up to 3,500 m (expanded to 3,900 m in 2008; www-6),
- the high rock strength (Tab. 26) and
- the high abrasiveness of the quartzite at face (Tab. 26)
- the low drilling performance (Fig. 74).

8.1 Geotechnical Model setup

8.1.1 Geometry

To obtain a faster computation time and to rebuild a more realistic modelling set-up, some simplifications have to be taken into account and the geological model shown in cross section in Fig. 5 has to be adjusted.

The adapted geometry is illustrated in Fig. 95 (cross section) and Fig. 96 (longitudinal section). The general stope in Tautona is dipping with an inclination angle of 20° in western direction. Due to the reef height of 30 cm the stope measures 1 m in height and 30 m in across slope and 30 m in upslope direction. 3 pulls were made to open the stope in full length. Length of a round is 10 m and depth 2 m.

The mine transportation gallery measures 2 x 3 m and is connected to the stope in a height of 1 m and has the same length as the stope itself.

To simplify the geotechnical model to reduce calculation time all overlying material is generalized to only one material. The overburden is assumed to consist only of quartzite. All overlying materials of the Witwatersrand supergroup weren't differentiated. Also the material of the venterstorp supergroup.

For another simplification of the model it is important to look at the overburden in more detail. Approaching the density for the material of the venterstorp supergroup of 3.0 g/cm³ (typical density of basic volcanic rocks) and comparing this value to the density of quartzitic material with a density of 2.7 g/cm³ results in a density difference of 0.3 g/cm³. The error in vertical stress derived from material diversification calculated with Eqn. 20 using this density difference and assuming a maximal thickness of venterstorp supergroup of 3 km is 8.8 MPa.

Eqn. 20: Equation for an estimation of vertical stress.

$$\sigma_v = \rho \cdot g \cdot h$$

<i>with:</i>	σ_v	<i>vertical stress</i>	<i>[MPa]</i>
	ρ	<i>density</i>	<i>[g/cm³]</i>
	g	<i>standard acceleration due to gravity</i>	<i>[ms⁻²]</i>
	h	<i>height of overburden</i>	<i>[km]</i>

To simplify the model the in chapter 4.1 described dykes and veins were not drawn. Based on the assumption that all stopes as well as all other reefs are not influencing each other, only one gold bearing reef and the corresponding stope is used for the calculation.

Due to the great depth (closure of fissures) and the low occurrence of discontinuities the rock mass is modelled without joints and without taking groundwater into account.

The high rock temperature in this depth is excluded in all models due to the applied Rocscience software. All Rocscience codes are not supporting mechanical-thermal-coupling.

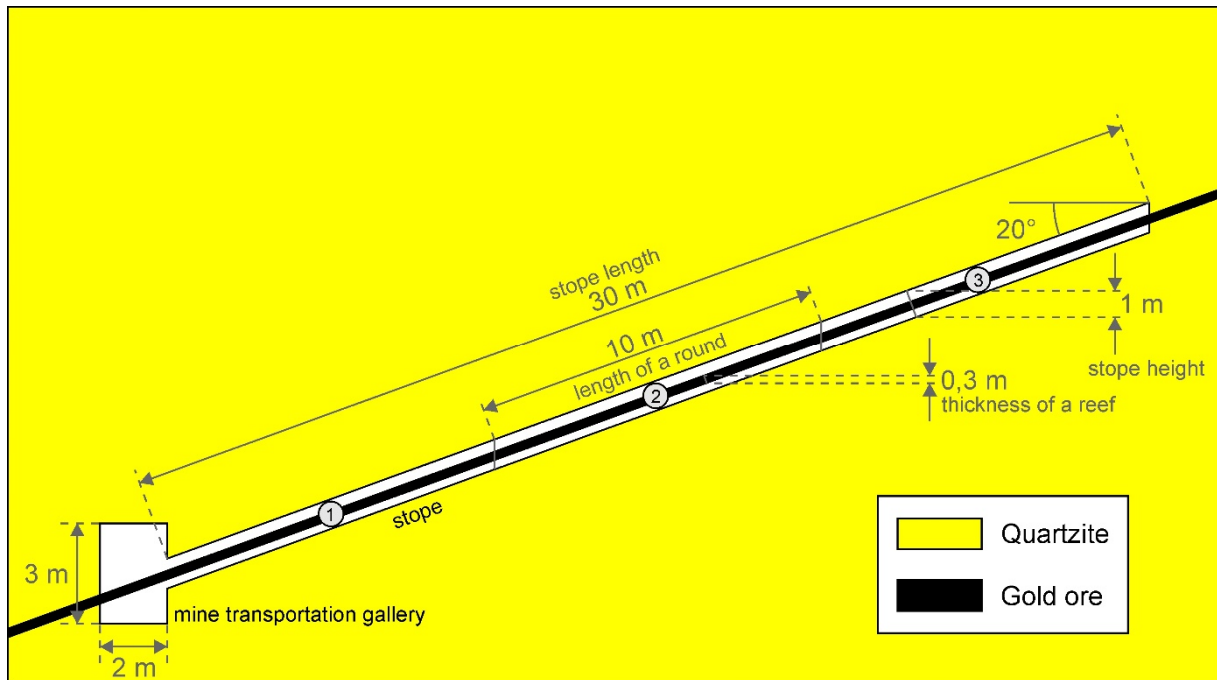


Fig. 95: Geotechnical model (cross section) of Tautona gold mine as basis for the subsequent numerical models.

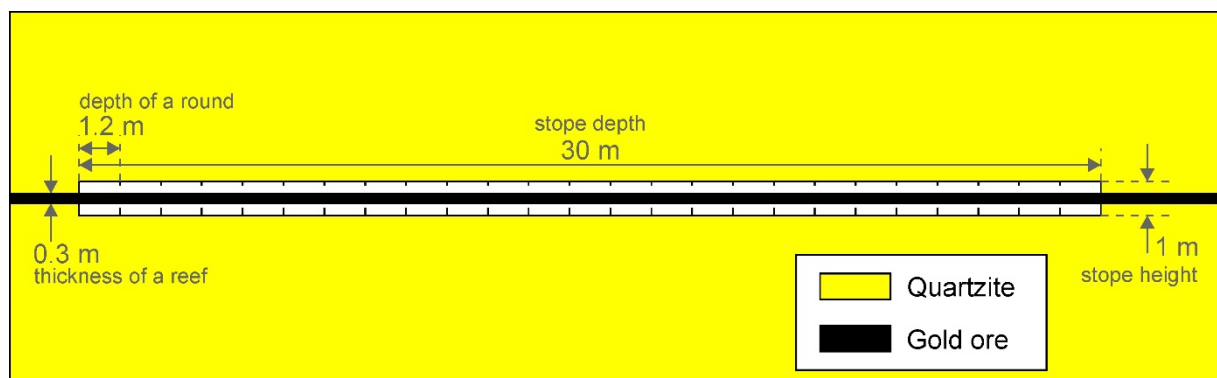


Fig. 96: Geotechnical model (longitudinal section) of Tautona gold mine as basis for the subsequent numerical models.

8.1.2 Material properties

The occurring materials can be characterized as quartzites, meta quartz conglomerates and gold bearing varieties of these rock types. To obtain a better understanding of the rock mechanical properties we performed several laboratory tests (chapter 6.8) and a parameter studies using the code Phase² in MENSCHIK (2009). The properties of the final materials in Phase² and RS³ are shown in Tab. 31 and

Tab. 32. All materials are considered as isotropic and plastic materials with full field stress and body force to be effective with the applied Generalized Hoek-Brown failure criterion. The switch to plastic mode is

required due to the high overburden and the occurring high stresses after the excavation to achieve better results.

The parametric study using Phase² (MENSCHIK 2009) provides certain evidence of a minor influence of the estimated rock strength, density and young's modulus on the principal stress after excavating the whole slope; for example, only + 5 MPa for a 20 % lower rock strength and + 5-10 MPa for a 20% higher rock strength.

An increased influence is given by the initial stress state, especially in the distribution of the occurring stress but also in the stress-level. The ratio of horizontal to vertical stress was varied from $\sigma_h/\sigma_v = 1:2$ (used for all subsequent calculations), 1:1 to 2:1. For equal horizontal and vertical stress the principal stress rises to 690 MPa and tops the 1:2-value by 100 MPa. The 2:1-case shows similar stress-values but a considerable different stress distribution (Fig. 97).

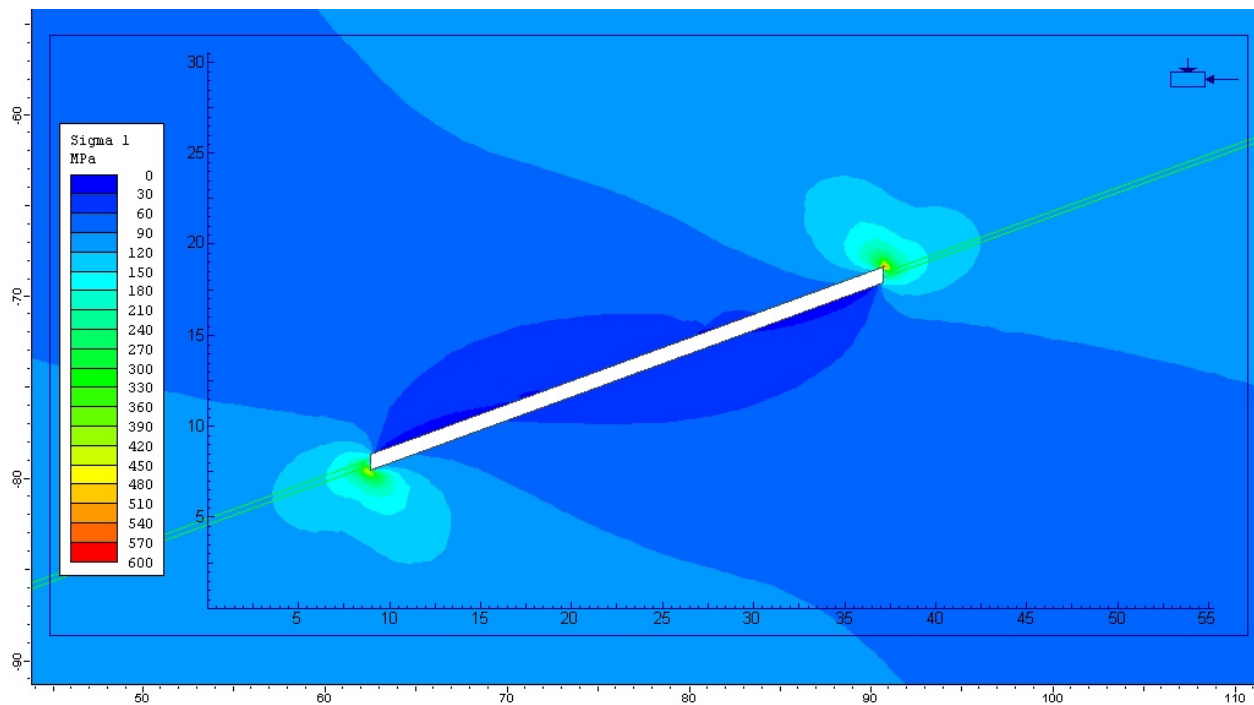


Fig. 97: Stress distribution of sigma 1 in case of an increased horizontal stress ($K=2$).

Due to the widely spaced discontinuities ISRM (1978b), as observed in the field, and the good joint surface conditions, but the wide opening of the stopes (30 m), the GSI is set to 95 for intact rock mass. For the disturbed rock mass, the GSI was reduced to 75. The intact compressive strength and the unit weight are measured in the laboratory. Due to a lack of sample material and missing triaxial tests, all other values are estimated by the help of literature values suggested by Rocscience RocData 5.0.

Tab. 31: Properties of quartzite used for numerical modelling in Phase² and RS³.

Material parameter	Unit	Value
Unit weight	MN/m ³	0.027
Young's modulus	MPa	81,597
Residual young's modulus	MPa	67,961.1
Poisson's ratio	-	0.3
Intact compressive strength	MPa	222

Material parameter (continued)	Unit	Value
mb (peak)	-	16.7293
mb (residual)	-	4.09484
s (peak)	-	0.573753
s (residual)	-	0.062177
a (peak)	-	0.500084
a (residual)	-	0.500911
GSI	-	95
GSI (residual)	-	75
mi	-	20
mi (residual)	-	10

Tab. 32: Properties of gold bearing quartzite used for numerical modelling in Phase² and RS³.

Material parameter	Unit	Value
Unit weight	MN/m ³	0.03
Young's modulus	MPa	73,510.8
Residual young's modulus	MPa	61,226.3
Poisson's ratio	-	0.3
Intact compressive strength	MPa	200
mb (peak)	-	16.7293
mb (residual)	-	4.09484
s (peak)	-	0.573753
s (residual)	-	0.062177
a (peak)	-	0.500084
a (residual)	-	0.500911
GSI	-	95
GSI (residual)	-	75
mi	-	20
mi (residual)	-	10

Modelling with FLAC 3D we decided to apply the Mohr-Coulomb failure criterion. To calculate the according properties we used RocData 5.0 from Rocscience and compared our synthetic data with quantitative triaxial data provided by HOEK (1965: 200) (Fig. 98) and converted the generalized Hoek-Brown properties to Mohr-Coulomb properties.

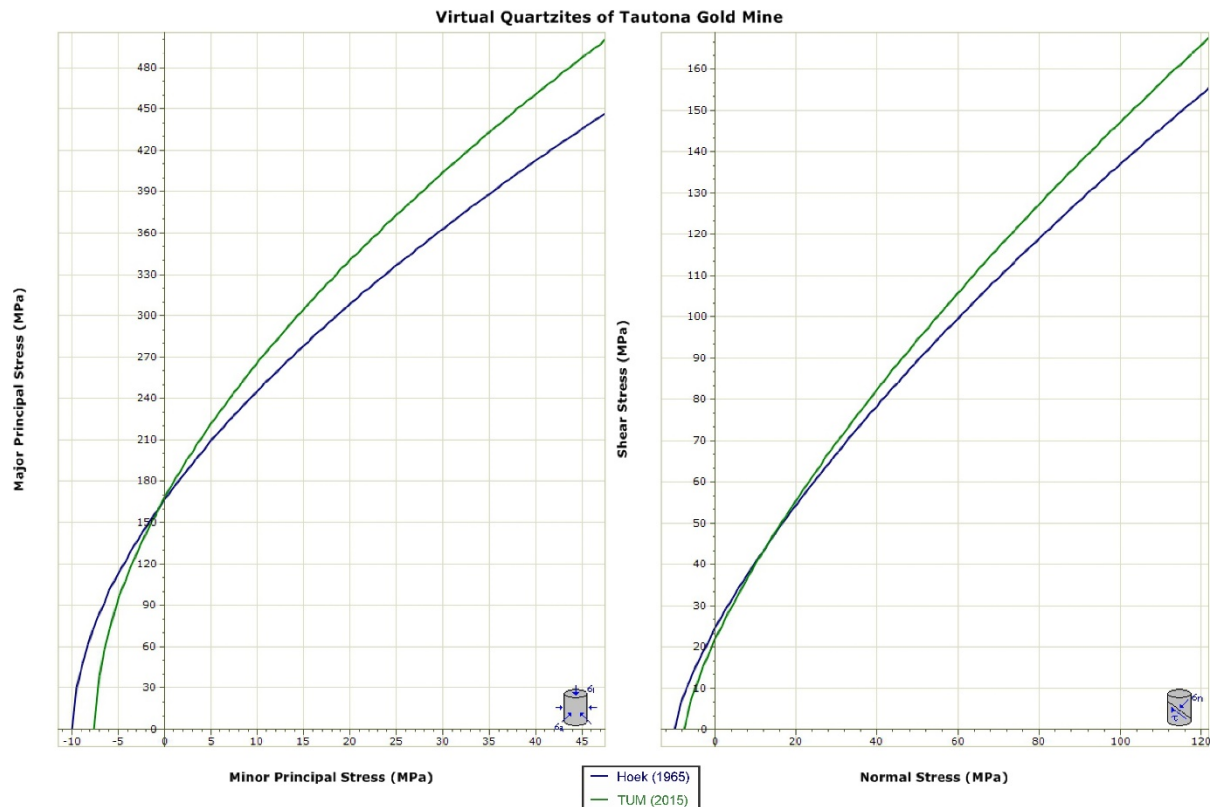


Fig. 98: Comparison of synthetic Hoek-Brown properties out of TUM uniaxial laboratory testing and the Hoek-Brown properties of the triaxial test data from HOEK (1965: 200).

As shown in Fig. 98 the data is comparable and shows a tensile strength of 7.6 MPa, a UCS of 168 MPa and a young's modulus of 81,597 MPa for our synthetic rock mass. The final rock properties can be found in the following table (Tab. 33).

Tab. 33: Mohr-Coulomb properties of gold bearing quartzites used for numerical modelling in FLAC 3D.

Material parameter	Unit	Quartzite	Gold bearing quartzite
Density	g/cm ³	2.7	3.0
Young's modulus	MPa	73,510	73,510
Poisson's ratio ν	-	0.3	0.3
Friction Angle φ	°	50	49
Cohesion	kPa	31	29
Tensile strength	kPa	8	8

8.2 2D Models (MSc) and recent models

During the master's thesis (MENSCHIK 2009) we analyzed with the help of Phase² the occurring stresses of Tautona gold mine. We started with a generalized overview model to determine the occurring stresses in a depth of 3,500 m and applied this parameter set for all subsequent detailed studies. By means of this analysis we obtained a value of 94 MPa for σ_1 and around 40 MPa for σ_3 .

In a next step we calculated a cross section and longitudinal section of one stope in a depth of 3,500 m as a detail model. The model was set up in 3 stages of excavation as it occurs typical in the mining process,

where the mining of a total stope length is done in three rounds. With this model it was possible to demonstrate the distribution of the complete occurring stresses (Fig. 99). As expected, the highest stresses could be verified at the stope walls with a maximum σ_1 after the third stage of 570 MPa. The stress distribution was found to be slightly asymmetric due to the dipping angle of 20° of the stope and the reef. The lowest stress was calculated for around the central part of the roof and foot wall.

The second detail model shows a longitudinal section through the mining stope to determine the occurring stresses at the mining face. This model shows a maximum principal stress of 420 MPa at the face which seems to be slightly underestimating the real occurring stresses due to the calculation mode of Phase².

Thus it is required to recalculate the models with a 3-dimensional code.

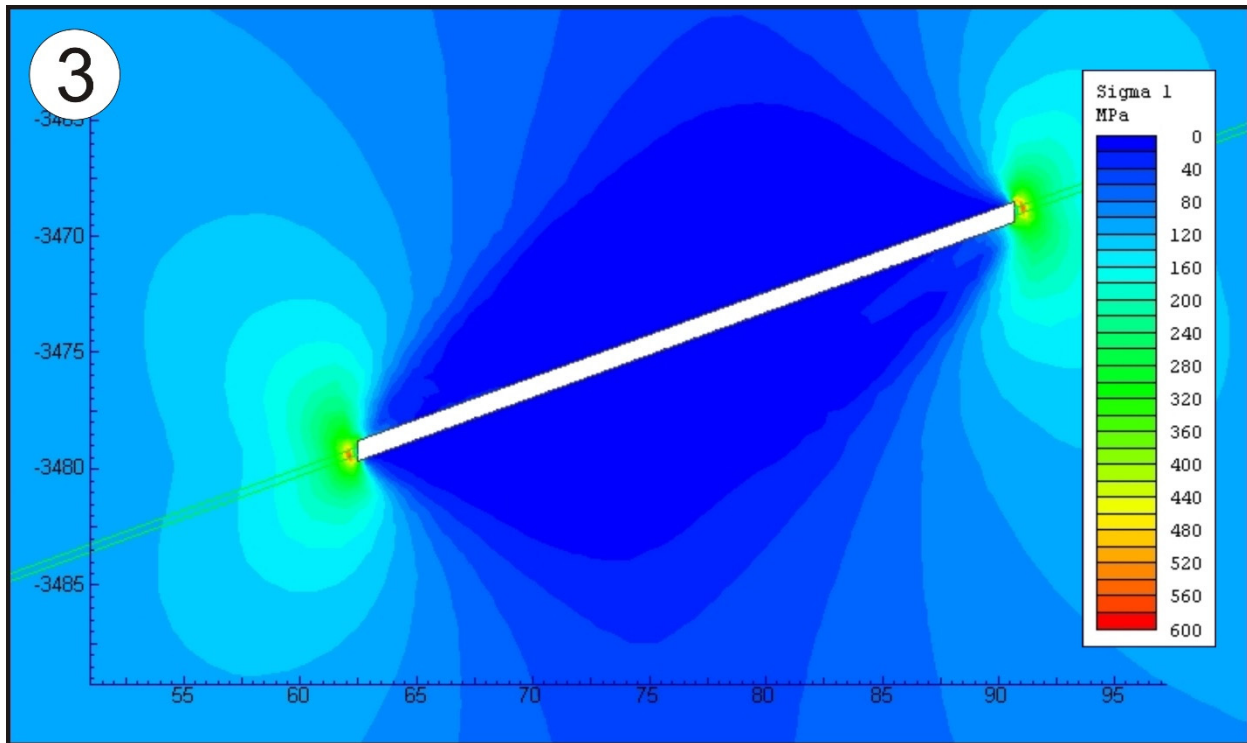


Fig. 99: Stress distribution of sigma 1 calculated with Phase² after the third excavation stage (MENSCHIK 2009: 27).

For an improved comparison of the test results all properties are recalculated (see chapter 8.1.2). The cross sectional detail model of the master's thesis (MENSCHIK 2009) was recomputed using the up-to-date version of Phase² and the optimized rock properties. The first model is an approach to the real geometry and the connecting link to the Master thesis. To gain more information, closer to reality, the geometry was adapted for a second model and a transportation gallery was inserted as it was observed during a site visit in the mine in 2011. Further models were calculated to check the influence of the edge rounding of the stope geometry. Third a second stope was drawn nearby the first one to check the interaction of generated stresses due to the excavation of both stopes.

8.2.1 Stope without transportation gallery

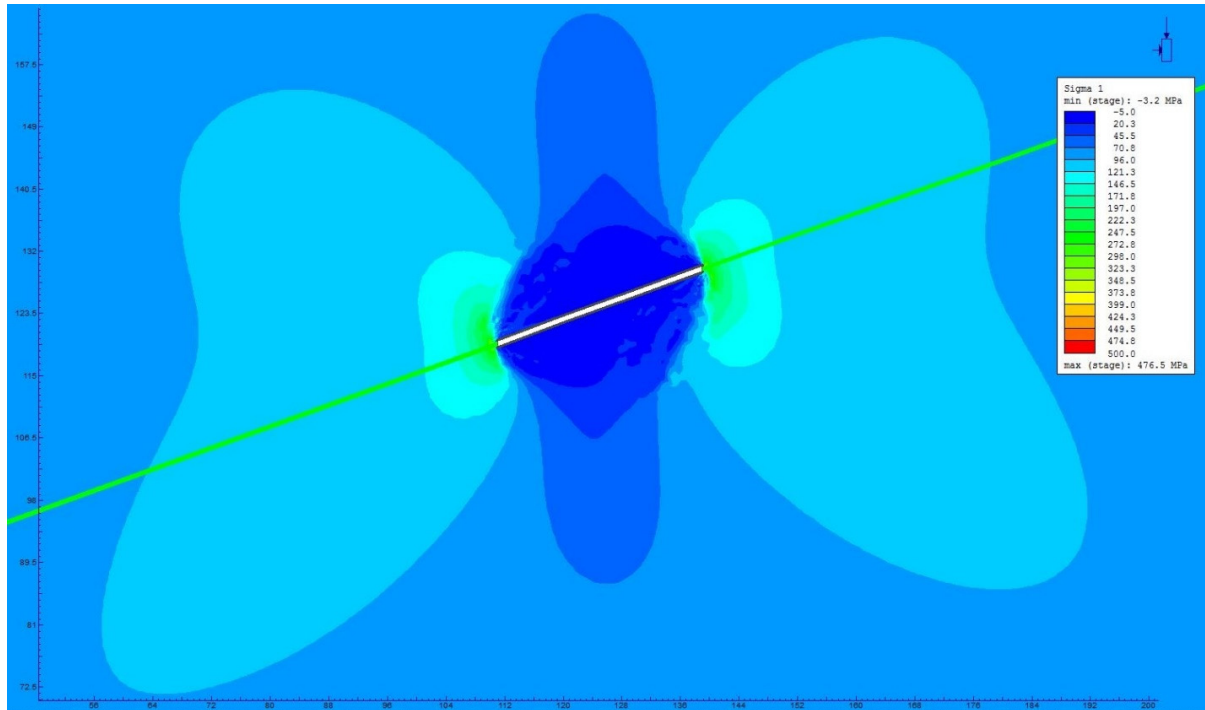


Fig. 100: Major stress distribution of model stope without transportation gallery.

After recalculation with adjusted properties and plastic behavior of the rock mass, σ_1 reaches its maximum after the third excavation stage with around 480 MPa. The stress distribution is similar to the one of the M.Sc. models (Fig. 100). The maximum stresses can be observed with an offset of about 1 m to the excavation wall inside the rock mass. On the downslope (left) (Fig. 101) side of the stope this zone of maximal stress is rotated a bit in direction to the lower corner due to the stope geometry. Also on the upslope (right) side this zone can be observed a bit rotated to the upper corner and 1 m off the wall. The maximum total displacement is located at the stope ceiling and the foot wall and reaches 3.6 cm (Fig. 102). The lower σ_1 direct at the side wall can be interpreted by the help of the yielded element. In these areas all finite elements have already yielded (Fig. 103) and could reduce the occurring principal stress. This could be seen in accordance to the generation of a minor rock mass supporting ring in fractured rock mass due to the rock strength exceeding stress.

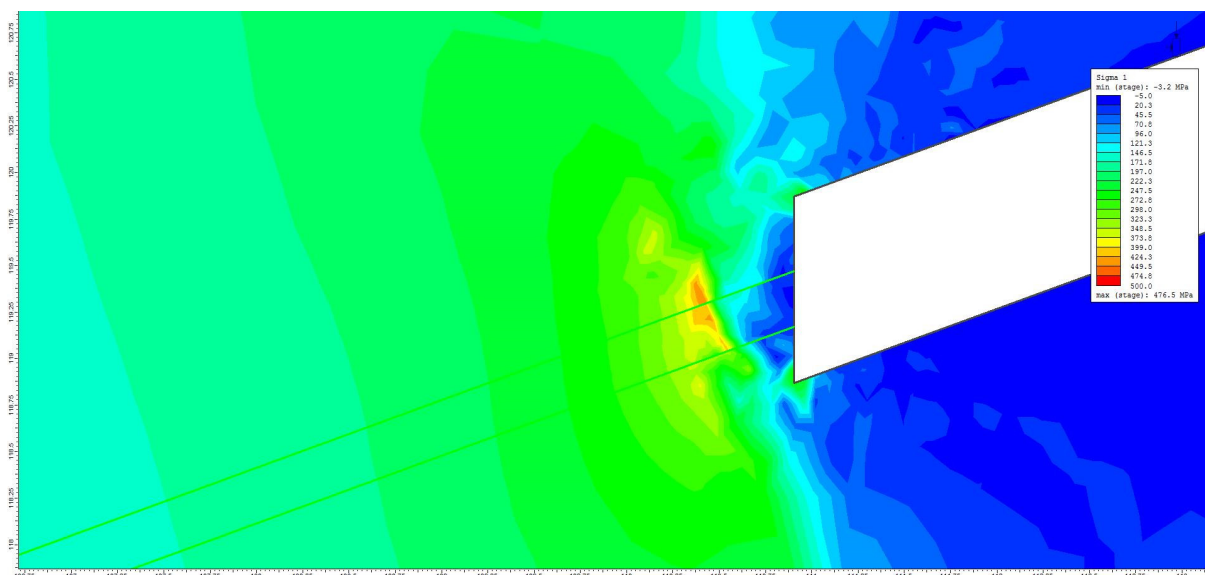


Fig. 101: Illustration of sigma 1 in a detailed view of the lower side wall after the third excavation stages.

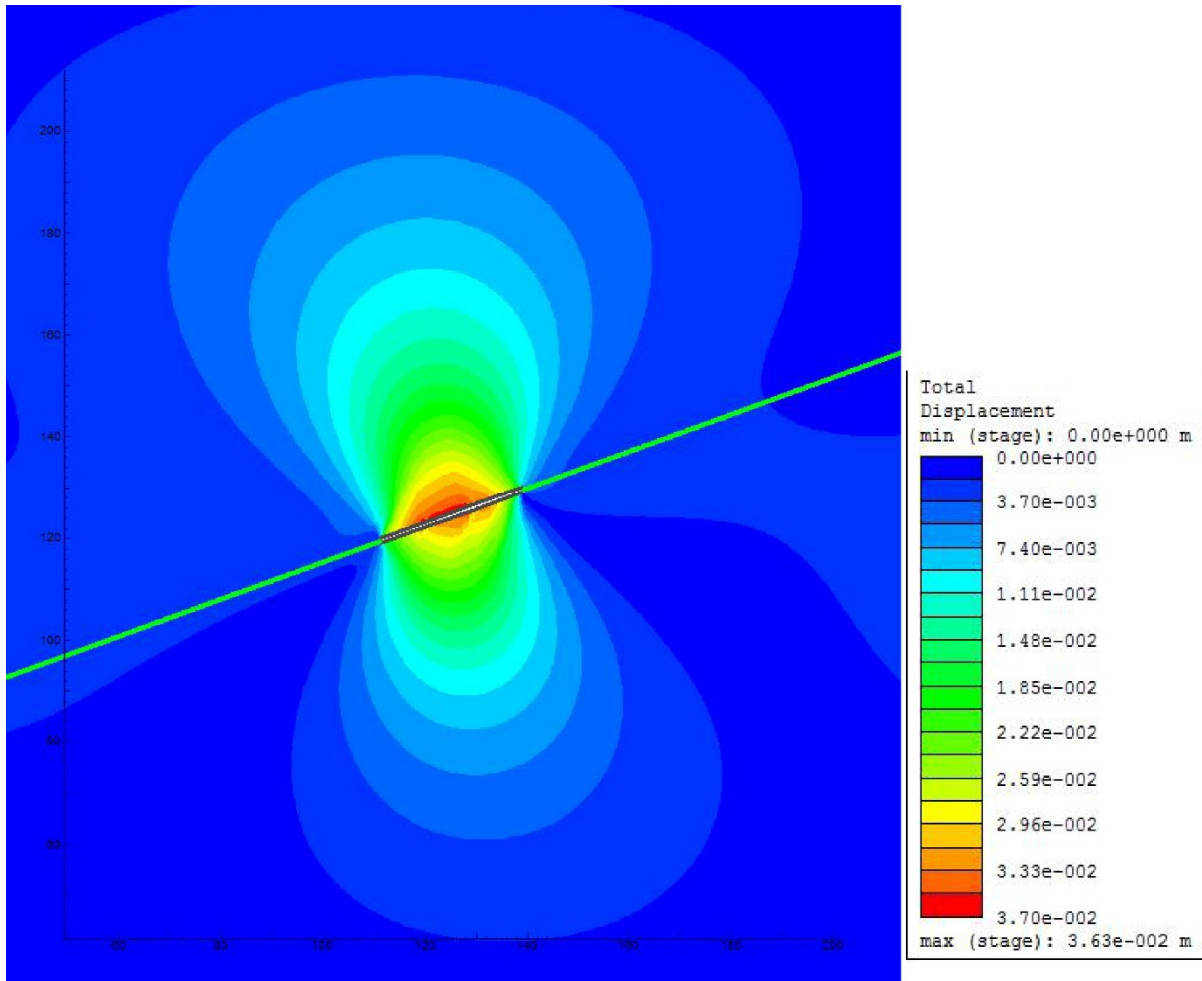


Fig. 102: Total displacement of the rock around the excavation after the third excavation stages.

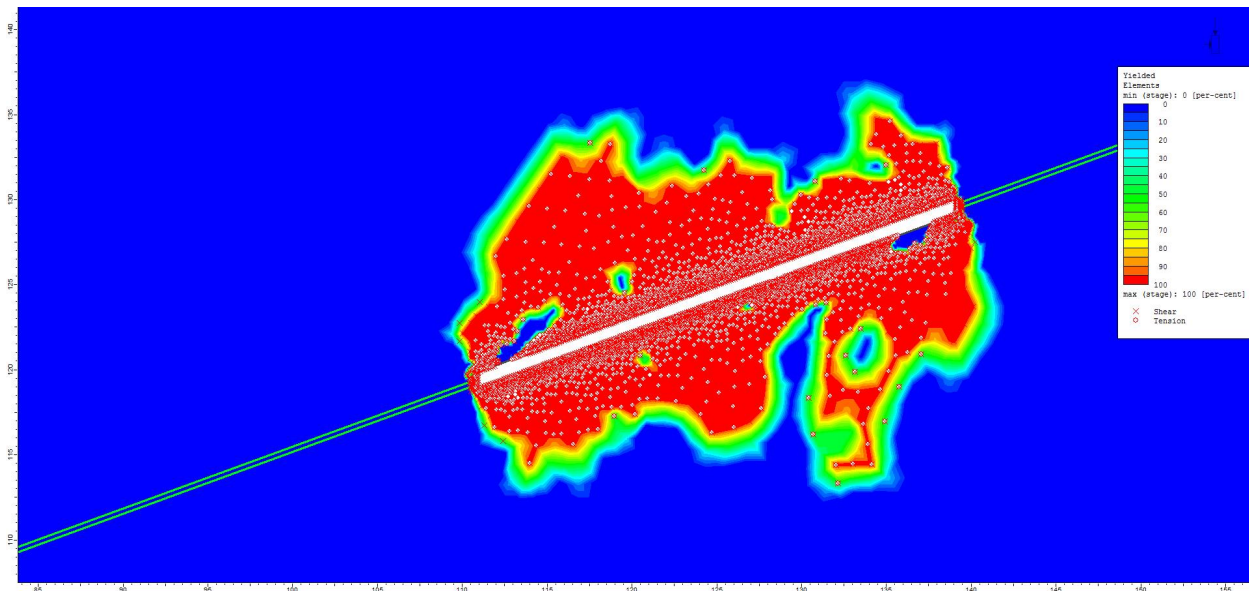


Fig. 103: Plot of yielded elements after the third excavation stage.

8.2.2 One Stope with the consideration of a transportation gallery

The illustration of this model shows almost no change in location on the upper side of the stope but the occurring stress and the deformation at the downslope side of the transportation gallery changes. The highest stress (σ_1) is located at about 1.5 m of the side wall of the transportation gallery and reaches values

of 350 MPa. On the upper side of the slope the value for σ_1 is about 470 MPa (Fig. 104). The maximum total displacement is situated at the stope ceiling as well as at the foot wall and reaches slightly higher values of 3.9 cm.

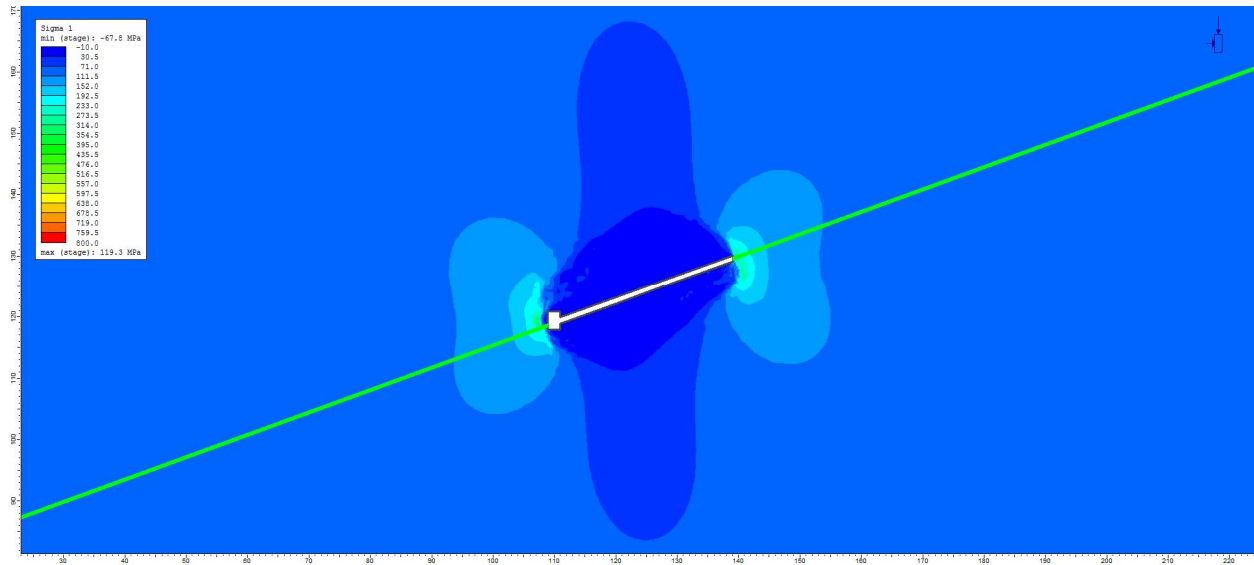


Fig. 104: Major Stress distribution of the model of one stope with a transportation gallery.

8.2.3 Stope with transportation gallery taking the rounded edges into account

As it is not possible to rebuild the real stope geometry, especially the corners of all excavations, we generate a model with all edges rounded to compare both extreme scenarios: Rounded Edges and sharp corners as usually used for all other models. As shown in Fig. 105 we introduced round edges at all occurring corners of the stope as well at the transportation gallery.

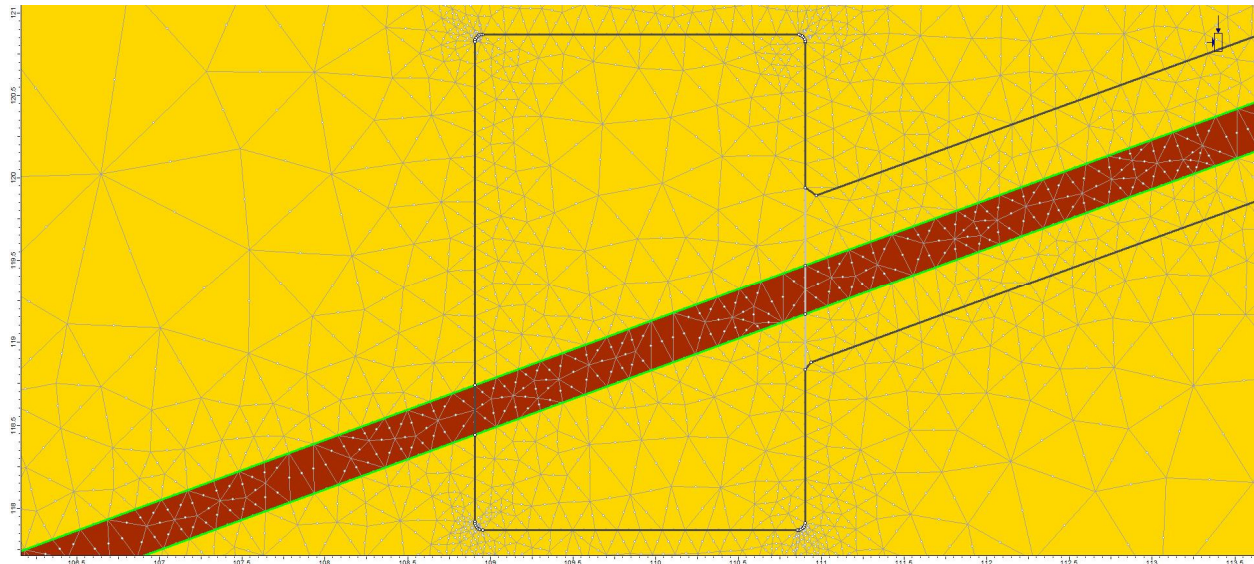


Fig. 105: Detail view of the geotechnical model of the transportation gallery with rounded edges.

As expected, the influence of the corners for the distribution of occurring stress is not observable. The highest value for σ_1 is reduced to 415 MPa (Fig. 106) as it was assumed.

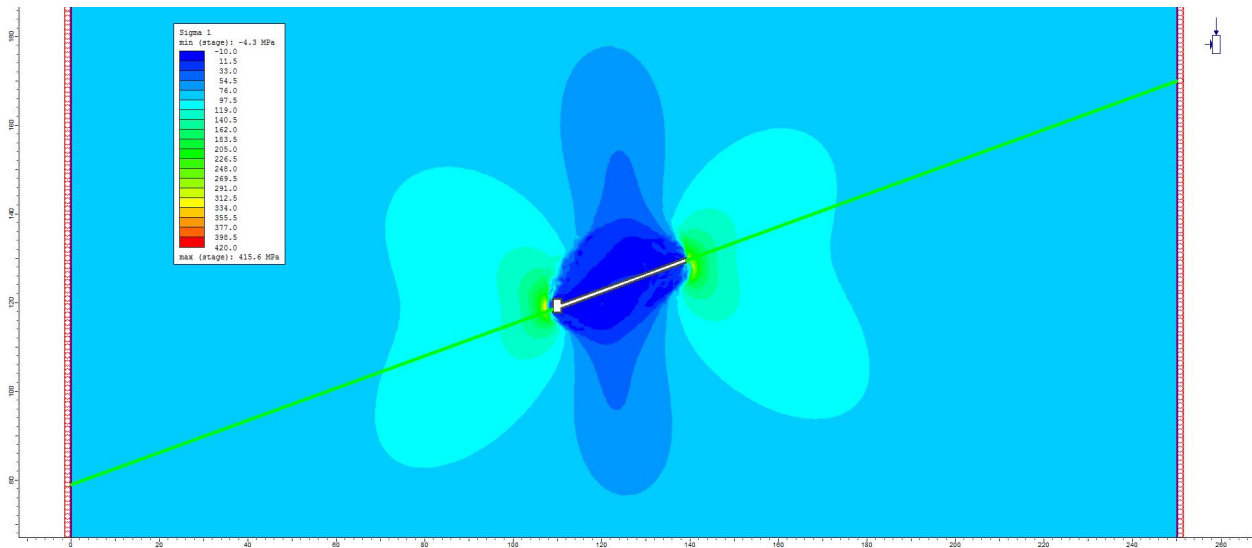


Fig. 106: Major Stress distribution of the model of one stope with the transportation gallery and rounded edges.

The maximum displacement is a bit higher with values of 3.99 due to geometrical reasons. The sharp corners, especially on the upslope (right) side of the stope cut off a developing shear plane. This shear plane can also be observed in the round edges model but here it is developed longer and is not cut off by the edge of the stope (Fig. 107). The developing shear plane is assumed to be responsible for the higher deformation rates until a groundarch is built.

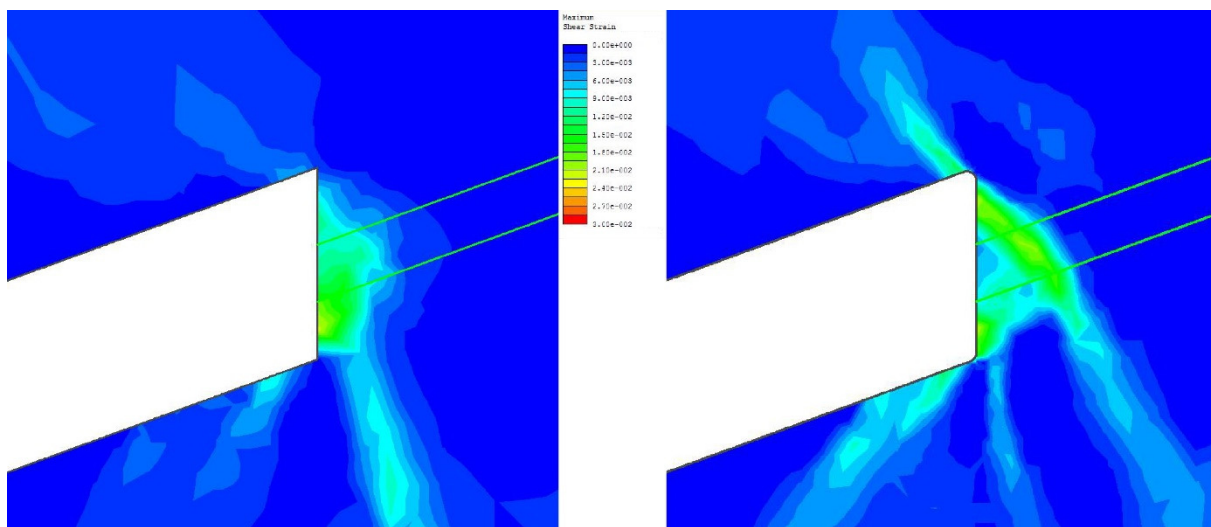


Fig. 107: Comparison of maximum shear strain of the models with sharp corners and rounded edges.

8.2.4 Two stacked stopes with transportation galleries

In some areas of the mines several stopes are situated near to each other. To gain information about the case of two stacked vertically to each other; the next model was set up. The distance was assumed with 30 m. As shown in Fig. 108 the maximum occurring stress σ_1 is higher than in the other models but only around 10 MPa with an absolute value of about 490 MPa. The maximum displacement is increasing compared to the model with one stope and shows a value of 4.3 cm. The highest values are observed at the ceiling of the upper stope and the foot wall of the lower stope. This difference in displacement distribution can be explained with an increasing area of yielded elements. The element distribution of plastic deformation of both stopes is different. The excavation of the first (upper) stope is comparable to the former models. While excavating the second stope (lower one), the area of yielded elements is not as big as at the first stope. During the three excavation steps the yielded zone grows bigger (Fig. 109), which can be

explained with the distortion of the rock mass during the first excavation and uplift of the material between both stopes. The yielded zone between both stopes stabilizes the whole mining building.

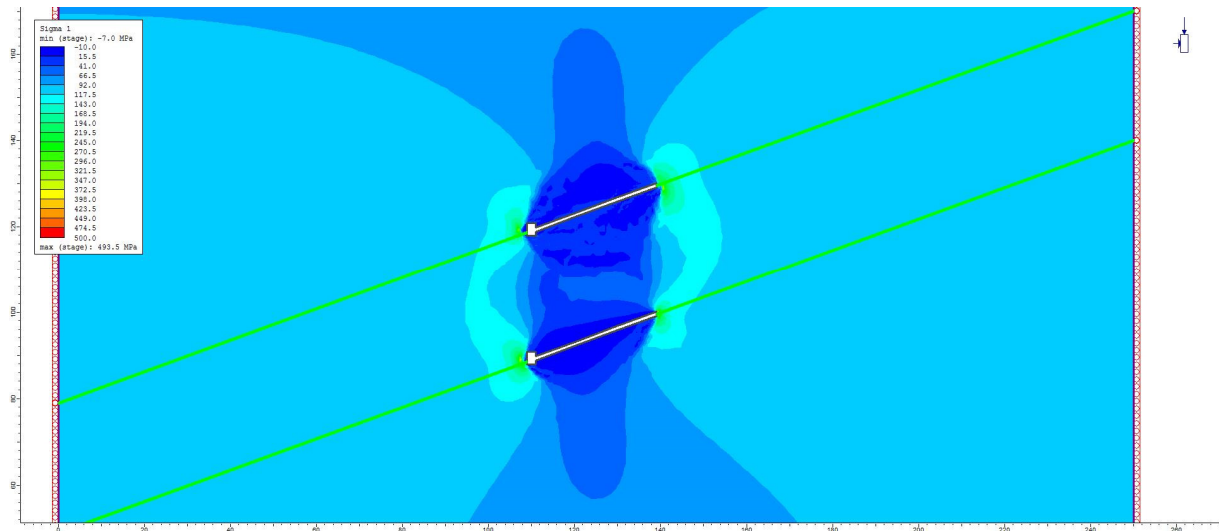


Fig. 108: Major Stress distribution of the model with two stacked stopes including transportation galleries.

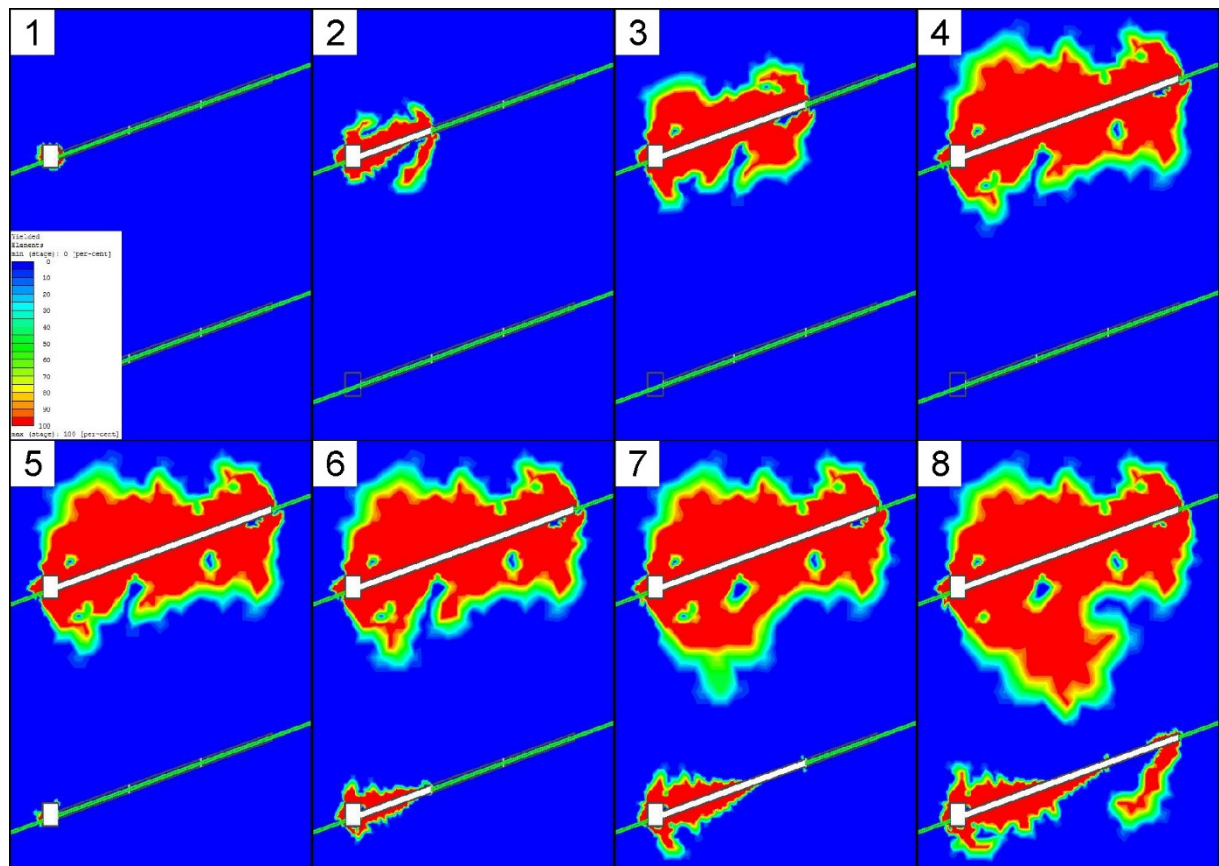


Fig. 109: Development of yielded zone (yielded elements) during the excavation stages.

8.3 3D Models

We applied the code FLAC 3D as commonly used for 3D underground excavations to model the scenery in a generalized setup to validate the more complex and detailed models which are computed using the currently available code RS³ of Rocscience. As this code was released in September 2014, this step is necessary to obtain more confidence to the modelling results and to feel confident about gaining adequate results with this easy to use code in comparison to an approved and more complex code, like FLAC 3D.

8.3.1 FLAC 3D

This model shows a similar distribution of stress (Fig. 110) and deformation (Fig. 111). The highest stresses reach values of 330 MPa and can be found at the central part of the edges of the stope walls. The corners have decreasing values of 160 MPa.

The minor values can be explained by the material parameters. These parameters are only recalculated using RocData from Rocscience. Further FLAC 3D has no residual values and is not calculating plasticity within the presented model. Within FLAC 3D we did not use staging for the excavated zone. All excavation is done in one step only.

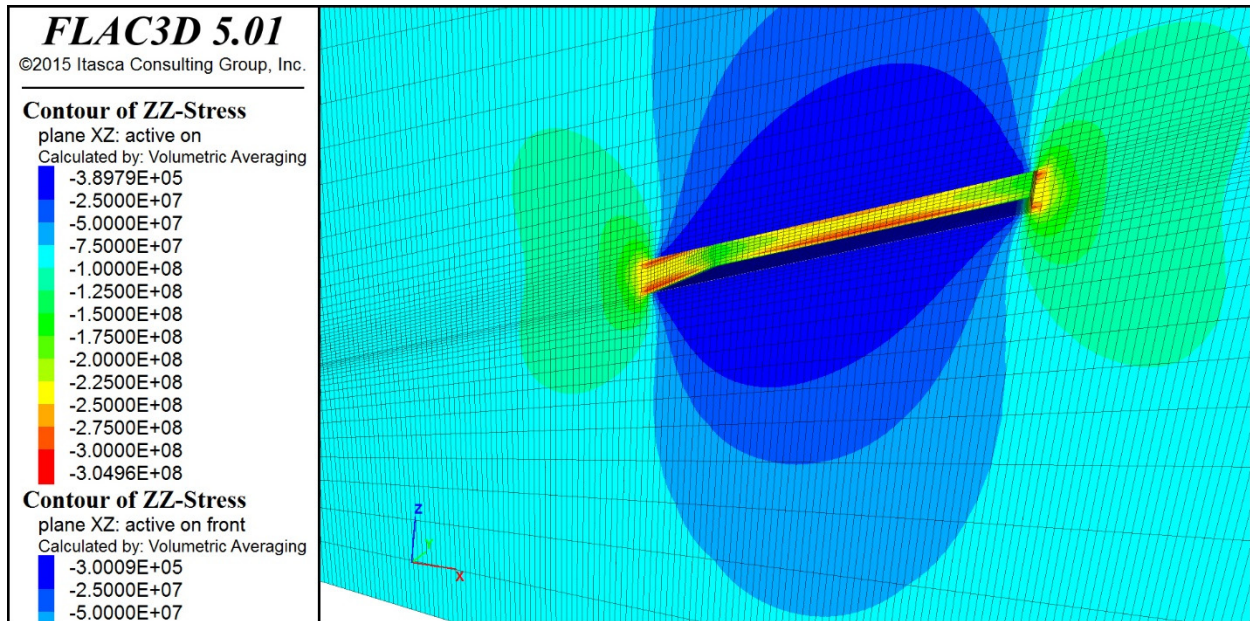


Fig. 110: Stress distribution of vertical stress of the FLAC3D model.

The total displacements are similar to the 2D models. The highest values can be found at the central part of the roof and the foot wall. The maximum lies by 2.2 cm in total.

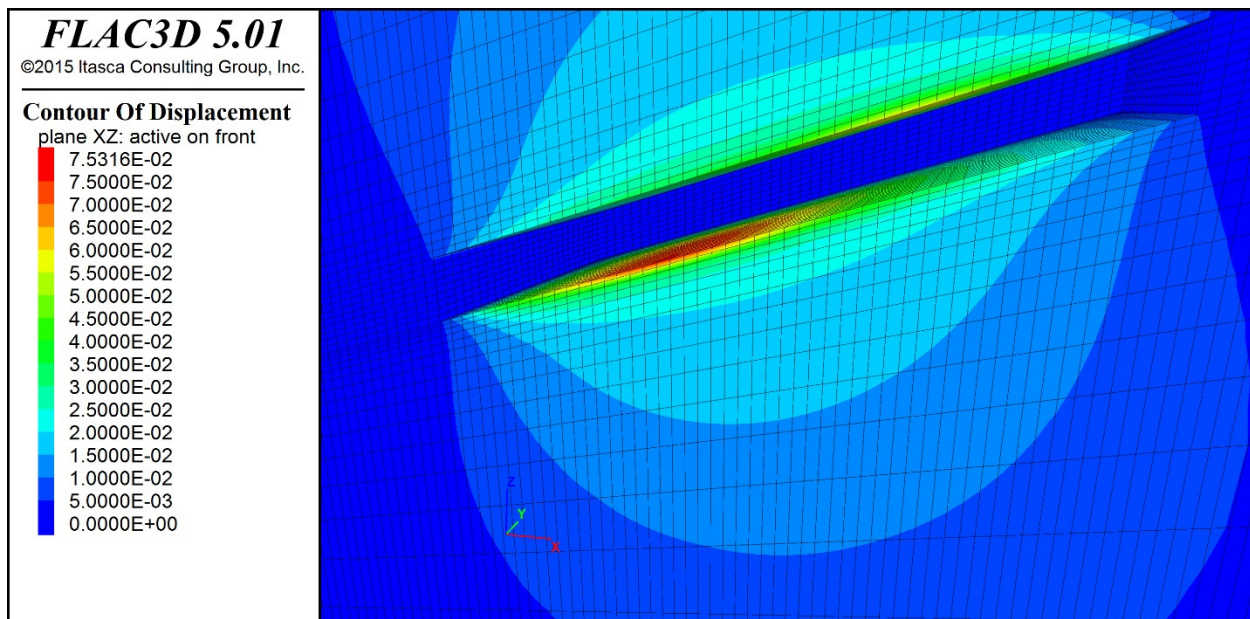


Fig. 111: Displacement of generalized FLAC3D model.

8.3.2 RS³

In comparison the RS³ model is similar to the FLAC 3D model. Due to the use of plasticity, the values of RS³ are higher and exceed the values of all 2D models due to the 3-dimensional setup. The maximum for σ_1 reaches around 600 MPa (Fig. 112). The highest values are situated as in the FLAC 3D model at the side walls in the crotches between the material boundary and stope wall and are concentrated at the center of the sidewalls, the back wall and the face wall. The Displacement rates are similarly distributed (in the middle of roof and foot wall) compared to the FLAC 3D model but are higher with values around 8 cm (Fig. 113).

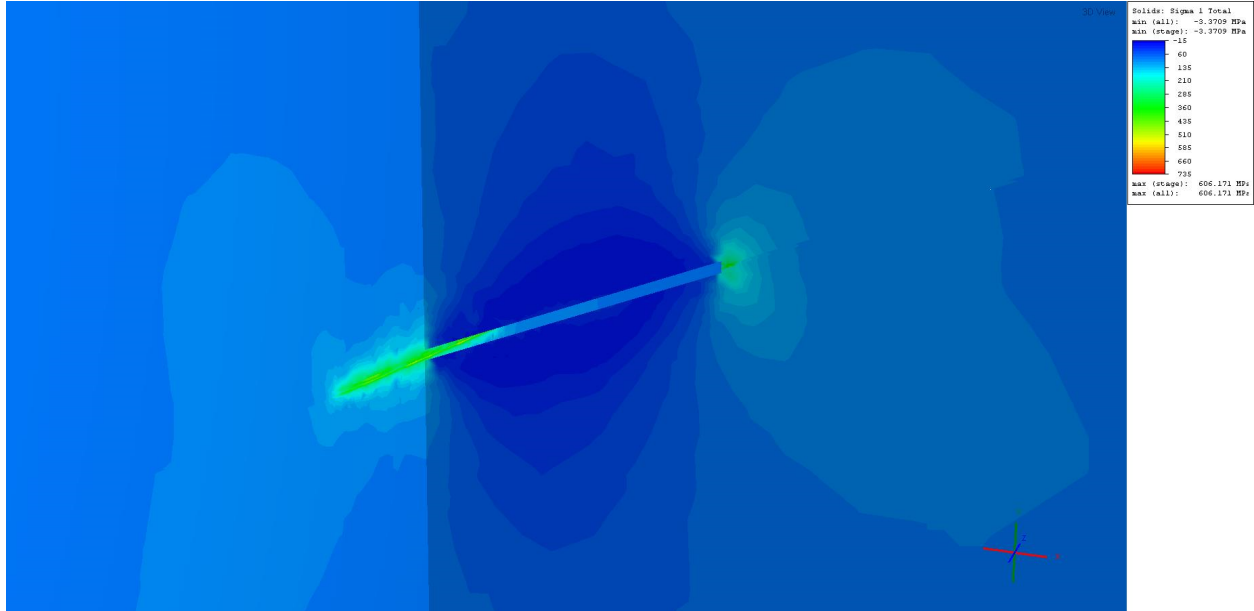


Fig. 112: Major Stress distribution of the RS³ model including one stope without transportation galleries.

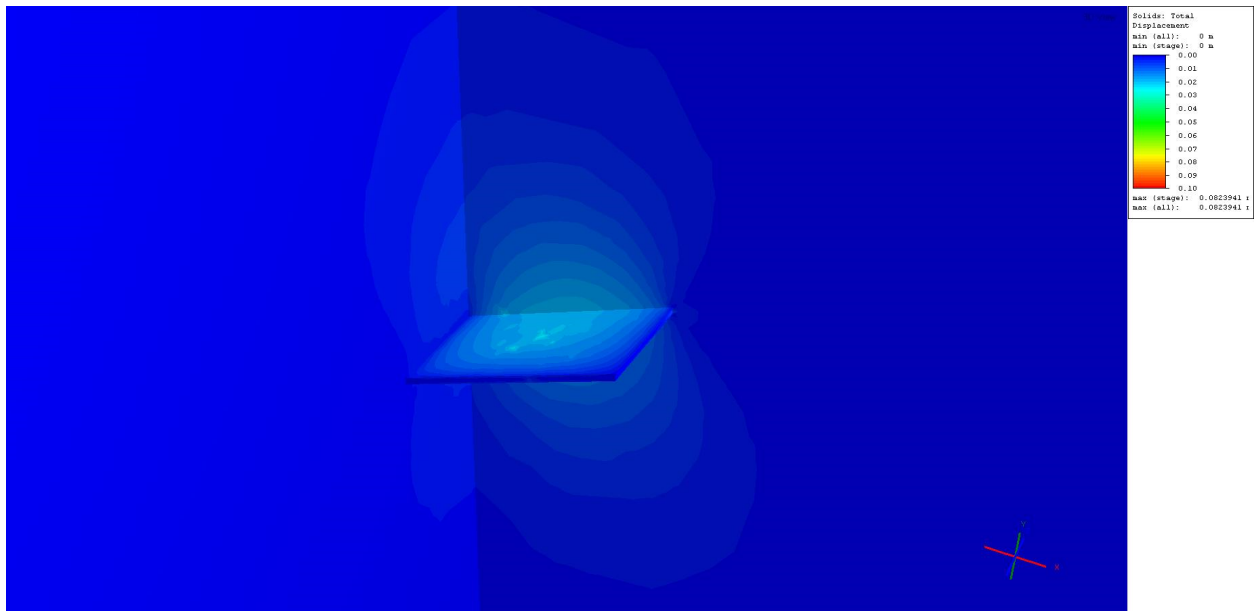


Fig. 113: Map of total displacements of the RS³ model including one stope without transportation galleries.

The second RS³ model with the transportation gallery shows very high values for σ_1 of max 685 MPa. After all excavation steps, the maximum can be named as around 550 MPa (Fig. 114). The overall maximum and all other higher values as the maximum after the last stage mentioned above, are reached after the first

excavation step of each stage (Fig. 115). This peak in principal stress results from the geometry. At this point of excavation, a step at the face wall with 90° angle to all other walls exists.

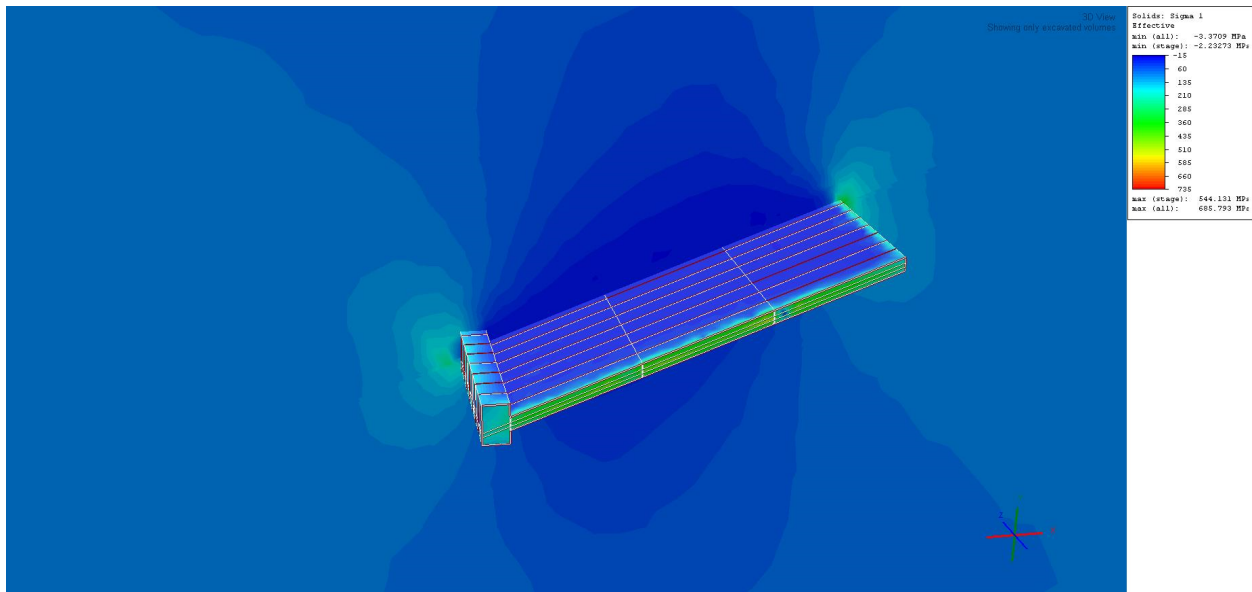


Fig. 114: Major stress distribution of the RS³ model including one stope with transportation galleries.

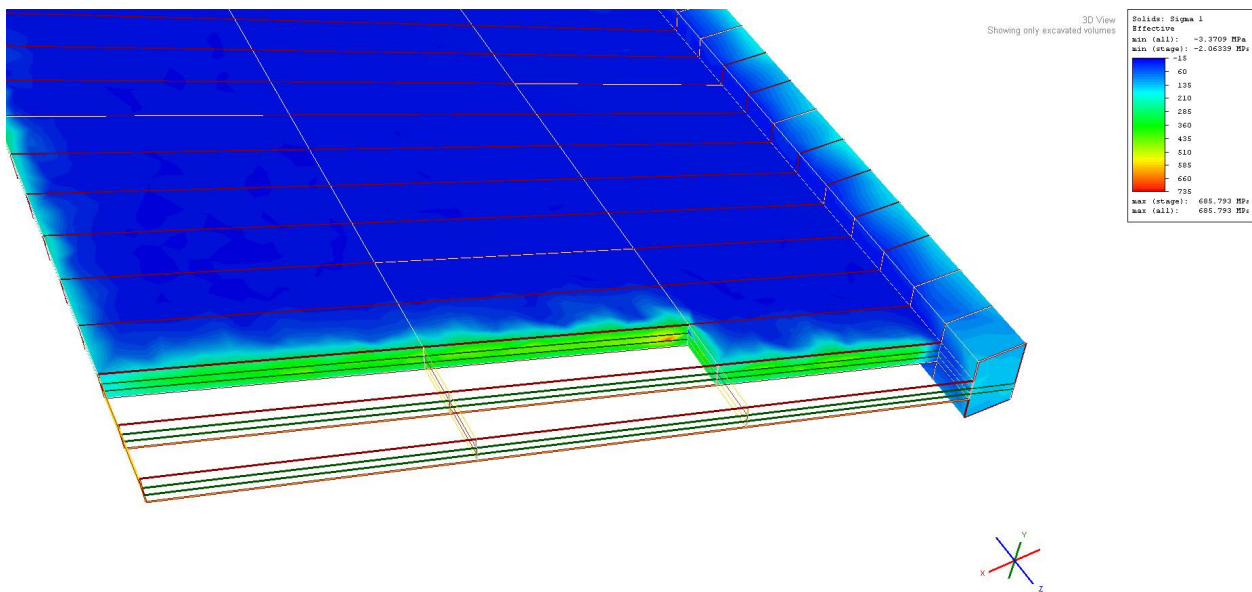


Fig. 115: Maximum major stress at a notch after first round after a completed excavation step of the RS³ model including one stope with transportation galleries.

8.4 Summary of all considered numerical models

All models show values of principal stress over 220 MPa which corresponds to the uniaxial compressive strength of the assumed material, namely quartzite. Supposing an even decreasing rock mass strength leads to the conclusion that there is a pre-fractured and disturbed zone at the side walls of the stopes. Also the yielded elements support this assumption. At the side walls shear planes are developing and provide certain evidence of a disturbed zone around the excavation. The depth of this zone varies between 1 and 2 m and can be observed throughout all models. The bulked rock mass zone is also well developed at the mining face.

9 Discussion

This chapter will compare all the data of laboratory and field testing and relate the drill data to the rock mechanical properties. Due to the creation of an internal database management, an increasing flexibility is granted and the transfer of this database system to another environment will be presented. Finally, the stress data derived from our numerical simulations will be compared to our field- observations as well as to literature.

9.1 Comparison of rock and drill data

One of the main issues of this thesis was the analysis of drill data as well as quantifying the influence of rock mechanical properties on the drilling process. We postulated the rock strength as the main rock feature in terms of the correlation with the drill performance by opposing the results of uniaxial compression strength test and drill tests. (Fig. 66, Fig. 72). Considering the correlation of wear and abrasiveness in the context of the rock - drill head interaction, we intended to compare the results of CAI, LAC and EQc to wear. In the following chapter the testing results as well as a comparison between the drill data and laboratory test data will be provided.

To characterize the influencing factors of the drilling process in more detail THURO (1996: 14) divided the drilling process in two steps: First the impact and second a rotational movement (Fig. 116). Due to this work, two main properties were characterized for the excavation of the material. Caused by the impact of the drill head, a zone of crushed material is created underneath the buttons of the drill bit. During the period of impact and the subsequent rotation the rock is set under a tensile load leading to radial fractures and initiating the chipping process.

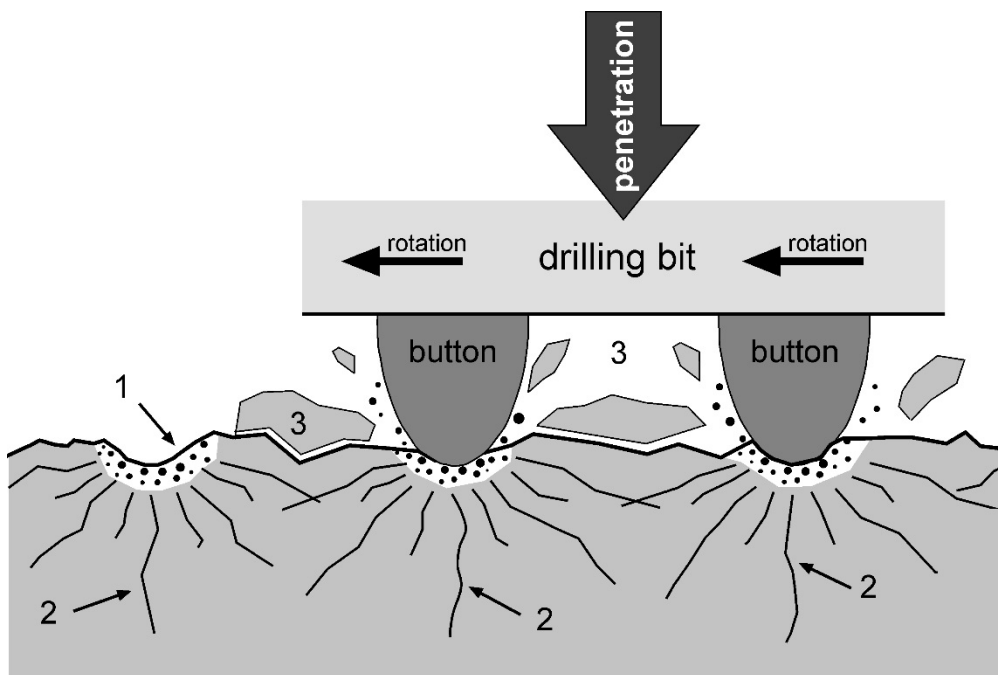


Fig. 116: Sketch of the physical drilling process during the rock drilling (THURO 1996: 14). Indicated with numbers are the zones in which the material excavation occurs (1 Zone where material is crushed due to compression; 2 Zone of radial fractures due to tensile stress; 3 Released rock chips which were loosened).

The uniaxial compression test is appropriate to determine the effectiveness of the drill head-impact on the rock mass and thus on the performance of the drill process. The uniaxial compressive strength could be the main rock property being taken into account. The energy which is produced by each impact of the machine could be compared to the energy which is required to fracture the rock. An adequate parameter could be the destruction work w_z . To improve the testing efficiency and to avoid long lasting sampling and

transportation, the application of a point load field testing device is conceivable. Thus the use of a field point load device for the determination of the destruction work was one objective of the current thesis. A further interesting aspect could be at the consideration of radial crack initiation during the impact and the rotational movement. The indirect tensile strength is suggested to be a suitable parameter for the indication of efficiency.

To analyze the wear potential of a certain rock, several abrasiveness tests are suitable. We decided to conduct the CERCHAR test, the LCPC test and the determination of the equivalent quartz content as parameters which influence the wear of a tool during the drilling process. To achieve quantitative and statistically reliable results, we conducted over 230 laboratory tests and performed 76 drill tests with over 4700 single drill holes. These preconditions allowed us to create a basis for further testing and could show a suitable way for future drill head testing. Due to difficulties in rock- sampling in the mines of South Africa and the associated limited number of samples and the sometimes smaller size, some testing was not feasible. In consequence the corresponding numbers are missing at the diagrams. A special problem is the determination of the wear of the drill head. During the mining process it is not possible to achieve suitable data for statistical analysis concerning the drill head diameter or the weight of the drill head. For the most producing mines the wear could not be measured and thus is missing in the corresponding graphs.

9.1.1 Performance

The main aspect of the parameter correlations is visible throughout all testing results: The higher the rock strength (UCS, PLI, BTS) the higher is the energy needed to excavate the material; and in consequence the lower is the performance of the drill.

As mentioned above we intended to correlate the performance to the rock strength. Starting with the most commonly used tests like the uniaxial compressive strength test, the point load test and the Brazilian tensile test can be enlisted. The diagrams of correlating the uniaxial compressive strength testing results with drill performance are illustrated in Fig. 117 and Fig. 119. Considering the uniaxial compressive strength, a correlation is suggested to be obvious, but only at first glance. The fit curve indicates a logarithmic connection between these two parameters. But no matter if a linear, exponential nor logarithmic fit curve is selected, at least the data of Oberbaumühle (amphibolite) is not fitting at all. The amphibolite samples of the quarry Oberbaumühle are characterized as very ductile whereas all other rocks are classified as brittle or at least in the limited range. A direct correlation between all rocks with brittle failure behavior concerning UCS and the performance can be suggested.

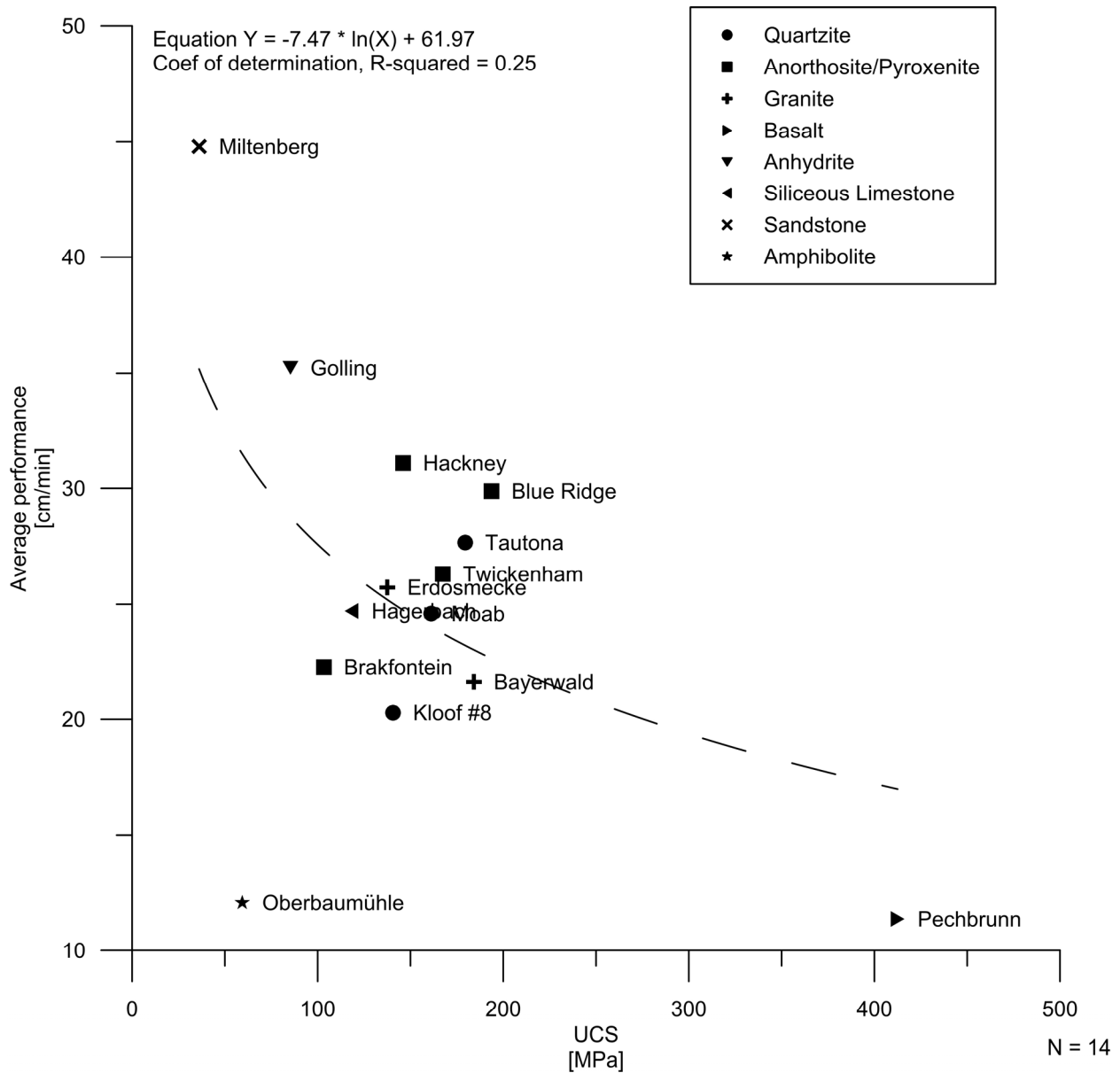


Fig. 117: Diagram of uniaxial compressive strength versus average drilling performance, providing certain evidence of a logarithmic correlation.

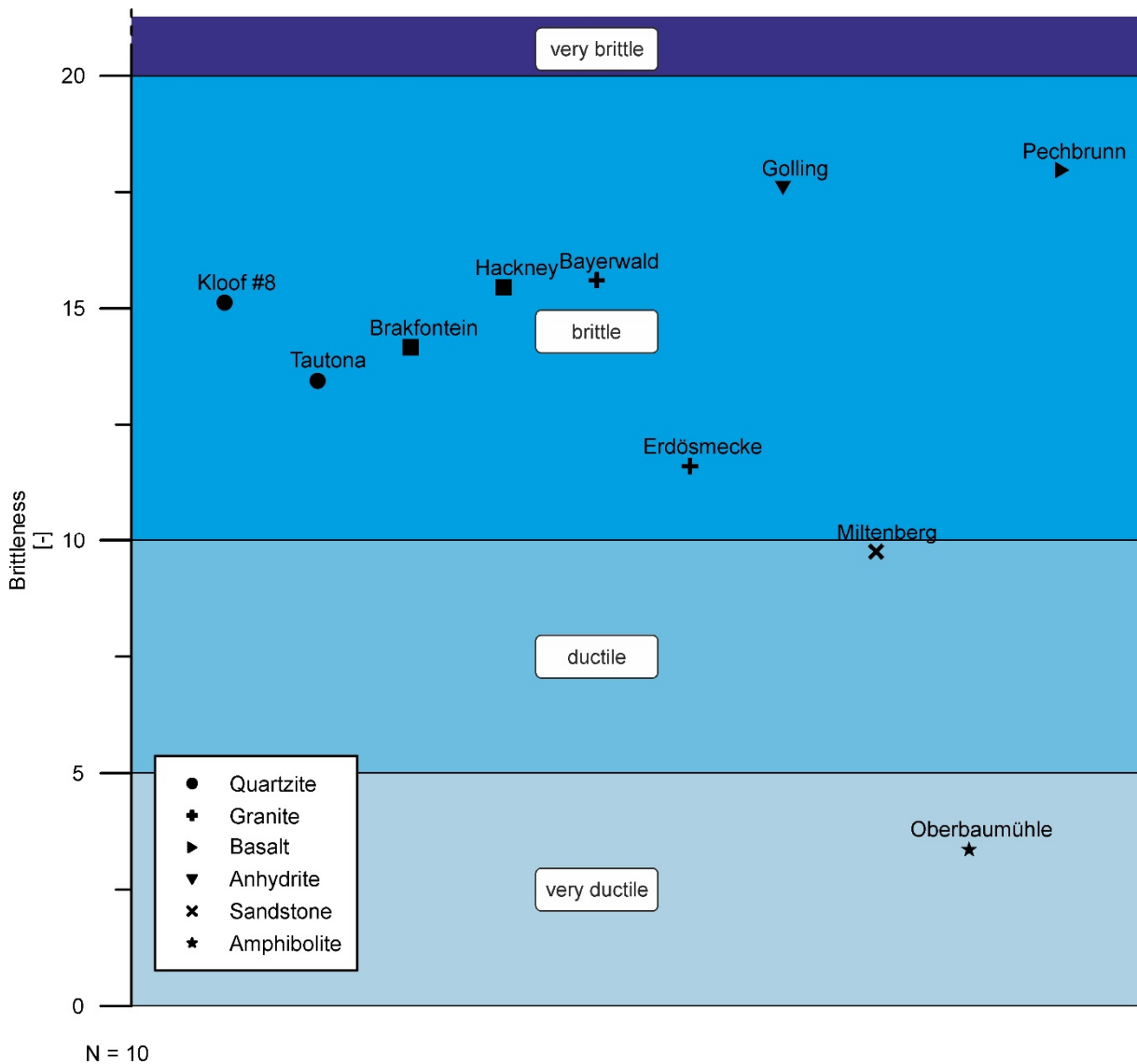


Fig. 118: Classification of brittleness as ratio of UCS/BTS of all tested rocks according to THURO (1996) showing the brittle behaviour of almost all samples except of the amphibolite of Oberbaumühle.

All tested rocks, independent of brittle or ductile failure, the results are indicating a more complex combination of rock mechanical properties, interacting and influencing the performance. In consequence, the uniaxial compressive strength is suggested not to be the adequate parameter or is just describing the problem insufficiently. Following the idea of an energy which is needed to excavate the material, the next parameter, the destruction work, could be taken into account. Considering the diagram in Fig. 119 this hypothesis could be confirmed.

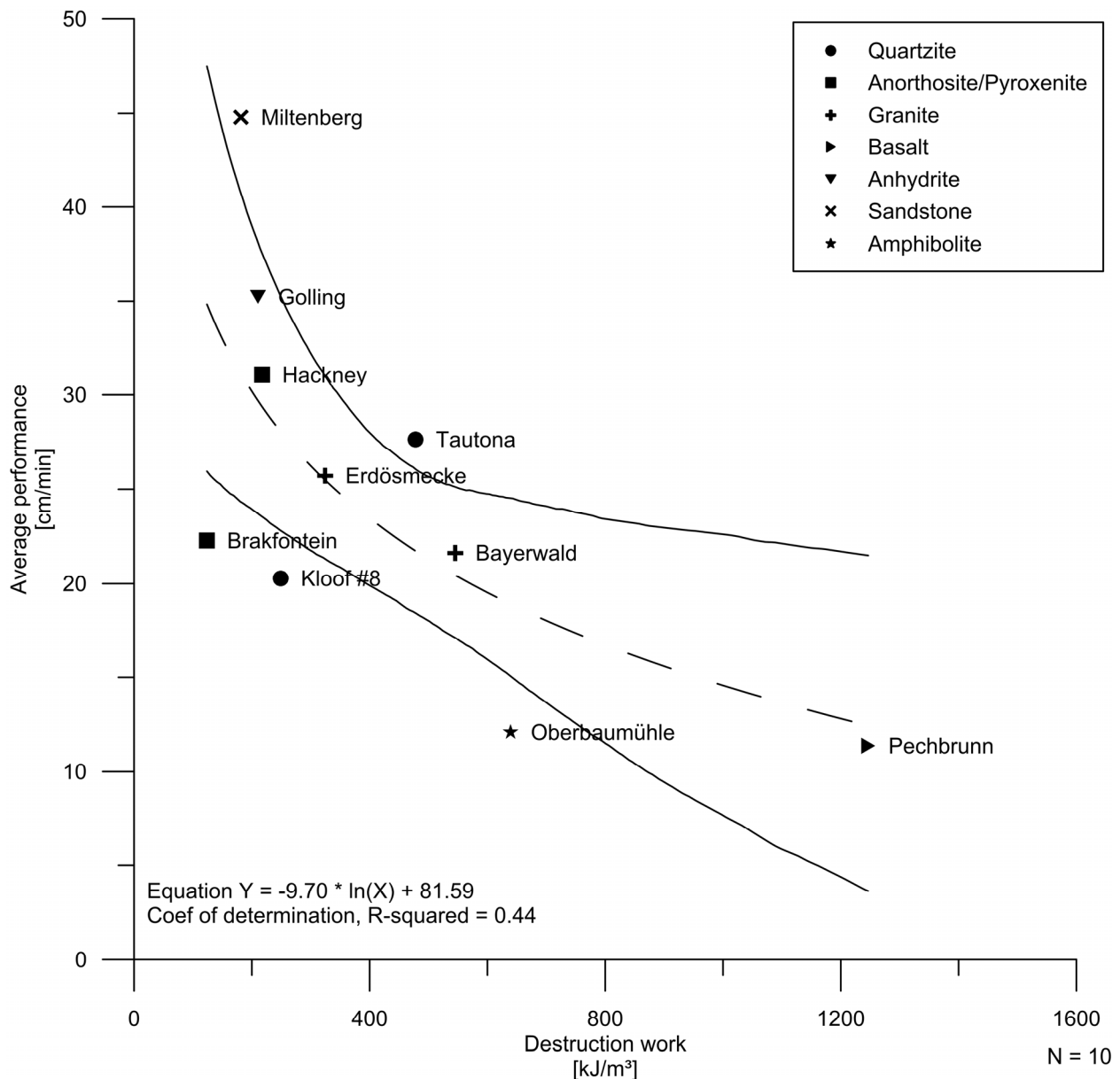


Fig. 119: Diagram of the destruction work versus average drilling performance. The fitted curve suggests a logarithmic correlation between both parameters.

According to WILFING et al. (2014) the destruction work is a suitable rock property which is suggested to lead to a more precise understanding of the energy needed to fracture the material. Due to the brittle failure mechanism, dominantly occurring during the accomplished tests, the test evaluations show no post-failure behavior, thus the destruction work is almost equal to the energy of failure recently defined by WILFING et al. (2014). The recording and calculation of the destruction work is very demanding, since the applied force needs to be adjusted in very fine steps by the testing software, especially when failure occurs. Due to these enhanced testing requirements, the parameter of destruction work is not trivial to determine using common UCS testing devices, also considering less well equipped laboratories. Also in case of testing rocks with a distinct ductile post-failure behavior the destruction work could be a misleading parameter and should be substituted by the energy of failure, as proposed by WILFING et al. (2014). Considering the confidence interval and the coefficient of determination of 0.44, the fit is insufficient for a suitable prediction of the performance in terms of rock drilling, respectively of the drill bit, but gives a much better fit than UCS.

During the impact stage, the rock gets compressed for a very short period of time which can be described by the help of the UCS. After the impact an immediate relaxation of the rock occurs and the material is set

under tensile load. Further the drilling process is very influenced by the tensile strength. Correlating the Brazilian tensile strength to the performance (Fig. 120), leads to improved results which can be compared to the application of the destruction work. The data points seem to correlate to a certain extend to a logarithmic fit considering the confidence interval and the R-squared value of 0.77.

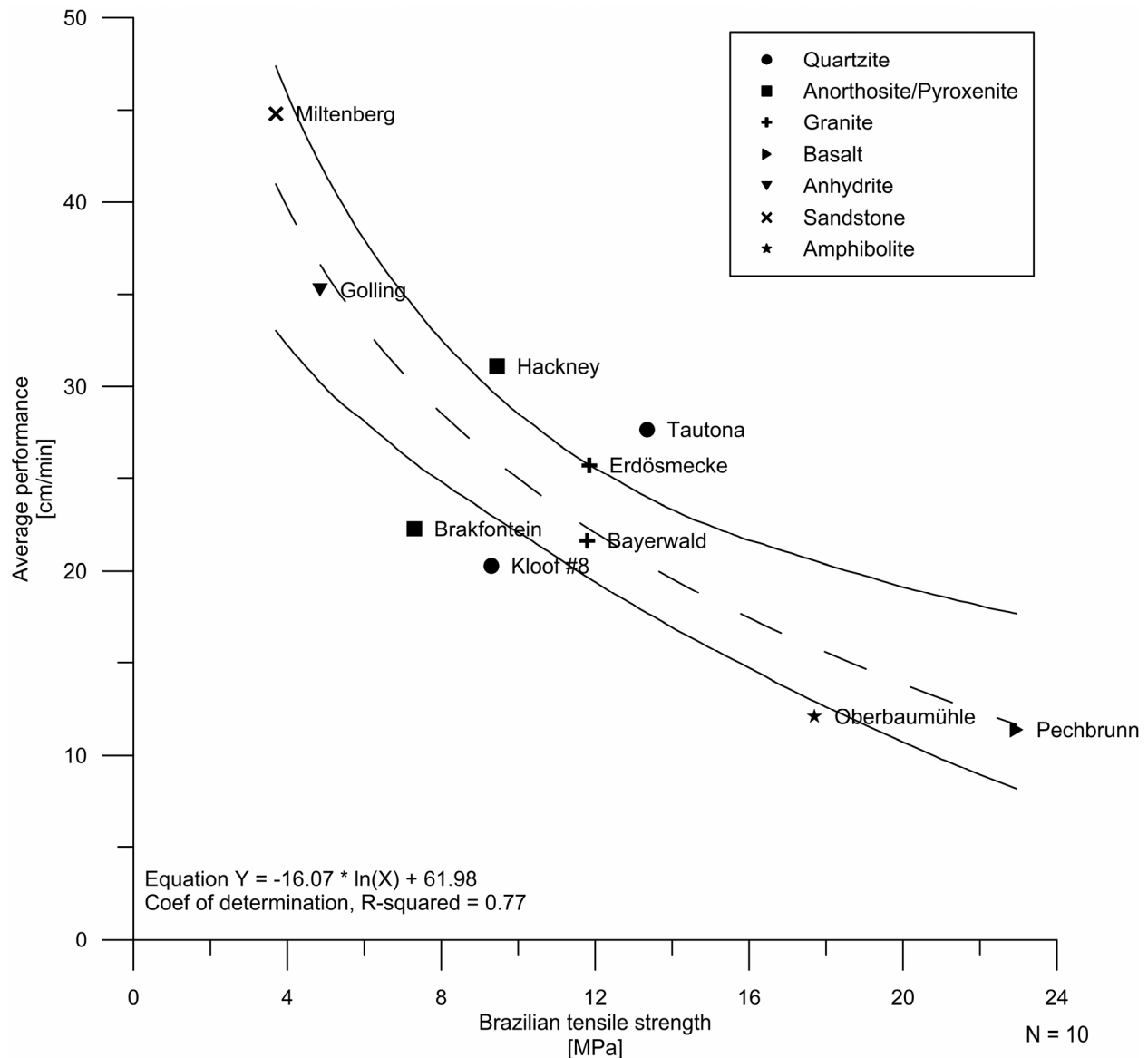


Fig. 120: Diagram, illustrating the logarithmic correlation between the results of the Brazilian tensile strength and the average drilling performance.

To test the Brazilian tensile strength, a proper sampling and sample preparation is required. The testing device is a very important factor of influence for the sensitivity of the stress regulator to increase the accuracy in terms of stress regulation improving the test accuracy. Thus the idea of applying a less complex test set-up for conducting tests on irregular samples was born. The point load test is a common test, which can also be performed in the field with a manual hydraulic device. The results of a combination of field and laboratory point load tests, plotted versus the performance are illustrated in Fig. 121.

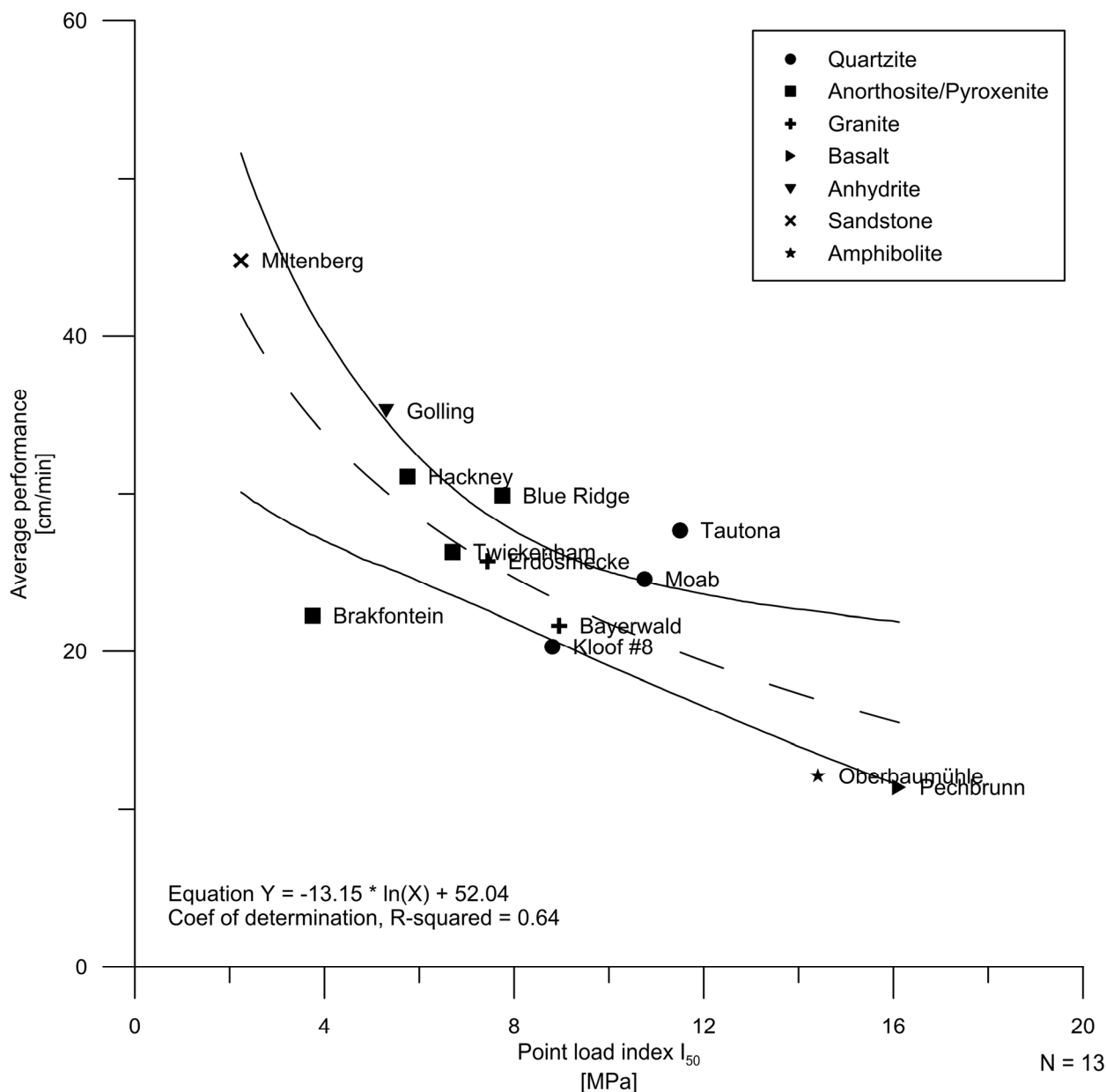


Fig. 121: Diagram illustrating the correlation between the point load index and the average drilling performance. The trend line indicates a correlation between these two parameters.

The point load index shows a little less correlation with the performance than the Brazilian tensile strength, which is indicated by the confidence interval and the coefficient of determination. Taking into consideration that the results are a combination of laboratory and field tests (Brakfontein, Hackney, Twickenham, Moab and Tautona), this kind of correlation should be followed in terms of further testing. Considering the testing results of the conducted field tests, the efficiency of this testing procedure is quite clear.

9.1.2 Wear

The data for some underground drill testing result from former tests, which were conducted in an early stage of this thesis or before. Thus the recommendation which parameters should be recorded was not set up to that time. At the platinum mines, tool wear was not a problem and was therefore not measured. To control the wear of the drill after each fifth drill hole is time and cost consuming for the mine operator. Therefore, less mines and rocks were analyzed in comparison to the performance testing. For approaching a new way of testing drill heads, the number of data sets is suggested to be sufficient. Facing the wear prediction as well as the correlation of the wear to the rock mechanical properties, the results should be

considered in combination. Starting with the CAI testing, (Fig. 122) which merely led to any correlation, going to the LAC (Fig. 123) with similar results, ending up at the equivalent quartz content (Fig. 124). Especially the results of the quarry of Oberbaumühle (amphibolite) are always outliers. One reason for this might be the occurring difficulties during the drilling process. Many of the drill heads got stuck, so the wear is a value of minor confidence. Nevertheless, during thin section analysis and in the test results of the destruction work, the special character of the amphibolite of Oberbaumühle becomes clearer. All mineral grains are strongly toothed and saturated along the boundaries. Especially columnar habitus of the amphiboles increasing the effect grain interlocking during compression. To loosen this structure much more energy is needed and the abrasive potential of the low quartz content will increase.

The higher wear at quarry Miltenberg is caused by the high quartz content. Due to the very low rock strength the CERCHAR test resulted in very low values. The testing pin would dig into the surface of the rock and not scratch at the surface resulting in a lower pin flattening.

The very low wear at Hagerbach compared to the very high CAI could be caused by the testing procedure. The rock testing in Hagerbach was conducted by Hagerbach Versuchsstollen GmbH. Thus for the CAI testing a steel pin with differing steel grade could have been applied and could have caused this deviation. The recordings concerning the experimental procedure were insufficient to clarify this fact finally.

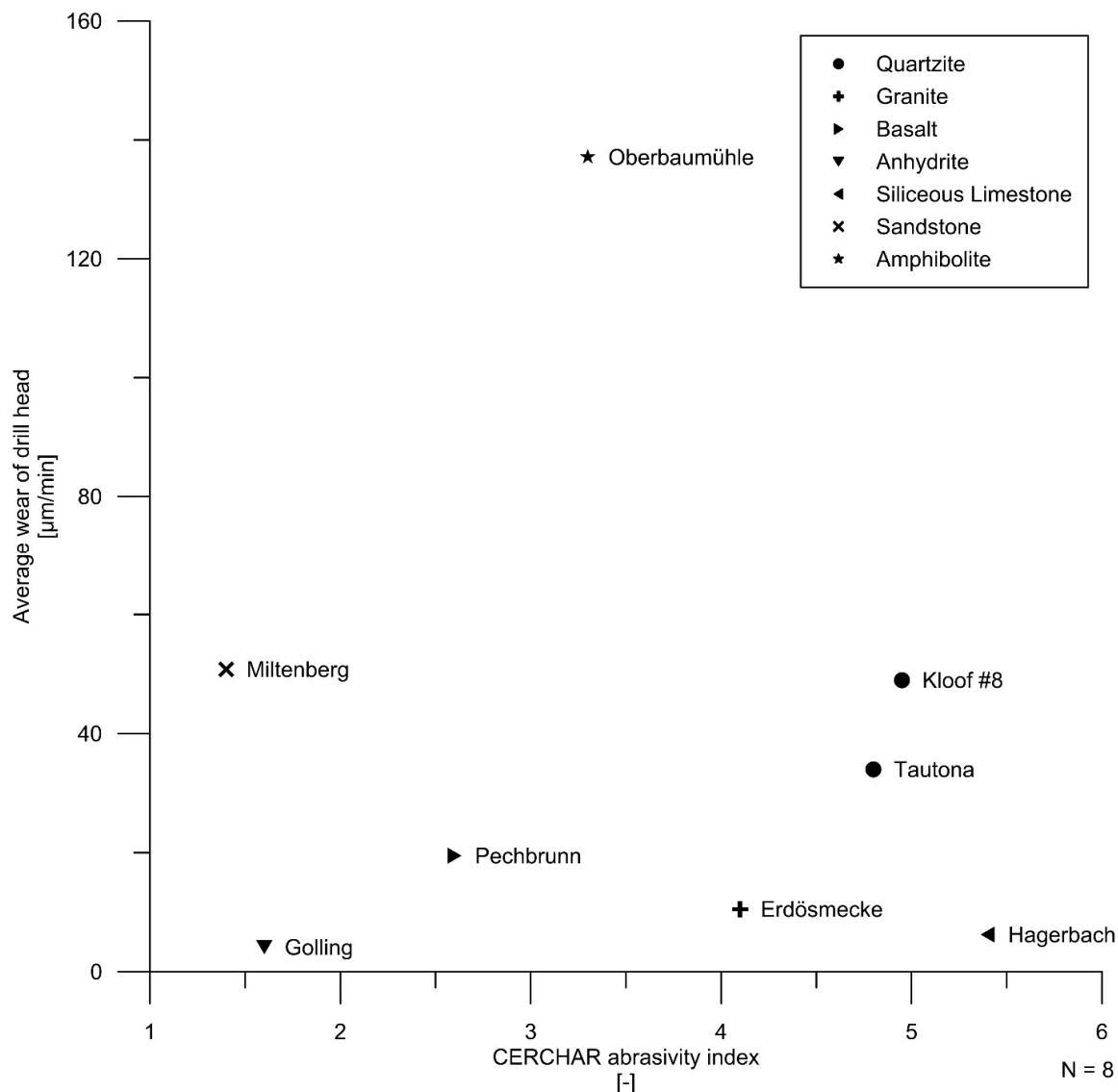


Fig. 122: Diagram of CAI versus the average wear of the drill head. Due to the scattering of the data no sufficient trend line could be plotted.

For LCPC testing the results are inducing an improved trend, but the rocks of Oberbaumühle were again insufficiently described with this index test. The results of the sandstones of Miltenberg yielded low abrasivity values. This could also be induced by the low rock strength. The quartz grains are loosened effortlessly during the testing procedure. Besides the releasing process, the grain shape plays a certain role. As the quartz grains are sometimes edge-rounded, the abrasive effect on the steel impeller is lower. The fine grained hematite could work as lubricant to lower the LAC.

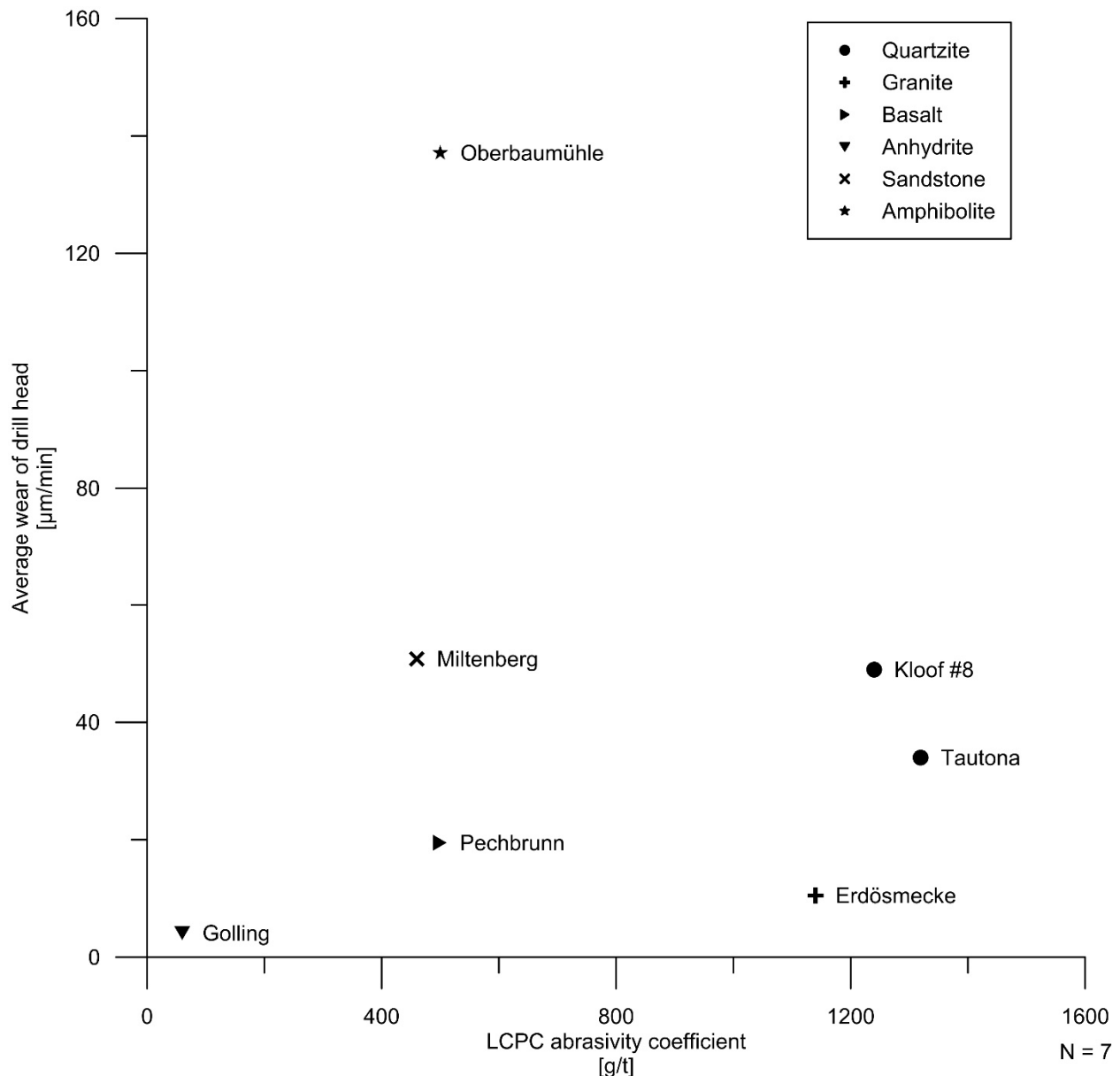


Fig. 123: Diagram of LAC versus average wear of the drill bit. Due to the scattering of the data no sufficient trend line could be plotted.

All previous results suggest a correlation of the mineral content especially of the equivalent quartz content and the average wear (Fig. 124). But again the amphibolite of Oberbaumühle does not fit in this correlation. The equivalent quartz content is not a suitable way of describing the structure and fabric of the rock as well. So, the strongly interlocking amphibolite will not fit. Thus the trend line was calculated without taking amphibolite of Oberbaumühle into account. The equivalent quartz content leads to an improved fit for the Miltenberg sandstone. The parameter of wear is represented in an enhanced way by the equivalent quartz content compared to the CAI or the LAC.

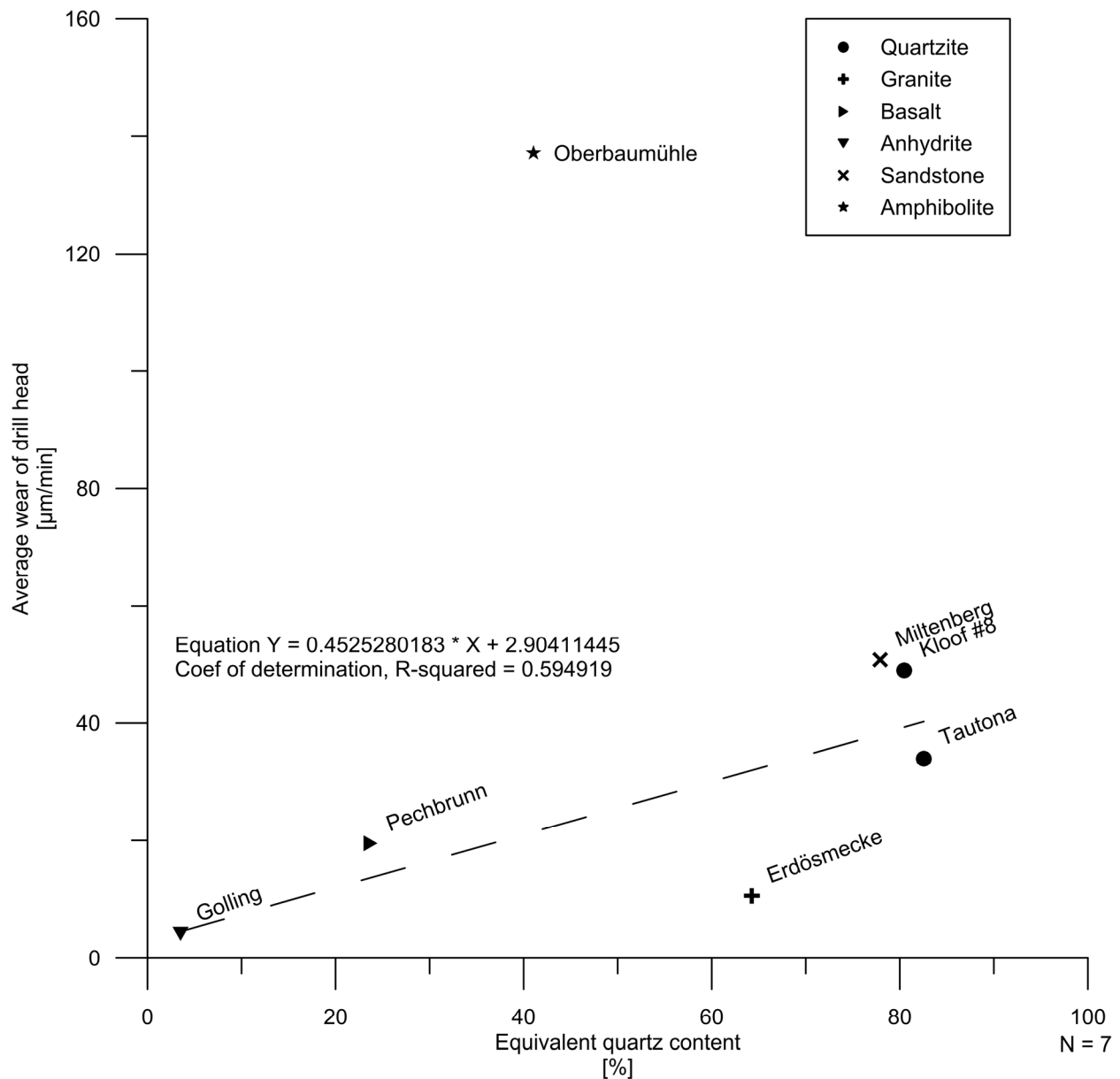


Fig. 124: Diagram of equivalent quartz content versus average wear with linear fit for all data except of Oberbaumühle.

As a final idea for a singular correlation we calculated the rock abrasivity index RAI (Eqn. 21) provided by PLINNINGER (2002: 95) and THURO & PLINNINGER (2007).

Eqn. 21: Calculation of the RAI with UCS and EQc as parameters PLINNINGER (2002: 95).

$$RAI = \sum_{i=1}^n A_i \cdot S_i \cdot UCS$$

with	<i>RAI</i>	<i>Rock abrasivity index</i>	<i>[-]</i>
	<i>UCS</i>	<i>Uniaxial compressive strength</i>	<i>[MPa]</i>
	<i>A_i</i>	<i>Percentage of the particular mineral</i>	<i>[%]</i>
	<i>S_i</i>	<i>Rosinwal-grinding hardness (related to quartz)</i>	<i>[%]</i>
	<i>n</i>	<i>Number of all considered minerals</i>	<i>[-]</i>

The correlation between the RAI and the average wear (Fig. 125) of the drill bit should account for the rock strength and the mineral content of abrasive minerals. But again the amphibolite of Oberbaumühle could not be fitted to the trend line.

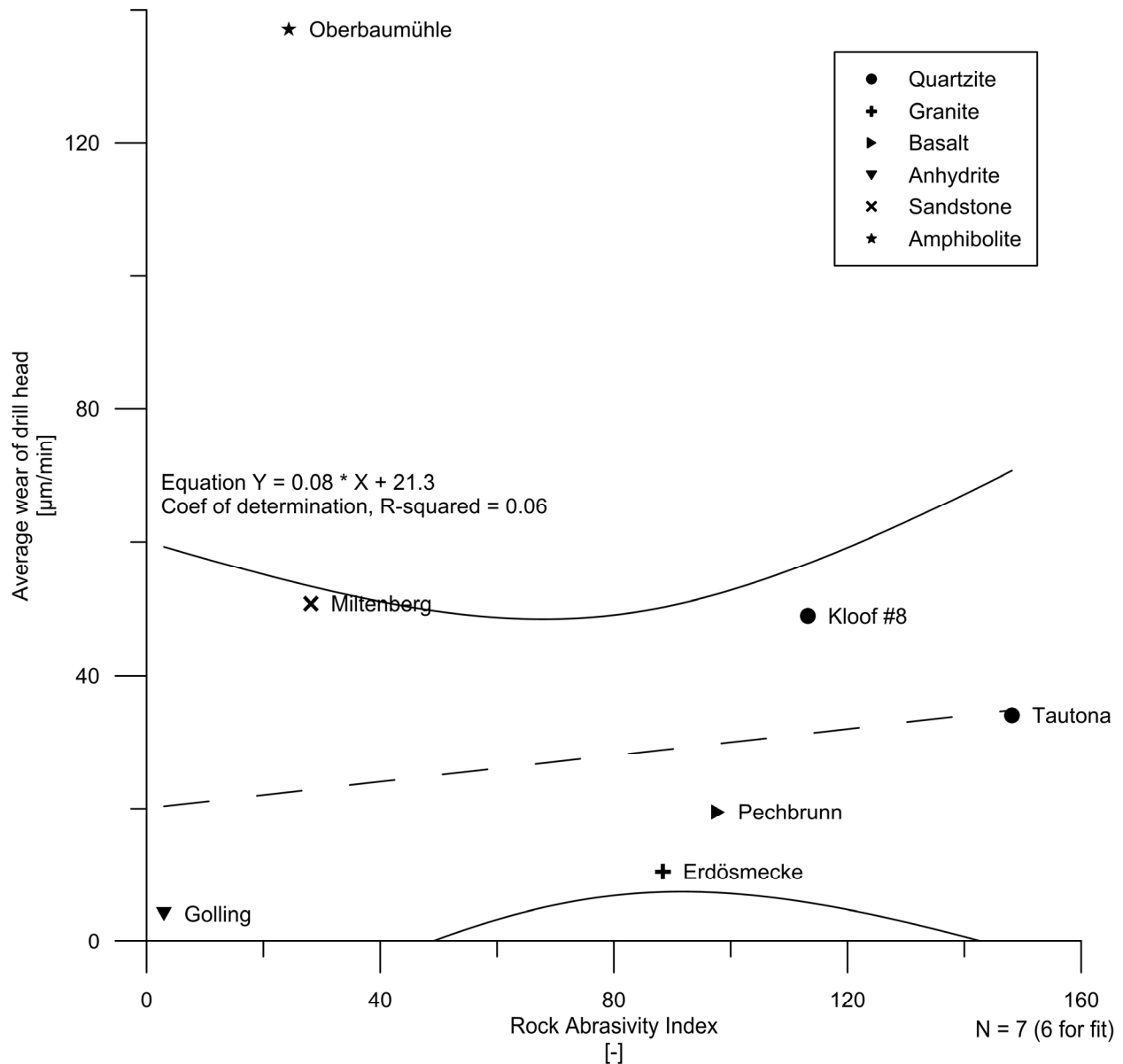


Fig. 125: Diagram of rock abrasivity index versus average performance with linear fit for all data except of Oberbaumühle.

The calculated RAI for the Miltenberg sandstone is suggested to be too low for the high abrasive potential. Besides of the mineral content and the rock strength, a more complex interaction of rock properties seems to influence the wear of the tools.

9.1.3 Rock landscape

Applying the suggested correlations, the interaction between drill head and rock mass in terms of performance and wear cannot be characterized with a single rock property. For this reason, the combination of the parameters rock strength and abrasivity was introduced. The basic idea was to create a diagram (Fig. 126), a kind of “map” which shows ranges of applicability of drill heads in relation to the rock properties. By means of this diagram the rock parameters and the corresponding drill head are illustrated. This diagram can be characterized as a “rock landscape”. The rock landscape illustrates the scope of application for every

single drill head. Besides the selection of the drill head in accordance with the geological conditions and the mined rock is possible.

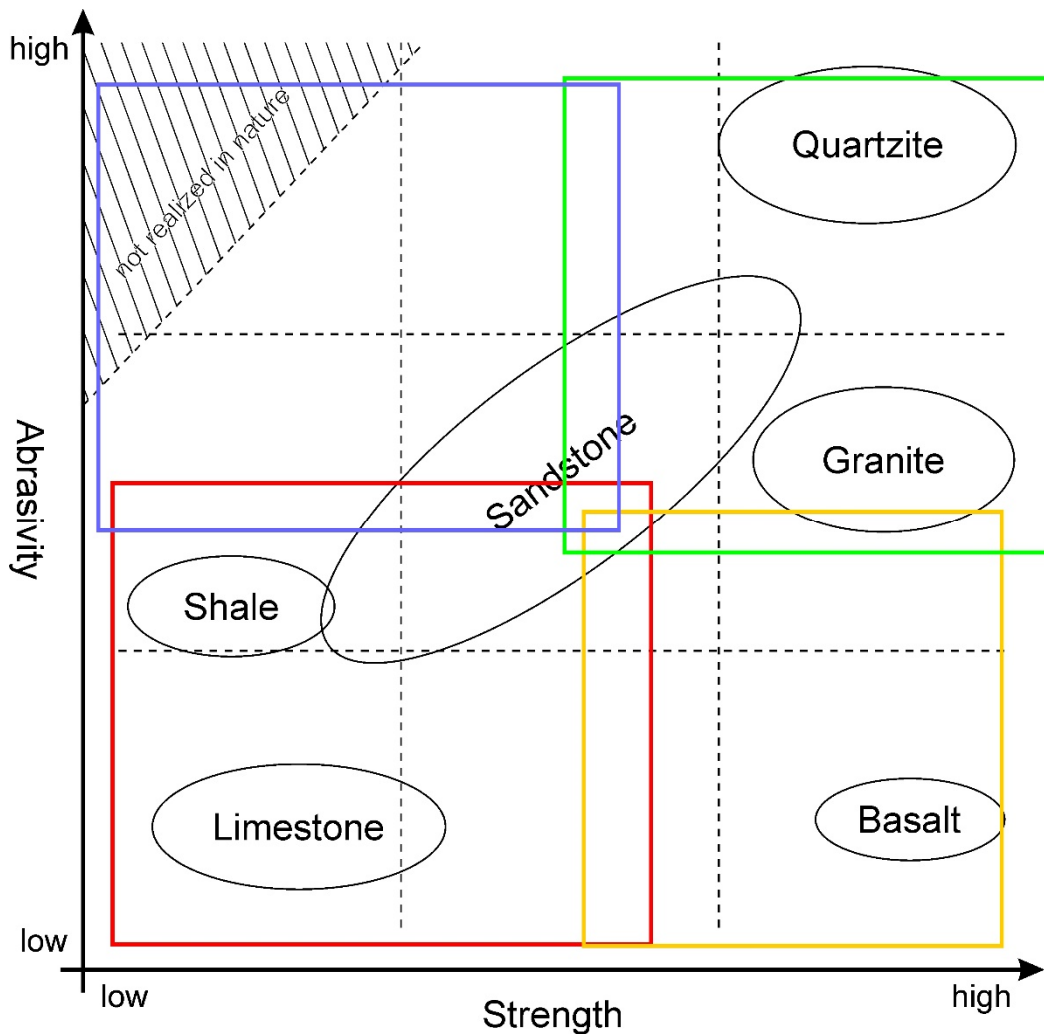


Fig. 126: Constitutional model of a “rock landscape” for drill head selection as an analysis tool for the current thesis. The colored frames represent the scope of application of each of 4 different drill heads.

As discussed in the previous chapters (9.1.1 and 9.1.2) Fig. 127 illustrates the combination of the recommended properties and the constitutional model of a rock landscape, describing the wear and performance of a single drill head. The point load index was taken into account since this test is well correlating with the performance. Further the testing can be performed in the field without any preparation of the samples. To determine the wear in a first approach we considered the equivalent quartz content as suitable since it provided the best correlation.

The scope of application of drill head 1 was selected empirically based on the background data of the equivalent quartz content, the point load index, the performance (upper chart) and the wear (lower chart) of Fig. 127.

Starting with the performance section of the landscape, the EQc is of minor importance for the scope of application. Thus the upper boundary is set to the maximum of the diagram of 90 %. The right boundary of the field of applicability, the maximum of the point load index for this drill head, was defined at 12 MPa. Considering Fig. 121, a value of 20 cm/min could be approached as the minimum of efficient performance for the selected drill head. Taking the different test locations into account, the point load index of 12 MPa would imply a sufficient performance for Tautona, but not for the quarries of Pechbrunn and

Oberbaumühle. The latter two quarries provide point load indices of more than 12 MPa resulting in decreasing performance values (Fig. 121).

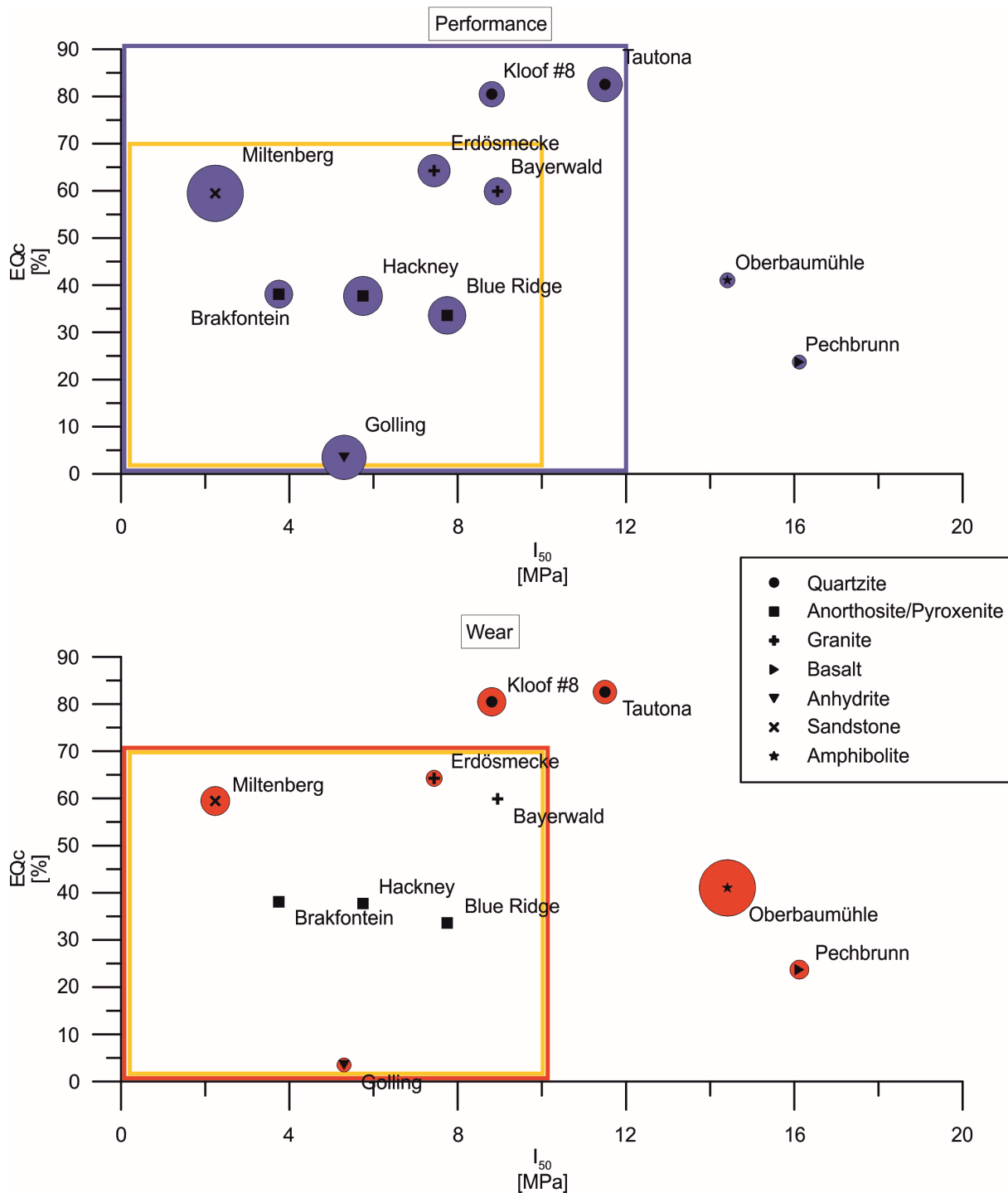


Fig. 127: The final rock landscape for point load index vs. equivalent quartz content. Areas of highest performance and lowest wear are printed in blue (performance) and red (wear). The landscape is divided in two parts. The upper one for performance and the lower part for wear. The best working conditions for drill head 1 are printed as intersecting area of the blue and red marked area in yellow.

Considering the wear (the bottom part of Fig. 127), the rock strength (point load index) and the abrasivity (EQc) have to be taken into account. Based on this assumption the scope of application was chosen to cover the granites of Erdösmecke and Bayerwald due to a low wear rate. Generally the threshold for the equivalent quartz content is chosen with help of the correlation of wear and EQc in Fig. 124. The wear occurring at Kloof and Tautona gold mines and at the quarry Oberbaumühle is exceeding the approached limit of

20 $\mu\text{m}/\text{m}$ loss in drill bit diameter, due to a considerable EQc. The sandstone of Miltenberg indicates a wear exceeding the limit of 20 $\mu\text{m}/\text{m}$ and shows an increased EQc. Due to the high performance rate at quarry Miltenberg the increased wear could be accepted and the scope of application tends to include this quarry. In consequence based on considerations of efficiency, the upper boundary of the scope of application is customized to 70 % EQc. Assuming that the rock strength and the quarry of Erdösmecke have to be included into the scope of application of drill head 1, the upper boundary of the point load index could be defined at 10 MPa but is customizable.

The resulting scope of application of drill head 1 is shown in Fig. 127 as the yellow colored rectangle with a range I_{50} between 0 and 10 MPa and EQc between 0 and 70 % as the intersecting area of the ranges of low wear and high performance.

A first approach and the introduction of this “tool” were accomplished by means of the current thesis with a sufficient data basis for the first drill head. But as shown in the example of drill head 1 the data acquisition is not trivial. To achieve the required information, much data meaning a high effort in terms of laboratory and field testing is required. Nevertheless, by the help of the introduced database system we are able to expand the data basis during the ongoing mining and the every-day work just by collecting an increasing amount of data applying different kinds of drill heads at different test locations.

9.2 Discussion of the used DBMS and Migration of data and DBMS to another system

At current stage we are dealing with almost 2500 laboratory tests within our database system and the number is still increasing. We are managing data of over 800 samples of almost 150 projects. With our status enquiry and the tools for mean value calculation and single value display we are able to achieve fast access to the produced data and to provide this data to our clients.

We could eliminate duplicated data and have a backup plan to store the data to avoid data loss. It is possible to access all data from everywhere around the world and to draw an excerpt of the database to work with other programs. The working with the database is as easy as writing a blog entry on a general home page.

The setup of this system was lightened due to the use of WYSIWYG (what you see is what you get) editors for web page programming like Adobe Dreamweaver and the help of phpMyAdmin for the setup of the database itself. The last program is also very useful to store big data within the database like it is done at the moment for all drill test data.

In contrast for the queries and the contained php code, to grant access and the data-application-tools a special know-how about database programming is required. The training period could be optimized and beginners could be able to obtain sufficient knowledge to create parts of the DBMS and to solve minor problems.

By programming the first add-on for drill head analysis and management of mine and drill head data, we created a tool for fast access to the conducted tests, in order to gain information about the tested items. This tool links the laboratory test results perfectly to the mine data which offers the possibility of a correlation to drill head data. These add-ons are fast programmable and allow a fast response to changed needs within a project.

The DBMS and the database can be migrated in a time efficient way. The files containing the web interface and the DBMS can be copied from one running server to another by the help of ftp clients or directly by accessing the web server via network. With the help of phpMyAdmin, the export of the database-data should not cause major problems. The import into the new database system is also supported by this administrative tool. The computer to which the DBMS should be transferred has to fulfill some requirements. The server must run a web server, the server must be accessible from the internet or intranet

and has to be able to run php code. Additionally, MySQL (version at least 5.5.41-43) and phpMyAdmin (version at least 4.0.10.10) must be installed and running on this machine.

This server should perform regularly backups of the files. A backup system for the database itself is already integrated in the DBMS.

9.3 Stress data in 3D modelling and in the field

All 2D and 3D models provided within the current thesis and in MENSCHIK (2009) indicate a zone of disturbed rock near the side walls of the stope. These zones are in 1-2 m distance to the side walls in the rock mass. Especially in a later stage of the stope as shown in Fig. 115 after the first round of an excavation step at the newly created sharp corner (Fig. 128), the stress maxima with 600-700 MPa (RS³ model one stope with transportation gallery) occurs and it exceeds the uniaxial compressive strength (220 MPa for quartzite) of the rock to a large extent.

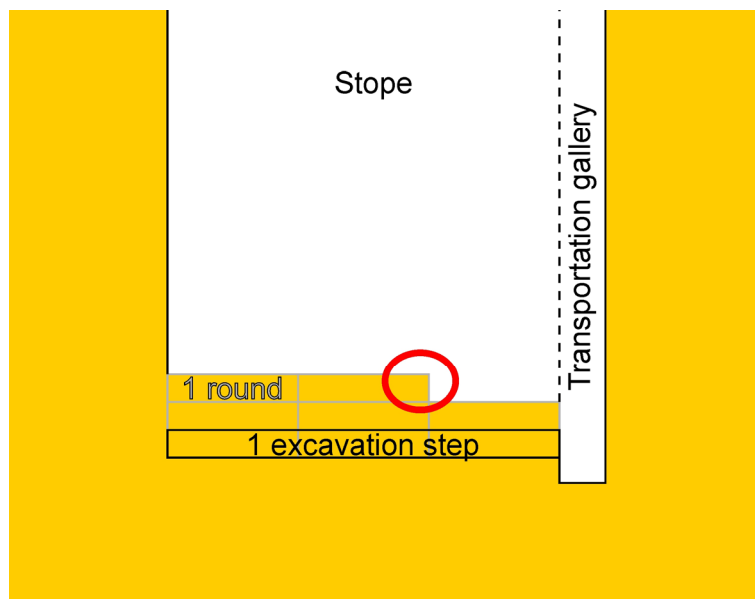


Fig. 128: Top view on the excavation stope. The highest stress concentrations are located with the red circle with definitions of the mining procedure.

This would lead to a pre-damage of the rock and creates disturbed zones causing a certain pressure at the side walls. These zones can be found around the whole area of the stope and the transportation gallery, which could result in an improvement of the drilling process especially for the middle holes. But a general problem with stress induced fracturing is the factor of time. Referring to MARTIN (1997: 708, Fig. 24) the creation of a notch at a circular shaped tunnel takes several months, but current projects show that around 80% of this yielding occurs after the first few hours and days of excavation. Due to geometrical reasons like rock ledges, sharp corners and the unknown sequence of the drill pattern, it is not possible to predict the occurrence of pre-fractured regions providing potential for increasing the drill speed.

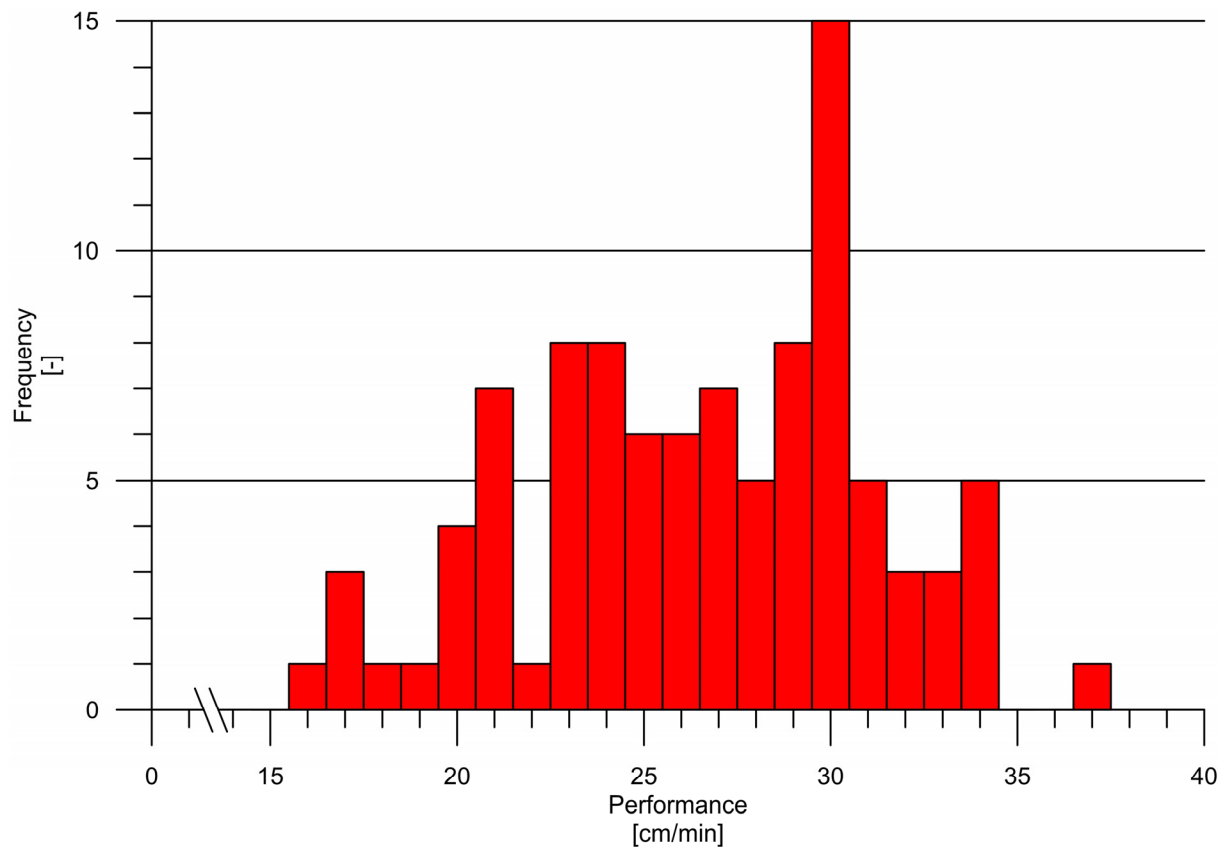


Fig. 129: Histogram illustrating the drill speeds of the total amount of single drillings of drill head 1 in Tautona gold mine.

The high stress rate could lead to a decreasing drilling performance and a higher tool wear, which can be followed in the testing results of Tautona gold mine (Fig. 129). This hypothesis could neither be rejected nor be confirmed within this research project. It was not possible to perform in-situ stress measurements where the drilling processes occur. Thus it would be desirable in the future to perform several drillings in comparable geological settings using similar machines and one specific drill head. Both effects are possible and maybe the reason for the bigger range of performance results of drill head 1 in Tautona (Fig. 129).

Looking at the side walls of the transportation galleries the fracturing effects are clearly visible (Fig. 130). Spalling and rock burst as phenomena typical for high stress are reported from Tautona rarely and only in the transportation galleries and access tunnels. Using the diagram of DIEDERICHS (2007: 1085, Fig 2) with σ_u of 220 MPa and $\sigma_{t,BTS}$ of 15 MPa the quartzites of Tautona (Fig. 131) have a high to very high energy retention but only a low spalling potential. In this classification, both lead to a very low strain burst potential. This is suggested to result in long term failure of rock slabs and no to fast processes, which can be observed in the field. The stopes have smooth walls and low support is needed.

At Tautona gold mine a typical round of max 1.2 m in depth and about 10 m in length is finished every two days. Due to the phenomena discussed in the previous paragraphs, it is not possible to create a drill pattern which could lead to an optimized drill performance and a decreasing wear. The disturbed zone occurs in a depth between 1 to 2 m from the side walls and could only be effective in the last centimeters of each drill hole.



Fig. 130: Stress induced loosening of rock mass at the side walls of the transportation gallery.

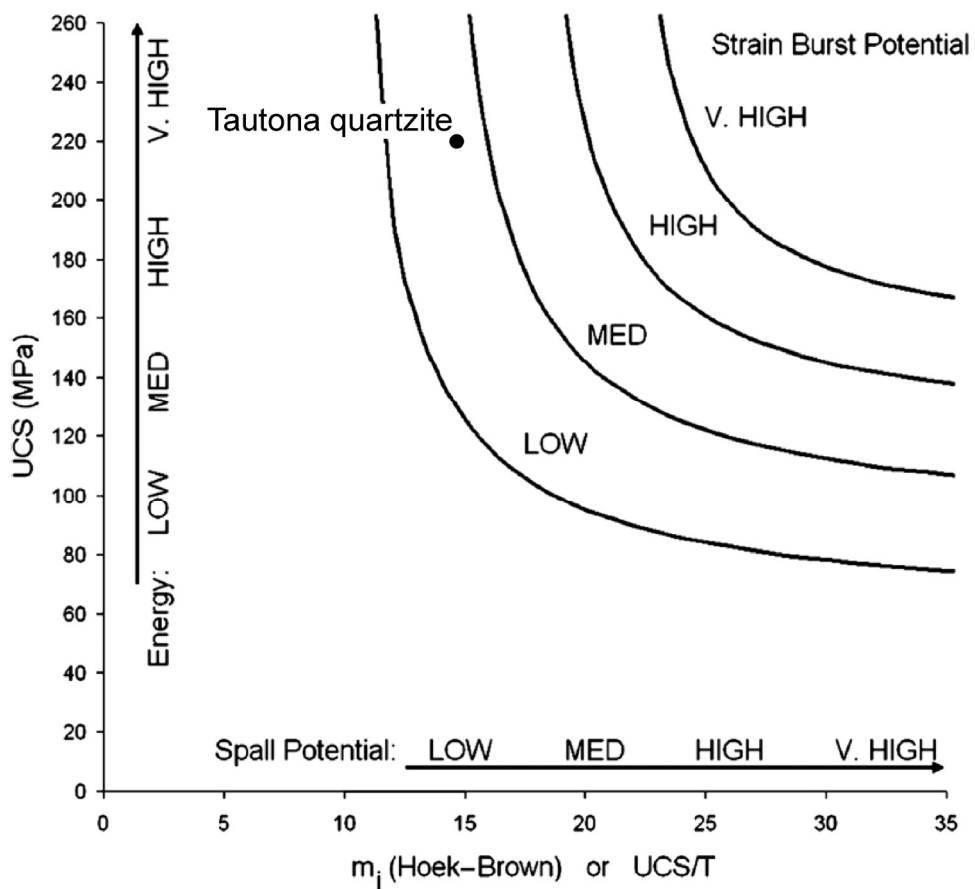


Fig. 131: Diagram illustrating the strain burst potential using a correlation between the UCS and m_i (Diederichs 2007: 1085, Fig 2).

10 Conclusions

To sum up some conclusions should be provided based on the findings discussed in the previous chapters.

The foundation of proper analysis of drilling performance in hard rock conditions is a database where all technical data, data of the construction site or mine and the results of the conducted laboratory testing program can be stored. In means of data management and to cover problems of data inconsistency and problems in data exchange we were able to solve the following issues within the established MySQL database:

- The database system is one system substituting all previous spreadsheet files for data exchange.
- All data is saved at one location and easy accessible from all around the world via HTML-PHP web interface.
- Due to the comfortable web-interface all problems concerning duplicated, inconsistent or unreadable data are solved.
- The first add-on, the drill bit add-on, allows access to all project relevant data (data about mines, geology, laboratory testing and tested drill heads) and supplies the user with all necessary data.
- An analysis tool for the drill bit add-on supports the user to analyze data from drill tests in the field or in mines.
- Additionally, a query tool for new mine sites allows an easy selection of the appropriate drill head. This tool compares and shows data concerning the available drill heads. The ranked query outputs indicate the best performing drill head or the one with minor tool in comparable geology (according to the given rock type) or the conducted rock laboratory testing (UCS and CAI).

In the second step, we wanted to correlate commonly used rock mechanical properties to drill test data like drilling performance and the drill head wear:

- The uniaxial compressive strength shows a good correlation for brittle rocks. Ductile rocks like the amphibolite of Oberbaumühle seem not fit to this model.
- The destruction work or the energy of failure is a suitable approach for the energy which is used to excavate the rock mass or face advance in mining.
- The Brazilian tensile strength (BTS) shows a good correlation with the drilling performance and should be considered as complementary parameter for the prediction of the drilling velocity. The BTS shows the highest correlation to the drill data.
- The point load test, used as an index test, is also a very good parameter for correlating with drilling performance. This test can also be conducted as a field test on compact irregular specimen with suitable results (so called “irregular lump test”). In this special case, the point load test index is not used as a substitute for the uniaxial compression test.
- The occurring wear of a drill head could not be sufficiently correlated with the CERCHAR abrasivity index (CAI), the LCPC abrasivity coefficient (LAC) nor the equivalent quartz content (EQc) in a singular dependency. It seems that tool wear is the result of an interaction between mineral content, the geometry of the grain boundaries, the existence of fissility or breakability and rock strength.
- Since a singular correlation was not found to be suitable to the drilling process, a so called “rock landscape” was developed. This “landscape” shows the scope of application including different drill heads according to rock strength and abrasivity or wear. For this approach the point load index and the equivalent quartz content were chosen as the best correlating properties.

Finally, we took a deeper look at the occurring stress situation and its effects on mining, especially the drilling process itself. For this purpose, a series of large and small scale 2D and 3D models had to be established to evaluate in-situ stress and the resulting interaction with the geometry of the given mine. The

proper code is crucial for the results and should be selected according to rock mass conditions, especially the given discontinuity pattern.

- The 2D Finite Element models (Phase² / RS², *Rocscience*) of the current thesis and MENSCHIK (2009) indicate zones of high stresses at the side walls in a distance of 1-2 m behind the wall. In these zones, pre-fracturing of the rock has to be expected.
- The computed 3D models using FLAC 3D (Fast Lagrange Code 3D, *Itasca*) and RS³ (3D Finite Element Code, *Rocscience*) could confirm these zones impressively.
- Since the excavation could be calculated in stages in RS³, these pre-fractured zones not only were located at the side walls but are developing in the newly blasted notch of the excavation after each round (drill-and-blast cycle).
- These zones can influence the drilling process in two ways:
 - (1) In regions, where high stresses predominate but does not exceed rock strength, drilling performance is lowered significantly apparently due to the triaxial stress state of the rock. This can be clearly seen in the gained data sets.
 - (2) In zones where high stresses exceed rock strength, pre-fracturing occurs resulting in higher drilling velocity can be much higher.
- Since the highly stressed zones vary between 1 and 2 m in depth at the center of the stope, normally the drilling process is not affected significantly, taking the length of the boreholes of 1.2 m into account.
- Due to the fast progression of excavation rounds (blasting is carried out at least every 2 days) and the low possibility of predicting local zones of high stress or pre fractured rock, it is not possible to give recommendations for a special drill pattern to optimize the drilling process.
- Although high stresses occur at the side walls of the stope, the quartzite of Tautona has high energy potential but only low spalling potential and a low strain burst potential (DIEDERICHS 2007). These facts can be observed and approved in the mines. Only in areas which were mined previously and left open for a certain amount of time e.g. rock slabs are spalling in the transportation galleries and walls have to be supported.

11 Recommendations for predicting drilling performance and wear based on rock properties

Taking into account the results of this extensive testing program, a suitable testing procedure to determine performance and wear of newly designed drill heads can be recommended.

1. The prototype drill head should be tested in at least 5 different rock types. Under the given circumstances this could be for example (a) Tautona gold mine quartzite (high stress conditions, high strength and high abrasivity rock conditions), (b) Bayerwald granite or (c) anorthosite of platinum mining (midfield of the rock landscape), (d) basalt (e.g. Pechbrunn for highest strength and low abrasivity rock), anhydrite (low strength and low abrasivity rock) and (e) quartz sandstone (for lower strength and high abrasivity rock).
2. Inevitable data is the performance of the drill head and the associated bit wear. Both has to be recorded precisely.
 - a. Drilling time should be recorded as net time (time to drill one single hole from top to the bottom).
 - b. Drill hole depth should be measured with a folding rule or depth gauge and not just be estimated with the length of the drill rod.
 - c. The wear has to be recorded at the beginning of the drilling process (zero value), repeated at least every 5 drill holes and after drilling the last drill hole. The measurement frequency

has to be adapted to geological conditions. If the rock mass is fractured, a measurement of every drill hole is recommended.

3. All new drill testing data must be uploaded to the drill head add-on of the database as csv-file as mentioned in chapter 7.3.3.3.
4. After processing the uploaded data within the database, the results can be plotted in the rock landscape (Fig. 127).

To select the best drill head according to the geological conditions of a new drill site, the following recommendations should be followed:

1. Check within the database if a mine of similar geological conditions has already been tested.
2. If this questions are answered with yes, a list of already tested and used drill heads for this mine should be available. Select the best drill bit of this mine.
3. If question 1 is answered with no, rock samples should be collected e.g. by core drilling or selection of large blocks. The rock sample should be at least 20 x 20 x 20 cm in size to provide enough material for laboratory testing (UCS, BTS, PLT, CAI, LCPC, XRD, EQc, v_p and thin section analysis). Best choice for performing an intensive laboratory testing program.
4. If large samples or drill cores cannot be obtained, collect smaller samples for a reduced laboratory program (BTS, PLT, CAI, LCPC, XRD, EQc, v_p and thin section analysis). Note, that BTS and PLT give quite good correlations with drilling performance. Good choice for performing a sufficient laboratory testing program.
5. If sampling for laboratory testing is not possible at all, collect one smaller sample 3 x 3 x 3 cm for a thin section analysis and XRD and conduct PLT field tests on at least 10 compact rocks of a size of around 5 x 5 x 5 cm. Low cost choice for performing a reduced laboratory testing program.
6. Enter all laboratory and field testing results into the database.
7. Perform a drill head query for the determined rock properties and the encountered rock type(s) for the selected drill head(s).
8. To double check the drill head selection, plot the rock properties of the new drill site in the rock landscape and verify the drill head offered by the database.

These two procedures provide the user with a work flow to optimize the data sets within our database and the rock landscape. In this respect, the introduced empirical model may simplify the selection of a drill bit according to the occurring geological conditions and rock types significantly.

12 References

12.1 Literature, standards and maps

- ALBER, M., YARALI, O., DAHL, F., BRULAND, A., KÄSLING, H., MICHALAKOPOULOS, T. N., CARDU, M., HAGAN, P., AYDIN, H. & ÖZARSLAN, A. (2014): ISRM Suggested Method for Determining the Abrasivity of Rock by the CERCHAR Abrasivity Test. – *Rock Mech. and Rock Eng.*, 47, 1: 261-266.
- ASTM D2938 (2002): Standard test method for unconfined compressive strength of intact rock core specimens (withdrawn 2005). – West Conshohocken (ASTM International).
- ASTM D7012 (2013): Standard test method for compressive strength and elastic moduli of intact rock core specimen under varying states of stress and temperatures. – West Conshohocken (ASTM International).
- BECKER, H. & LEMMES, F. (1984): Gesteinsphysikalische Untersuchungen im Streckenvortrieb. – *Tunnel*, 2: 71-76.
- BERGMANN, J., FRIEDEL, P. & KLEEBOEG, R. (1998): BGMN - a new fundamental parameters based Rietveld program for laboratory X-ray sources, its use in quantitative analysis and structure investigations. – *CPD Newsletter*, 20: 5-8.
- BESTER, A. F. (1998): Geologiese Opname van Suid-Afrika 1:250,000 of map 2826 Winburg. – Pretoria (Geological Survey of South Africa).
- BROOK, N. (1993): The measurement and estimation of basic rock strength. – In: HUDSON, J. (Ed.): *Comprehensive rock engineering. Principles, practice & projects. Vol. 3: Rock testing and site characterization.*: 41-81, Oxford, New York (Pergamon).
- BÜCHI, E., MATHIER, J.-F. & WYSS, C. (1995): Gesteinsabrasivität - ein bedeutender Kostenfaktor beim mechanischen Abbau von Fest- und Lockergestein. – *Tunnel*, 5: 38-43.
- CAWTHORN, R. & BOERST, K. (2006): Origin of the Pegmatitic Pyroxenite in the Merensky Unit, Bushveld Complex, South Africa. – *Journal of Petrology*, 47, 8: 1509-1530.
- CERCHAR (1986): The CERCHAR Abrasiveness Index. – 12 p., Verneuil (Eigenverlag).
- CHEN, P. P.-S. (1976): The Entity-Relationship Model. Toward a Unified View of Data. – *ACM Transactions on Database Systems*, 1, 1: 9-36.
- CODD, E. (1970): A Relational Model of Data for Large Shared Data Banks. – *Communications of the ACM*, 13, 6: 377-387.
- DGEG (1979): Empfehlungen für die Versuchstechnik im Fels. Empfehlung Nr. 1: Einaxiale Druckversuche an Gesteinsproben. – *Bautechnik*, 7: 217-220.
- DGGT (2004): Einaxiale Druckversuche an zylindrischen Gesteinsprüfkörpern. Neufassung der Empfehlung Nr. 1 des Arbeitskreises 3.3 „Versuchstechnik Fels“ der Deutschen Gesellschaft für Geotechnik e.V. – *Bautechnik*, 81: 825-834.
- DGGT (2008): Indirekter Zugversuch an Gesteinsproben – Spaltzugversuch. Empfehlung Nr. 10 des Arbeitskreises 3.3 „Versuchstechnik Fels“ der Deutschen Gesellschaft für Geotechnik e.V. – *Bautechnik*, 85: 623-627.
- DGGT (2010): Punktlastversuche an Gesteinsproben. Empfehlung Nr. 10 des Arbeitskreises 3.3 „Versuchstechnik Fels“ der Deutschen Gesellschaft für Geotechnik e.V. – *Bautechnik*, 87: 322-330.

- DIEDERICHS, M. (2007): Mechanic interpretation of damage and spalling prediction for deep tunnels. – Canadian Geotechnical Journal, 44: 1082-1116.
- DILL, H., SCHRÖDER, B. & STETTNER, G. (1991): Geologische Karte des KTB-Umfeldes Oberpfalz 1 : 50,000. – Hannover (Niedersächsisches Landesamt für Bodenforschung und Bayerisches Geologisches Landesamt).
- DIMROTH, E. & SÖLLNER, K. (1964): Geologische Karte von Bayern 1 : 25,000 - 6038 Waldershof. – München (Bayerisches Geologisches Landesamt).
- DIN 51220 (2003): Werkstoffprüfmaschinen - Allgemeines zu Anforderungen an Werkstoffprüfmaschinen und zu deren Prüfung und Kalibrierung. – Berlin (Beuth Verlag).
- DIN EN 14579 (2005): Prüfverfahren für Naturstein - Bestimmung der Geschwindigkeit der Schallausbreitung. – Berlin (Beuth Verlag).
- EALLES, H. V. (2007): Riddles in stone. – 361 p., Johannesburg (Witwatersrand University Press).
- EITSCHBERGER, C. (2010): Konzeptionierung und Programmierung einer Festgesteinsdatenbank für geotechnische Kennwerte. – 73 p., Unpublished Master Thesis, Technische Universität München, München.
- FELLINGER, G. & BERGLER, C. (2009): 2DOC in der Praxis. Teil IV: Das Tunnelbauprojekt Harter Plateau/Linz. – Felsbau, 5/6: 284-288.
- FRIMMEL, H. E. (2005): Archean atmospheric evolution. Evidence from the Witwatersrand gold fields, South Africa. – Earth-Science Review, 70: 1-46.
- GEHRING, K. (1995): Leistungs- und Verschleißprognosen im maschinellen Tunnelbau. – Felsbau, 13: 439-448.
- GRIMM, W.-D., SCHWARZ, U., CLEMENS, K., POSCHLOD, K., NIEHAUS, F., LUKAS, R., SCHÜRMEISTER, R., BALLERSTÄDT, N., SIMPER, M. & ERFLE, E. (1990): Bildtafeln und Erläuterungen zu 200 Naturwerksteinen der Bundesrepublik Deutschland. – In: GRIMM, W.-D. (Ed.): Bildatlas wichtiger Denkmalgesteine der Bundesrepublik Deutschland: 252–655, Arbeitshefte des Bayerischen Landesamtes für Denkmalpflege, Bd. 50, München (Lipp).
- GUILBERT, J. M. & PARK JR., C. F. (1986): The Geology of Ore Deposits. – 985 p., New York (W. H. Freeman and Company).
- HAMMERBECK, E. & ALLOCK, R. (1985): Geological Map of Southern Africa 1 : 4 Mio. – Pretoria (The Geological Society of South Africa).
- HENNING, E., ANDRÉE, K., BROUWER, H. & BUCHER, W. (1938): Afrika (ohne Atlasländer und Madagaskar) nebst Arabien. – 142 p., Regionale Geologie der Erde, 1, Leipzig (Akademischer Verlag).
- HOEK, E. (1965): Rock fracture under static stress conditions. – 470 p., Pretoria (National Mechanical Engineering Research Institute).
- ISRM (1978a): Suggested methods for determining the uniaxial compressive strength and deformability of rock materials. – Int. J. Rock Mech. & Min. Sci. & Geomech. Abstr., 16: 135-140.
- ISRM (1978b): Suggested methods for the quantitative description of discontinuities in rock masses. – Int. J. Rock Mech. & Min. Sci. & Geomech. Abstr., 1978, 15: 319-368.

- ISRM (1985): Suggested method for determining point load strength. ISRM Commission on testing methods, working group on revision of the point load test method. – *Int. J. Rock Mech. & Min. Sci. & Geomech. Abstr.*, 22: 51-60.
- KÄSLING, H. & THURO, K. (2010): Determining abrasivity of rock and soil in the laboratory. – In: WILLIAMS, A. L. (Ed.): *Geologically active: 1973-1980*, Leiden (CRC Press/Balkema).
- KÄSLING, H., THURO, K., SINGER, J. & BAUER, M. (2006): Abrasivitätsuntersuchungen an Lockergesteinen im Hinblick auf die Gebirgslösung. – In: DGGT (Ed.): *Beiträge zur 29. Baugrundtagung: 283-290*, 29. Baugrundtagung, Bremen, 27. - 29. Sept. 2006, Bremen.
- KEMPER, A. & EICKLER, A. (2011): *Datenbanksysteme: Eine Einführung*. – 792 p., München (Oldenburg Wissenschaftsverlag).
- KLÖTZLI, U. S., BUDA, G. & SKIÖLD, T. (2004): Zircon typology, geochronology and whole rock Sr-Nd isotope systematics of the Mecsek Mountain granitoids in the Tisia Terrane (Hungary). – *Mineralogy and Petrology*, 81, 1-2: 113-134.
- LEHRBERGER, G. (2013): Granit - das Höchste und das Tiefste. – In: HELM, W. (Ed.): *Granit: 19-48*, Hauzenberg (Granitzentrum Bayerischer Wald).
- MAIER, W. D., BARNES, S.-J., CHINYEPI, G., BARTON, J. M., EGLINGTON, B. & SETSHEDI, I. (2007): The composition of magmatic Ni–Cu–(PGE) sulfide deposits in the Tati and Selebi-Phikwe belts of eastern Botswana. – *Miner Deposita*, 43, 1: 37-60.
- MARTIN, C. (1997): Seventeenth Canadian Geotechnical Colloquium: The effect of cohesion loss and stress path on brittle rock strength. – *Canadian Geotechnical Journal*, 34: 698-725.
- MENSCHIK, F. (2009): *Geotechnische Einflussfaktoren beim Bohren mit elektrischen Schlagbohrhämmern*. – 53 p., Unpublished Master Thesis, Technische Universität München, München.
- MESCHEDE, M. (2015): *Geologie Deutschlands*. – 249 p. Berlin (Springer Spektrum).
- MONDAL, S. K. & MATHEZ, E. A. (2007): Origin of the UG2 chromitite layer, Bushveld Complex. – *Journal of Petrology*, 48, 3: 495-510.
- MOORE & REYNOLDS (1997): *X-ray diffraction and the identification and analysis of clay minerals*. – x p., Oxford (Oxford University Press).
- NORMALISATION FRANÇAISE P 18-579 (AFNOR) (1990): *Granulats - Détermination des coefficients d'abrasivité et de broyabilité*. – Paris (Association française de normalisation, AFNOR).
- OBERT, L. & DUVALL, W. I. (1967): *Rock mechanics and the design of structures in rock*. – 650 p., New York (Wiley).
- PETERS, S. W. (1991): *Regional geology of Africa*. – 722 p., Berlin (Springer-Verlag).
- PLINNINGER, R. J. (2002): *Klassifizierung und Prognose von Werkzeugverschleiß bei konventionellen Gebirgslösungsverfahren im Festgestein*. – 146 p., Münchner geologische Hefte Reihe B, *Angewandte Geologie*, 17, München (Lehrstuhl für Allgemeine Angewandte und Ingenieur-Geologie Techn. Univ).
- PLÖCHINGER, B. (1987): *Geologische Karte der Republik Österreich 1 : 50,000 of Map 94 Hallein*. – Wien (Geologische Bundesanstalt).

- PLÖCHINGER, B. (1990): Erläuterungen zu Blatt 94 Hallein. – 76 p., Wien (Ferdinand Berger und Söhne OHG).
- POHL, W. (2005): Mineralische und Energie-Rohstoffe: Eine Einführung zur Entstehung und nachhaltigen Nutzung von Lagerstätten. – 527 p., Stuttgart (Schweizerbart'sche Verlagsbuchhandlung).
- RAUM, G. (2013): Geologische Karte von Bayern 1 : 25,000 - 6039 Mitterteich. – Augsburg (Bayerisches Landesamt für Umwelt).
- ROSIWAL, A. (1896): Neue Untersuchungsergebnisse über die Härte von Mineralien und Gesteinen. – Verhandlg. d. k.k. geol. R.-A. Wien: 475-491.
- ROSIWAL, A. (1916): Neuere Ergebnisse der Härtebestimmung von Mineralien und Gesteinen. Ein absolutes Maß für die Härte spröder Körper. – Verhandlg. d. k.k. geol. R.-A. Wien: 117-147.
- SAAKE, G., SATTLER, K.-U. & HEUER, A. (2010): Datenbanken. Konzepte und Sprachen. – 784 p., Heidelberg (mitp-Verlag).
- SCHIMAZEK, G. & KNATZ, H. (1976): Die Beurteilung von Gesteinen durch Schneid- und Rollenbohrwerkzeuge. – Erzmetall, 29: 113-119.
- SCHLÜTER, T. (2008): Geological Atlas of Africa: with notes on stratigraphy, tectonics, economic geology, geohazards, geosites and geoscientific education of each country. – 307 p., Berlin (Springer).
- SCHOUWSTRA, R., KINLOCH, E. & LEE, C. (2000): A Short Geological Review of the Bushveld Complex. – Platinum Metals Review and Sustainability, 1, 44: 33-39.
- SCHÜSSLER, U. (1990): Petrographie, Geochemie und Metamorphosealter von Metabasiten im KTB-Zielgebiet Oberpfalz. – Geologica Bavarica, 1990, 95: 5-99.
- SCHWARZMEIER, J. & WEINELT, W. (1993): Geologische Karte 1 : 100,000 Naturpark Spessart. – München (Bayerisches Geologisches Landesamt).
- SPICHER, A. (1980): Geologische Karte der Schweiz 1 : 500,000. – Bern (Schweizerischen Geologischen Kommission).
- STETTNER, G. (1992): Geologie im Umfeld der Kontinentalen Tiefbohrung Oberpfalz. – 244 p., München (Bayerisches Geologisches Landesamt).
- THE GEOLOGICAL SOCIETY OF SOUTH AFRICA (1986): The Witwatersrand Basin 1 : 500,000. – Johannesburg (The Geological Society of South Africa).
- THURO, K. (1996): Bohrbarkeit beim konventionellen Sprengvortrieb. – 145 p., Münchner geologische Hefte Reihe B, 1, München (Lehrstuhl für Allgem. Angew. und Ingenieur-Geologie).
- THURO, K. & KÄSLING, H. (2009): Classification of the abrasiveness of soil and rock. – Geomechanik und Tunnelbau, 2, 2: 179-188.
- THURO, K. & PLINNINGER, R. (2007): Geologisch-geotechnische Grundlagen der Gebirgslösung im Fels. - In: EICHLER, K. (Ed.): Fels- und Tunnelbau II. Verfahren und Kenngrößen – Technologie und Umwelt – Vortrieb und Sicherung – Baustoffe und Eigenschaften. – 314 S Renningen-Malmsheim (Expert): 112-160.
- VILJOEN, M. J. & REIMOLD, W. U. (1999): An introduction to South Africa's geological and mining heritage. –193 p., Randburg (Mintek in association with the Geological Society of South Africa).

-
- WEISSERT, H. & STÖSSEL, I. (2010): Der Ozean im Gebirge. – 192 p., Zürich (vdf Hochschulvlg).
- WEST, G. (1989): Technical Note - Rock Abrasiveness Testing for Tunneling. – *Int. J. Rock Mech. & Min. Sci. & Geomech. Abstr.*, 26, 2: 151-160.
- WILFING, L., KÄSLING, H. & THURO, K. (2014): Towards a uniform definition of rock toughness for penetration prediction in TBM-tunneling. – In: LOLLINO, G., GIORDANO, D., THURO, K., CARRANZA-TORRES, C., WU, F., MARINOS, P. & DELGADO, C. (Eds.): *Engineering Geology for Society and Territory – Volume 6: 469-473*, IAEG XII Congress, Turin, IAEG, Turin (Springer).

12.2 Online references

- www-1: http://www.hilti.com/fstore/holcom/LinkFiles/Leaflet_TE_MD20_W3134_English.pdf,
last access on 16.04.2014.
- www-2: <http://www.miningweekly.com/article/moab-khotsong-mine-south-africa-2015-05-01>,
last access on 25.09.2015.
- www-3: <http://www.miningweekly.com/article/kloof-mine-south-africa-2015-04-10>,
last access on 25.09.2015.
- www-4: http://aquariusplatinum.com/blue_ridge,
last access on 17.7.2015.
- www-5: <http://www.bcl.bw/index.php?id=16>,
last access on 18.07.2015.
- www-6: <http://www.mining-technology.com/features/feature-top-ten-deepest-mines-world-south-africa/>,
last access on 17.10.2014.

13 Appendices

A) Database structure – entities (tables) and attributes (fields) with properties

A.1) Explanation of database structure

Attribute (Field)	Datatype	Null allowed	Standard
Name of the attribute (Database) this name is also used as variable in php/html code	Integer Float/Decimal Text Date	Yes/No Are Null values allowed for this field	Standard value if no other value is defined

A.2) User management module

Anmeldung

Attribute (Field)	Datatype	Null allowed	Standard
ID	int(11)	No	
Name	text	No	
Zeit	timestamp	No	CURRENT_TIMESTAMP

tblbenutzer

Attribute (Field)	Datatype	Null allowed	Standard
benID	int(5)	No	
benName	varchar(50)	No	
b	varchar(50)	No	
benEbene	varchar(50)	No	
BenAuftraggeberID	int(11)	Yes	NULL

A.3) General project data module

bearbeitung

Attribute (Field)	Datatype	Null allowed	Standard
bearbID	int(11)	No	
bearbProjektID	int(11)	No	
Teilprojekt	text	No	
Auftragseingang	date	No	
Abgabefrist	date	Yes	NULL
Bearbeiter	text	No	
HIWI	text	Yes	NULL
Laborstatus	text	No	
LaborstatusDate	date	Yes	NULL
Laborbericht	text	No	

LaborberichtDate	date	Yes	NULL
Rechnung	text	No	
RechnungDate	date	Yes	NULL
BKZ	text	No	
Preis	float	No	
Aktualisierung	timestamp	No	0000-00-00 00:00:00

tblansprechpartner

Attribute (Field)	Datatype	Null allowed	Standard
AnsAnsprechpartnerID	int(11)	No	
AnsVorname	varchar(50)	Yes	NULL
AnsNachname	varchar(50)	Yes	NULL
AnsTelefon	varchar(20)	Yes	NULL
AnsEmail	varchar(50)	Yes	NULL
AnsStrasse	varchar(50)	Yes	NULL
AnsPostleitzahl	varchar(20)	Yes	NULL
AnsOrt	varchar(50)	Yes	NULL
AnsArbeitgeber	tinyint(4)	No	

tblauftraggeber

Attribute (Field)	Datatype	Null allowed	Standard
AufAuftraggeberID	int(11)	No	
AufFirmenname	varchar(100)	No	
AufCode	varchar(4)	Yes	NULL
AufStrasse	varchar(100)	Yes	NULL
AufPostleitzahl	varchar(20)	Yes	NULL
AufOrt	varchar(50)	Yes	NULL

tblgesteinsart

Attribute (Field)	Datatype	Null allowed	Standard
GesID	smallint(4)	No	
GesName	varchar(50)	No	
GesName_e	varchar(50)	No	

tblmitarbeiter

Attribute (Field)	Datatype	Null allowed	Standard
MitMitarbeiterID	tinyint(11)	No	
MitVorname	varchar(100)	No	
MitNachname	varchar(100)	No	

MitTelefon	varchar(20)	Yes	NULL
MitEmail	varchar(100)	Yes	NULL

tblproben

Attribute (Field)	Datatype	Null allowed	Standard
PrbProbenID	int(11)	No	
PrbProjektID	int(11)	No	
PrbName	varchar(100)	Yes	NULL
PrbGesteinsart	smallint(4)	Yes	NULL
PrbGestein	varchar(50)	Yes	NULL
PrbBeschreibung	text	Yes	NULL
PrbTrennflaechen	text	Yes	NULL
PrbEntnahmeArt	varchar(100)	Yes	NULL
PrbEntnahmeOrt	varchar(100)	Yes	NULL
PrbEntnahmeTiefe	varchar(20)	Yes	NULL
PrbEntnahmeDatum	date	Yes	NULL
PrbBearbeiter	varchar(100)	Yes	NULL

tblprojekte

Attribute (Field)	Datatype	Null allowed	Standard
ProProjektID	int(11)	No	
ProMitarbeiterID	int(11)	No	
ProName	varchar(100)	No	
ProCode	varchar(5)	Yes	NULL
ProBeschreibung	text	Yes	NULL
ProAuftraggeberID	int(11)	No	
ProAnsprechpartnerID	int(11)	Yes	NULL

A.4) Laboratory data module

tbl1dv

Attribute (Field)	Datatype	Null allowed	Standard
1DVProbenID	int(11)	No	
1DVPruefkoerperID	int(11)	No	
1DVPruefkoerper	varchar(100)	No	
1DVMitarbeiter	varchar(100)	Yes	NULL
1DVDatum	date	No	
1DVWassergehalt	varchar(20)	Yes	NULL
1DVGroesstkorn	varchar(20)	Yes	NULL
1DVDurchmesser	decimal(7,1)	Yes	NULL
1DVLaeenge	decimal(7,1)	Yes	NULL
1DVDichte	decimal(4,3)	Yes	NULL

1DVWinkel	varchar(10)	Yes	NULL
1DVEinaxiale_Druckfestigkeit	decimal(7,1)	Yes	NULL
1DVE_Modul	decimal(7,2)	Yes	NULL
1DVV_Modul	decimal(7,2)	Yes	NULL
1DVZerstoerungsarbeit	decimal(7,1)	Yes	NULL
1DVTyp	varchar(4)	Yes	1DV
1DVFormblatt	varchar(100)	Yes	NULL
1DVwb	decimal(7,3)	No	

tblcai

Attribute (Field)	Datatype	Null allowed	Standard
CAIProbenID	int(11)	No	
CAIPruefkoerperID	int(11)	No	
CAIPruefkoerper	varchar(50)	No	
CAIMitarbeiter	varchar(100)	Yes	NULL
CAIDatum	date	No	
CAIWassergehalt	varchar(20)	Yes	NULL
CAIOrientierung	int(2)	Yes	NULL
CAIZustand	int(2)	Yes	NULL
CAIEinzelversuche	int(2)	Yes	NULL
CAIStandardabweichung	decimal(7,2)	Yes	NULL
CAIStandardfehler	decimal(7,2)	Yes	NULL
CAIWert	decimal(7,1)	Yes	NULL
CAITyp	varchar(4)	Yes	CAI
CAIFormblatt	varchar(100)	Yes	NULL

tblcpc

Attribute (Field)	Datatype	Null allowed	Standard
LCPCProbenID	int(11)	No	
LCPCPruefkoerperID	int(11)	No	
LCPCPruefkoerper	varchar(100)	No	
LCPCMitarbeiter	varchar(100)	Yes	NULL
LCPCDatum	date	No	
LCPCVersuchsoption	int(11)	No	
LCPCLAK	int(4)	Yes	NULL
LCPCLBK	int(3)	Yes	NULL
LCPCTyp	varchar(4)	Yes	LCPC
LCPCFormblatt	varchar(100)	Yes	NULL

tblplt

Attribute (Field)	Datatype	Null allowed	Standard
-------------------	----------	--------------	----------

PLTProbenID	int(11)	No	
PLTPruefkoerperID	int(11)	No	
PLTPruefkoerper	varchar(100)	No	
PLTMitarbeiter	varchar(100)	Yes	NULL
PLTDatum	date	No	
PLTWassergehalt	varchar(20)	Yes	NULL
PLTGroesstkorn	varchar(20)	Yes	NULL
PLTPruefoption	varchar(50)	Yes	NULL
PLTAnzahl	int(3)	Yes	NULL
PLTPunktlastindex	decimal(7,2)	Yes	NULL
PLTUCS	decimal(7,2)	Yes	NULL
PLTUmrechnungsfaktor	decimal(6,2)	Yes	NULL
PLTTyp	varchar(3)	Yes	PLT
PLTFormblatt	varchar(100)	Yes	NULL

tblspz

Attribute (Field)	Datatype	Null allowed	Standard
SPZProbenID	int(11)	No	
SPZPruefkoerperID	int(11)	No	
SPZPruefkoerper	varchar(100)	No	
SPZMitarbeiter	varchar(100)	Yes	NULL
SPZDatum	date	No	
SPZWassergehalt	varchar(20)	Yes	NULL
SPZGroesstkorn	varchar(20)	Yes	NULL
SPZDurchmesser	decimal(7,2)	Yes	NULL
SPZLaenge	decimal(7,2)	Yes	NULL
SPZMasse	decimal(7,2)	Yes	NULL
SPZDichte	decimal(5,3)	No	
SPZBelastungsfall	tinyint(2)	No	
SPZSpaltzugfestigkeit	decimal(7,1)	Yes	NULL
SPZTyp	varchar(4)	Yes	SPZ
SPZFormblatt	varchar(100)	Yes	NULL

tblus_p

Attribute (Field)	Datatype	Null allowed	Standard
USPPruefkoerperID	int(11)	No	
USPProbenID	int(11)	No	
USPPruefkoerpername	varchar(20)	No	
USPMitarbeiter	varchar(20)	Yes	NULL
USPDatum	date	No	
USPDurchmesser	double(7,2)	No	
USPHoehe	double(7,2)	No	
USPGewicht	double(7,2)	No	

USPQuerschnitt	int(1)	No	
USPvp_p	double(7,2)	No	
USPTyp	varchar(4)	Yes	USP
USPFormblatt	varchar(100)	Yes	NULL

A.5) Hilti add on module

hil-drill

Attribute (Field)	Datatype	Null allowed	Standard
DrillID	int(11)	No	
Kennung	text	No	
CID	int(11)	No	

hil-drilldata

Attribute (Field)	Datatype	Null allowed	Standard
DatID	int(11)	No	
DrilltestID	int(11)	No	
DrillID	int(11)	No	
DrillHeadCount	int(11)	No	
MineID	int(11)	No	
BohrlochNr	tinyint(4)	No	
Bohrlochtiefe	decimal(5,3)	No	
TiefenSumme	decimal(6,3)	No	
BohrzeitMin	tinyint(4)	No	
BohrzeitSek	tinyint(4)	No	
Probleme	tinyint(1)	No	
Problembeschreibung	text	No	
Durchmesser	decimal(6,3)	Yes	NULL
Gewicht	decimal(6,2)	Yes	NULL
Bohrer	text	No	

hil-drmi

Attribute (Field)	Datatype	Null allowed	Standard
drmiID	int(11)	No	
MineID	int(11)	No	
DrillID	int(11)	No	
Perf	float	No	
Wear	float	No	
Drop	float	No	

hil-mines

Attribute (Field)	Datatype	Null allowed	Standard
MineID	int(11)	No	
Land	text	No	
Name	text	No	
Resource	text	No	
Descript	text	No	
Reefs	text	No	
Coord	varchar(35)	No	
ProjektID	int(11)	No	
Depth	text	No	
City	text	No	
Company	text	No	
Openup	text	No	

hil-rocks

Attribute (Field)	Datatype	Null allowed	Standard
RockID	int(11)	No	
MineID	int(11)	No	
Rocktype	text	No	